Water Management in Mature Oil Fields using Advanced Particle Gels

Final Report

Contract no.: 11123-32

Jan. 15, 2016

- Prime Contractor: The University of Texas at Austin
- Participant: Missouri University of Science and Technology

Contacts: – Mojdeh Delshad, 512-471-3219, delshad@mail.utexas.edu

Baojun Bai, 573-341-4016, baib@mst.edu

Research Partnership to Secure Energy for America (RPSEA)

Project Manager: John R. Terneus

Start Date: January 18, 2013

End Date: January 17, 2015

Table of Content

Section 1: Executive Summary

This project provided a better understanding of recent particle gel processes based on systematic laboratory experiments and development of a numerical tool to solve excess water production taking into account the reservoir heterogeneity and operating conditions. The ultimate purpose of the project was to provide a simulation tool to optimize particle gel treatments to increase oil recovery and reduce water production.

Coreflood experiments helped in understanding the prevailing mechanisms of preformed particle gel transport in porous media. The experiments provided the necessary data to develop and validate mechanistic models for each process that were implemented in a reservoir simulator to design and predict the performance of such treatments in field projects. The proposed research included designing and performing experiments, development of mathematical models and a water shut off reservoir simulator, validation and verification, and feasibility of the proposed treatment for a particular field. The simulator will aid in providing guidelines for the application in candidate reservoirs.

Major Accomplishment

- Investigated the extent to what the particle gel can reduce the permeability to water much more than that to oil using two closed conduit model and super-K permeability sandstone cores.
- Used sandpack models and Berea sandstone cores to study the effect of milli-sized particle gel and nanogels on oil recovery improvement and determined the factors that affect particle gel transport behavior.
- Designed heterogeneous experimental models and conducted experiments to evaluate the ability of PPGs to solve the conformance problem for the reservoirs with and without cross flow.
- Designed screen plate models and ran experiments to establish the passing criteria for PPG transport through different pore sizes of throat and different widths of fractures.
- Built a novel discrete fracture model to investigate the PPG capability to block the fracture network and improve oil recovery from the matrix.
- Developed models/correlations for gel viscosity, plugging, swelling ratio, resistance factor, residual resistance factor, and retention for a wide range of flow rate and brine salinity and hardness, conduit size.
- Successfully modeled the laboratory tests using the reservoir simulator for conformance control, UTGEL.

Significant Findings

- Particle gel (PG) injection cannot only improve oil recovery for heterogeneous model resulted from conformance improvement but it can also increase the oil recovery from homogenous models, which could be attributed to the elastic effect from the swelling gels.
- Proper selections of particle gels (particle size and strength) can lead to particle gels selectively enter super-K zones with no penetration into non-swept zones. This can minimize the risk of formation damage and significantly improve conformance.
- For in-depth fluid diversion applications, the retention of PG strongly affected the propagation of particles through porous media. However, the gel retention can be controlled by selecting proper particle gel strength, concentration, and size.
- The numerical studies indicated that main PG design variables are treatment size, PPG concentration, permeability contrast between layers, mobility ratio, and the ratio of vertical to horizontal permeability.
- Pilot scale field simulations showed that PG has the capability to generate high resistance factor in high permeability thief zones and increase the oil recovery by around 10-15% and decrease water cut by about 5-10 % over waterflood.
- Numerical simulations illustrated that higher permeability contrast between layers and lower crossflow are favorable design parameters for PG treatment.
- Comprehensively studied the swelling kinetics where swelling time will be less than two hours for PPG in most cases. Therefore, swelling kinetics may not be critical for field cases.

PUBLICATIONS

1. **A. Almohsin** et al.," Transport of Nanogel through Porous Media and Its Resistance to Water Flow," SPE paper 169078, SPE Improved Oil Recovery Symposium, Tulsa, OK, April 2014. http://dx.doi.org/10.2118/169078-MS.
2. **F. Muhammed** et al., "A Simple Technique to Determine Gel Strength of Millimeter-sized Particle Gel," SPE paper 169106, SPE Improved Oil Recovery Symposium, Tulsa, OK, April 2014. http://dx.doi.org/10.2118/169106-MS.
3. **Goudarzi**, A. et al "Water Management in Mature Oil Fields using Preformed Particle Gels," SPE paper 165356, SPE Western Regional & AAPG Pacific Section Meeting, 2013 Joint Technical Conference, Apr 19 - 25, 2013, Monterey, CA, USA. http://dx.doi.org/10.2118/165356-MS
4. **Goudarzi**, A. et al., "New Experiments and Mechanistic Models for Conformance Control Microgels," SPE paper 169159, SPE Improved Oil

Recovery Symposium, Tulsa, OK, April 2014. http://dx.doi.org/10.2118/169159-MS.

5. **Goudarzi**, A., Zhang, H., Varavei, A., Taksausdom, P., Hu, Y., Delshad, M., Bai, B., and Sepehmoori, K. 2015. A laboratory and simulation study of preformed particle gels for water Conformance Control. Fuel Journal*;* 140**:** 502-513.
6. **Imqam**, A. et al., "Preformed Particle Gel Extrusion through Open Conduits during Conformance Control Treatments," SPE paper 169107, SPE Improved Oil Recovery Symposium, Tulsa, OK, April 2014. http://dx.doi.org/10.2118/169107-MS.
7. **Imqam** A. et al "Characterizations of Disproportionate Permeability Reduction of Particle Gels Through Fractures" SPE-171531-MS**,** Asia Pacific Oil & Gas Conference and Exhibition, October 2014, Adelaide, Australia. http://dx.doi.org/10.2118/171531-MS
8. **Imqam**, A., Bai, B., Al-Ramadan, M., Delshad, M., Sepehrnoori, K. 2015. Preformed Particle Gel Extrusion through Open Conduits during Conformance Control Treatments. SPE Journal. SPE-169107-PA, SPE- Journal. 20 (5):1083 – 1093. http://dx.doi.org/10.2118/169107-PA.
9. **Imqam**, A., Bai, B., Delshad, M. 2015. Preformed Particle Gel Propagation through Super-K Permeability and its Resistance to Water Flow during Conformance Control. Paper SPE 176429 presented at the SPE Asia Pacific Oil & Gas Conference and Exhibition held in Bali, Indonesia, 20–22 October. http://dx.doi.org/10.2118/176429-MS.
10. **Imqam**, A., Goudarzi, A., Delshad, M., Bai, B. 2015. Development a Mechanistic Numerical Simulator for Preformed Particle Gel Applications in Non-Cross Flow Heterogeneous Reservoirs. Paper SPE 175058 presented to the SPE Annual Technical Conference and Exhibition held in Houston, Texas, USA, 28-30 September. http://dx.doi.org/10.2118/175058-MS.
11. **Imqam, A**., Bai, B., Wang, Z., M., Delshad, M. 2016. Effect of Heterogeneity on Propagation, Placement, and Conformance Control of Preformed Particle Gel Treatment in Fractures. Paper SPE 179705 presented at the SPE Improved Oil Recovery Symposium, Tulsa, Oklahoma, 9-13 April**.** http://dx.doi.org/10.2118/179705-MS.

Section 2: Preformed Particle Gel properties

2.1 Summary

Preformed particle gel (PPG) has been injected into mature oil reservoirs as a conformance control agent to decrease reservoir heterogeneity and also to improve sweep efficiencies during water injection for reduced water production and enhanced oil recovery. The ultimate purpose of this chapter is to provide a fundamental basis for gel selection. This work involves the study of swelling and de-swelling kinetics of cross-linked acrylamide and potassium acrylate copolymer preformed particle gels. The swelling and de-swelling kinetic curves of the PPG were measured, and their swelling and de-swelling kinetic parameters were estimated. The equilibrium swelling ratios of the PPG in brine solutions of different concentrations were determined from both the swelling and de-swelling processes. Results showed that PPG swelling capacity increases with temperature but decreases with salinity. PPG de-swelling capacity increases with salinity and temperature.

2.2 Experimental Description

2.2.1 Materials

The PPG used in this study is commercially known as Liquid Block^{TM} 40K. Its chemical name is crosslinked acrylamide and potassium acrylate copolymer. Its basic chemical components are 2-propenoic acid, potassium salt, and 2- propenamide polymer. This PPG has an apparent bulk density (g/l) of 540, its moisture content is 5%, and it has a pH value of 5.5-6.0. For this study, PPG having particle sizes of 425–600 μm were chosen.

2.2.2 Swelling Kinetics Studies

2.2.2.1 Effect of Salinity on PPG Swelling Capacity

Experiments to determine the effect of salinity on PPG swelling capacity were carried out by adding known amounts of dry PPG to different concentrations of brine solutions. All brine solutions were predetermined to have a pH of 7. The volumes of the PPG were measured at different time intervals until the PPG ceased to swell. The swelling ratios of PPG in different brine solutions were measured using the equation $\frac{V_f}{V_i}$, where V_f is the final volume of the PPG in ml and V_i is the initial volume of the PPG in ml. Finally, swelling kinetic data were obtained and swelling kinetic curves drawn.

2.2.2.2 Effect of Temperature on PPG Swelling Capacity

PPG swelling ratios were measured by using brine solutions initially heated to 45 ^{o}C and 60 ^{o}C. All brine solutions were predetermined to have pH's of 7. The swelling kinetic curves of PPG immersed in brine solutions having temperatures of 45 ^{o}C and 60 ^{o}C were compared with the swelling kinetic curve of PPGs swollen in different brine solution at 25 ^{0}C.

2.2.3 De-swelling Kinetic Studies

2.2.3.1 Effect of Salinity on PPG De-swelling Capacity

De-swelling kinetics experiments were carried out by first fully swelling six samples of PPG immersed in distilled water. Varying amounts of NaCl powder were added to each of the samples to increase salinity to 0.05%, 0.25%, 1.0%, 5.0%, 10.0% and 20.0%. The graduate tubes holding the samples were then shaken to ensure homogeneity. Once the gels were settled at the bottom of the tubes, the volumes of the PPG (ml) were measured at different time intervals until the PPG ceased to deswell. The swelling ratios of the PPG in different concentrations of brine solutions were calculated using the equation $\frac{V_i}{V_f}$, where V_i is the initial volume of the PPG in ml and V_f is the final

volume of the PPG in ml. Finally, de-swelling kinetic data were obtained and deswelling kinetic curves drawn.

2.2.4 Gel Strength Measurements

The storage moduli (G`) for gels swollen in brine were measured at room temperature (around 23 ^{o}C) using a rheometer. After being swelled in brine, gel strengths were measured and compared to see if the gel strength increased or decreased after swollen in different brine solutions. The sensor used for these measurements was PP335 TiPoLO2 016 with a gap of 0.8 mm between the sensor and the plate. G`were measured at a frequency of 1 Hz for each sample.

2.3 Results and Analysis

2.3.1 PPG Swelling and De-swelling Capacities

2.3.1.1 Effect of Salinity on PPG Swelling Capacity

Figure 2-1 shows the influence of salinity on the swelling capacities of PPG. It shows that salinity decreases the swelling capabilities of PPG. In distilled water, PPG swells up to 500 times. Also, a small increase in salt concentration greatly decreases PPG swelling capacity. On average, an increase of 0.05% of salt concentration decreases the swelling capacity of the PPG from 504 to 156 times.

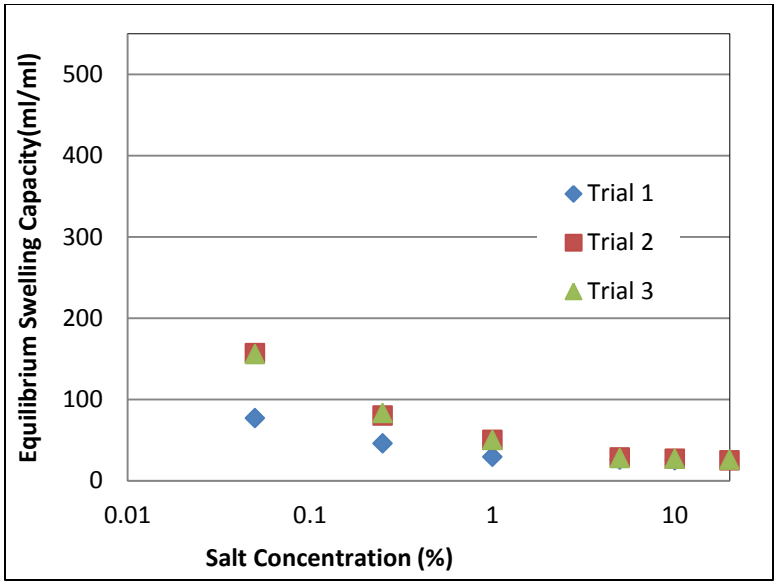

Figure 2-1. Effect of salt concentration on PPG swelling capacity

Table 2-1. PPG Swelling Ratios

PPG Swelling Ratios	
Salt Concentrations (%)	Average
0.00	504.167
0.05	156.111
0.25	80.000
1.00	48.611
5.00	28.426
10.00	26.389
20.00	25.185

PPG used is a superabsorbent polymer that is capable of swelling more than 500 times in DIW. This is due to the PPG being negatively charged and creating hydrogen bonds between the positively charged hydrogen ions in water. As the hydrogen ions get used up, the solution becomes increasingly negatively charged. This further enhances the reaction between the polymer and hydrogen ion for a charge-balancing effect. This

accounts for the superabsorbent property of PPG. As NaCl concentration increases, however, the concentration of Na^+ also increases. The negatively charged polymer group will be balanced by the sodium cations instead, which restricts further water absorption.

2.3.1.2 Effect of Temperature on PPG Swelling Capacity

Increasing the temperature of the solution in which the PPG is immersed induces the breakage of the porous structure of PPG. The endothermic reaction of chemical bond breaking is accelerated by the increase in temperature. As the porous structure of the PPG is broken, more water can be absorbed into the PPG. This explains the increase in the swelling capacities of PPG with increasing temperature as shown in **Fig. 2-2.**

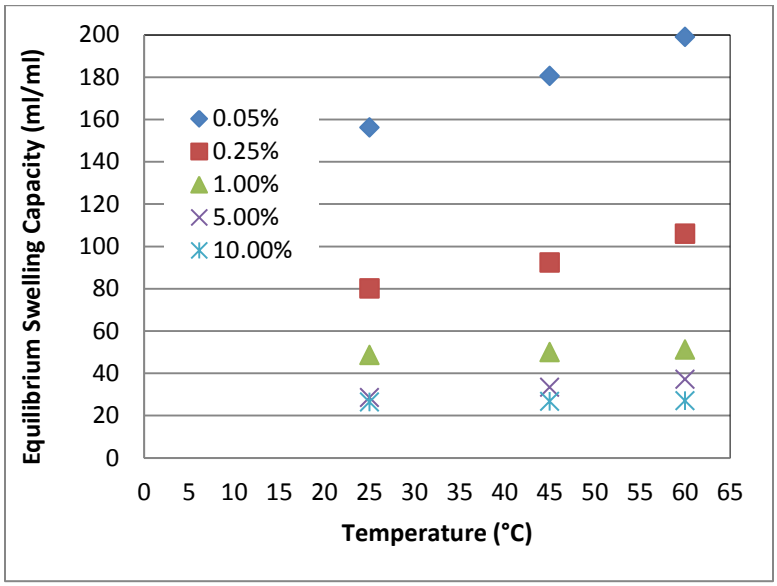

Figure 2-2. Effect of Temperature on PPG Swelling Capacity

Table 2-2 Effect of Temperature on PPG Swelling Capacity

Salt Conc (%)	Temperature (°C) 25	45	60
0.05	156.111	180.560	198.876
0.25	80.000	92.200	103.862
1.00	48.611	50.000	51.076
5.00	28.426	33.300	37.052
10.00	26.389	26.670	26.882

Increasing the temperature of the brine solution that PPG is immersed will induce the breakage of the PPG's porous matrix. As the pore space in between the molecular structure of PPG increases, more water is able to diffuse in, subsequently increasing the volume of PPG and its equilibrium swelling capacity.

2.3.1.3 Effect of Salinity on PPG Deswelling Capacity

Figure 2-3 shows the influence of salinity on the deswelling capacities of PPG. It shows that salinity increases PPG deswelling ratios. Also, comparing **Figure 2-3** with **Figure 2-1**, a smaller deswelling ratios is observed more often than swelling ratios for PPG.

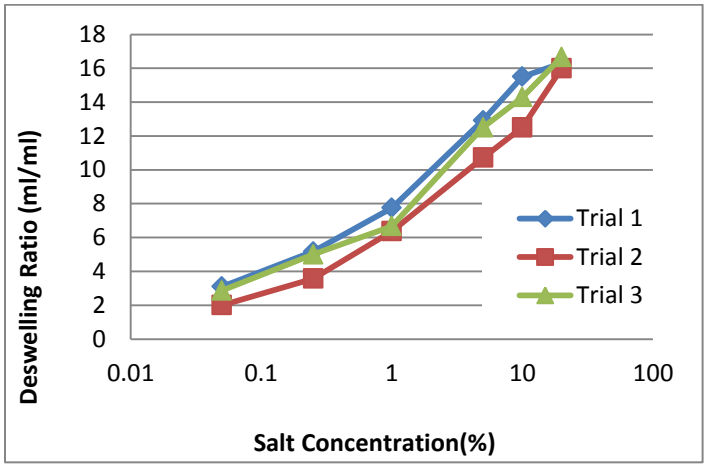

Figure 2-3. Effect of Salinity on PPG Deswelling Capacity

Table 2-3. Deswelling Ratios

PPG Deswelling Ratios	
Salt Concentrations (%)	Average
0.05	2.45
0.25	4.74
1.00	7.52
5.00	13.40
10.00	15.50
20.00	17.40

Increasing the salinity of the solution will cause a chemical potential disequilibrium between the polymer and the surrounding solution. To regain equilibrium, the Na^+ cations will diffuse into the polymer and replace the hydrogen cations. Hence, water is expelled from the gel. Increasing salinity will only make more water to be expelled thereby creating a larger deswelling ratio.

2.3.2 Swelling Kinetics of PPG

Dry PPG particles were placed separately in test tubes filled with different brine concentrations. The stable swelling ratio was computed for each concentration. **Figure 2-4** shows the influence of the brine concentration on the swelling capacity. The PPG showed normal swelling ratio behavior in that its swelling capacity initially increased with time and then attained equilibrium swelling capacity (ESC). The swelling degree is generally determined as a balance between water absorption (due to the hydrophobicity of polymer chains) and network elasticity (proportional to crosslink density).

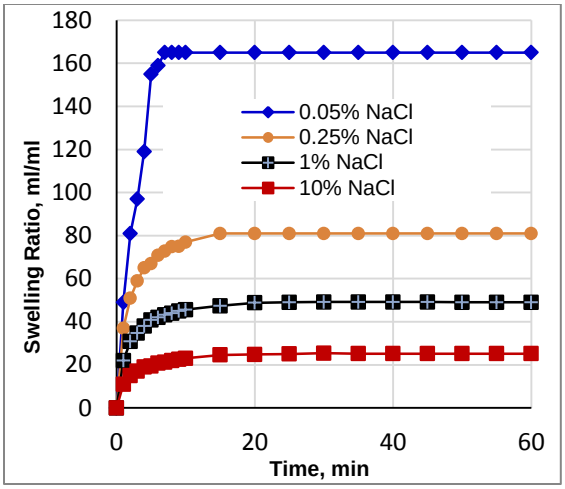

Figure 2-4. Swelling ratio of gel in different brine concentrations

The ESC data obtained from **Figure 2-4** was used in **Figure 2-5** to show how brine concentration correlations can be applied to predict the ESC values of concentrations. **Figure 2-5** illustrates that the higher the concentration, the smaller the ESC value. **Equation 2-1** is the correlation obtained to predict the ESC of gel swollen in brine. These empirical correlations were fitted with the power law model, with a high R^2 accuracy:

$$ESC = 53.084 \times C_{brine}^{-0.352} \qquad (2\text{-}1)$$

where ESC is the equilibrium swelling capacity, C_{brine} is the sodium chloride concentration in wt.-%. Using this correlation serves as a simple, quick, and practical method to estimate the equilibrium swelling capacity of PPG for a range of NaCl concentrations either in the laboratory or on-site during the PPG treatment process.

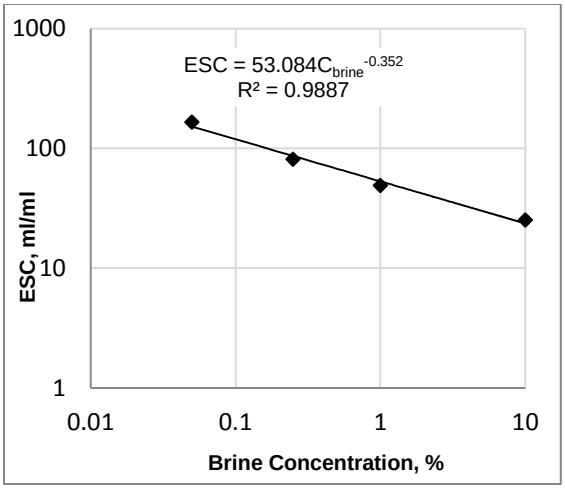

Figure 2-5. Effect of brine concentration on the ESC.

2.3.3 Gel Strength Measurements

Figure 2-6 shows the measurement of the PPG storage modulus for gels swollen in different brine concentrations. The results exhibit a significant increase in gel strength as the brine solution increased. PPG swollen in higher salt concentrations was much stronger than the PPG swollen in lower salt concentrations. There are two possible reasons for this increase in gel strength. First, the elastic pressure of the PPG was more dominant than the osmotic pressure for the PPG swollen in high brine concentrations. Hence, the swelling ratio was restricted, which caused an increase in gel strength. Second, the screen effect reduced efficient water absorbency, which resulted in the PPG shrinking and its strength increasing.

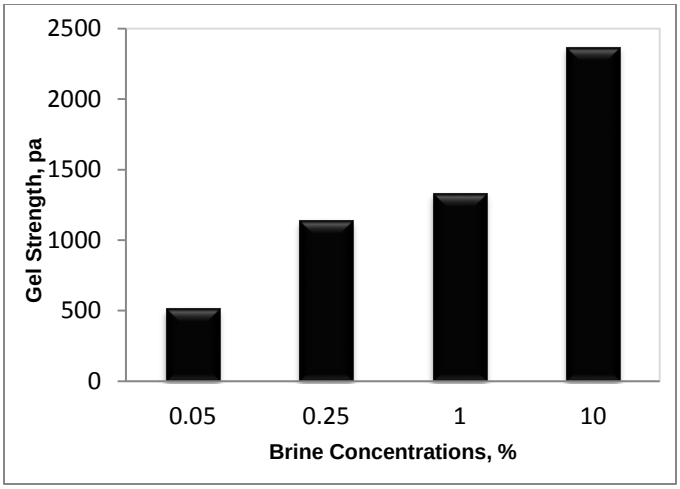

Figure 2-6. Gel strength measurements for different NaCl solutions.

2.4 Summary and Conclusions

The swelling and deswelling capacities of PPG were analyzed and the following conclusions were made:

- Salinity decreases the swelling capacities of PPG.
- PPG is capable of swelling up to 500 times in distilled water.
- An increase of 0.05% salinity can decrease the PPG swelling ratio up to 400 times.
- Swelling capacities of PPG increase with solution temperature.
- Salinity increases PPG deswelling ratio.
- PPG will always reach the same equilibrium swelling ratio regardless of whether the process is swelling or deswelling.
- PPG strength increased as the brine concentration increased.

Section 3: Using Screen Plate Models to Determine Gel Strength

3.1 Summary

The strength of PPGs is important to the optimization of their performance as plugging agents. Conventional gel strength has always been measured by applying load to single, isolated sample with certain geometry. However, determining the strength of sugar-like PPGs with irregular shapes is a challenging task. Previous publications have proposed different methods to evaluate gel strength. However, those methods are not suitable for rapid quantitative evaluation of PPG strength on site. We designed a simplified experimental apparatus to evaluate gel strength in the laboratory or on site during gel treatment.

3.2 Objectives

This method can serve as a simple, fast, and practical technique to quantitatively evaluate particle gel strength in the laboratory and on site during a PPG treatment process.

3.3 Experimental Description

Preformed Particle Gel. A commercial SAP comprised mainly of a potassium salt of cross-linked polyacrylamide copolymer was used as the PPGs in all experiments. When dry, these PPGs are white, sugar-like, granular powder. **Table 3-1** lists the typical characteristics of the PPGs used in this study.

Table 3-1—Characteristics of PPG used in the experiments

Properties	**Value**
Absorption of De-ionized Water (g/g)	>200
Apparent Bulk Density (g/l)	540
Moisture Content (%)	5
pH Value	5.5-6.0 (+/- 0.5; 1% gel in 0.9%

In the aqueous solution, PPGs can absorb a large amount of water because of its hydrophilicity which allows a hydrogen bond with the water molecules, although the swelling solution salinity affects its ability to adsorb water. **Figure 3-1** shows a comparison of dry gel particles and fully swollen particles in 1.0 wt % sodium chloride (NaCl). Standard U.S. sieves were used to select 18/20 mesh size (0.85/1000 mm) of dry PPGs, which we used in all experiments. In the following subsections, we present a conventional analysis of the PPG before the screen model experiment.

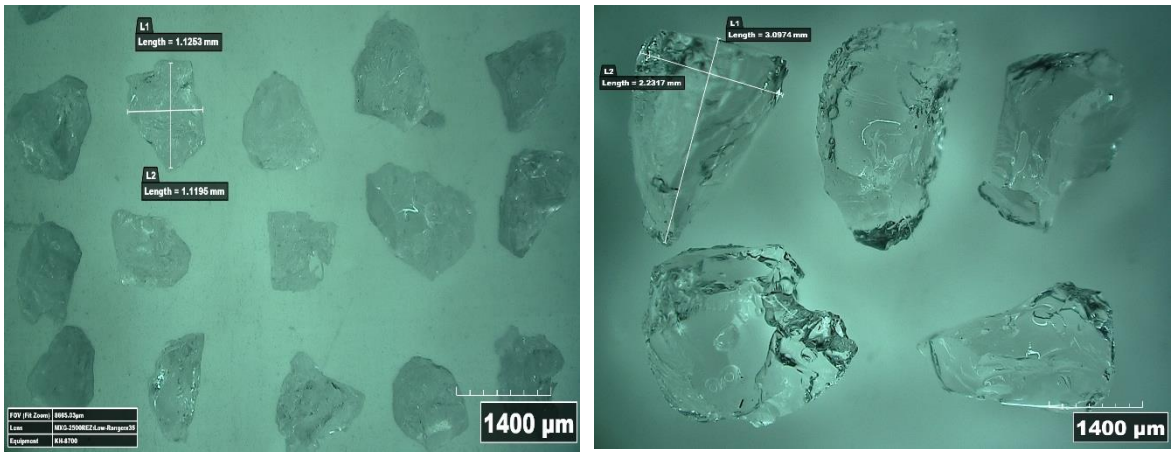

(a) **(b)**

Figure 3-1—Comparison of dry and swollen PPG: (a) Dry granular PPGs with 18/20 mesh size, (b) Fully swollen PPGs in 1.0 wt% NaCl

Particle Size Distribution (PSD). We adapted a microscopic image analysis technique to determine the PSD of the PPG; this method is time intensive but yields accurate results. A digital microscope was used to measure the size of the particle samples. We observed that the dry PPGs used in this study had a median size of 0.92 mm. **Figure 3-2** shows the PSD of the PPGs fully swollen in different brine salinities before the PPG extrusion through the screen plates.

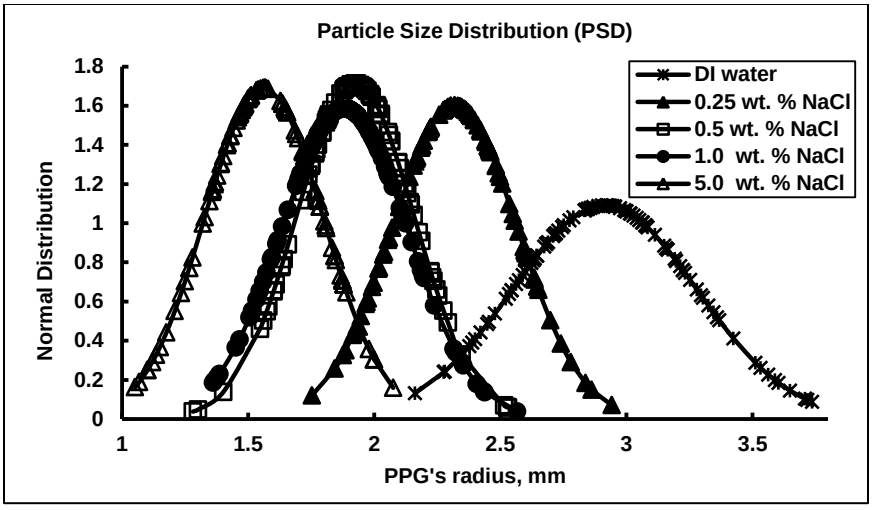

Figure 3-2—PSD of PPGs swollen in different brine salinities

Clearly, the PPG swollen in distilled (DI) water had the highest median size, 5.8 mm, while the PPG swollen in brine with a salinity of 5.0 wt% NaCl had the lowest median size, 3.1 mm. This observation is consistent with the swelling ratio measurement presented in **Figure. 3-3**. Thus, the swelling ratio and particle size were affected greatly by the brine salinity.

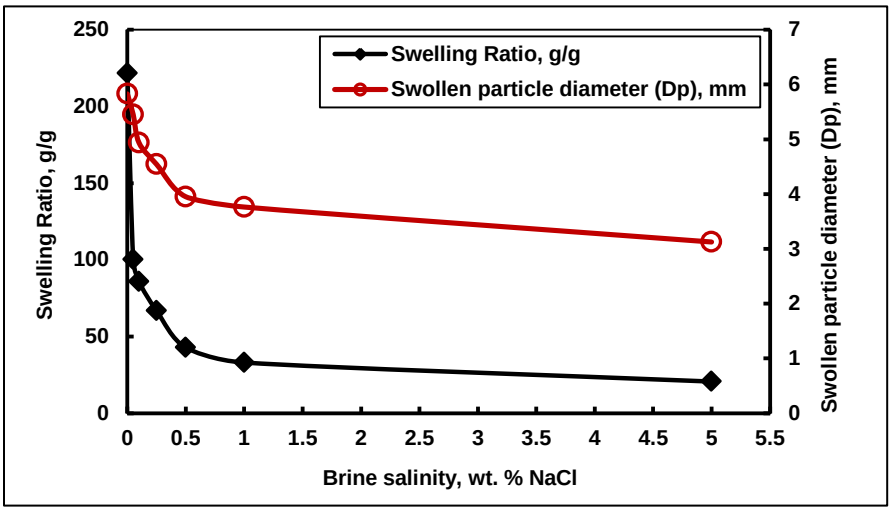

Figure 3-3—Effect of brine salinity on swelling ratio and particle size

SW evolution. Dry gel particles were immersed in six different brine salinities for 24 hours. The PPGs then were separated, and the excess water was blotted from them using wire gauze. **Figure 3-3** depicts a plot of the swelling ratio in g/g in the Y-axis and brine salinity in wt% NaCl in the X-axis. The higher the brine salinity the lower the SW because of the difference in the osmotic pressure between the gel particle's internal network and the external brine solution, this osmotic pressure decreased as the ionic strength of the brine increased. This figure also shows a plot of the gel particle size after swelling as a function of brine salinity.

G' measurement. The viscoelastic properties of PPGs usually are evaluated by dynamic oscillatory measurements using parallel plate geometries with a plate and a senor. A sample with defined geometry normally is placed between the plate and the sensor of the rheometer. However, commercial PPGs are irregular granule particles, which makes measuring the G' difficult because the swollen particles tend to slide out of the gap when the sensor begins to press on them. In this experiment, we used gap heights of 0.5, 1.0, and 1.5 mm between the sensor and the plate on which the PPG samples were placed. The oscillation time sweep curve model was selected for these measurements; it represents the elastic modulus logarithmically in Pascal (Pa) as a function of time in seconds. The frequency was set at 1.00 Hz. For each sample, the G' reading was taken every 30 seconds for 300 seconds. All experiments were conducted at an ambient temperature of 25 °C. **Figure 3-4** depicts the G' as a function of the gap height between the rheometer's plate and sensor. PPGs swollen in high-salinity brine had smaller particles with stronger polymer network bonds which resulted in a high G'.

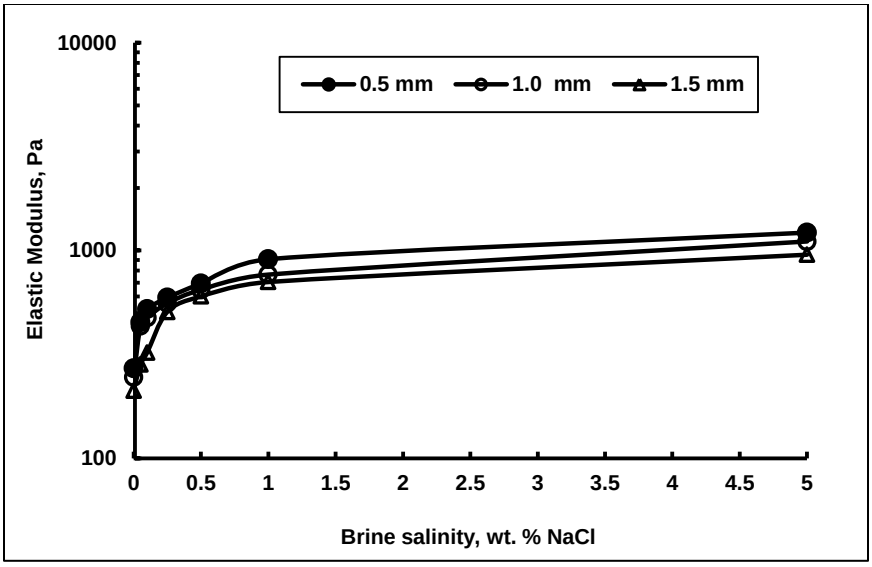

Figure 3-4—Effect of the gap height on the elastic modulus of swollen PPG

While useful, this method requires attention to the preparation of the samples for measurement. The excess solution must be blotted from these samples with care because if too little water is removed, the particles will move in the excess solution, and the measured G' will be too small as a result of interparticle slippage. If too much water is removed, the PPG will not swell fully. Improper sample preparation leads to measurement discrepancies between analyses even with the same PPG sample.

Brine. In order to have different PPG strengths available for evaluating the proposed technique, we used six different brine (NaCl) weight concentrations (0.05, 0.1, 0.25, 0.5, 1.0, and 5.0 wt%) and DI water, which yielded PPGs with various swelling ratios and strength.

3.4 Screen Model Description

Model Setup. The experimental apparatus, presented in **Figure 3-5**, is easy to assemble and use. It consists of a positive displacement hand pump and a specially designed piston accumulator. The top cap of the accumulator has a hole connected to the pump by tubing and fittings; the bottom cap is a stainless steel screen plate with multiple holes.

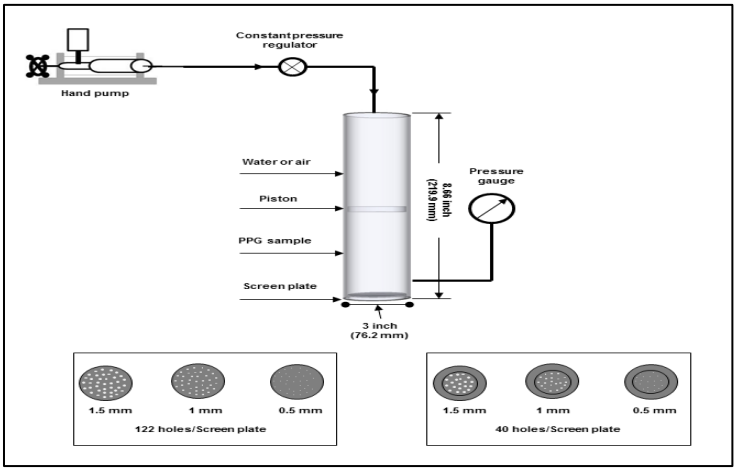

Figure 3-5—Schematic diagram of the screen plate experimental apparatus

We used two sets of screen plates in this study; their dimensions are presented in **Table 3-1**. This apparatus was designed to isolate the PPG sample from injection fluid (i.e., air or liquid) by piston, so any fluid can be used to push the piston and force the gel particle to extrude through the screen plate. A pressure gauge is mounted in the lower part of the accumulator near the screen plate to record the threshold and extrusion pressure. The accumulator is made of stainless steel material, so it is easy to clean and will not wear easily.

3.4.1 Model Experimental Procedure

1. *Sample preparation and loading*

- Depending on the brine salinity, 10 to 20 g of dry PPG was added slowly to the brine solution. The mixture then was stirred for 5 to 10 minutes and left for 24 hours until the PPG was fully swollen.
- 500 ml of fully swollen PPG samples from which excess water has been blotted was loaded inside the accumulator between the piston and a screen plate by putting first the piston and then the gel sample inside the container, placing the screen plate on top of the sample, and tightening the caps. **Figure 3-6** shows the sample loading procedures.
- During the experiment, the accumulator was turned upside down in vertical position so that the screen plate would be on the bottom.

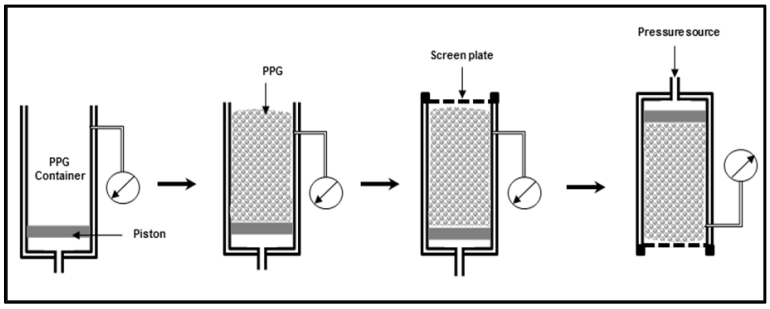

Figure 3-6—PPG sample loading procedure

2. *Threshold pressure measurement*

- A positive displacement hand pump was used to deliver constant pressure to push the PPG through the screen plate hole.
- The initial constant pressure was 34.4 KPa, which then was increased gradually (13.78 KPa at a time) until the PPG began to extrude through the screen plate. The pressure gauge reading at the time of the first PPG extrusion was considered the threshold pressure.
- We repeated these procedures for each combination of screen hole size and brine salinity; recording the threshold pressure each time.

3. *Apparent viscosity determination*

- A syringe Isco pump was used to provide a constant flow rate to determine the pressure during PPG extrusion.
- The pump was set to different flow rates (0.1, 0.2, 0.5, 0.75, 1.0, 1.5, 2.0, 2.5, 3.0, 5.0, 7.5, and 10 ml/min), and the stabilized pressure was recorded at the pressure gauge connected to the bottom of the accumulator at each flow rate.

- The procedure was repeated until the pressure differences were negligible, even when the injection rate increase was significant. The stabilized pressure was plotted against the injection flow rate.
- We repeated these procedures for different combinations of screen size and brine salinity.

3.5 Results and Analysis

3.5.1 Threshold Pressure Evaluation

Several factors can affect the threshold pressure of PPGs. In this study, we investigated the following factors:

1. *Brine salinity*. In this study, PPGs were swollen in brine salinities ranging from DI water to 5.0 wt% NaCl**.** Increasing the brine salinity cause the PPGs stiffness to increase, making it more difficult for PPG to pass through the screen hole. **Figure 3-7** shows a plot of three curves of the threshold pressure of swollen PPGs in different brine salinities passing through different hole sizes; as shown, the threshold pressure increased with the brine salinity when the hole size was the same. The threshold pressure increased rapidly as the brine salinity increased until the salinity was 0.5 wt% NaCl, at which point the threshold pressure reached an almost stable value. This indicates that PPG is prone to stiffness when the swelling medium has a higher salinity. The figure also depicts a plot comparing three screen hole sizes. The threshold pressure values were highest with a small hole size (0.5 mm).

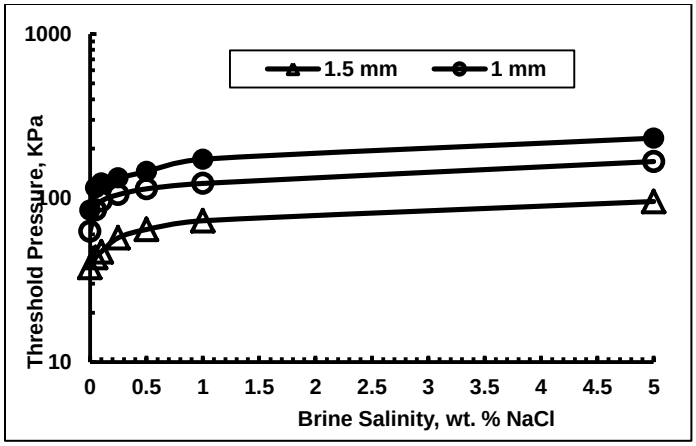

Figure 3-7—Effect of brine salinity on the threshold pressure of PPG using three different screen plate hole sizes

2. *Ratio of hole size (D_{pt}) to swollen PPG size (D_p).* **Figure 3-8** shows the prominent effect of the ratio of D_{pt} to D_p on the threshold pressure. . The threshold pressure significantly increases with brine salinity when the ratio is the same. Note that the particle prepared by high-salinity brine has higher strength than that prepared by low-salinity brine. Therefore, the result indicates strong particles need higher pressure to push them through holes than weak particles.

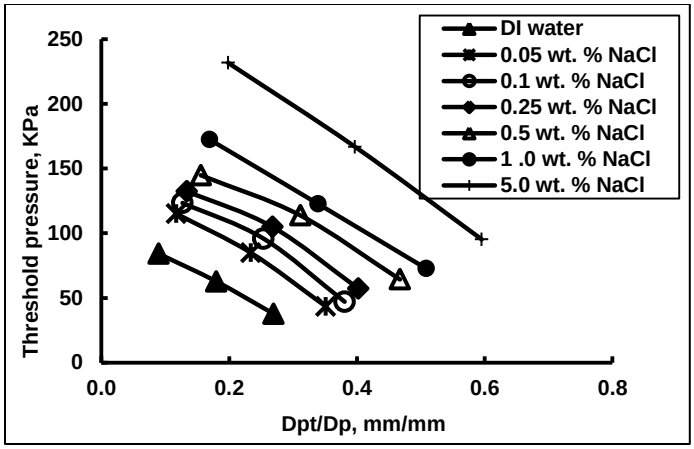

Figure 3-8—Effect of the ratio of hole size (D_{pt}) to swollen PPG size (D_p) on threshold pressure

3. *Holes density.* We investigated the effect of the density (number) of holes per screen plate on the threshold pressure measurement. Three additional screen plates were designed with the same three hole sizes (0.5, 1.0, and 5.0 mm), but with 40 holes per screen plate. The evaluation of this parameter is important because it relates to the porosity and permeability of the porous media and can be used as a criterion in PPG treatment design. **Figures 3- 9a** through **3-9g** present the threshold pressure values using 122 holes per plate compared to the threshold pressure values using 40 holes per plate. All seven figures show an identical trend, the difference between the threshold pressure values was moderate for the 1.0 mm and 1.5 mm screen plate. However, a huge difference existed in the threshold pressure values when using 0.5 mm hole size. For example, in **Figure 3-9a**, the threshold pressure value of PPGs swollen in DI water was 84.1 KPa when the hole density was 122 holes/plate, but that value jumped to 372.3 KPa given 40 holes/plate.

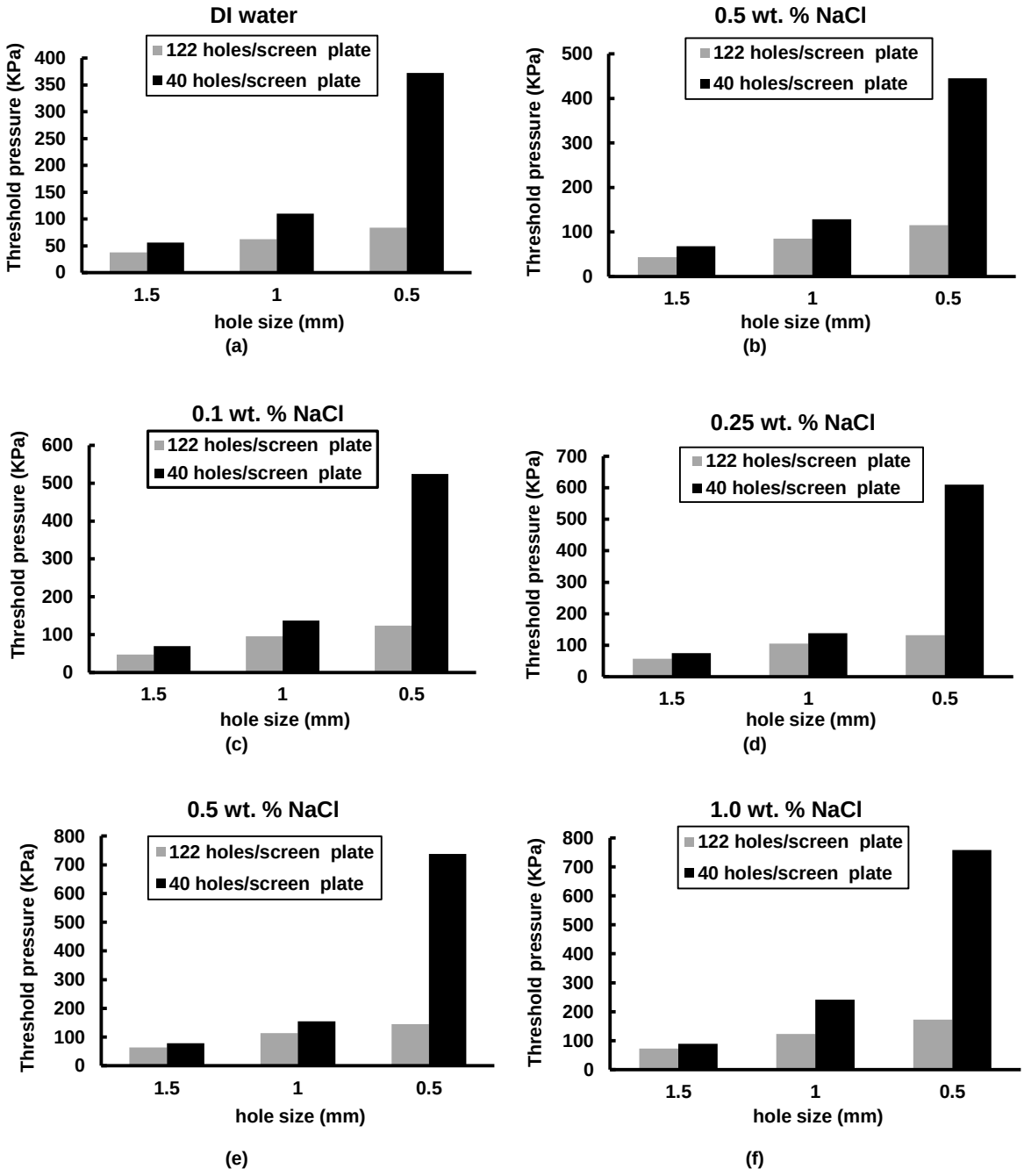
DI water
122 holes/screen plate
40 holes/screen plate
Threshold pressure (KPa)
400
350
300
250
200
150
100
50
0
1.5
1
0.5
hole size (mm)
(a)
0.5 wt. % NaCl
122 holes/screen plate
40 holes/screen plate
Threshold pressure (KPa)
500
400
300
200
100
0
1.5
1
0.5
hole size (mm)
(b)
0.1 wt. % NaCl
122 holes/screen plate
40 holes/screen plate
Threshold pressure (KPa)
600
500
400
300
200
100
0
1.5
1
0.5
hole size (mm)
(c)
0.25 wt. % NaCl
122 holes/screen plate
40 holes/screen plate
Threshold pressure (KPa)
700
600
500
400
300
200
100
0
1.5
1
0.5
hole size (mm)
(d)
0.5 wt. % NaCl
122 holes/screen plate
40 holes/screen plate
Threshold pressure (KPa)
800
700
600
500
400
300
200
100
0
1.5
1
0.5
hole size (mm)
(e)
1.0 wt. % NaCl
122 holes/screen plate
40 holes/screen plate
Threshold pressure (KPa)
800
700
600
500
400
300
200
100
0
1.5
1
0.5
hole size (mm)
(f)

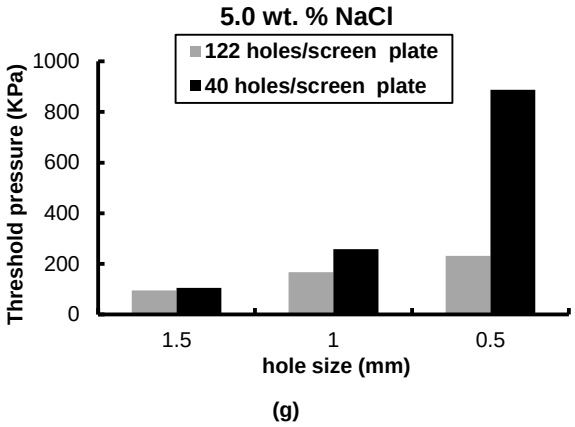

Figure 3-9—Comparison of threshold pressure using different screen plate hole densities

3.5.2 Apparent Viscosity Determination

We sought to examine whether this apparatus can be used to determine the apparent viscosity of PPGs, which is an important parameter in evaluating their rheological behavior. To accomplish this task, we first measured the stabilized extrusion pressure as a function of the flow rate. **Figure 3-10** shows a plot of the effect of the flow rate on the PPG extrusion pressure through three different sizes of screen holes. In all three cases, the pressure increased rapidly when the injection rate was low. However, the pressure plateaued to some extent when the injection rate exceeded 1.0 ml/min. The stabilized pressure curves were the highest when the 0.5 mm screen plate was used with a peak of 300 KPa when PPGs were swollen in 5.0 wt% NaCl. The lowest stabilized pressure curve was recorded when the 1.5 mm screen plate was used with PPG swollen in DI water.

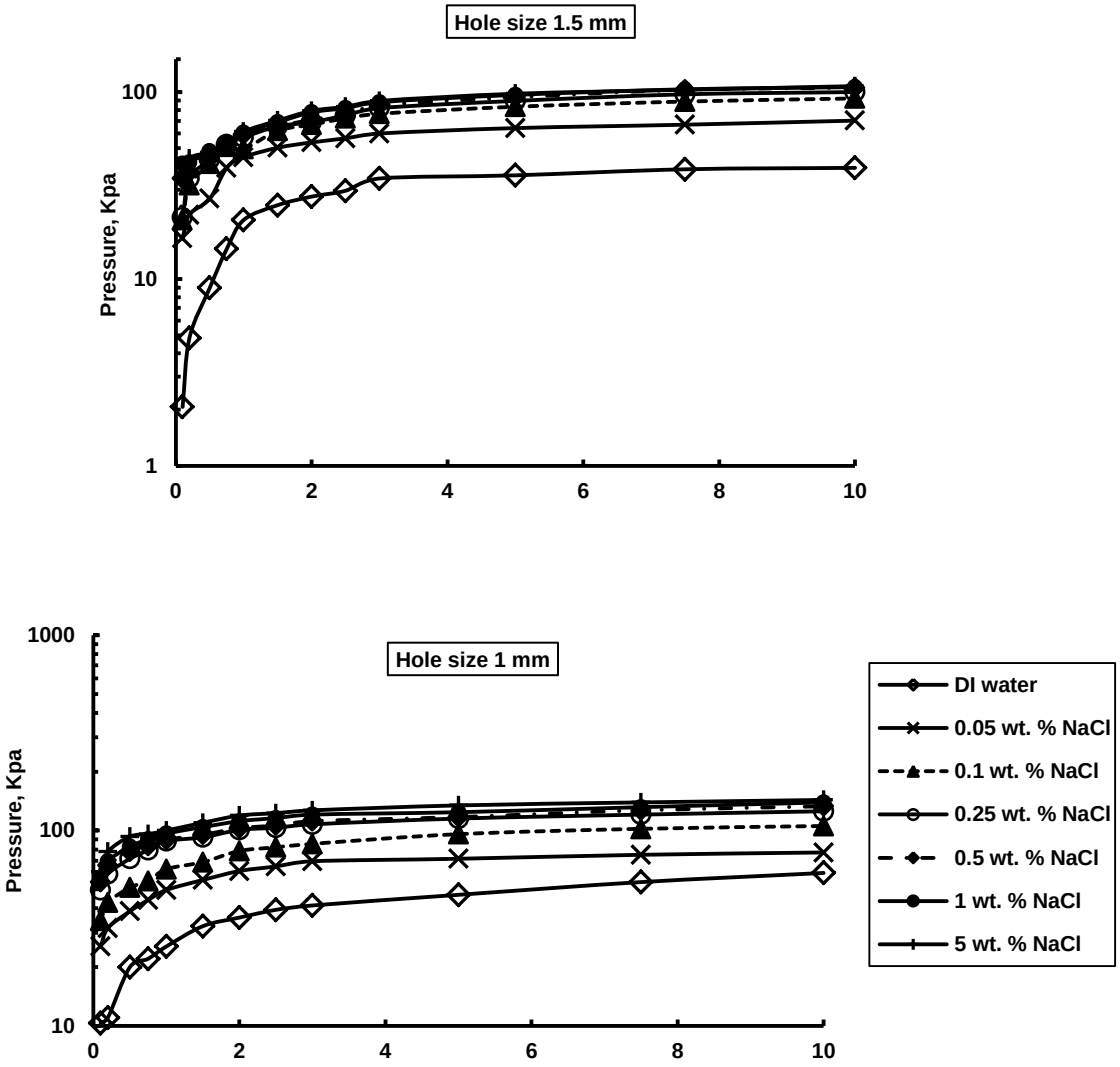
Hole size 1.5 mm
Pressure, Kpa
100
10
1
0
2
4
6
8
10
Hole size 1 mm
1000
100
10
DI water
0.05 wt. % NaCl
0.1 wt. % NaCl
0.25 wt. % NaCl
0.5 wt. % NaCl
1 wt. % NaCl
5 wt. % NaCl

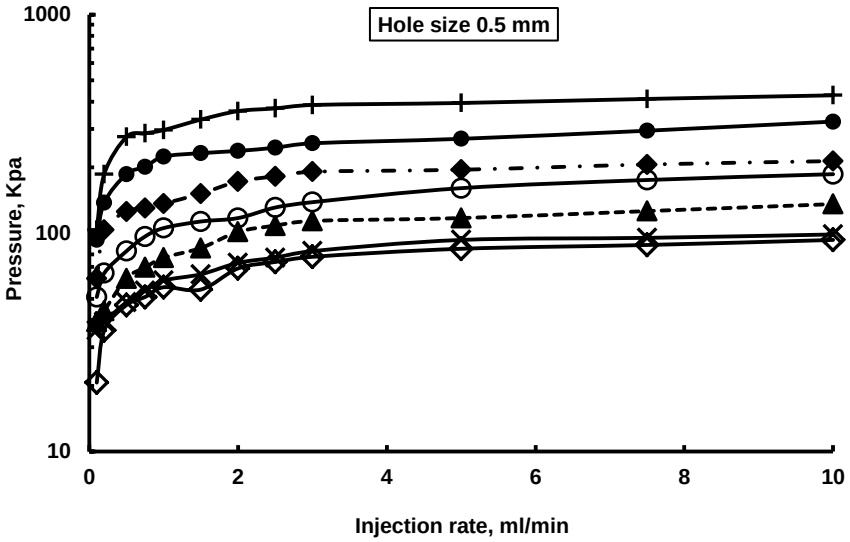

Figure 3-10—Injection rate, brine salinity, and pore size effect on PPG extrusion pressure of swollen PPG

The Δp_{gel} was considered to be the value of the stabilized pressure drop as depicted in **Figure 3- 10**. Δp_{brine} was calculated using Darcy's equation, where k is calculated using **Equation 3-1**:

$$k = 20 \times 10^6 d^2 \varphi \quad \text{..... (3-1)}$$

where k is the screen plate permeability in darcys, d is the screen hole diameter in inches, and the porosity is from **Table 3-1**.

The length term in Darcy's equation is considered to be the plate thickness, and the area was calculated using the diameter of the screen plate. The flow rate was taken from the injection flow rates used.

The apparent viscosity was plotted against the shear rate, which we calculated by converting the flow rate to a velocity and then using **Equation 3- 2,** which divides it by the diameter of the holes in the screen plates.

$$\gamma = \frac{v}{d} \quad \text{……..……..…..} \quad (3\text{-}2)$$

where γ is the shear rate in sec^{-1}, v is the velocity in *mm/sec*, and d is the diameter of the holes in the screen plates in *mm*. **Figure 3-11** presents the relationship between the apparent viscosity and shear rates. We found that the apparent viscosity values from the experimental results in different size of the holes follow the same line in a log-log plot when the brine salinity is the same, indicating that the hole size does not affect the apparent viscosity. We also found that the apparent viscosity values decreased as the shear rate increased, indicating that all of the swollen PPG samples were shear-thinning materials.

The apparent viscosity of non-Newtonian fluids can be expressed using the power-law model (Bourgoyne, 1991):

$$\mu_{app} = K\gamma^{n-1} \quad \text{……..……} \quad (3\text{-}3)$$

where K is the flow consistency constant ($Pa \bullet s^n$), and n is the flow behavior index. These terms, also called the Ostwald-de Waele flow indices, represent the degree of non-Newtonian behavior of the fluids.

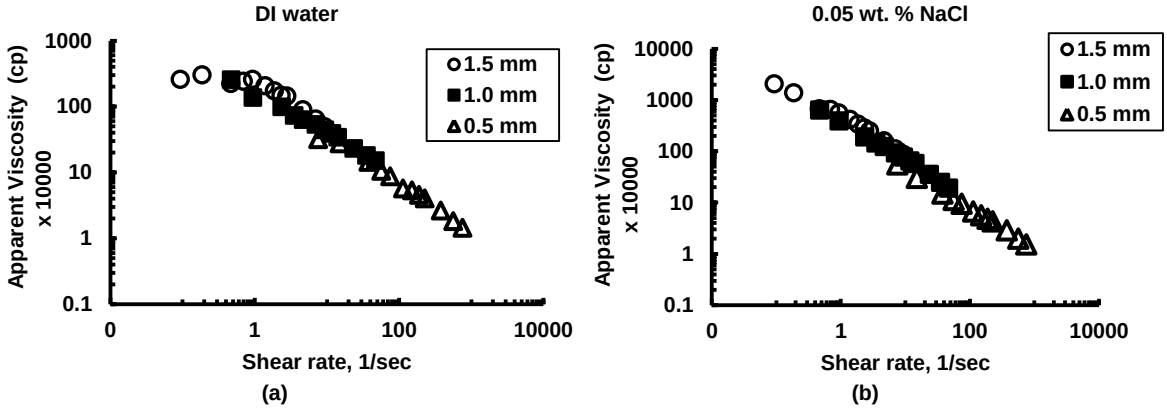

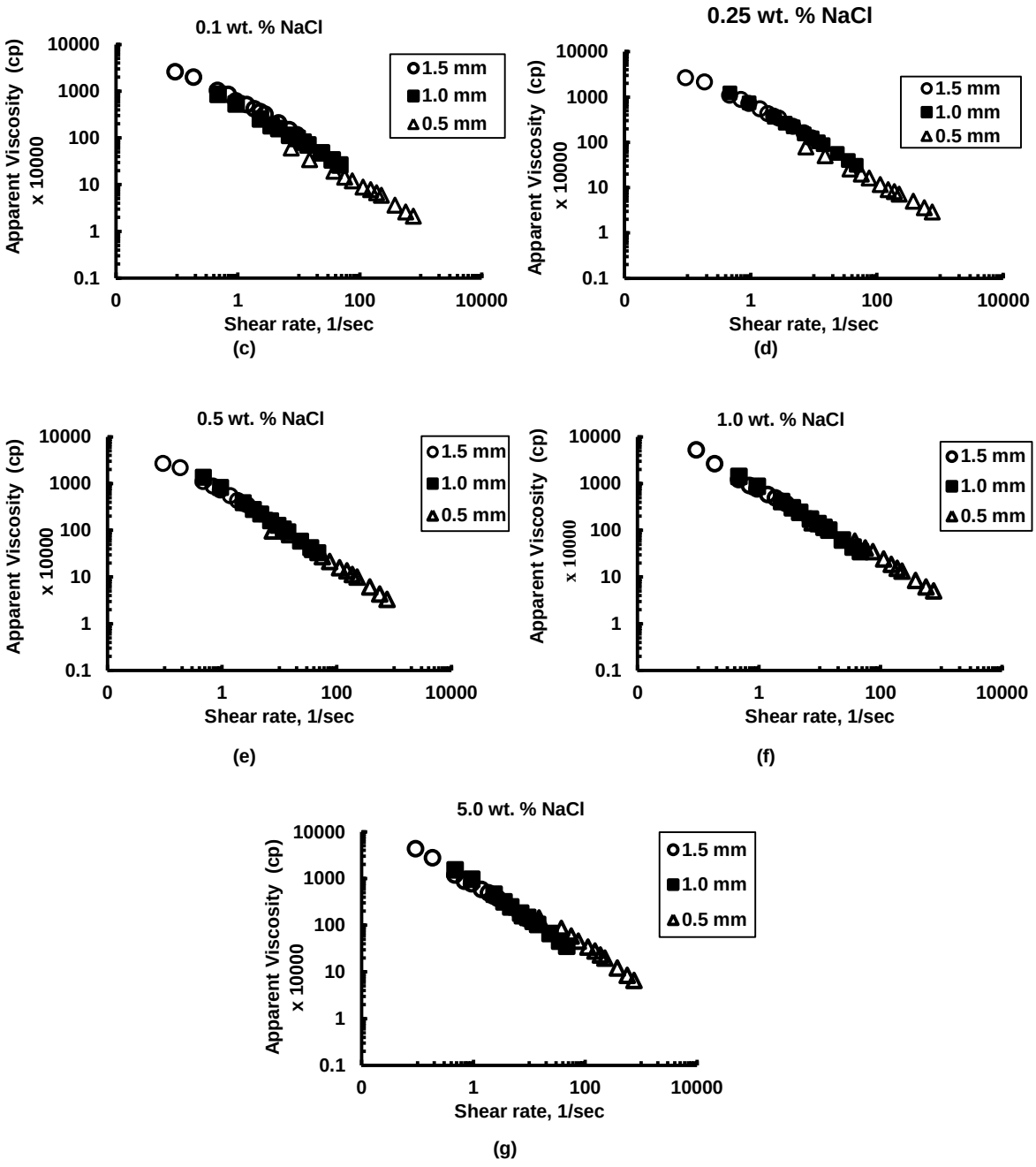

Figure 3-11—Share rate effect on apparent viscosity as a function of brine salinity and hole size

Table 3-2 lists the *K* and *n* for all PPG samples and screen plates tested in this study. Using the fitting equations in the various screen plates, the rheological behavior of the PPG in terms of the apparent viscosity can be evaluated quantitatively, and the performance of swollen PPG products for reservoir applications can be compared.

Table 3-2—Fitting equations for apparent viscosity versus shear rate in screen plates using: $\mu_{app} = K\gamma^{n-1}$

Screen plate hole size	**Brine salinity (%)**	**Flow consistency constant (*K*) c**	**Flow behavior index (*n*)**	R^2
1.5 mm	DI water	1.74×10^6	0.366	0.766
	0.05	4.66×10^6	0.674	0.986
	0.1	6.05×10^6	0.683	0.992
	0.25	6.44×10^6	0.678	0.992
	0.5	7.01×10^6	0.731	0.997
	1.0	7.52×10^6	0.762	0.996
	5.0	7.43×10^6	0.74	0.996
1.0 mm	DI water	1.57×10^6	0.592	0.992
	0.05	3.79×10^6	0.746	0.996
	0.1	4.94×10^6	0.748	0.998
	0.25	7.12×10^6	0.797	0.998
	0.5	7.66×10^6	0.812	0.999
	1.0	8.15×10^6	0.809	0.998
	5.0	8.91×10^6	0.821	0.998
0.5 mm	DI water	1.67×10^6	0.700	0.988
	0.05	2.46×10^6	0.759	0.998
	0.1	2.57×10^6	0.713	0.996
	0.25	3.54×10^6	0.722	0.999
	0.5	5.55×10^6	0.757	0.991
	1.0	8.30×10^6	0.763	0.992
	5.0	9.98×10^6	0.731	0.978

3.5.3 Injectivity versus Flow Rate

Injectivity, defined as the flow rate divided by the pressure, is an important measure of the difficulty of injecting a gel, with higher injectivity indicating easier PPGs injection. **Figure 3-12** depicts a plot of the injectivity versus the flow rate as a function of brine salinity and screen holes. The injectivity decreased with brine salinity, meaning that PPGs swollen in lower brine salinity were easier to inject into a screen than those prepared with higher brine salinity. Because PPG swollen in low-salinity brine is larger than that swollen in high-salinity brine, the deformability of the swollen gel particles has a more significant influence on gel injectivity than does the particle size. PPG injectivity depends highly on the flow rate, with which it increases linearly, as shown in **Figure 3-12**. This relationship varies drastically from water injection in that water injectivity does not change with the flow rate. Water injection and particle gel injection differ because water is a Newtonian fluid, while swollen PPGs are pseudo-plastic materials. Particle gel injectivity increases with larger screen pore sizes.

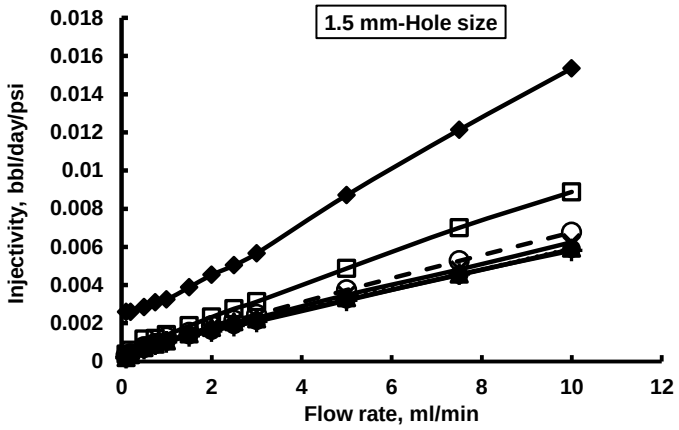

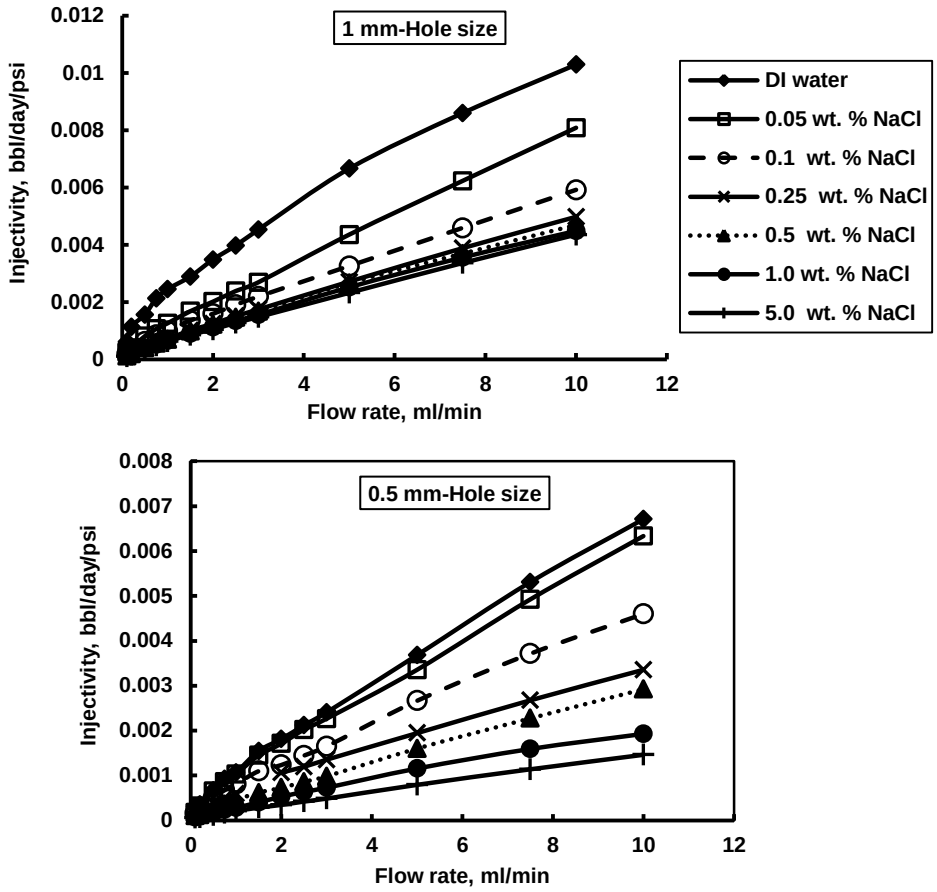

Figure 3-12—Injectivity versus flow rate as a function of brine salinity and hole size

3.5.4 Correlation of Threshold Pressure and PPG Elastic Modulus

To validate our results, we plotted the threshold pressure against the elastic modulus values. **Figure 3- 13** shows the relationship between the threshold pressure and the elastic modulus of swollen PPG under different numbers of screen plate holes and different gap heights. A linear relationship between threshold pressure and elastic modulus was plotted for the PPGs swollen in media having different salinities. **Equation 3-4** can be used to quantify the elastic modulus when the threshold pressure is measured using this proposed method.

$$P_t = KG' + C \text{ , } \ldots\ldots\ldots\ldots\ldots\ldots \text{ (3-4)}$$

where P_t is the threshold pressure in Pa, K, and C are constants that are dependent on the brine salinity, hole size and density per screen plate, and G' is the elastic modulus in Pa. **Table 3-3** summarizes the values of K and C taken from fitting **Equation 3-4** in **Figure 3-13a** and **3-13b.**

The constants K and C are a function of the variables affecting the threshold pressure. More research is needed to clarify the nature of these constants.

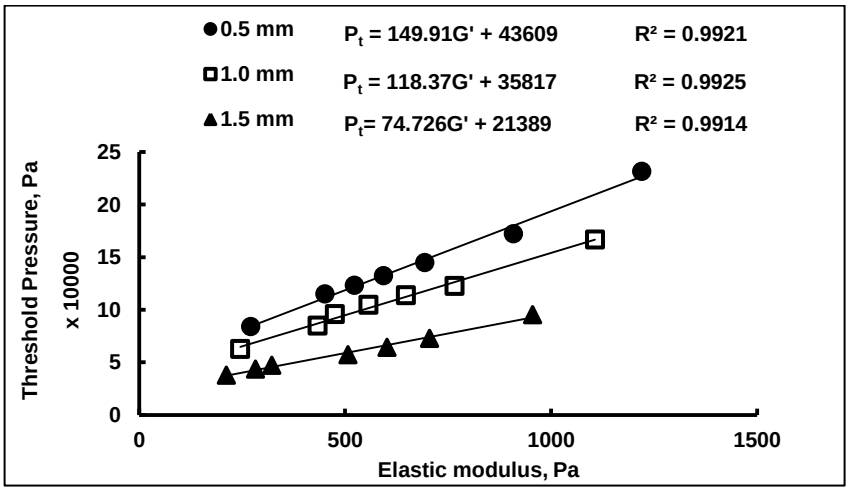

(a)

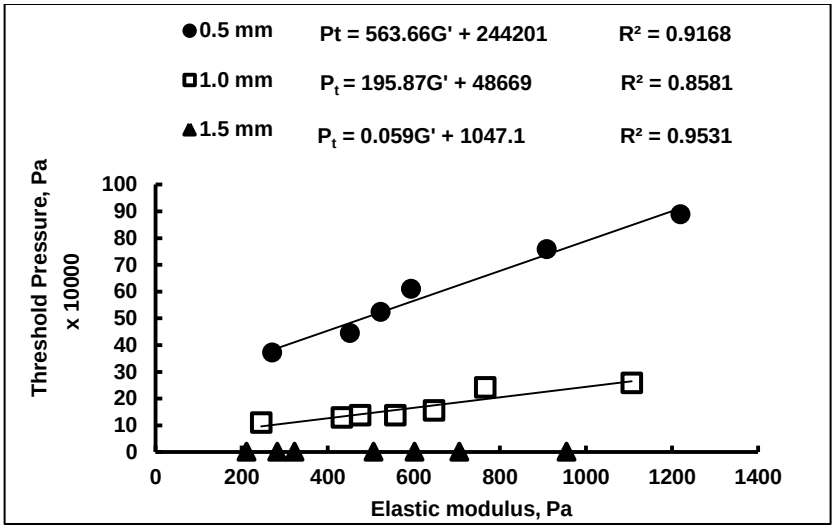

Figure 3-13—Correlation of threshold pressure to elastic modulus for PPG swollen in 0 to 5.0 wt% NaCI solutions at different hole sizes and gap heights: (a) correlation for 122 holes per screen plate, (b) correlation for 40 holes/ screen plate

Table 3-3— Fitting equations for threshold pressure to the elastic modulus for PPG, using: $P_t = KG' + C$

Screen plate #	Number of holes per screen plate	Hole size (D_{pt}), mm	Constant *K*	Constant C	R^2
1	122	1.5	74.726	21389	0.9914
2	122	1	118.37	35817	0.9925
3	122	0.5	149.91	43609	0.9921
4	40	1.5	0.059	1047.1	0.9531
5	40	1	195.87	48669	0.8581
6	40	0.5	563.66	244201	0.9168

3.6 Discussion

The results of this study indicate that this simplified experimental apparatus can be used to quantitatively determine two major parameters, the threshold pressure (P_t) and apparent viscosity (μ_{app}), which are important in the characterization of gel particle transport through porous media. The P_t correlates very well with the gel strength so it can

be used to determine how easily a gel particle will begin to move into a constriction. However, P_t depends on the holes density per screen plate so the hole density of a plate should not be changed when comparing different particles. The μ_{app} correlates very well with the shear rate but is not affected by the hole density; therefore, this parameter can be used to characterize the ability of gel particles to propagate through constriction. In addition, the size and shape of PPG before and after they pass through restrictions can be observed visually to qualitatively determine the rigidity or deformability of the particle sample. For example, **Figure 3-14** shows pictures of particles swollen in 1.0 wt% NaCl before and after their extrusion through a screen plate with hole size of 1.0 mm. Clearly, the particles were broken down into smaller sizes after passing through the constriction, indicating that they break down easily and are not very deformable.

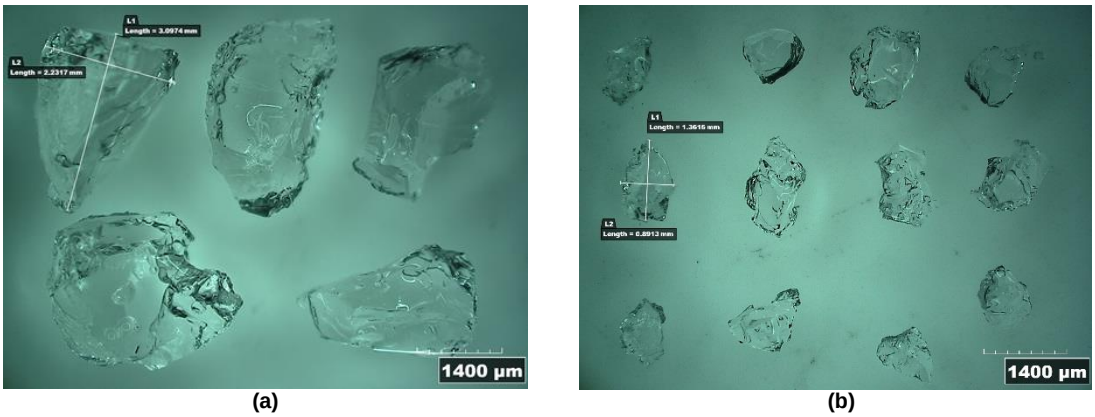

(a) (b)

Figure 3-14—Comparison of PPG sizes before and after extrusion: (a) PPGs, swollen in 1. Wt. % NaCl, before extrusion, (b) PPG after extrusion though 1.0 mm screen plate holes

3.7 Summary and Conclusion

In this study, experiments were conducted to quantitatively evaluate the strength of PPG samples swollen in different saline media using screen plate models that we designed. The major contributions of this study are as follows:

1. A simple technique was introduced that can provide a fast, practical method by which to quantitatively evaluate particle gel strength in the laboratory and on site during a PPGs treatment process.

2. Two parameters of PPGs characterization, the threshold pressure and apparent viscosity, can be quantitatively determined using this method. The ratio of particle size to hole size and hole density impact the threshold pressure but they do not impact the apparent viscosity of the swollen PPGs.
3. PPGs swollen in high-salinity brine require a higher injection pressure than that swollen in low-salinity brine, even though the former are bigger than the latter.
4. Two mathematical models were introduced based on the experimental lab results: one model correlates the threshold pressure with the gel strength and the other correlates the apparent viscosity with the shear rate. Both correlation equations have reasonably good correlation factors.
5. PPGs injection pressure depends chiefly on the gel particles strength. However, the injection pressure does not increase significantly with the injection rate.

Section 4: Using Plate Models to Evaluate Gel Extrusion through Fractures

4.1 Summary

This chapter presents the experiments that were conducted to examine the PPG extrusion and propagation behavior through various widths of open fracture screen plates. Several factors that impact the PPG extrusion behavior were considered in this study. These factors include the effect of brine concentration, flow rate, and size of the fracture. Additionally, this section presents a fully designed factorial analysis conducted to gain understanding of which factor can influence PPG injection pressure, resistance factor, and injectivity.

4.2 Objectives

The objectives of this study were to understand PPG propagation through the open fracture screen plates. The open fracture screen plates were used to mimic the fractures and the fracture-like channels that exist in the mature reservoirs.

Injecting the PPGs through the open fracture screen plates can facilitate identifying the major parameters that can be utilized to yield efficient gel treatments through fractures for better conformance control treatments.

4.3 Summary of Experiments

A total of 12 experiments were performed to examine PPG transportation behavior through fracture screen plates. **Figure 4-1** presents the major experiment outcomes and shows how DI water and three different brine concentrations (0.25, 1.0 and 5.0 wt% NaCl) were used in this study to obtain different swollen PPGs of different gel strengths and swelling ratios, accordingly. Three open fracture screen plates with different fracture widths (0.25, 0.50 and 1.0 mm) were used to examine how fracture width size can be related to PPG injection pressure, resistance factor and injectivity). A

full-factorial design was developed to examine the most influential parameters on injection pressure, resistance factor and PPG injectivity.

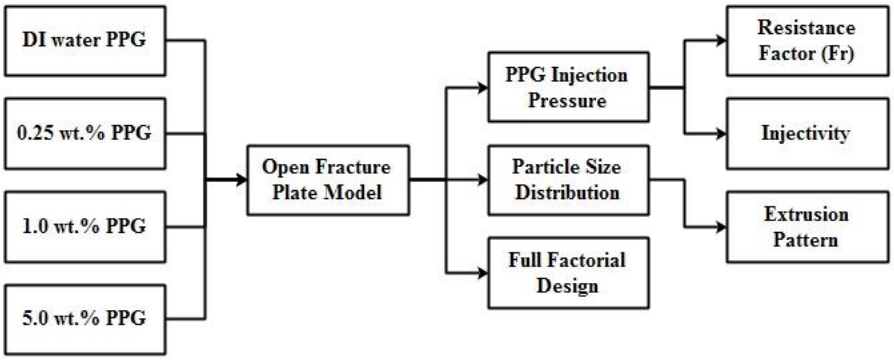

Figure 4-1. The Outcomes of the Experiments.

4.4 Open Fracture Screen Plates

Three different stainless steel open fracture screen plates of various fracture width were used in this study as shown in **Figure 4-2**. The fractures were designed to be in the center of the plates to fit the model. The open fracture screen plates have a total diameter of 63.5 mm and a thickness and a total length of 7.5 and 66 mm, respectively. The equivalent permeability of each open fracture screen plate was measured using the following equation

$$k = 5.4476 \times 10^{10}\, b^2 \qquad (4\text{-}1)$$

where k is the permeability in (md), and b is the fracture width in (inches). **Equation 4-1** can be used to estimate the permeability of open, smooth-walled fractures, with parallel faces where the permeability is dependent on fracture width (Witherspoon et al. 1980). **Table 4-1** summarizes the dimensions of the open fracture screen plates and the equivalent permeability calculations. The high values of the equivalent permeability calculations are due to the fact that the fractures have a significant effect on fluid flow through fractures since they are isolated.

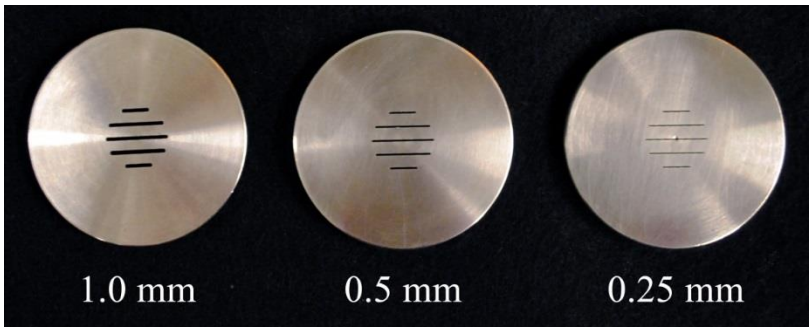

Figure 4-2. The Open Fracture Screen Plates of Various Fracture Widths.

Table 4-1. The Dimensions of The open fracture screen plates and the equivalent permeability calculations.

Fracture width (mm)	Thickness (mm)	Total fracture length (mm)	Diameter (mm)	Permeability (Darcy)
0.25	7.8	66	63.5	5277
0.50	7.8	66	63.5	21109
1.0	7.8	66	63.5	84438

4.5 Experimental Setup and Procedure

The screen plates of different fracture widths were placed between the swollen PPGs particles and the bottom of the accumulator. The threshold pressure and the PPG injection pressure were measured through the pressure gauge mounted on the lower part of the accumulator.

The following experimental procedure was performed:

- Initially, 10 to 20 g of dry PPG particles with a mesh size of (18/20) were added to the desired brine solution, where the mixture was left for 24 hours to allow the PPG particles to fully swell.
- Then, 500 ml of the fully swollen gel particles from which excess water has been blotted were put into the accumulator and the open fracture screen plate was attached to it.
- Gas between the piston and the top cap was released, and the gap was filled with distilled water to avoid a two phase medium.
- The ISCO pump was initially run at constant pressure starting at 10 psi to obtain the threshold pressure.

- After recording the threshold pressure, the pump was stopped for about one hour.
- Then, the pump was run using constant flow rates of 1.0, 2.0 3.0, 4.0 and 5.0 ml/min. The stabilized pressure was recorded for each flow rate.

4.6 Results and Discussions

4.6.1 PPGs Threshold Pressure Measurements.

Threshold pressure can be defined as the minimum pressure required for PPG to be extruded through the fracture screen plate. The threshold pressure was measured in the experiment by applying a constant pressure of 10 psi, which is the minimum pressure that can be obtained using the ISCO pump. **Figure 4-3*a*** through ***c*** show the effect of brine concentration and the fracture width on the threshold pressure. The results indicate that for certain brine concentrations, the threshold pressure increased as the width of the fracture screen plate decreased. For example, the threshold pressure for 1.0 wt% PPG through 1.0, 0.50, and 0.25 mm fractures were 9.7, 5.2, and 0.68 psi , respectively. Moreover, it is evident form the figure that for a certain fracture width, increasing the brine concentration will result in an increase in the threshold pressure. For instance, at 0.25 mm fracture, the threshold pressure for DI water and 0.25, 1.0 and 5.0 wt% PPGs were 10.9, 9.7, 8.3, and 7.9 psi, respectively. However, the effect of brine concentration is less prominent compared to the fracture size, which is due to the high fluid conductivity within the fractures.

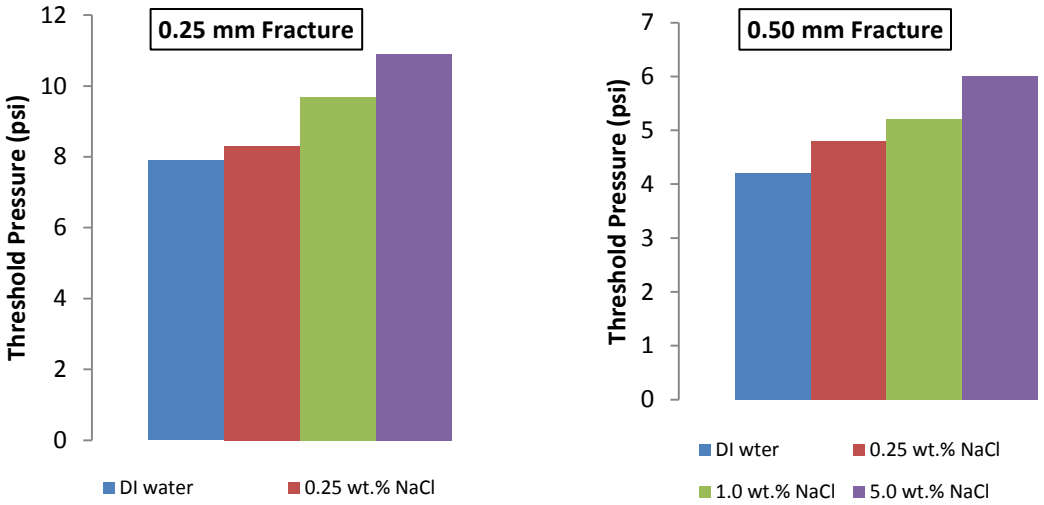

(a)

(b)

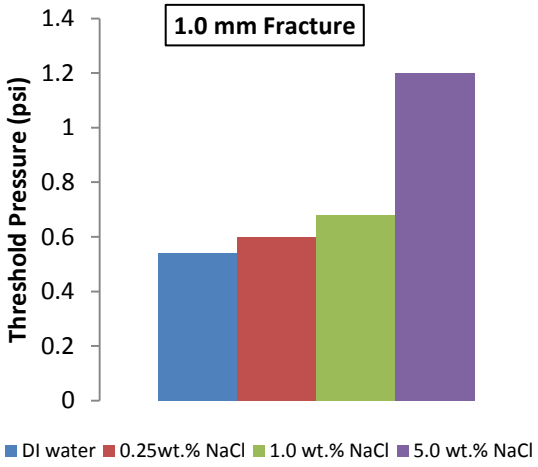

(c)

Figure 4-3. The Effect of Brine Concentration and Fracture Width on PPGs Threshold Pressure.

4.6.2 PPGs Injection Pressure Trend.

After obtaining the threshold pressure, the experiments were run using a constant flow rate supplied by a Teledyne Isco syringe pump. An erratic PPG injection pressure response was noted fluctuating in a certain range. **Figures 4-4** and **4-5** show two examples of the PPG injection pressure response that occurred during PPG injection. A

fluctuation trend in the injection pressure was obvious regardless of fracture width and concentration of the swollen PPG used, respectively. To understand the reasons for the injection pressure fluctuation, possible causes in the experiment that might lead to such a response were examined. It was found out that are there two possible reasons for such a response: 1) orientation of the fracture screen plates or 2) heterogeneity of swollen PPG particles. Since the fractures screen plates were designed and manufactured according to standards, the scope of investigation was directed to the second possible factor which is the heterogeneity of swollen PPG particles.

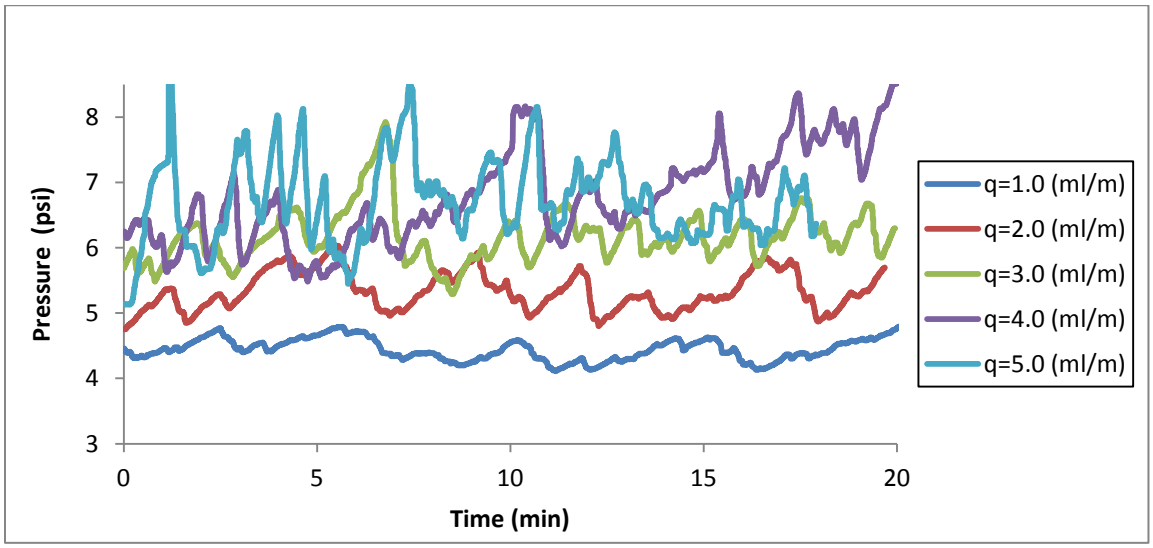

Figure 4-4. DI PPG Injection Pressure through 0.50 mm Fracture as a Function of Time and Flow Rate.

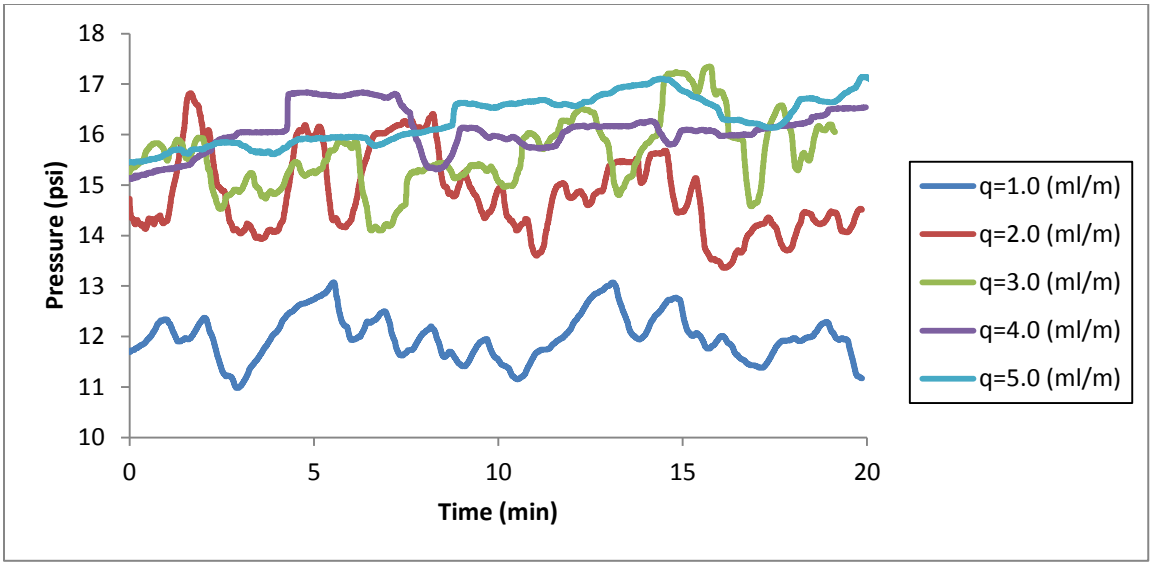

Figure 4-5. 5.0 wt. % NaCl PPG Injection Pressure through 0.25 mm Fracture As a Function of Time and Flow Rate.

4.6.3 Effect of Injection Flow Rate on Injection Pressure of PPGs.

After obtaining the threshold pressure for each set of brine concentrations and widths of the open fracture screen plates, five different constant injection flow rates were used to examine the effect of changing the flow rates on PPG injection pressure. **Figures 4-6** to **4-8** show the effect of changing the flow rate on PPG injection pressure. These figures clearly show that increasing the flow rate will yield an increase in PPG injection pressure for all the brine concentrations and for all the different open fracture screen plates. However, the increase is not significant especially at high flow rates. The PPG injection pressure will increase slightly at the beginning and then reach a plateau.

For PPG particles that were swollen in a 5.0 wt% NaCl brine and extruded through a 0.25 mm open fracture screen plate, the injection pressure increased from 11.8 psi to 14.5 psi when the injection flow rate increased from 1.0 to 2.0 ml/m. Then, the injection pressure only increased 0.1 psi when the injection flow rate increased from 4.0 to 5.0 ml/m. (Seright, 1999) attributed such a trend to a strong slip effect exhibited by the

gel where little or no viscous dissipation of energy occurred within the moving gel plug. Thus, the hydrodynamic lift force acting on particles to transport them through the pores will increase with flow rate resulting in an increase in particle mobilizations (Baghdkian et al., 1989). Moreover, this trend is consistent with the findings from PPG injection reports from the oil fields where it was observed that PPG injection pressure did not increase significantly in accordance with the increase in the injection pumping rate (Bai et al., 2007a).

4.6.4 Effect of Brine Concentration on Injection Pressure of PPGs.

The dry gel particles were swollen in four different brine concentrations (0, 0.25, 1.0, and 5.0 wt% NaCl) to obtain fully swollen PPG particles that vary in their strength and swelling ratio. Then, the swollen PPG results were uploaded into the model to examine how the brine concentration can impact the PPG injection pressure through the different open fracture screen plates. **Figures 4-6** to **4-8** show the effect of the brine concentration on PPG injection pressure. The results reveal that at a constant flow rate, increasing the brine concentration will result in an increase in PPG injection pressure regardless of the size of the fracture.

For instance, at a constant flow rate of 5.0 ml/m for PPG prepared with DI, 0.25, 1.0, and 5.0 wt% NaCl and extruded through an 0.25 mm open fracture screen plate, the injection pressures were 11.4, 12.6, 14.2, and 16.2 psi, respectively. However, at a 5.0 ml/m injection flow rate for the same brine concentrations, the PPG injection pressures increased slightly at 6.5, 6.8, 7.8, and 8.2 psi when the PPG extruded through the 0.50 mm open fracture screen plate. The results clearly show that PPG particles swollen at low brine concentrations are softer and more deformable compared to PPG particles swollen in high brine concentration. However, in the case where PPG particles were swollen in DI and propagated through the 1.0 mm open fracture screen plate, the injection pressure was higher than that of the other swollen PPG particles. This can be explained by the low

injection pressure that was observed in general for all the different swollen gel particles where the pressure only ranged from 0.80 psi to 2.2 psi. The latter deviation might indicate that since the DI PPG particles were bigger in size and the injection pressure was low, the effect of brine concentration might be insignificant compared to the results recorded for the smaller fracture widths in the other two cases of 0.25 and 0.50 mm, respectively.

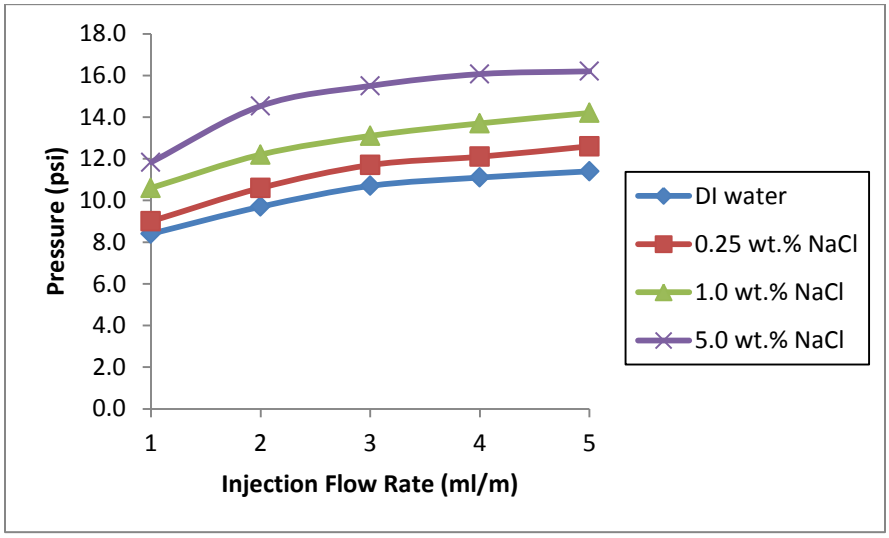

Figure 4-6. PPGs Injection Pressure through 0.25 mm Fracture vs. Injection flow Rate and Brine Concentration.

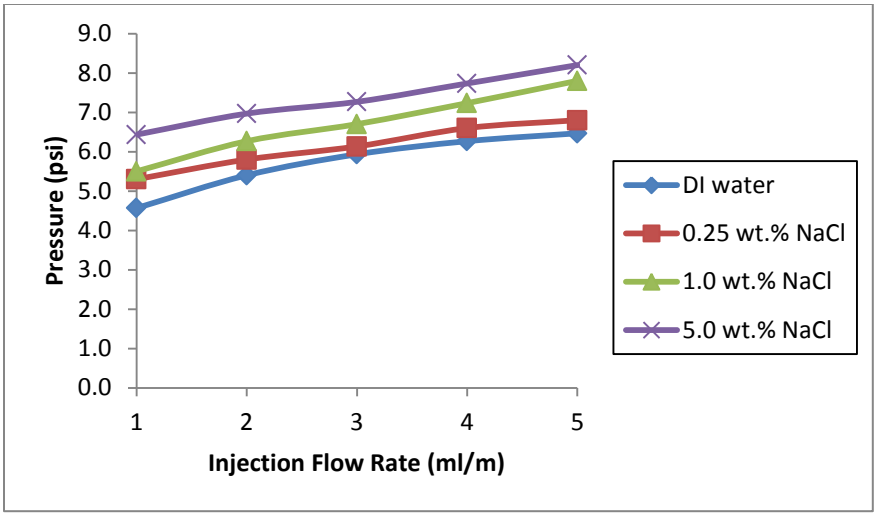

Figure 4-7. PPGs Injection Pressure through 0.50 mm fracture vs. Injection Flow Rate and Brine Concentration.

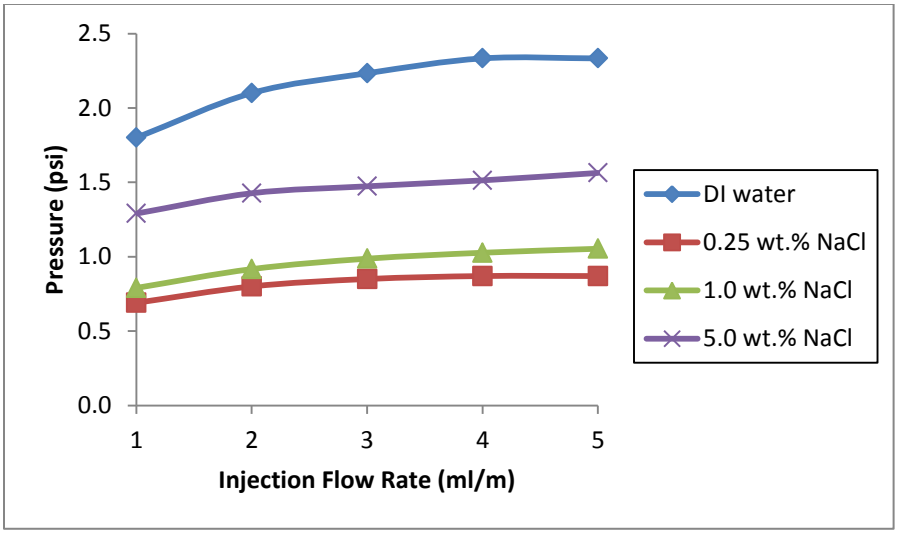

Figure 4-8. PPGs Injection Pressure through 1.0 mm fracture vs. Injection Flow Rate and Brine Concentration

4.6.5 Effect of Fracture Width on Injection Pressure of PPGs.

Three different open fracture screen plates with widths of 0.25, 0.50 and 1.0 mm were used to investigate how PPG injection pressure changes with respect to varying the width of the open fracture screen plate. **Figures 4–9** to **4–12** indicate that for a given flow rate and brine concentration, PPG injection pressure decreased as the fracture width increased. For example, for the PPG particles that were swollen in 1.0 wt% NaCl at a constant injection flow rate of 1.0 ml/m, the injection pressure was 10.6 psi at 0.25 mm fracture size. However, when the 1.0 wt% PPG particles were extruded through the 0.50 mm fracture, the injection pressure was almost reduced to half, i.e., 5.5 psi, and sequentially the injection pressure was pretty low at 0.79 psi when the same composition at the same flow rate was transported through the largest fracture width, which is 1.0 mm. In this case, the same trend was observed in the all the different PPG particles that were swollen in different brine concentration.

For the PPG particles that were prepared with 5.0 wt% at a constant injection pressure of 5.0 ml/min, the PPG injection pressures were 16.2, 8.2, and 1.56 psi for the open fracture screen plates with widths of 0.25, 0.50 and 1.0 mm, respectively. The results imply that the bigger the size of the open fracture, the more conductive it is and thus less injection pressure is required for PPG particles to be transported. Furthermore, these results indicate that at a certain brine concentration and flow rate, the PPG injection pressure is inversely proportional to the size of the fracture. This finding is consistent with Zhang (2011) and Seright (1988) who both determined that gel extrusion pressure is inversely proportional to open fracture width size.

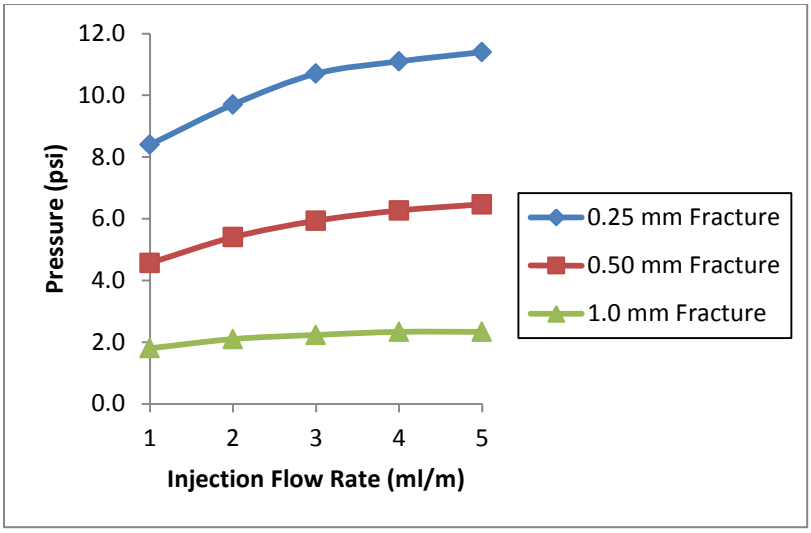

Figure 4-9. DI water PPGs Injection Pressure through Open Fracture Screen Plates.

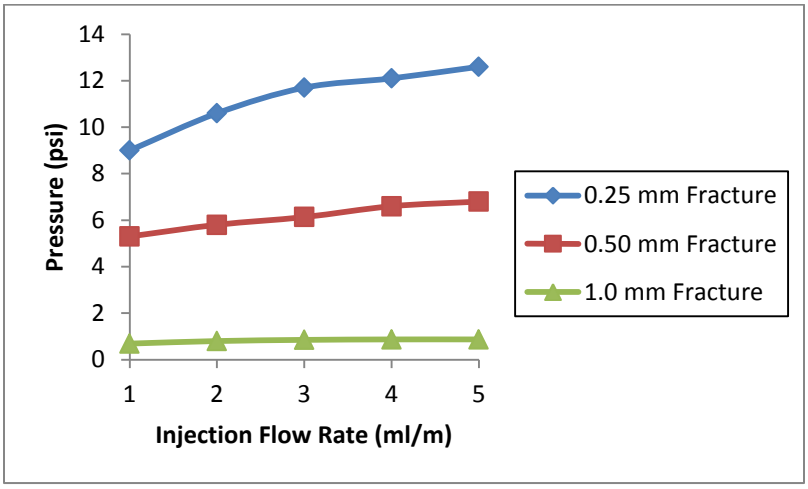

Figure 4-10. 0.25 wt% PPGs Injection Pressure through Open Fracture Screen Plates.

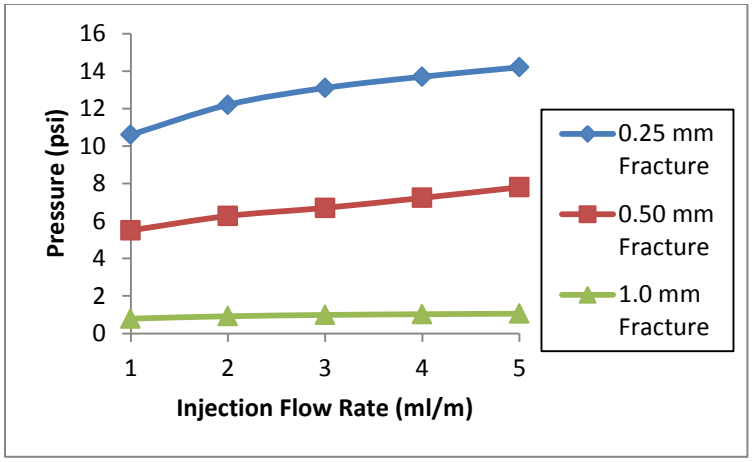

Figure 4-11. 1.0 wt% PPGs Injection Pressure through Open Fracture Screen Plates.

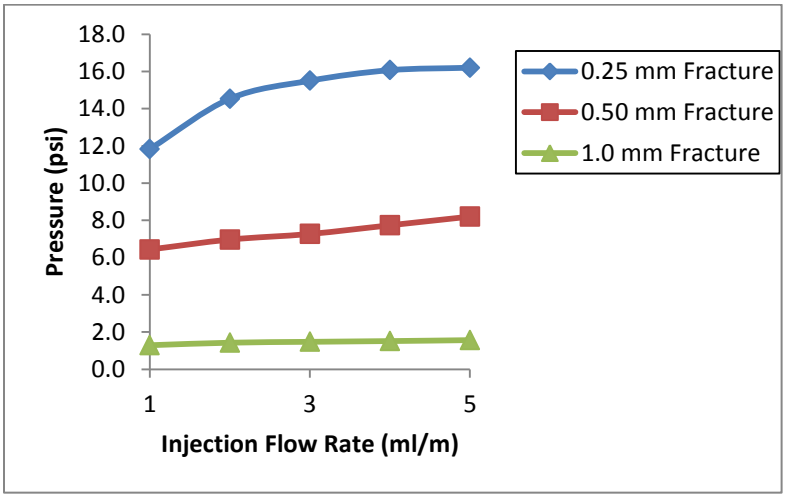

Figure 4-12. 5.0 wt% PPGs Injection Pressure through Open Fracture Screen Plates.

4.6.6 Rheological Model of PPGs through Open fracture Screen Plate.

PPGs injection pressure vs the flow rate can be fitted using the power law which indicates that PPG particles are shear-thinning materials. **Table 4-2** summarizes the fitting equation for the stable injection pressure of PPG particles vs the flow rate for all brine concentrations and through the different open fracture screens plate where the

apparent consistency constant and the flow index can be referred to as the brine concentration and fracture width, respectively.

Table 4-2. Fitting Equation for PPGs Resistance Factor through Open Fracture Screen Plates.

Fracture width (mm)	Brine Concentration. (%)	Fitting Equations	R^2
0.25	DI	$P = 8.463q^{0.1948}$	0.9883
	0.25	$P = 9.0918q^{0.2105}$	0.9891
	1.0	$P = 10.668q^{0.1816}$	0.9965
	5.0	$P = 12.189q^{0.1979}$	0.9396
0.50	DI	$P = 4.6046q^{0.2198}$	0.994
	0.25	$P = 5.2515q^{0.1568}$	0.9845
	1.0	$P = 5.4428q^{0.2096}$	0.9837
	5.0	$P = 6.3527q^{0.1444}$	0.9617
1.0	DI	$P = 1.8321q^{0.1672}$	0.962
	0.25	$P = 0.7048q^{0.1491}$	0.9367
	1.0	$P = 0.7988q^{0.1807}$	0.988
	5.0	$P = 1.2989q^{0.1151}$	0.9866

4.6.7 Resistance Factor Calculations for PPGs through Open fracture Screen Plate

The resistance factor can be defined as the ratio of PPG injection pressure drop to water injection pressure at the same injection flow rate. It can also be referred to as the apparent viscosity which describes the macroscopic rheology of gel in porous media relative to that of water. The water injection pressure could not be measured in this study due to the fact that the PPG particles were injected through open fractures. Therefore, the following equation was used to calculate the water injection pressure drop through the fracture screen plate as described by Buckingham's equation for flow through slots of fine clearance (Engler, 2010).

$$\Delta P_w = \frac{(12)(14.7)}{9.86\times10^9}\frac{q_f\ l_f \mu}{(n_f A)h_f {w_f}^3} \qquad (4\text{-}2)$$

where**:**

ΔP_w is the water pressure drop across the fracture screen plate in (psi)
q_f is the injection flow rate in (cc/s)
l_f is the total fracture length in (cm)
μ is the water viscosity in (cp)
n_f is the number of fractures per unit area
A is the cross sectional area of the fracture screen plate in (cm^2)
h_f is the fracture height in (cm)
w_f is the width of the fracture in (cm)

4.6.7.1 Effect of injection flow rate on resistance factor

Figures 4-13 to **4-15** plot the resistance factor against the injection flow rate in a log-log scale. It is clear that that the resistance factor decreases with an increase in injection flow rate. This relationship demonstrates that the apparent viscosity of PPG decreases with an increase in the injection flow rate. This behavior occurs due to the elasticity nature of PPG, which exhibits a shear-thinning fluid while flowing through open fractures in porous media. The relationship between the resistance factor and the flow rate can be fitted with a high accuracy using the power-law equation expressed as:

$$Fr = Kq^n \qquad (4\text{-}3)$$

where F_r is the resistance factor, q is the flow rate in ml/m, and K and n are constant coefficients. Table 4-3 lists the fitting equations and their correlations coefficients.

4.6.7.2 Effect of brine concentration on resistance factor

Figures 4-13 to **4-15** indicate that the resistance factor for PPG transportation through the open fracture screen plate increases with the increase in brine concentration. This relationship indicates that PPG particles swollen in high brine concentration have a higher apparent viscosity than the PPG particles swollen in a low brine concentration.

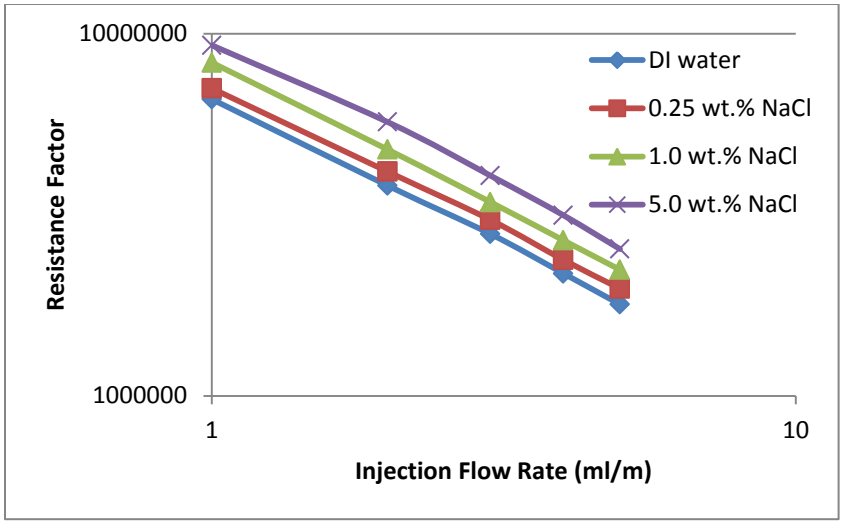

Figure 4-13. Resistance Factor through 0.25 mm Fracture vs. Injection flow Rate and Brine Concentration.

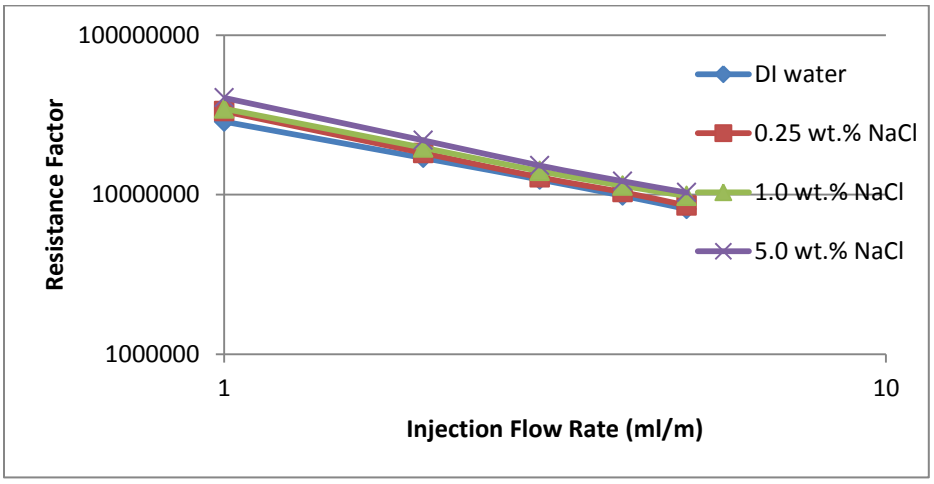

Figure 4-14. Resistance Factor through 0.50 mm Fracture vs. Injection flow Rate and Brine Concentration.

.

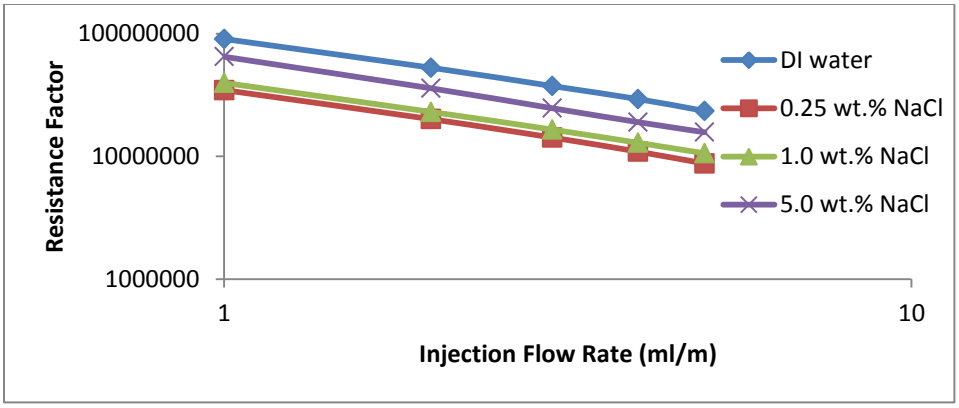

Figure 4-15. Resistance Factor through 1.0 mm Fracture vs. Injection flow Rate and Brine Concentration

4.6.7.3 Fracture Width Effect on Resistance Factor

It can be seen from **Figs. 4-16** to **4-19** that the resistance factor of PPG increases with the increase in fracture width. This trend is consistent with the behavior of bulk gel in fractures and porous media (Seright, 2001) and the flow of PPG particles through open fracture models (Zhang, 2011) as well as PPG extrusion through open conduits (Imqam, 2014). Results might be in contradiction with the common assumption that the narrower the fracture, the more resistance force will be exerted on PPG to pass through the fracture. However, since resistance factor is defined as PPG pressure drop to the pressure drop of water in the same fracture, we can infer that water pressure decreases significantly with an increase in fracture width. Furthermore, such a decrease in the water pressure leads to a high resistance factor. Moreover, from the results it can be concluded that the apparent viscosity of PPG increases with the increase in the fracture width.

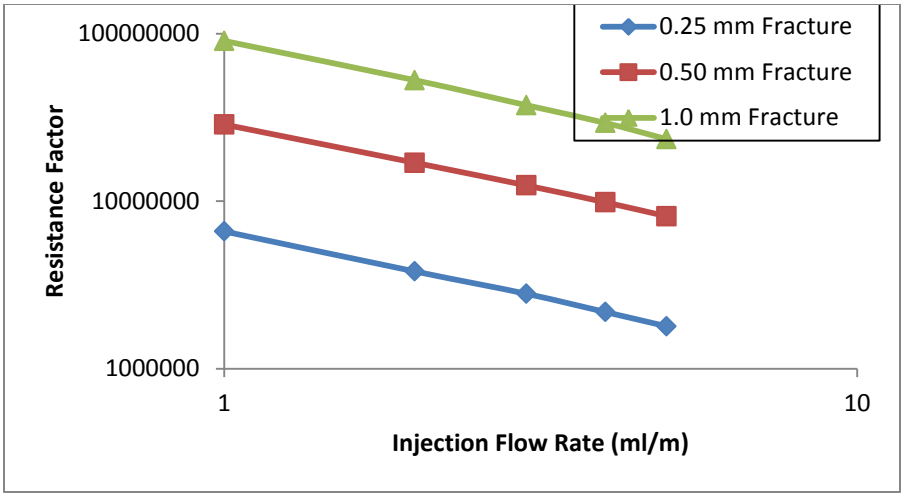

Figure 4-16. DI water PPGs Resistance Factor through Open Fracture Screen Plates.

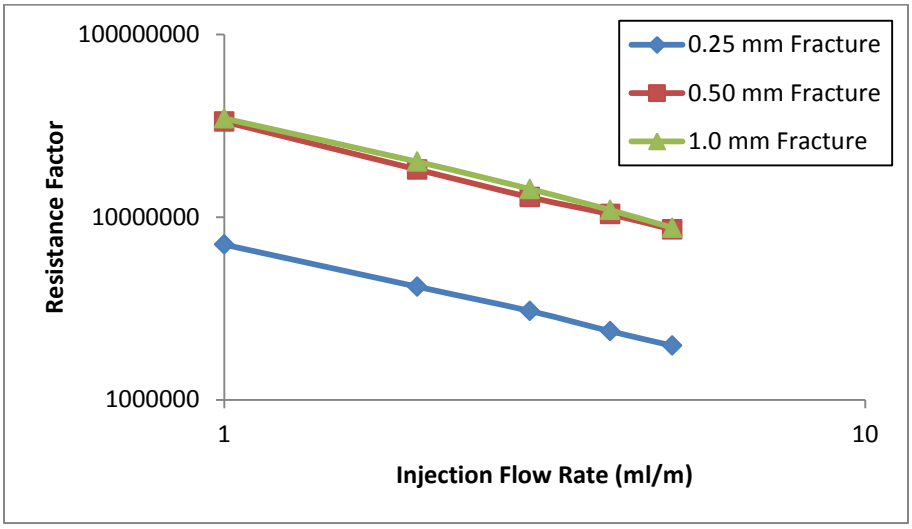

Figure 4-17. 0.25 wt.% PPGs Resistance Factor through Open Fracture Screen Plates.

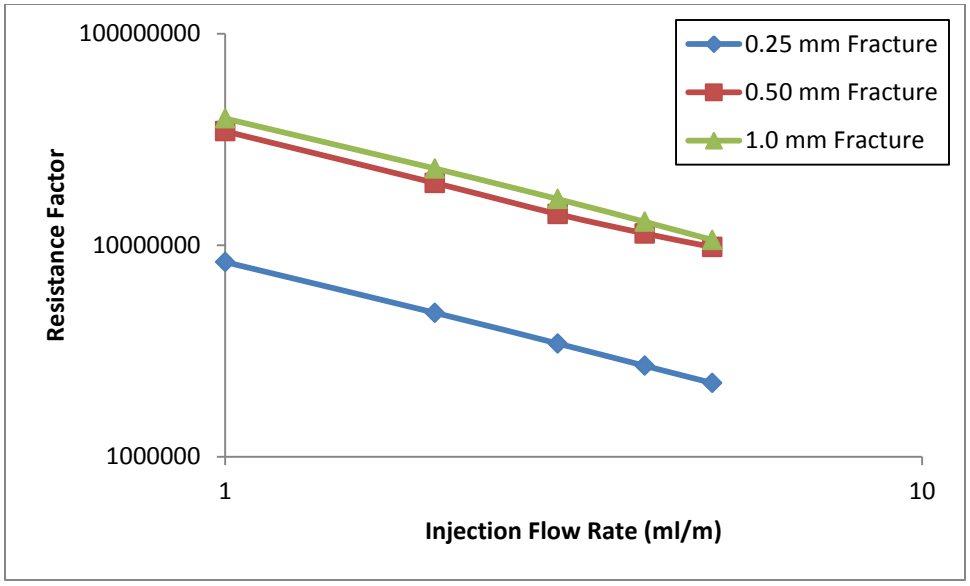

Figure 4-18. 1.0 wt % PPGs Resistance Factor through Open Fracture Screen Plates.

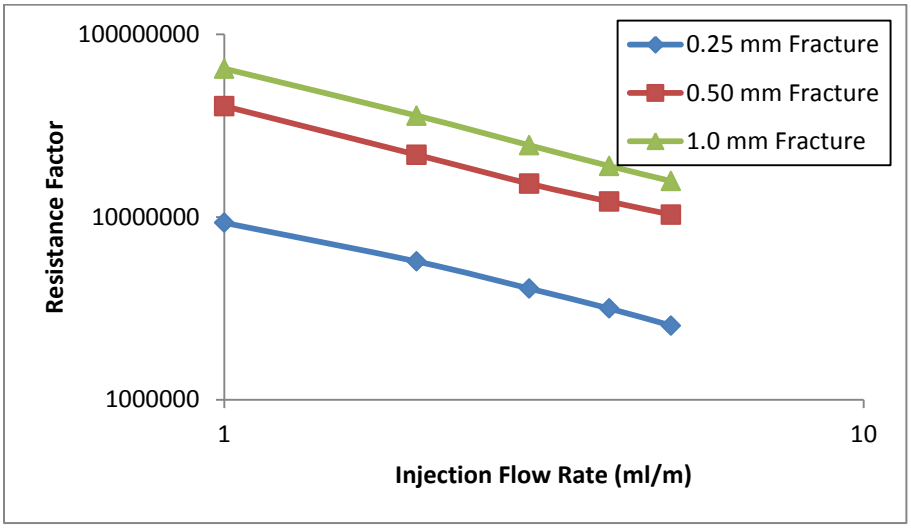

Figure 4-19. 5.0 wt% PPGs Resistance Factor through Open Fracture Screen Plates.

Table 4-3. Fitting Equation For Resistance Factor .

Fracture width (mm)	Brine Concentration. (%)	Fitting Equations	R^2
0.25	DI	$F_r = 6.64E+06q^{-0.805}$	0.9993
	0.25	$F_r = 7.13E+06q^{-0.79}$	0.9992
	1.0	$F_r = 8.37E+06q^{-0.818}$	0.9998
	5.0	$F_r = 9.56E+06q^{-0.802}$	0.9961
0.50	DI	$F_r = 2.89E+07q^{-0.78}$	0.9995
	0.25	$F_r = 3.30E+07q^{-0.843}$	0.9995
	1.0	$F_r = 3.42E+07q^{-0.79}$	0.9988
	5.0	$F_r = 3.99E+07q^{-0.856}$	0.9989
1.0	DI	$F_r = 9.20E+07q^{-0.833}$	0.9984
	0.25	$F_r = 3.54E+07q^{-0.851}$	0.9979
	1.0	$F_r = 4.01E+07q^{-0.819}$	0.9994
	5.0	$F_r = 6.52E+07q^{-0.885}$	0.9998

4.6.7.4 General Full-Factorial Design.

Minitab statistical software was used to conduct a full-factorial design to determine the most influential factor on PPG injection pressure, resistance factor, and injectivity. Three parameters were considered in this study: fracture width, swelling ratio (which is related to brine concentration) and PPG injection flow rate. **Fig. 4-20** demonstrates the Pareto Chart of standardized effects considering PPG injection pressure as a response. The factorial design results show that the fracture width of the open fracture screen plates had the most influential effect on the PPG injection pressure. The swelling ratio ranked second and the injection flow rate had the least influential effect on PPG injection pressure.

For the resistance factor, the Pareto Chart in **Fig. 4-21** reveals that the injection flow rate is the factor that mostly influences the resistance factor. However, the fracture width effect was close to the effect of the injection flow rate. Additionally, the figure shows that the swelling ratio had the least effect on the resistance factor calculations.

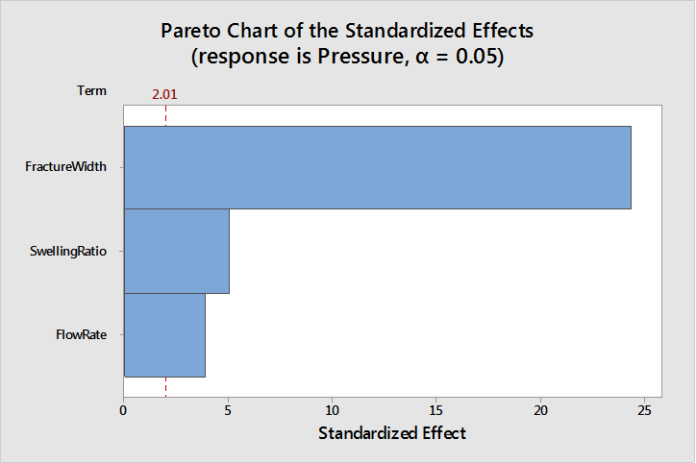

Figure 4-20. Pareto Chart of Injection Pressure as a Response.

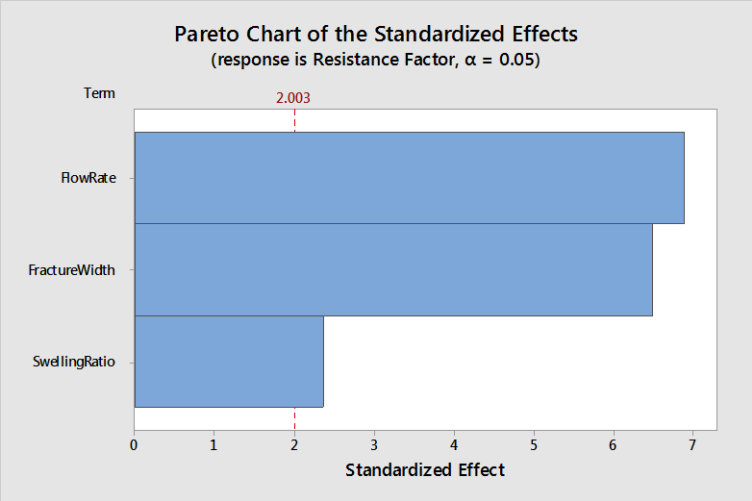

Figure 4-21. Pareto Chart of Resistance Factor as a Response

4.7 Summary and Conclusions

This section examined the evaluation of millimeter-size PPG particles through open-fracture screen plates the major outcomes of this study can be summarized in the following points:

- PPG injection pressure increases as both the brine concentration and the injection flow rate increase. However, the increase is not significant due to the high fluid conductivity within the fractures.

- As demonstrated by the power law rheology model, PPG exhibits shear thinning or pseudo-elastic behavior.
- The PPG resistance factor increases as the injection flow rate decreases.
- The PPG resistance factor increases with the increase in the fracture width size.
- PPG threshold pressure increases as the brine concentration increases regardless the size of the fracture.
- Evaluation of the extruded PPG particles from the various fractures can facilitate an understanding or the transportation pattern of PPG through fractures.
- The full-factorial design shows fracture width as the most influential factor on both the PPG injection pressure and injectivity, whereas flow rate affects the resistance factor the most.

Section 5: Gel Pack Model to Evaluate Gel Pack Permeability

5.1 Summary

Gel pack permeability is a new concept is introduced through this study. It introduced to study factors that have a significant effect on particle gel propagation through either super-k or fracture systems. Gel was found that partially plugs undesired formations rather than fully blocking. This section investigates what factors significantly effect on particle gel pack permeability. This investigation is a crucial for a successful gel treatment because it gives an idea about how much gel pack permeability can minimize the permeability of the target zone.

5.2 Objectives

This study aimed to provide an intensive insight on the gel rheology properties for PPG during water flow. The following are summaries of the objectives of this section and expected technical contribution gained from this investigation.

- Determine the PPG pack permeability for water flow.
- Examine the effect of change brine concentrations, particle gel sizes, and injection flow rates on PPG pack permeability.
- Study the effect of compressed gel on the blocking efficiency of PPG.
- Determine the PPG pack compressibility under the different load pressure.
- This investigation is very important for a gel treatment to be successful where gel treatment target is to reduce the undesired permeability formations to the level as we planned.
- The findings from this section will be used to optimize a particle gel conformance control design. A gel pack with the desired permeability can be designed by selecting both gel strength and particle sizes that correspond with reservoir pressures.

5.3 Experimental Description

5.3.1 Preformed Particle Gel (PPG).

A super absorbent polymer (SAP) was used as the preformed particle gel for this study. The particle was synthesized by a free radical process using acrylamide, acrylic acid, and N, N'-methylenebisacrylamide. Most PPGs reach full swelling in half an hour, but a field operation usually take a few hour to a few months, so fully swelling particles were used in experiments.

Various sizes of PPG were selected for experiments: 18-20, 20-30, 50-60, and 80-100 mesh. **Table 5-1** illustrates the PPG size distribution before and after being swollen in 1% NaCl solution.

Table 5-1—PPG size before and after swelling in 1% NaCl.

No	PPG (mesh size)	PPG size before swelling, μm	PPG size after being swollen, mm
1	18-20	850	42.5
2	20-30	600	30
3	50-60	250	12.5
4	80-100	150	7.5

5.3.2 Brine Concentrations.

Sodium chloride (NaCl) with three concentrations (0.05, 1, and 10 wt%) was used to prepare the swollen gels. **Figure 5-1** depicts the PPG before and after being swollen in different brine concentrations.

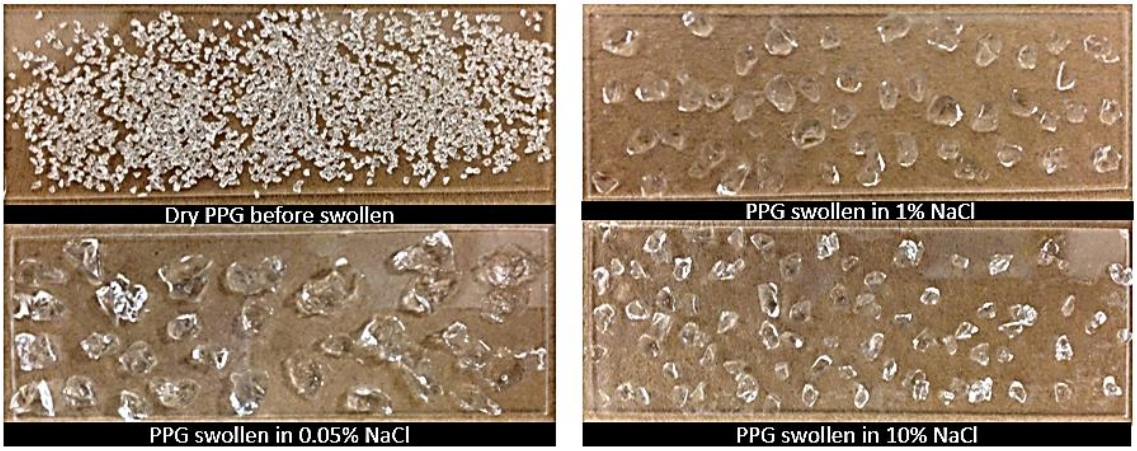

Figure 5-1—PPG (30-mesh size) before and after being swollen in different brine concentrations

The brine concentration was carefully selected according to the gel strength and swelling ratio where the gel prepared in the low salinity brine had less strength and more swelling ratio than the gel prepared in the high salinity brine. **Table 5-2** illustrates the swelling ratio and gel strength measurements for different brine concentrations. Storage moduli (G´) for the PPG prepared in different brine concentrations were measured at room temperature (23^{o}C) using a rheometer. The sensor used for measurements was PP335 TiPoLO2 016, with a gap of 0.2 mm between the sensor and the plate. G' were measured at a frequency of 1 Hz for each sample.

Table 5-2—PPG swelling ratio and strength measurements of 30 mesh size.

No	Brine concentration, % NaCl	PPG concentration, wt %	Swelling ratio	Gel strength, pa
1	0.05	0.60	165	515
2	1	2.0	50	870
3	10	4.0	25	1300

5.4 Experimental Setup

An apparatus was built to evaluate the factors impacting the permeability of the gel pack, as presented in **Figure 5-2**. The apparatus (simple channel) was built from an

acrylic transparent tube and its square cross–section was 5.06 cm^2 and 26.5 cm long. Different brine concentrations were injected into the PPG-filled transparent tube, using a syringe pump. Two caps with four stainless steel rods and nuts were used to hold the transparent tube channel. The core sample was fitted inside the tube with an O–ring to prevent any leakage of gel that might occur during brine injection. A piston made from an acrylic rod was located at the top of the tube to compress the gel inside the channel tube. A hole inside the piston was made to permit brine to be injected through the gel after it was compressed. Two pressure gauges were connected, one at the inlet and the other at the bottom of the gel, to measure the differential pressure across the PPG.

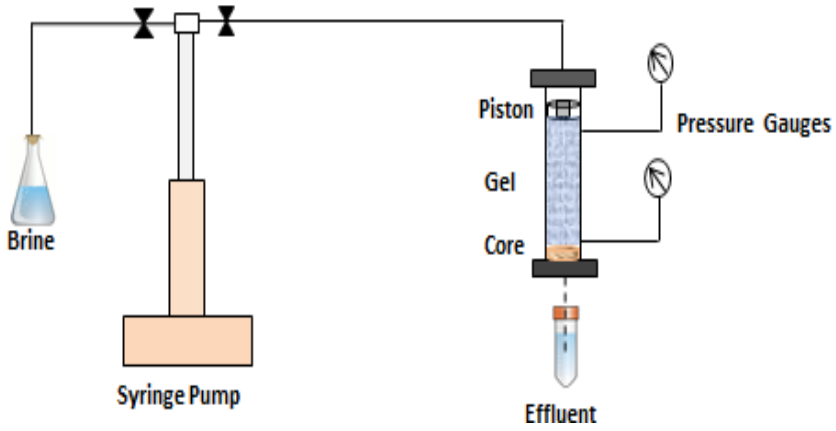

Figure 5-2—PPG pack permeability setup.

5.5 Experimental Procedure

A consolidated sandstone core was fitted at the bottom of the channel tube model to prevent gel movement from reaching the outlet. Swollen PPG was then placed inside the transparent tube model. Six different injection brine flow rates (0.1, 0.2, 0.3, 0.4, 0.5, and 0.6 ml/min) were used for each experiment to measure the PPG pack permeability.

A piston was then fitted inside the channel, and the gel was compressed at eight different load pressures: 75, 125, 150, 175, 200, 225, 250, and 275 psi. At each load pressure, the same injection flow rates were used to measure the gel pack permeability.

The pressure drop across the PPG, the change in the length of the gel, and the fluid produced at the outlet were all recorded at the ambient temperature. In addition, to study the effect of load pressure on gel strength measurements, a sample of gel was taken before and after the gel was compressed.

5.6 Results and Analysis

5.6.1 PPG Pack Permeability Measurements

5.6.1.1 Brine concentration effect

Stabilized pressures for each concentration of brine were obtained at the different injection flow rates **(Figure 5-3).** The results showed that the stabilized pressure of the PPG rose as the flow rate increased. This increase, however, was significant only at a low flow rate (0.1 to 0.3 ml/min). For example, in the case of no piston effect, the stabilized pressure for the gel swollen in 10% brine started to increase from 1 psi to 2.8 psi at low flow rates (0.1 to 0.3 ml/min). At high flow rates (0.4 to 0.6 ml/min), the pressure slightly increased from 3.5 to 4.1 psi. Additionally, Fig. 4 provides a gel stabilized pressure comparison between the brine concentrations of 0.05% NaCl and 10% NaCl before and after the load pressure was introduced. The results showed that the pressure measurement at 0.05% did not increase significantly after the gel was compressed to 275 psi as compared to the results for the 10% solution. The pressure measurement increased almost 1 psi for the former and almost 13 psi for the latter. This behavior revealed that the permeability of a strong gel (swollen in a high brine concentrations) decreased more rapidly than that of a weak gel (swollen in a low brine concentrations) if high pressure was applied. All the measurements of gel particle compression were performed until 275 psi because it was observed that the gel pack permeability became almost at higher pressure. The results suggest that strong gel applications in an oil field will be more effective than weak gels at controlling water production.

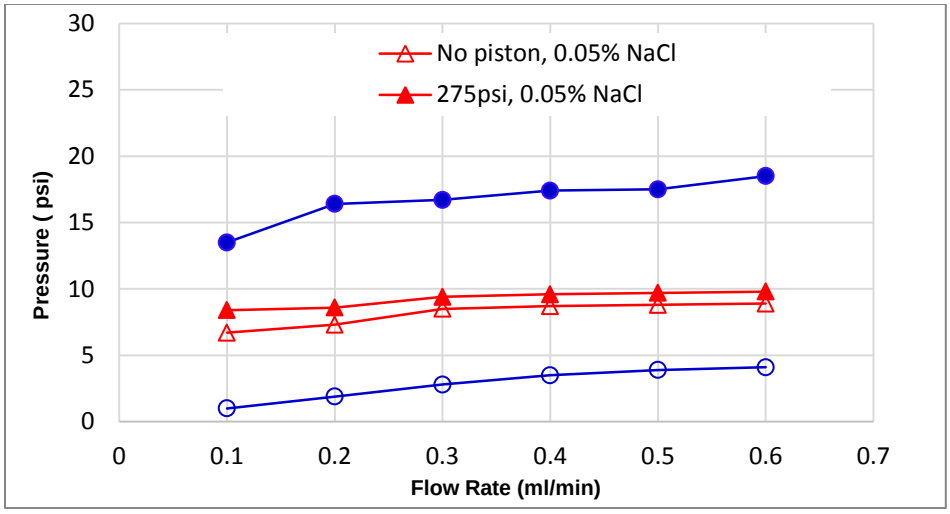

Figure 5-3 Stabilized pressure for different brine concentrations before and after applying load pressure

The PPG pack permeability calculated for the different brine concentrations was determined according to the power law equation and plotted as shown in **Figure 5-4**. At the initial load pressure, gel swollen in 10% NaCl started with higher gel pack permeability than did gels swollen in either 0.05% NaCl or 1% NaCl. The gel pack permeability with a 10% brine concentration started at 103 md before the gel was compressed. The gel compressed gradually when the load pressure was applied. The gel pack permeability began to decrease continuously until 200 psi, it fluctuated between 5 and 7 md. The gel pack permeability with a 0.05% NaCl brine began at 20 md before the load pressure was applied. It started decreasing after the load pressure was applied. When the load pressure reached 175 psi, the gel pack permeability had a different trend. It started to form channels inside the gel, and the permeability increased to 11.8 md. When the pressure was released, the gel network reformed and the gel pack permeability continued to decrease after the gel compressed to 200 psi.

Figure 5-4 indicates also that the strong gel had a higher gel pack permeability than did a weak gel before the load pressure was introduced. At a high load pressure,

however, the gel pack permeability exhibited a different trend. The decrease in the PPG pack permeability with high gel strength was significantly less than that of the PPG pack permeability with low gel strength.

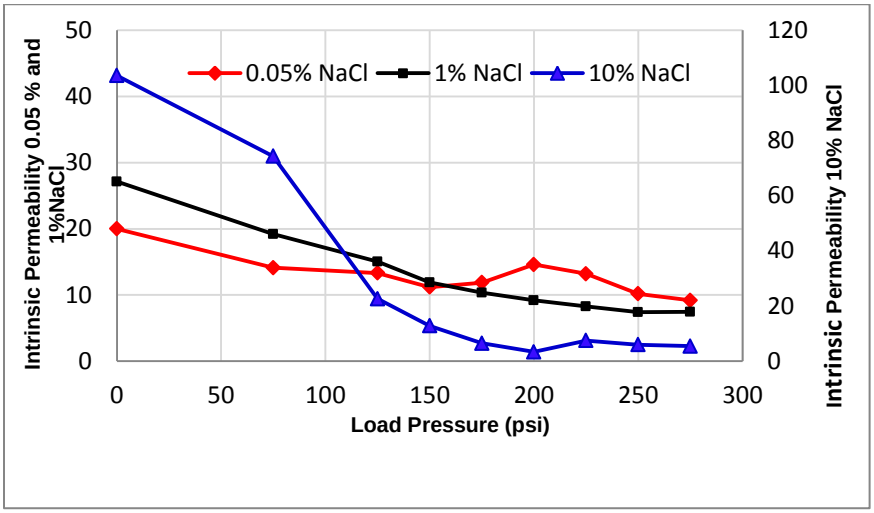

Figure 5-4 Comparison between PPG pack permeabilities with different brine concentrations.

Tables 5-3, **5-4**, and **5-5** summarize both the permeability and elasticity measurements for the different brine concentrations as determined by using the power law equation. The elasticity index for the PPG varied between 0.7 and 0.9 for weak gels, while for strong gels, it varied between 0.3 and 0.8.

Table 5.3—PPG pack permeability measurements for 0.05% NaCl.

P (psi)	Intrinsic Permeability, ko (md)	Elasticity Index	R^2
No load	19.987	0.8417	0.9916
75	14.105	0.7792	0.991
125	13.316	0.7555	0.9803
150	11.196	0.9418	0.9924
175	11.856	0.9661	0.9986
200	14.594	0.7939	0.9901
225	13.201	1.381	0.9159
250	10.182	0.9003	0.9693
275	9.1823	0.9444	0.9961

Table 5.4—PPG pack permeability measurements for 1% NaCl.

P (psi)	Intrinsic Permeability, ko (md)	Elasticity Index	R^2
No load	27.114	0.8399	0.992
75	19.185	0.8464	0.9964
125	15.035	0.7729	0.9956
150	11.889	0.8575	0.9988
175	10.345	0.8055	0.9849
200	9.1845	0.8934	0.9937
225	8.2749	0.9505	0.999
250	7.4038	0.9349	0.9963
275	7.4382	0.9192	0.997

Table 5.5—PPG pack permeability measurements for 10% NaCl.

P (psi)	Intrinsic Permeability, ko (md)	Elasticity Index	R^2
No load	103.53	0.311	0.9372
75	74.323	0.1297	0.9699
125	22.643	0.4809	0.9287
150	12.809	0.6346	0.9743
175	6.4912	0.5848	0.9308
200	3.3611	0.8532	0.9963
225	7.5038	0.7202	0.9833
250	5.9863	0.6923	0.9659
275	5.4555	0.7136	0.9606

5.6.1.2 Preformed particle gel size effect.

Various particle sizes were used to investigate how the PPG size affects the permeability measurements**.** Particles of all experimental sizes were swollen in the same brine concentrations (1% NaCl). **Figure 5-5** reveals that the PPG pack permeability was affected by particle size. Large particle sizes had a lower gel pack permeability than did smaller particle sizes across all of the load pressure ranges. The gel pack permeability with a particle size of 20-30 mesh was 27 md before adding the load pressure. The gel pack permeability then started to decrease gradually after the load pressure was

introduced. The permeability decreased to almost 8 md at 200 psi. Gel with a particle size of 80-100 mesh had a gel pack permeability of 33 md before applying the load pressure. Permeability then decreased to almost 20 md at 200s psi.

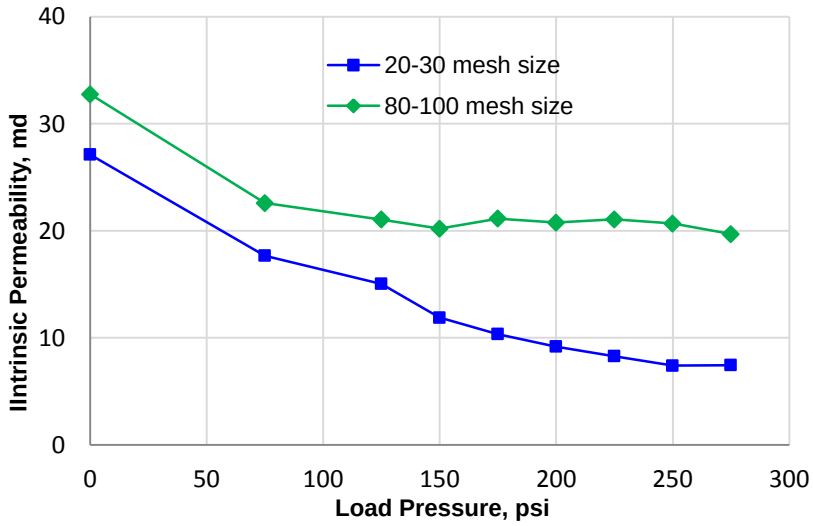

Figure 5-5—PPG pack permeabilities with different particle sizes.

In addition, the results showed that the PPG pack permeability before applying the load pressure was much larger than the PPG pack permeability after applying the load pressure. The PPG pack permeability decreased significantly when the load pressure was first applied. The permeability then became almost constant because the gel particles were compressed substantially, forcing them closer to one another during the earlier stages of the applied load pressure and less during the later stages. Similarly, this new finding indicated that the PPG pack permeability would have lower permeability at reservoir pressure conditions than it would at surface conditions. It also suggested that using smaller particles in the conformance control treatment would not result in a better gel resistance to water flow inside the high permeability channels.

5.6.2 Gel Pack Permeability Reduction

This section presents a comparison between the gels pack permeability determined before and after load pressure for both effects of brine concentration and particle size. The results obtained from this comparison are important to quantifying the change in the gel permeability and the rheology that occurred during the PPG compression.

5.6.2.1 Reduction of PPG pack permeability for brine concentrations

The effect of brine concentration on the PPG pack permeability can be expressed using the Permeability Gel Reduction (KGR) factor. It can be defined as the ratio between the PPG pack permeability measured after using the load pressure (KGA) and the PPG pack permeability measured before the load pressure (KGB). This concept, which is expressed in a percentage, is used to determine how much the PPG permeability can be decreased.

Table 5-6 illustrates the permeability results obtained for 30-mesh size PPG swollen in three different brine concentrations. The results indicated that the KGB increased as the brine concentration increased. When the load pressure was applied, however, the KGA decreased as the brine concentration increased. Consequently, the PPG permeability reduction (KGR %) rose as the gel strength increased. The KGR for a gel swollen in 0.05% NaCl was 54.05%; the KGR for a gel swollen in 10% NaCl was 94.73%. These results suggested that the plugging efficiency can be improved if a strong gel is selected for the conformance control treatment.

Table 5.6—Reduction of PPG pack permeability as a function of brine concentration.

Particle Size (mesh)	Brine Concentration, % NaCl	KGB	KGA@275psi	KGR (%)
30	0.05	19.987	9.1823	54.05
30	1	27.114	7.4382	72.56
30	10	103.53	5.455	94.73

5.6.2.2 Reduction of PPG pack permeability for particles sizes

Table 5-7 displays the effect of different particle sizes on the PPG pack permeability reduction. Particles of various sizes were swollen in the same brine concentration (1% NaCl). The findings show that the PPG pack permeability before and after applying the load pressure was greater for smaller particle sizes than for larger particle sizes. The PPG permeability reduction (KGR %) did not significantly change for the experimental particle sizes. Compared with the effect of brine concentration, particle size had less effect on the KGR.

Table 5-7—Reduction of PPG pack permeability as a function of particle size.

Brine Concentration % NaCl	Particle Size (mesh)	KGB (md)	KGA@275 psi	KGR (%)
1	18-20	22.201	6.167	72.2
1	20-30	27.114	7.4382	72.56
1	50-60	27.351	16.846	38.4
1	80-100	32.756	19.592	40.1

5.6.3 PPG Strength

A rheometer was used to measure the strength of the gel swollen in 0.05, 1, or 10% NaCl. **Figure 5-6** presents the PPG strength measurements before and after the load pressure was applied. G`A and G`B are gel strengths measured before and after the load pressure was introduced, respectively. The results suggested that the gel strength increased as the brine concentration and load pressure increased. Analogously, this result revealed that the gel strength would increase when gel is injected into the target formation under reservoir pressure conditions.

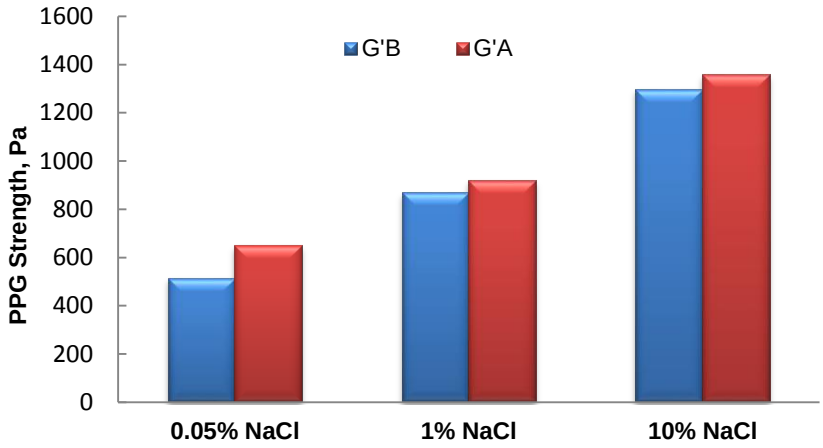

Figure 5-6—PPG strength before (G`B) and after (G`A) load pressure.

5.6.4 PPG Compressibility Measurement

The results obtained from the experiments demonstrated that the PPG can be compressed at various values based on both different brine concentrations and load pressures. Gel compressibility was obtained and plotted in **Figure 5-7** for the different brine concentrations. The PPG for all brine concentrations had a large compressibility value at the beginning of the introduced load pressure. For instance, the PPG swollen in 10% NaCl had a compressibility of 0.0037 psi^{-1} at 75 psi and then decreased gradually to 0.00172 psi^{-1} at 275 psi. The findings obtained from the compressibility measurements are consistent with data obtained from the PPG pack permeability measurements. At the initial load pressure of 75 psi, the gel compressibility of the solution with 10% NaCl was 0.0037 psi^{-1}, while the gel compressibility of the 1% brine concentration at 75 psi load pressure was only 0.000527 psi^{-1}. The compressibility for both brine concentrations 1% NaCl and 10% NaCl is fairly fitted by Equation 5.1 and Equation 5.2**,** respectively, as follows:

$$C_{ppg} = 0.0091\ P^{-0.614} \quad \text{.....(5.1)}$$

$$C_{ppg} = 0.0437\ P^{-0.573} \quad \text{.....(5.2)}$$

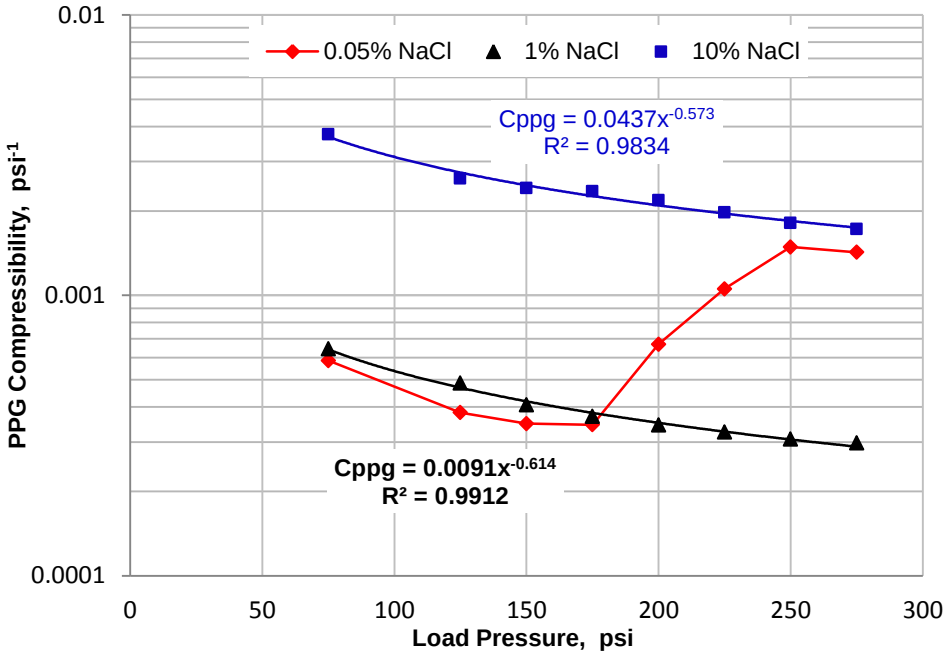

Figure 5-7—PPG compressibility (psi^{-1}) and load pressure (psi).

Additionally, the results in **Figure 5-7** indicated that the compressibility for a PPG swollen in 0.05% NaCl decreased gradually and then suddenly increased at 175 psi. This increase most likely occurred due to the channel created during the PPG permeability measurement process. Data also suggested that PPGs swollen in high brine concentrations are more compressible than PPGs swollen in low brine concentrations. The average PPG compressibility obtained for all brine concentrations ranged between 0.0003 psi^{-1} and 0.003 psi^{-1}. **Table 5-8** shows the procedure for finding the compressibility in relation to the load pressure.

Table 5.8—Compressibility of 30-mesh size with 1% NaCl.

P (psi)	*L*	Vo	*V2*	Delt V	Delt P	Cppg (Psi^{-1})

75	22.5	118.5093	113.9513	4.55805	73	0.000527
125	22.4	118.5093	113.4448	5.0645	123	0.000347
150	22.3	118.5093	112.9384	5.57095	147	0.00032
175	22.1	118.5093	111.9255	6.58385	173	0.000321
200	21.9	118.5093	110.9126	7.59675	198	0.000324
225	21.7	118.5093	109.8997	8.60965	223	0.000326
250	21.6	118.5093	109.3932	9.1161	250	0.000308
275	21.5	118.5093	108.8868	9.62255	273	0.000297

5.7 Summary and Conclusions

During these investigations of factors affecting the gel pack permeability formed inside large channeled features, the following are conclusions observed from the study:

- A PPG partially blocks the large channel rather than fully blocking it. The PPG will do so because the gel can formed channels for water to pass through. Therefore, we strongly recommend that operators in the field consider the effect of both particle size and brine concentration when designing PPGs for water production control purposes.
- Gel-plugging efficiency is affected by particle size selection. Our results indicated that gel resistance to water flow improved when larger particles were selected.
- Brine concentration had a significant effect on the PPG resistance to water flow. We observed that strong gels had a lower permeability than did weak gels. Therefore, a strong PPG would be the right choice for more effectively plugging an undesired zone than a weak gel.
- Brine concentration had a more pronounced effect on the PPG pack permeability than did gel particle size.
- The gel pack permeability decreased significantly at the beginning of the compression process. Then, after the gel became slightly rigid because of the load pressure effect, the compressibility reduction became less obvious. The PPG was compressible between 0.0003 psi^{-1} and 0.003 psi^{-1}. This compressibility varied according to both brine concentration and particle size.
- The PPG strength increased as both the brine concentration and the load pressure increased. A weak gel creates internal channels more easily than a strong gel when the PPG is subjected to continuous load pressure.
- Gel pack permeability is lower at reservoir conditions compared to the gel pack permeability at surface conditions. The gel pack permeability measurements registered a few hundred *millidarcies* before the load pressure was applied; the gel permeability decreased to less than 10 md after the load pressure was introduced.

Section 6: Tubing Model to Evaluate PPGs Extrusion through Conduits

6.1 Summary

The success of gel treatments depends heavily on the gel's ability to extrude through fractures and channels during the placement process (Seright, 1999a and 1999b). Thus, understanding both the mechanism and the behavior of gel extrusion is the key to a successful conformance control treatment.

6.2 Objectives

The objective of this work is to conduct an in-depth examination of several factors that can have an important impact on the PPG extrusion mechanism and placement performance in opening conduits. The following summarizes the detailed objectives and expected technical outcomes of this work.

- Examines the effect of the conduit's opening size and brine concentration (PPG strength) on the injectivity index, resistance factor, gel dehydration, particle opening ratio, gel wash-out, and plugging efficiency.
- Determine the matching ratio measured between gel particle size and conduit opening size.
- Study the effect of gel strength on the blocking efficiency of PPG.
- Determine the residual resistance factor (*Frr*) for water flow through PPG filled the conduit.
- This work will provide a significant guidance about how to better design millimeter-size particle gel treatments for large openings, like open fractures, cave, worm hole and conduits.
- Based on the laboratory data, correlation models were developed to quantitatively calculate the resistance factor as a function of particle strength, passing ratio, and shear rate. The two developed models were embedded into an existing reservoir simulator (UT-gel) for particle gel treatment optimization design and performance prediction.

6.3 Experimental Description

6.3.1 Preformed Particle Gel.

A superabsorbent polymer was used as a PPG to conduct the experiments. The particle was synthesized using acrylamide, acrylic acid and N, N'-methylenebisacrylamide by a free radical process. Dry particles with a mesh size of 30 were swollen in different concentrations of NaCl brine (0.05%, 0.25%, 1%, and 10%). The brine concentration was carefully selected based on the swelling ratio and the gel strength after swelling, as shown in **Table 6.1.**

Table 6-1—Summary effect of brine concentration on PPG.

No	Brine conc., %NaCl	PPG Conc., wt%	Swelling ratio	Gel Strength, Pa
1	0.05	0.60	165	515
2	0.25	1.25	80	657
3	1	2	50	870
4	10	4	25	1300

PPG swollen in low NaCl concentrations will have high swelling ratio and low gel strength. PPG concentration was determined using the initial weight of dry gel divided by the final weight of completely swollen gel. PPG concentration is changed as a result of the brine concentration effect.

6.3.2 Description of Tubes

Tubes five feet (1.5 meter) long with varying internal diameters (10.922, 3.048, 1.752, and 0.774 millimeters) were used to emulate different conduit sizes. Three pressure taps were mounted along the tube to monitor PPG propagation performances. The internal diameters were carefully selected to be larger than, equal to, and smaller than the swollen particles.

6.3.3 Microscope.

A microscope was used to determine the particle size before and after particle extrusion through the conduit models. An image analysis technique was used to obtain the particle gel size distribution.

RheoScope Device

Storage moduli (G´) for PPG prepared in different brine concentrations were measured at room temperature (23 ^{o}C) using a rheoscope. The PPG strength was measured before and after gel propagation into the conduit to determine the effect of the extrusion process on strength. The sensor used for measurements is PP335 TiPoLO2 016 with a gap of 0.2 mm between the sensor and the plate. G' were measured at a frequency of 1 Hz for each sample.

6.4 Experimental Setup

Figure 6-1 provides the schematic of the conduit model used to conduct the experiments. This model contained a syringe pump that was used to inject brine and gel through the accumulator into a five-foot tube. The tube was divided into three sections, the first two of which were two feet long, with last section being one foot long. Effluent gel and brine were both collected to evaluate the gel's properties after the extrusion.

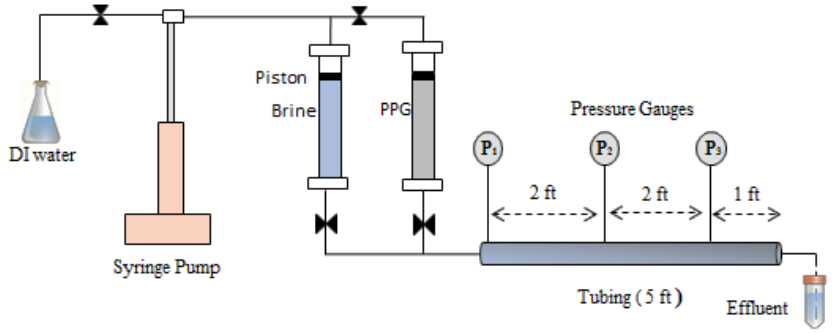

Figure 6-1—Schematic of the conduit model.

6.5 Experimental Procedure

Dry PPG's of 30 mesh size were placed in different concentration brines and left overnight to swell fully. A sieve was used to allow the swollen gel to separate from the excess brine solution. The gel then was packed into a stainless steel accumulator so that it could be injected into a conduit model. The gel injection process at the ambient temperature is summarized as follows:

The PPGs were injected into different internal tubes at the same designed velocity. **Table 6.2** summarizes the velocities used for the different inner diameters. The gel initially was injected at a high velocity, which then was reduced gradually for all experiments. The pressure needed to be stable for each gel injection velocity. Following pressure stabilization, gel samples were taken for each gel injection velocity to measure gel strength and particle size. Finally, when the gel injection process was complete, the same concentration brine was injected into the tube filled with particles from a low to a high velocity to determine gel resistance to water flow.

Table 6-2—Gel velocities designed for each conduit inner diameter.

Conduit inner diameter, mm	Injection flow rate, ml/min	Injection velocity, ft/day
10.922	39.2	1979
	29.2	1476
	19.2	970
	9.8	495
	4.9	247
	3.9	198
	1.9	99
	1	49
	0.2	10
3.048	3	1928
	2.3	1446
	1.5	964
	0.75	482
	0.37	241
	0.30	193
	0.15	96
	0.07	48
	0.01	10
1.752	1	1931

	0.75	1448
	0.5	966
	0.25	483
	0.125	241
	0.1	193
	0.05	96
	0.025	48
	0.005	10

6.6 Results and Analysis

PPGs swollen in four different concentration brines were injected into three sizes of conduits at various injection velocities to investigate the effect of brine concentration (related to gel strength) on injectivity, the resistance factor, and the threshold pressure. The resistance factor and gel injection pressure data were used to develop new correlation models for PPG to predict the resistance factor and the initial stable injection pressure during gel extrusion in conduits.

6.6.1 Injectivity Index Calculation

An injectivity index was obtained as a function of the brine concentration, injection velocity, and conduit inner diameter to observe the behavior of PPG that had extruded through the conduit systems. **Figure 6-2** shows the effect of the brine concentrations and gel injection velocity on the gel injection pressure through three different sizes of conduits. At the same injection velocity, the gel injection pressure increased as the brine concentration increased. This occurred because PPG swollen in low brine concentration swelled more and became weaker than the PPG swollen in high brine concentration. The gel injection volume required to achieve stable pressure is varied; it depends on the brine concentration and the conduit inner diameter size. Large volume of gel was injected as the gel become stronger and the conduit inner diameter become smaller. In conduit inner diameter 1.752 mm for gel injected at velocity 1931.26

ft/day, PPG injected pore volume required to get stable pressure increased from 11.5 PV to 33.9 PV when brine concentration increased from 0.05% NaCl to 10% NaCl.

The results also show that the gel injection pressure increased as the injection velocity increased. This increase in the gel injection pressure became insignificant when the gel injection velocity exceeded 500 ft/day. This suggests that the gel injection pressure did not increase linearly through all of the gel injection velocities, but rather tended to reach a plateau after a certain injection velocity. This insignificant increase most likely occurred because of the gel slip that can occur when extruding through conduits at a high velocity (Seright, 1997). Our results were consistent with Seright (1997, 1998) for gel extrusion through tubes where he observed that gel injection pressure became independent of injection velocity after a specific velocity value.

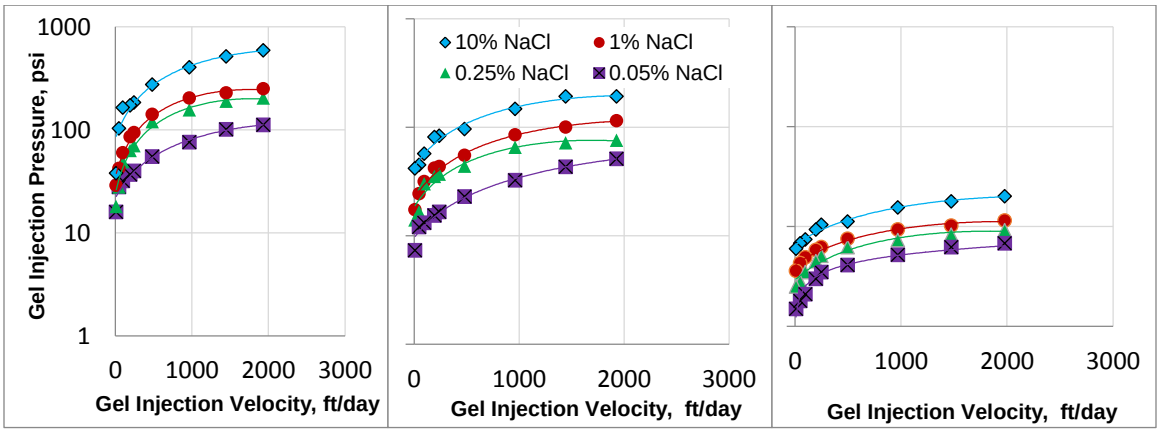

Figure 6-2—PPG injection pressure as a function of brine concentration and conduit diameter.

The data from **Figure 6-2** were used to obtain the gel injectivity index through the conduit systems. PPGs with a high injectivity index required a lower injection pressure to be propagated through the conduit. In this study, the injectivity index increased as the brine concentrations decreased, as shown in **Figure 6-3**. This likely occurred as a result of the swelling ratio effect. PPGs swollen in low brine concentrations contain a high

percentage of aqueous phase and a low percentage of solid phase. This composition allows PPGs swollen in low brine concentrations to be more injectable than PPGs swollen in high brine concentrations. These results also indicate that the injectivity index increased as both the conduit inner diameter and the velocity increased. For the conduit size, this behavior is easy to understand, but for the velocity, this occurred because the gel followed the shear thinning or pseudo plastic behavior in the conduit systems.

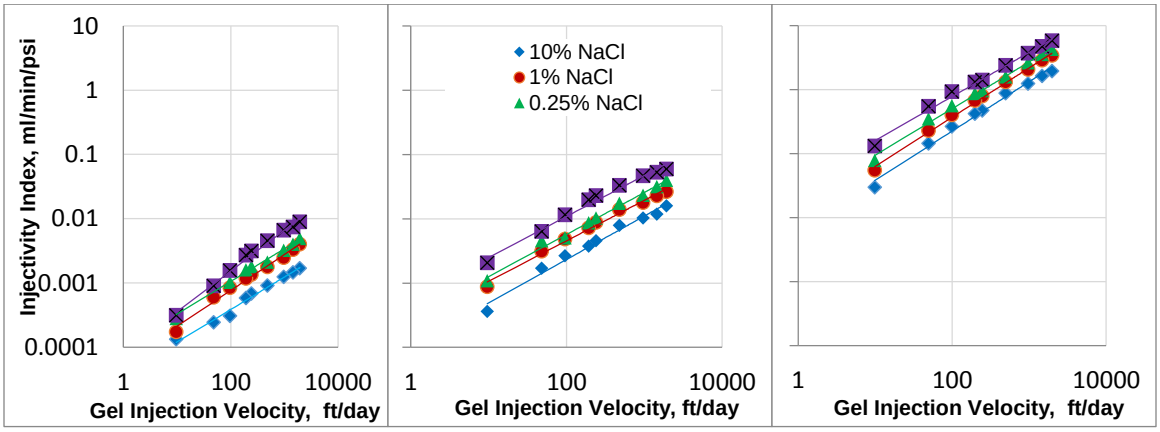

Figure 6-3—Injectivity index results.

6.6.3 Resistance Factor Calculation

In analogy to porous media experiment, resistance factor (Fr) was estimated from the injectivity index and geometry of the conduit, namely QL/AΔP for the brine and the gel injection. It can be defined as the ratio of the particle gel injection pressure drop to the brine injection pressure drop at the same flow rate and can be calculated from the following equation:

$$Fr = \Delta p_{PPG} / \Delta p_{brine} \quad \text{.....(6-1)}$$

where Δp_{PPG} is the PPG injection pressure drop and Δp_{brine} is the brine injection pressure drop before PPG placement.

PPGs swollen in four different concentrations of brines were injected into three conduits at various injection velocities to determine the effect of brine concentration and conduit inner diameter on the resistance factor. The injection began with the highest injection velocity until the injection pressure became stable. Then the injection continued at reduced velocities. A stable pressure was recorded at each injection velocity. **Figure 6-4** indicates that for all gel velocity injections, Fr increased as the brine concentration and conduit inner diameter increased. The Fr measured across all three conduits became an independent factor on velocity when it exceeded 500 ft/day. The Fr value for the gel swollen in 10% NaCl extruded in 10.922 mm was 99133; it then decreased substantially to 3364 as the velocity increased from 10 ft/day to 500 ft/day. However, as the velocity increased above 500 ft/day, the Fr values decreased only slightly during the gel injection process.

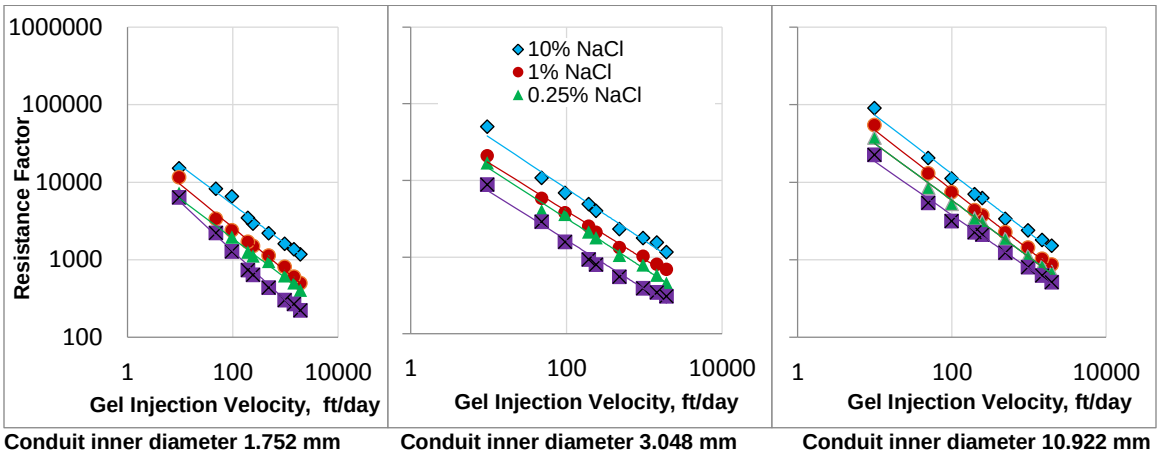

Figure 6-4—Resistance factor as a function of brine concentration and conduit inner diameter.

6.6.4 Gel Threshold Pressure vs Particle Opening Ratio

The particle opening ratio is defined as the ratio of the gel particle diameter (D_g) before the extrusion to the pore opening conduit diameter (D_p). The 30-mesh PPGs swollen in different concentration brines had different sizes and strengths, as shown in **Table 6.1**. *The gel threshold pressure (Pt)* is the minimum pressure required to initiate

gel flow through the conduit. **Figure 6-5** illustrates the relationship between the threshold pressure and the particle opening ratio. Strong gel requires a higher threshold pressure than weak gel in order for it to pass through an opening. The result obtained agrees with Seright (1997, 1998) who observed that some threshold pressure was required before the gel would extrude through a given opening size. The data also suggest that when the particle opening ratio exceeded two, the threshold pressure for both strong and weak gel increased much less compared to when the ratio was below two. This may have occurred for two reasons. First, the swollen particle dehydration during extrusion process may have reduced the size of the particles as the ratio increased. Secondly, the gel particles broke into small pieces, which may lead to smaller increases in the threshold pressure with increasing particle opening ratio.

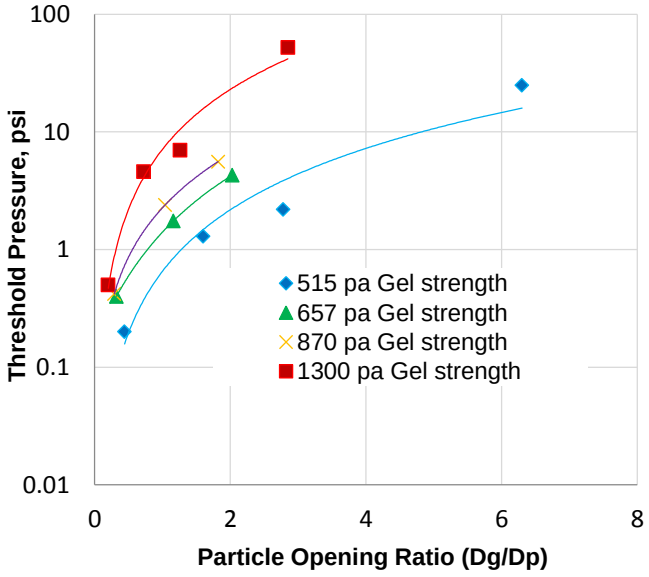

Figure 6-5—Effect of particle opening ratio on threshold pressure.

6.6.5 Stabilized Gel Injection Pressure vs Particle Opening Ratio

After the PPGs passed through the conduit, gel was injected continuously until the injection pressure stabilized. The injection pressure of the stable gel was measured as a

function of the gel strength and particle opening ratio, as shown in **Figure 6-6**. The results show that the stable injection pressure increased with the gel strength and particle opening ratio. The gel strength had a significant effect on the stability of the injection pressure, more than did the particle opening ratio. The gel injection pressure increased by around ten times (100 to 1320 psi) when the gel strength approximately doubled from 515 to 1300 pa. The injection pressure only tripled (191.7 to 590 psi) when the particle opening ratio approximately doubled from 0.72 to 1.26 at the gel strength of 1300 pa.

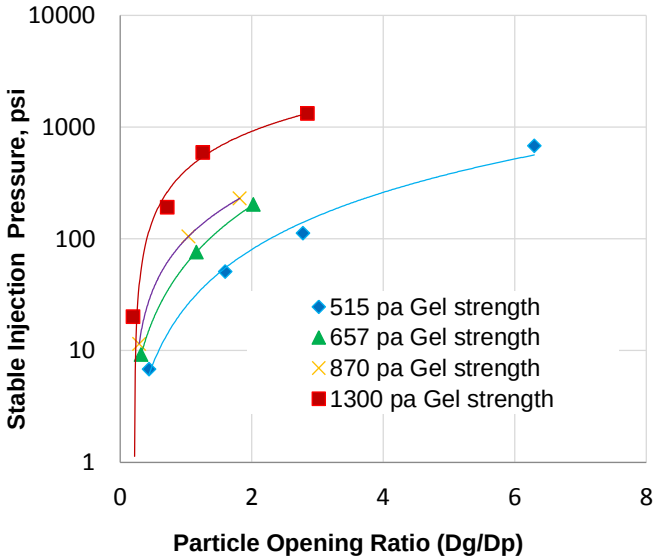

Figure 6-6—Stabilized injection pressure as a function of particle opening ratio and gel strength.

6.6.7 Correlation Models

Having correlation models that can predict the resistance factor (apparent viscosity) and stabilized injection pressure for PPGs during gel treatments is important to quantify gel transport process. Such models not only can be inserted into a simulator to yield better predictions of PPG performance, but also can provide results more quickly, as conducting all of these experiments in the lab would be time consuming and would require a great amount of effort to achieve reliable results.

6.6.7.1 PPG resistance factor model.

Polymer or polymer gel viscosity is often expressed as a function of shear rate; therefore, we tried to correlate the resistance factor with shear rate. In the paper, we use the maximum shear rate at the pore wall to obtain shear rate values and the equation is given as follows (Zaitoun et al., 2012):

$$\gamma = 8v/D \quad \text{..... (6.2)}$$

where γ is the shear rate, v is the superficial velocity, and D is the conduit inner diameter.

The data in **Figure 6-4** was reorganized to **Figure 6-7** after converting velocity to shear rate. It can be seen that all data is in the same line for the particle prepared by the same concentration brine even though their particle opening ratios are different, indicating that Fr was independent of conduit inner diameter. This phenomenon is not very surprising because we know the polymer gel viscosity is a function of shear rate but does not depend on the gap between cylinder and spindle when we measure the bulk gel viscosity.

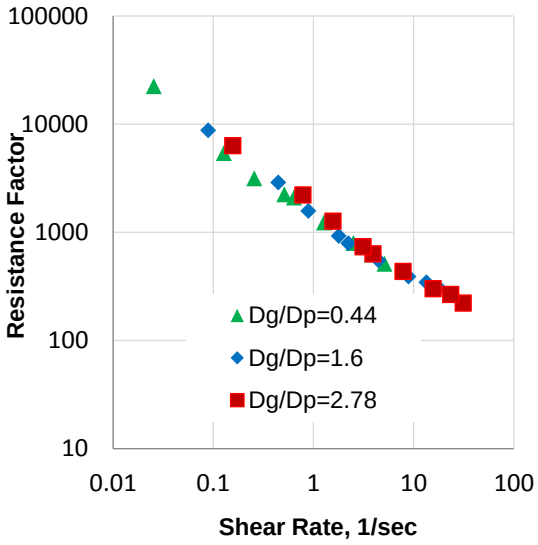

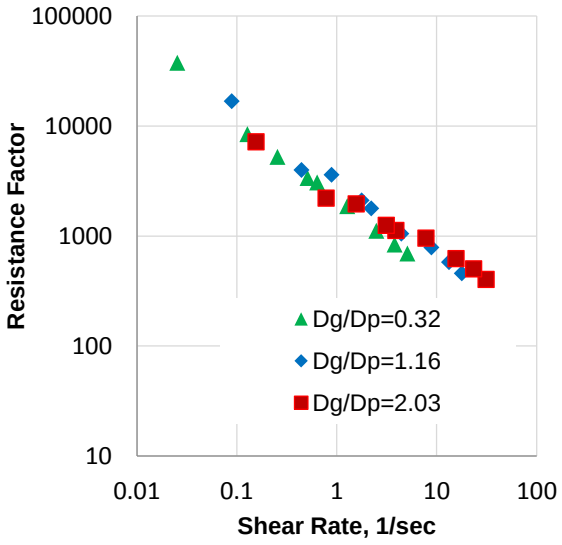

0.05% brine concentration

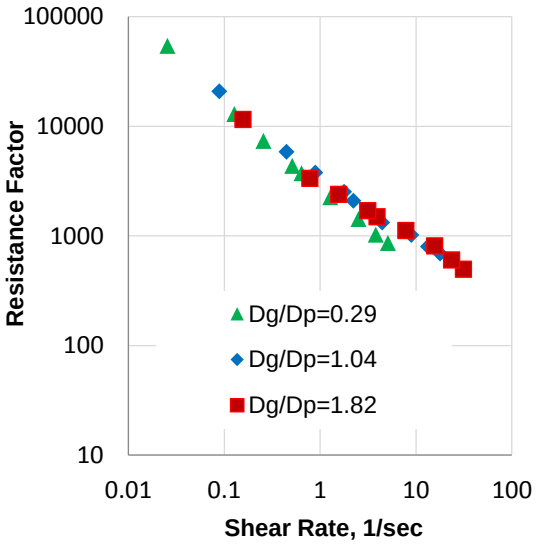

0.25% brine concntrations

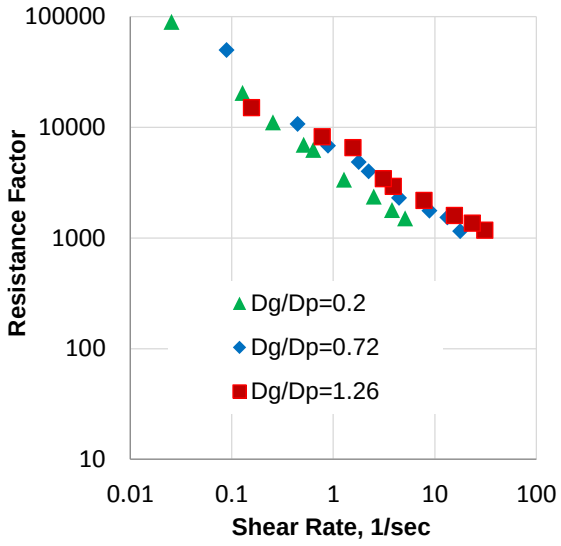

1% brine concentration

10% brine concentration

Figure 6-7—Resistance factor for gel swollen in brine concentrations as a function of both shear rate and particle opening ratio.

A good fit was noticed using power law equation for resistance factor results plotted against shear rate. The fit is even better with a particle opening ratio greater than one or equal to one. Therefore, the developed model will includes the data for particle opening ratios greater than and equal to one. The resistance factor obtained as a function of the shear rate can be expressed as:

$$Fr = M\,\gamma^{-E} \quad \text{.....(6.3)}$$

where M and E are constant coefficients related to brine concentration and particle opening ratio, both were obtained from gel extrusion through conduits. **Table 6.3** summarizes the results obtained for both M and E for each brine concentration.

Table 6-3—Fitting equations for resistance factor for each brine concentration.

Brine concentration, %NaCl	*M*	*E*	R^2
0.05	1618.4	0.62	0.98
0.25	2917.9	0.61	0.97
1	3643.7	0.596	0.98
10	7128.5	0.588	0.96

To develop a general correlation that can be used to predict the resistance factor for all brine concentrations, both constant coefficients *M* and *E* need to be determined. **Table 6-3** indicates that *E* was not affected very much by brine concentration but M was strongly affected. To obtain these coefficients, both constants were plotted as a function of the brine concentration(*C*), as shown in **Figure 6-8.** Power-law equation was used again to obtain the proper fitting correlation for the coefficients.

The constant coefficient (*M*) was fitted with goodness of fit of 99%:

$$M = 3831.3\ C^{0.2709} \quad \text{..... (5.4)}$$

The constant coefficient (*E*) was fitted with goodness of fit of 96%:

$$E = 0.6001\ C^{-0.01} \quad \text{.....(5.5)}$$

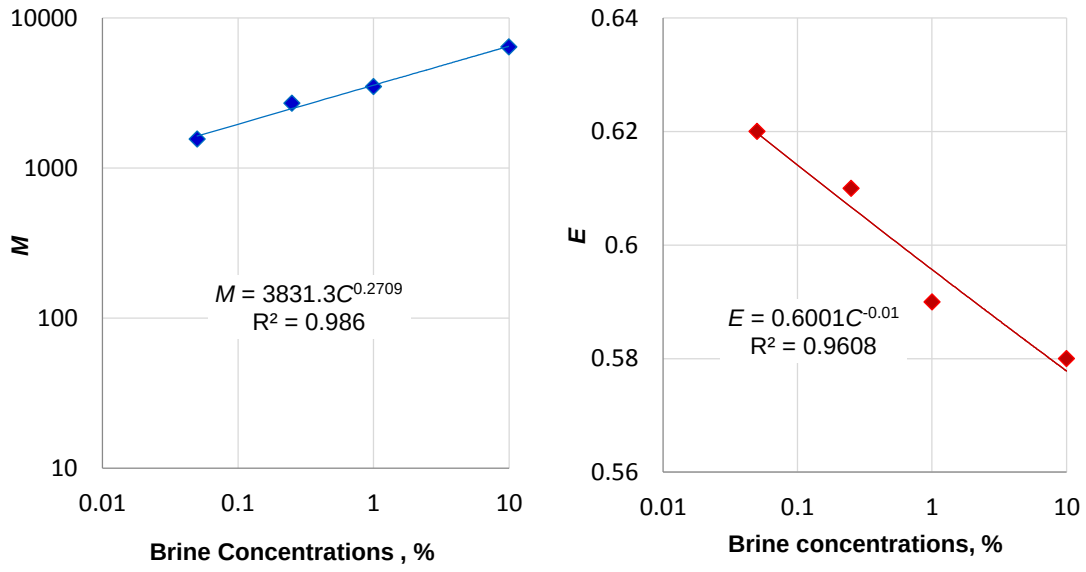

Figure 6-8—The constant coefficients as a function of brine concentration.

Then, the general form of the correlation (which can be used to predict the resistance factor in conduit systems) can be written as:

$$\mathrm{Fr} = 3831.3\, C^{0.2709}\gamma^{-0.6001\, C^{-0.01}} \quad \text{.....(6.6)}$$

The obtained correlation also can be expressed as a function of the gel strength. **Table 6.1** clearly indicates that the gel strength depends heavily on the brine concentrations; the following correlation was fitted with goodness of fit of 99.7% to expresses the relationship between brine concentrations and gel strength:

$$C = 3\times10^{-17}\, G'^{\,5.6391} \quad \text{..... (5.7)}$$

Then, the correlation can be modified to be a function of gel strength (G´):

$$\mathrm{Fr} = 3831.3 \times (3\times10^{-17}\, G'^{5.6391})^{0.2709}\gamma^{-0.6001\,(3\times10^{-17}\, G'^{\,5.6391})^{-0.01}} \text{.(5.8)}$$

External data that were not included in the newly developed model were used to not only validate but also ensure the accuracy of the correlation**. Figure 6.9** provides a comparison between the Fr obtained from the new model and the measured data obtained from lab measurements. The Fr measurements from external lab experiments were for gel extruded through different particle opening ratios ranging from 1.02 to 6.29. There was good agreement over the entire resistance factor, which indicates that the newly developed correlation can be used successfully to predict the resistance factor of PPGs extruded through open conduit systems.

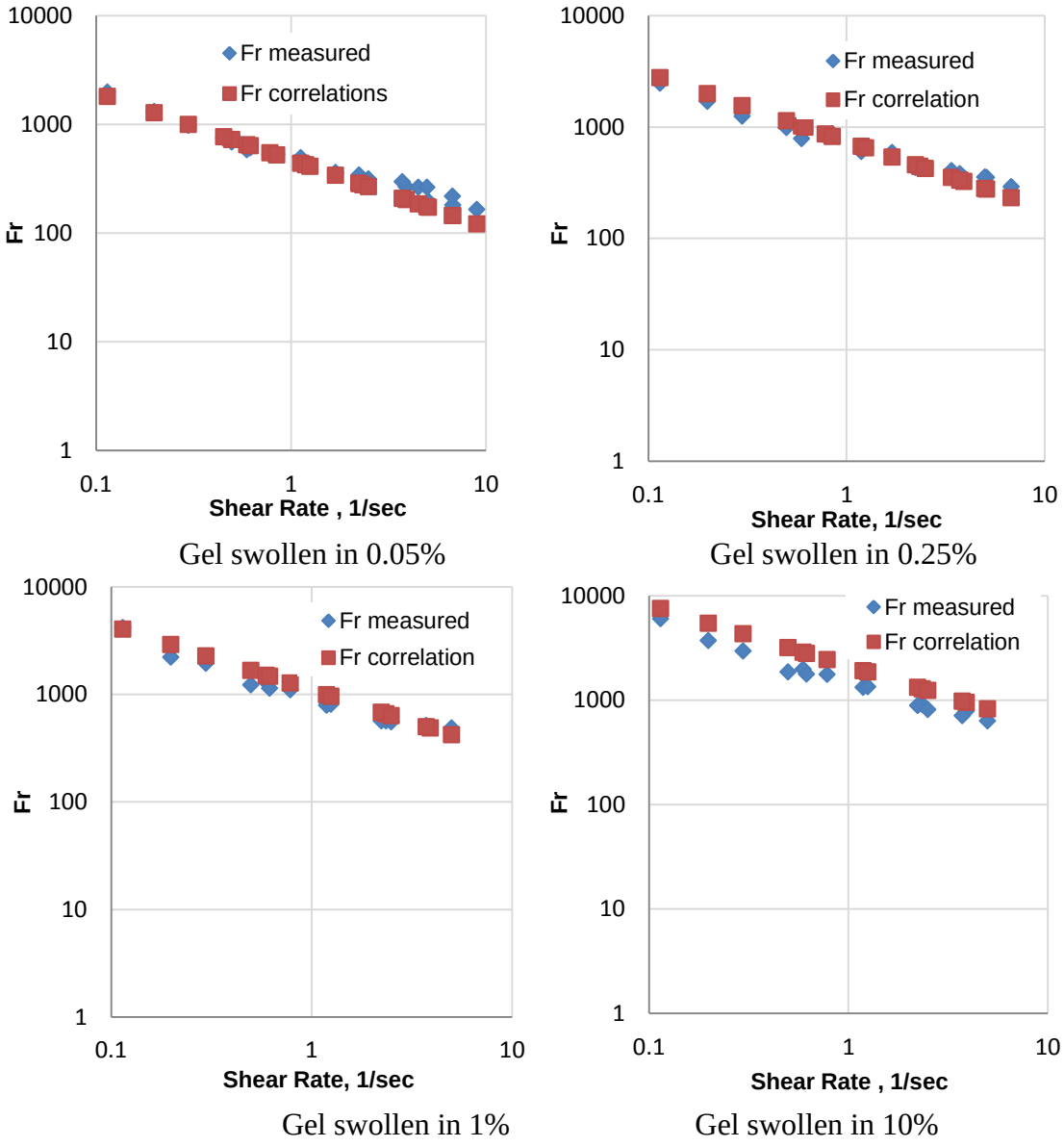

Figure 6-9—Comparison between resistance factors measured in the lab and data obtained from the correlations.

6.6.7.4 PPG stabilized injection pressure model.

The data in **Figure 6-6** were drawn in log-log scale as shown in **Figure 6-10**, and were fitted well using the following power law equation:

$$P_{inj} = a(Dg/Dp)^b \quad \text{..... (5.9)}$$

where P_{inj} is the initial stable injection pressure in psi, and a and b are coefficient factors obtained for PPGs extruded through different particle opening ratios. **Table 6-4** shows the results obtained for these two factors for the different gel strengths.

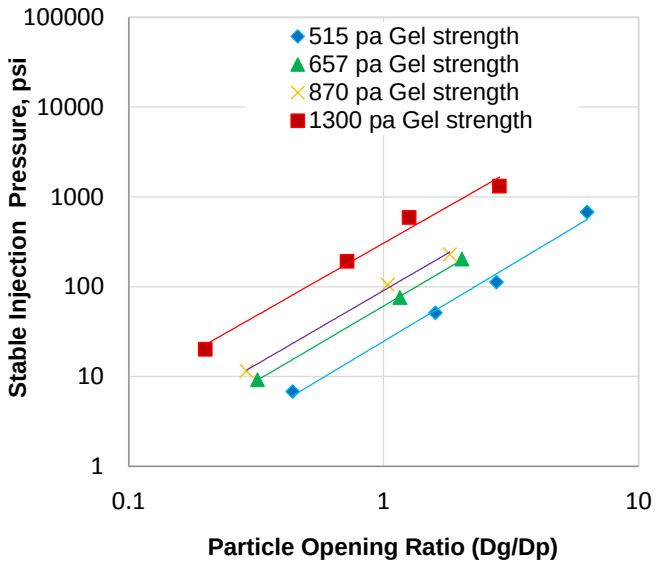

Figure 6-10—Stable injection pressure as a function of particle opening ratio and gel strength.

With fitting equations obtained for the various particle opening ratios and gel strengths, PPG's stable injection pressure can be evaluated quantitatively to obtain a better prediction of the PPG injection pressure in conduit systems.

Table 6-4—Fitting equations for stable injection pressure.

Gel strength, pa	*a*	*b*	R^2
515	24.669	1.6987	0.99
657	61.055	1.6686	0.99
870	90.713	1.6484	0.99
1300	305.49	1.6156	0.98

To develop a general correlation that can predict the PPG's stable injection pressure for all gel strengths, another regression analysis was performed to correlate these two coefficients with the gel strengths, as shown in **Figure 6.11**. Then, *a* and *b* were substituted into the new general fitting equations.

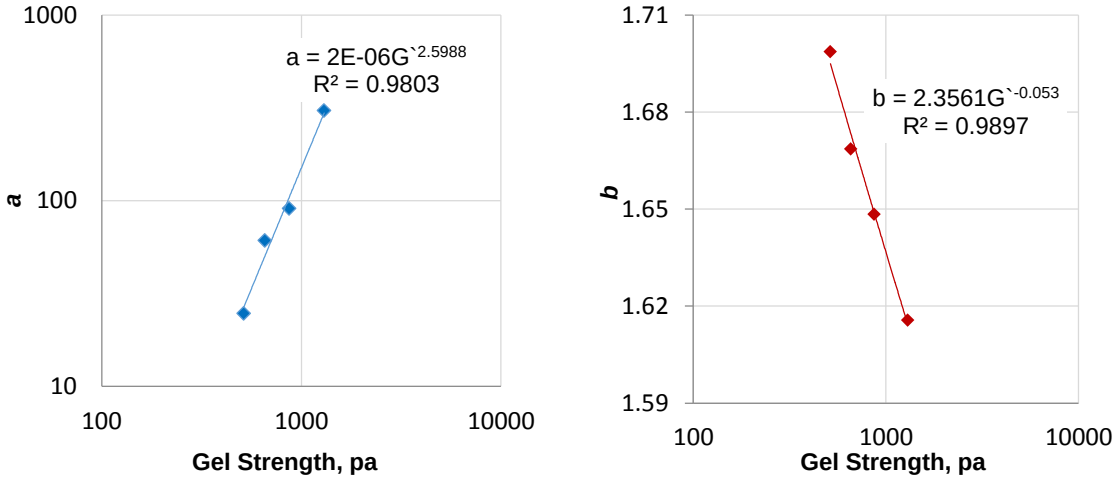

Figure 6-11—The correlation coefficients (*a*) and (*b*) as a function of gel strength.

Finally, the general form of the new correlation that can be used to predict the initial stable injection pressure in conduit systems can be written as:

$$P_{inj} = 2 \times 10^{-6}\, G'^{2.5988}\, (Dg/Dp)^{2.3561\, G'^{-0.053}} \quad \text{..... (5.10)}$$

A validation test, as described in **Table 6-5**, was performed to ensure the accuracy of the new model. Various ranges of particle opening ratios were not included in the developed correlation used to test the model. The initial injection pressures measured in the lab for four gel strengths in different particle opening ratios were compared with values obtained from the correlation. The relative error indicates that the new correlation can be used with relatively negligible error to determine the stable injection pressure for gel strengths of 515, 657, and 870 pa. While the correlation can be used for gel strength of 1300 pa, the relative error is higher.

Table 6-5—New developed model validation for initial stable injection pressure.

Gel strength (pa)	Dg/Dp	Initial stable injection pressure (psi)		Relative Error (%)
		Measured	Calculated	
515	2.78	120	125	-4.1
	4.74	326	311	4.6
	3.49	184.3	184.9	-0.3
657	2.03	153	137	10.4
	3.46	375	334	10.9
870	1.82	218	233.5	-7.1
	2.29	339.5	340.8	0.38
1300	0.72	183.3	145	20.8
	1.58	440	517	-17.5

6.6.8 Resistance to Water Flow after Gel Placement in Conduits

After gel placement within the conduit system, brine was injected with different velocities, from low to high, to extrude the gel inside a conduit. In this way, four parameters were systematically obtained to characterize particle blocking behavior to water. These four sequence parameters include the pressure gradient peak, critical water breakthrough pressure, residual resistance factor, and plugging efficiency.

6.6.8.1 Pressure gradient peak (PGP)

PGP is defined as the pressure gradient at which the gel began to move and washout from the conduit as a result of brine injection. **Figure 6-12** provides an example of the brine injection pressure gradient at each section through the gel swollen in 0.05% concentration brine within a conduit inner diameter of 10.922 mm. Brine was injected through the gel at a velocity of 9.89 ft/day. Gel washout and water movement were measured by observing the pressure changes in all three sections and monitoring both the effluent produced gel and brine. In all experiments, we noticed that the injection pressure gradient in all sections increased sharply until reaching a certain peak, at which point it began to decline. This peak indicates the point at which gel failure and washout began to occur in each section (Seright, 2003). After each peak, the pressure gradient declined significantly before becoming stable in all sections. In the first section, the peak occurred at 1.85 psi/ft after 0.03 PV of brine was injected. While in the second section, the

pressure gradient peak occurred at 1.05 psi/ft after injecting 0.04 PV of brine. In the last section, the peak occurred at 0.53 psi/ft after injecting 0.05 PV of brine. Then after injecting 0.15PV of brine, the water pressure gradient in all sections became stable. The pressure gradient variations in all three sections exhibited a difference in gel movement and washout along the conduit systems.

The conduit inner diameter was checked visibly after the brine injection process was complete. For gel swollen in 0.05% NaCl, about 20% of gel was found remaining inside the conduit while for gel swollen in 10% NaCl about 70% of gel was found remaining inside the same conduit inner diameter size. This remaining volume suggests that the conduit was filled with a concentrated immobile gel.

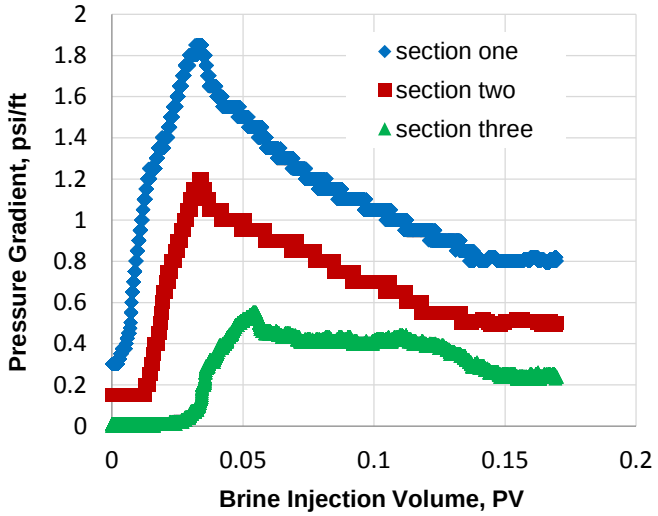

Figure 6-12—Brine injection gradient through gel in three sections for 10.922 mm conduit.

Table 6.6 provides a summary and comparison of the results obtained from the first section for all of the concentration brines. These results include the brine volume injected, as associated with its pressure gradients, for gels placed inside a conduit within an opening size of 3.0488 mm. The results suggest that gel swollen in high brine concentrations exhibit more stability inside the conduit than gel swollen in low brine concentrations when subjected to the same injection velocity.

Table 6-6—Brine concentrations effect on gel movement at 9.62 ft/day.

Brine concentration, %NaCl	Brine injected volume for peak, PV	Pressure gradient peak through brine injection, psi/ft
0.05	0.12	4.25
0.25	0.31	7.85
1	0.52	12.05
10	0.67	25.6

Table 6.7 summarizes the results obtained from the injection of brine through gel swollen in 10% brine for three conduit inner diameters. Differing from the results obtained in large conduit opening, these results indicate that gel washout began to occur in a small conduit inner diameter when both a high injection pressure gradient and large volume of water were applied. Gel washout began to occur through an opening of 1.752 mm when 1.17 PV of brine was injected and the pressure gradient reached 245.3 psi/ft. In contrast, the gel injected through a larger opening size (10.922 mm) began to move when 0.16 PV of brine was injected and the pressure gradient was only 4.9 psi/ft. These findings indicate that less gel movement occurred in smaller conduit diameters than in larger conduit diameters.

Table 6-7—Conduit diameter effect on gel extrusion for gel swollen in 10% NaCl.

Inner diameter, mm	Brine injected volume for peak, PV	Pressure gradient peak through water injection, psi/ft
10.922	0.16	4.9
3.048	0.67	25.6
1.752	1.17	245.3

6.6.8.2 Critical water breakthrough pressure (PCW).

PCW is defined as the pressure at which the first drop of water can be seen from the outlet. **Figure 6-13** provides information about this variable as a function of both the brine concentration and conduit inner diameter. The small water breakthrough pressure indicates that water could start propagate easily through the gel. This result suggests that as the gel became stronger (swollen in high brine concentration), the water breakthrough pressure increased. Differences in water breakthrough are clear when comparing weak gel (swollen in low brine concentrations) against strong gel. **Figure 5.13*a*** shows the

water breakthrough measurement for gel swollen in different concentration brines when gel was placed within a 3.0488 mm opening. When gel was swollen in 0.05% brine, water was able to pass through it at 8.8 psi. Water could not pass through gel swollen in 10% brine until the pressure reached 46 psi. **Figure 6.13*b*** shows the results obtained for water breakthrough through gel swollen in 0.05% brine concentration as a function of different conduit sizes. Water was less likely to pass through a smaller pore opening than a larger opening. Water passed through a 10.922 mm opening at a pressure of 2.1 psi, and through a 1.752 mm opening at a pressure of 60.2 psi.

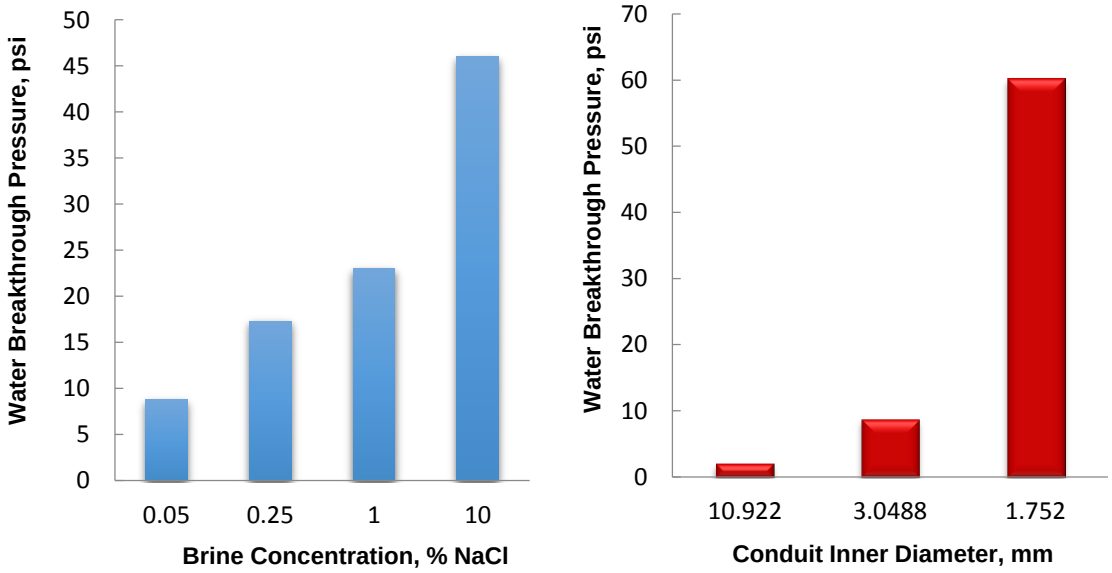

a. Conduit inner diameter 3.0488 mm *b*. Gel swollen in 0.05% brine concentration

Figure 6-13—Critical water breakthrough pressure as a function of brine concentration and conduit inner diameter.

6.6.8.4 Residual resistance factor and plugging efficiency (E).

F_{rrw} is defined as the ratio of water phase permeability before and after particle gel treatment and (E) refers to the percentage of permeability reduction, which can be calculated from the following equation $E\ (\%) = [1- (1 / F_{rrw})]*100$. The stabilized water injection pressures at different velocities were used to calculate F_{rrw} and E. **Figure 6-14**

shows the residual resistance factor as a function of brine concentration and brine velocity. F_{rrw} increased as the gel strength and conduit inner diameter increased. **Figure 6-15** shows the gel plugging efficiency as a function of the brine concentration and brine velocity. The PPG plugging efficiency increased when a strong gel was selected as a plugging agent for large conduit sizes. The results suggest that gel swollen in 10% brine can provide a 97% plugging, as compared to 76% plugging for gel swollen in 0.05% brine for a conduit with inner diameter of 1.752 mm. This percentage increased to 98% for the former and 93% for the latter when gel was placed into a large opening (10.922 mm). These findings indicate that the plugging efficiency of the PPG did not decrease significantly in spite of the gel washout occurring after gel placement.

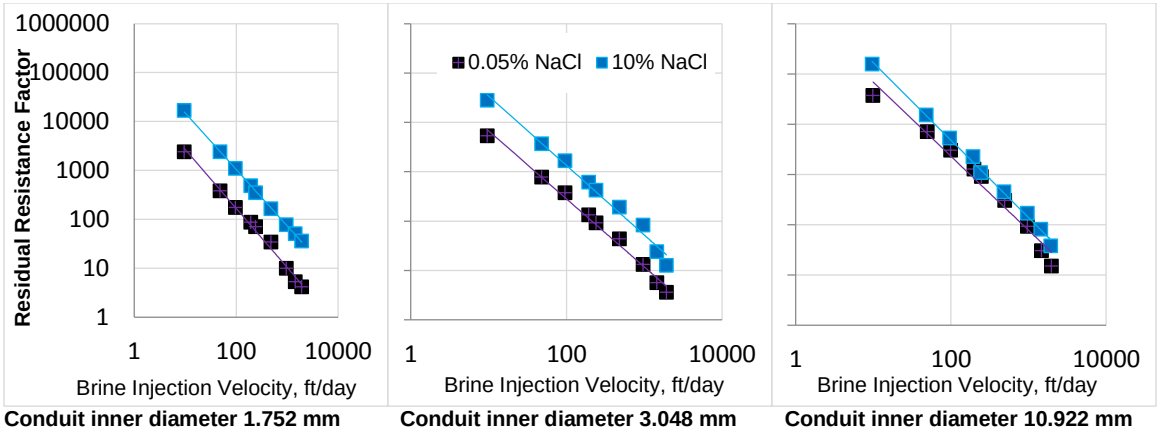

Figure 6-14—Residual resistance factor as a function of brine conc. and conduit inner diameter.

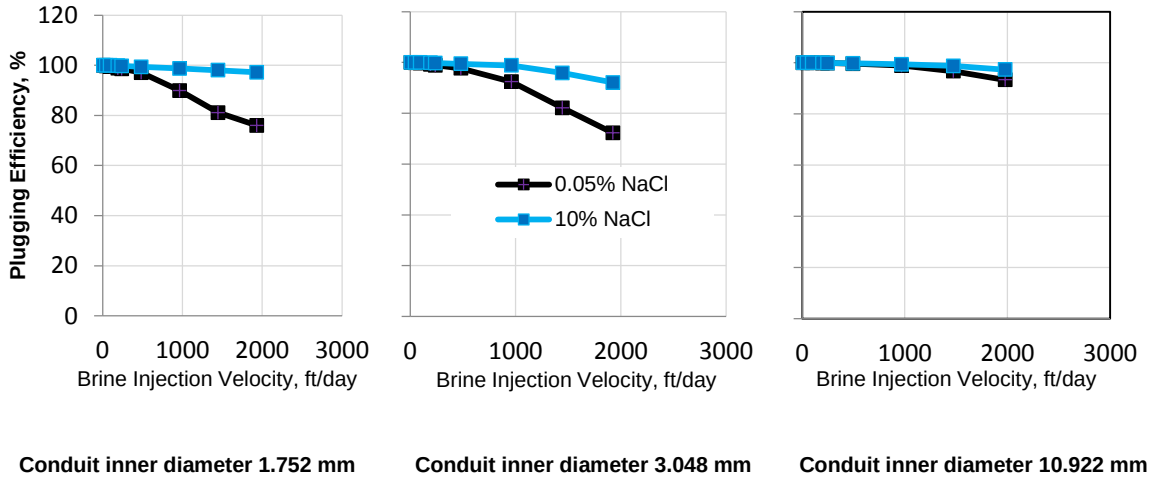

Figure 6-15—Plugging efficiency as a function of brine conc. and conduit inner diameter.

6.7 Discussion

When investigating particle injection, many researchers are interested in the passing ratio, which is the ratio of the particle size to the pore throat size at which the particle can pass through a constriction. For stiff, hard particle, this question is easy to answer. Extensive experimental results have shown that stiff particles can pass through pore throats only if their particle sizes are less than 1/9 of the pore size. However, swollen gel particles are deformable and breakable, so they can pass through porous media much easier than stiff particles. Swollen gel particle transport mechanism through porous media exhibit different patterns of behavior (Bai et al., 2007). **Table 6-8** provides the ratio of particle size to opening size (D_g/D_p), as well as the particle size before and after extrusion. Weak particles still were able to transport through the opening when the D_g/D_p was as high as 6.3 but required a relatively high injection pressure gradient of 12.5 psi/ft in order to do so. These results are consistent with Seright (1997) where he observed that pressure gradient increased significantly with decreased tube diameter.

Table 6-8—Particle opening ratio measurements results.

Gel strength, Pa	Particle gel size before extrusion, mm	Pore opening size, mm	Dg/Dp	Gel particle size after extrusion, mm	Gel Particle size decrease, %	Gel threshold pressure gradient, psi/ft	Gel Injection stable pressure, psi
515	4.88	10.922	0.44	3.57	26.8	0.1	6.8
		3.048	1.60	2.58	47.13	0.65	51
		1.752	2.78	2.391	51	1.1	112
		0.774	6.3	0.902	81.51	12.5	680
657	3.56	10.922	0.32	2.90	18.5	0.2	9.2
		3.048	1.16	2.17	39.04	0.85	76
		1.752	2.03	2.19	38.4	2.1	203
870	3.2	10.922	0.29	2.30	28.1	0.21	11.5
		3.048	1.04	1.99	37.81	1.2	105
		1.752	1.82	1.87	41.5	2.8	230
1300	2.21	10.922	0.20	1.945	11.99	0.25	20.1
		3.048	0.72	1.808	18.19	2.3	191.7
		1.752	1.26	1.923	12.98	3.5	590
		0.774	2.85	1.73	21.7	26.2	1320

The results shown in **Table 6-8** indicate that gel particle size was reduced after extrusion when Dg/Dp larger than, equal to, and even smaller than one. **Figure 6-16** shows particle sizes measurement before and after extrusion for the sample with gel strength of 515 pa. The weak gel particles experienced a significant decrease in particle size, up to 81.5%, when they moved through conduit with a 0.774 mm opening for D_g/D_p equal to 6.3. However, a strong gel decreased only by 21.7% when moving through the same conduit size but with Dg/Dp equal to 2.85. Based on previous knowledge (Bai et al., 2007), this particle size reduction could be explained by two reasons: breakdown, dehydration or both. To determine if the particle size reduction was caused by gel dehydration, we collected effluent particle gel samples from 3.048 mm conduit, where D_g/D_p have smaller than and equal to one, measured their strength and also placed them in the same concentration brine to observe their re-swelling. **Figure 6-17** shows how much the gel volume increased at different injection rates for four different strength gels. The results show that the weakest particles can regain 50% of water, while the strong gels can regain only approximately 20% of water, indicating that weak gel can be dehydrated

more than strong gel during conformance control treatments. In another words, the weakest particles shrunk 50% of its original volume while the strongest one shrunk 20% when they passed through the conduit. The strength measurement taken after extrusion, shown in **Figure 6-18** also indicates that the gel became more concentrated due to water loss from its cluster. When we compared the significant reduction in particle size to the gel particle volume shrunk, we observed that gel particle size reduction was caused by both particle breakdown and dehydration.

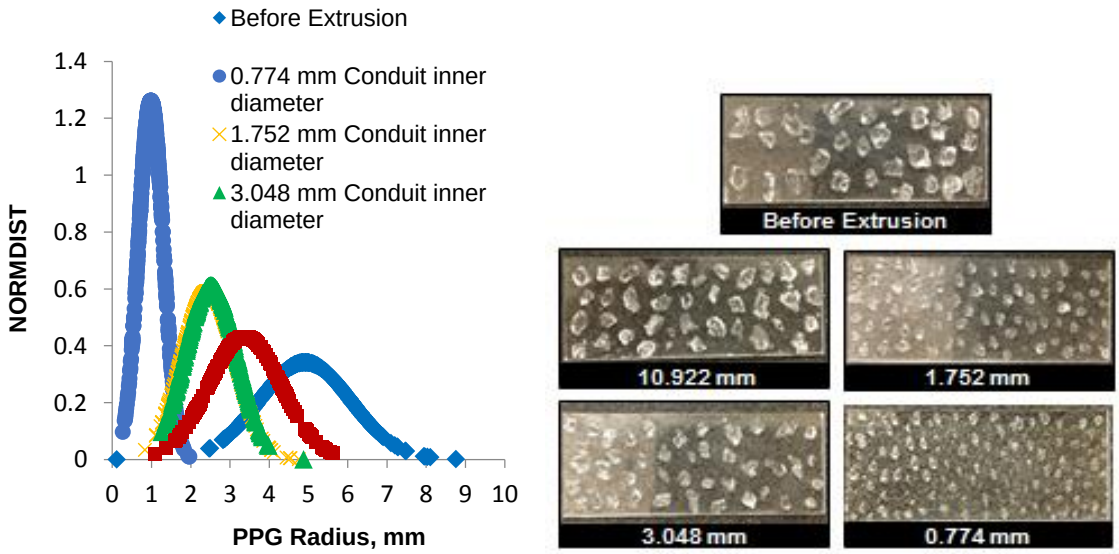

Figure 6-16—PPG size distributions and images for gel with strength of 515 pa before and after extrusion.

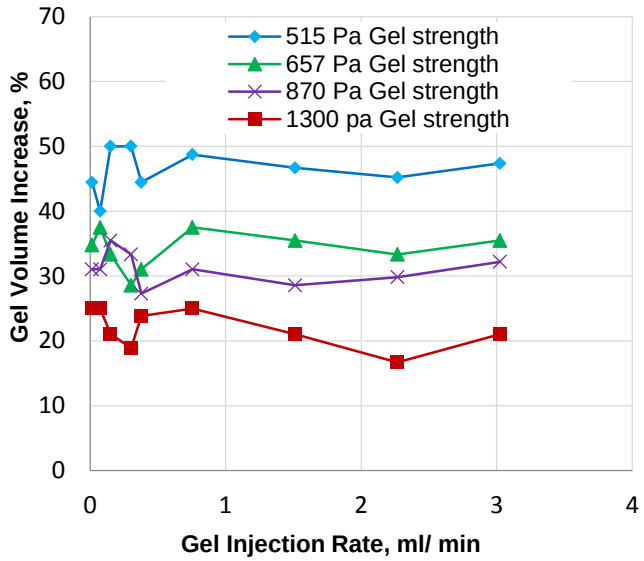

Figure 6-17—Particle volume increased after soaking in same brine.

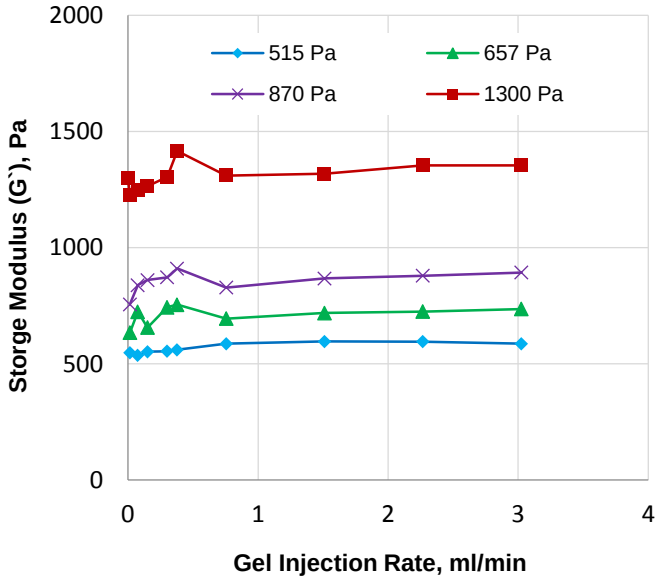

Figure 6-18—Particle storage moduli (G`) after extrusion

6.8 Summary and Conclusions

A number of factors that affect PPG extrusion and blocking efficiency through conduit systems were intensively examined in this study. The mechanisms associated

with gel propagation and placement, such as dehydration and gel washout, were investigated during the experiments. The following conclusions can be drawn from the research:

- PPG injection pressure increased as the brine concentration and injection velocity increased. This increase, however, after a certain velocity became unsubstantial.
- The resistance factor increased when the gel strength increased and/or when the conduit inner diameter becomes wider but it decreased if the velocity increased.
- Both the gel threshold pressure and the stable injection pressure increased as the particle opening ratio increased. Both pressures, however, would not increase significantly after a specific ratio. Additionally, the gel strength impacted the gel injection pressure more than did the particle opening ratio.
- Two new empirical correlation models were successfully developed to predict both PPG resistance factor and stable injection pressure.
- The resistance factor measurements are not dependent on the particle opening ratio when it is measured against shear rate.
- PPG blocking performance increased as the gel strength and conduit inner diameter increased. This finding reveals that the conduit size conductivity can significantly decrease if a strong gel is selected for the conformance treatment.
- Weak gels can be injected into large particle opening ratio with relative small increase in injection pressure compared to strong gels. Weak gels break into small sizes so it could pass through.
- Weak gels tend to dehydrate more than strong gels. The gel becomes stronger after the extrusion process, as a result of the dehydration mechanism.
- PPG size reduced during transportation through conduits due to dehydration and breakdown.

Section 7: Using Partially Open Fracture Model to Evaluate Disproportionate Permeability Reduction Effect

7.1 Summary

When gels are placed throughout fractures or conduits, water permeability decreases significantly and water flow into the well is minimized. However, if oil is produced from reservoir through fractures or conduits, oil permeability will not be significantly decreased. This work will provide a better understanding of preformed particle gel performance when two phase fluids propagate through fractures filled with gel.

7.2 Objectives

This work intends to examine in-depth several factors such as particle size, gel strength, and fracture width effects on Disproportionate Permeability Reduction (DPR) and gel extrusion through fracture systems.

- Alternate banks of both brine and oil were used to determine the extent to which PPGs can reduce water permeability more than oil permeability within fracture systems.
- Examine the effect of brine concentrations, particle gel sizes, and injection flow rates on PPG injection pressure.
- Determine the residual resistance factor (*Frr*) for oil and water during the different multiple injection cycles.
- Evaluate different DPR mechanisms using PPG as divergent materials.

7.3 Experimental Description

7.3.1 Preformed Particle Gel

Super-absorbent polymer (SAP) was used as a PPG sample. PPG is comprised primarily of potassium salts with crosslinked polyacrylic acid / polyacrylamide copolymer.

Two sizes of particle gels, 20-30 and 100-120 mesh size, were selected for the experiments. **Table 7-1** illustrates the size distribution of the PPG before swelling, as determined by a sieving test.

Table 7-1—Size distribution of particle gel.

Sieves (mesh)	Size (microns)
20-30	850-600
100-120	150-125

7.3.2 Brine Concentrations and Oil Viscosities

Sodium chloride (NaCl) with four concentrations (0.05, 0.25, 1, and 10 wt% NaCl) was used to prepare the swelling gels. The brine concentration was selected carefully according to both the swelling ratio and the gel strength; the high-salinity brine resulted in high gel strength and a low swelling ratio. Two oils with viscosities of 37 and 195cp were used in the study.

7.3.3 Description of Tubes.

In this experiment, stainless steel tubes with internal diameters of 0.12 inches and 0.069 inches were used to represent fractures. These tubes were originally 20 ft long and were cut into 5 ft in lengths.

7.4 Experimental Setup

Figure 7-1 presents the experimental apparatus, which consisted of a syringe pump used to inject brine, gel, and oil through the accumulator into a fracture model. The fracture model was essentially five long tubes with two different internal diameters. A check valve was used at the inlet of the fracture model to ensure that no back flow of gel occurred when pressure was released from the pump. A 0.5-micron filter was installed at the outlet of the tube to ensure that no gel washout occurred during either the brine or the oil injection process. Pressure sensors were connected at both the inlet and the outlet to measure the differential pressure across the gel.

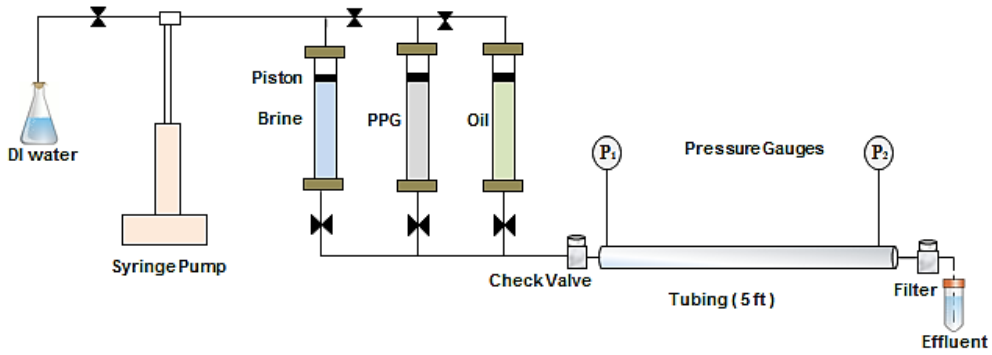

Figure 7-1—Schematic diagram of PPG placement in fractures.

7.5 Experimental Procedures

First, we obtained the effects of brine concentrations (gel strength), particle size, and fracture width on the gel extrusion and DPR behavior through fractures. PPGs with mesh sizes of 20-30 swollen in 0.05%, 0.25%, 1%, and 10% brine solution were extruded through tubes with internal diameters of 0.069 inches. From high to low, nine flow rates, 3.0246, 2.2684, 1.5123, 0.7561, 0.3781, 0.3025, 0.1512, 0.0756, and 0.0151ml/min, were used to extrude the PPG. Stable PPG injection pressures were achieved and resistance factors determined for each flow rate. Then, a filter was installed at the outlet, and PPG was injected again and compressed through the tube until the injection pressure reached 100 psi. The same type of brine used to prepare the swollen PPG then was injected. Oil with a 37 cp viscosity was injected after each injected brine concentration. Residual resistance factors for both water and oil were determined during the experiments.

The second objective of this study was to understand gel performance under a sequence of brine and oil cycles. PPGs with mesh sizes of 20-30 swollen in 1% NaCl were extruded through a tube with a diameter of 0.12 inches using the nine different flow rates. Stable pressure was achieved for each gel injection rate. After a filter was installed and the PPG was compressed, brine and oil cycles were alternated in sequence. Both brine and oil were injected through the tube model with seven flow rates starting from

low to high: 0.0151, 0.0756, 0.1512, 0.3025, 0.3781, 0.7561, and 1.5123 ml/ min. This sequence can be summarized in the following steps:

1) Concentration of 1% NaCl (first cycle) was injected with seven flow rates through PPG-filled tubes. Stable pressure was achieved for each flow rate, and the residual resistance factors for water (F_{rrw}) were determined.
2) Oil with a 37 cp viscosity was injected to displace water inside the gel. Residual resistance factors for oil (*Frro*) were obtained for the seven flow rates.
3) Oil with a 195 cp viscosity was injected, and the F_{rro} were again obtained for each flow rate.
4) 1% NaCl brine (second cycle) was injected after the injection of oils with same flow rates, and F_{rrw} was calculated.
5) After the second cycle of brine injection, oil with a 37 cp viscosity was injected again to obtain the F_{rro}.
6) High-viscosity (195 cp) oil was injected, and the F_{rro} were determined.
7) Finally, 1% NaCl brine (third cycle) was injected in the same model with the same flow rates to determine the F_{rrw}.

The above seven steps were repeated using PPG with a mesh size of 100-120 swollen in the same NaCl concentrations (1%).

7.6 Results and Analysis

Data showing the effects of the gel particle size, gel strength, and fracture width on gel extrusions and placements were obtained. These data include the PPG injection pressure, resistance factor, residual resistance factors, and results for the brine and oil cycles.

7.6.1 PPG Injections and Residual Resistance Factor

This section presents and discusses the results obtained for the injection pressure and residual resistance factors for the effects of gel strength, particle gel size, and fracture width.

7.6.1.1 Stabilized PPG injection pressure versus injection rate

The stable pressure measurements obtained during the gel extrusion process were recorded and plotted against the PPG injection flow rate for each different gel strength and particle size. **Figure 7-2 *a*** illustrates the stable injection pressure of the gels for gel storage moduli of 515, 657, 870, and 1300 pa injected through a tube with an internal diameter of 0.069 inches. **Figure 7-2 *b*** presents the measurements taken for both 20-30 mesh size and 100-120 mesh size injected through a fracture 0.12 inches wide. The results show that the stable injection pressure for each flow rate increased as the gel strength and particle size increased. For instance, a particle gel with a 100-120 mesh size had a stable pressure of 65 psi at a gel injection rate of 3.0256 ml/min, while a particle gel with a 20-30 mesh size had a stable pressure of 71 psi at the same injection flow rate. This increase in pressure occurred because larger particles are more resistant to flow through fractures than smaller particles. This behavior, however, was most pronounced at low flow rates. This finding could imply that at a high injection rate, the stable pressure for both particle sizes is an independent factor.

The stable pressure for all of the gel strengths and particle sizes increased significantly as the injection rate increased. Though to an insignificant extent, the pressure continued to build up as the PPG injection rate increased. The results also indicate that as the gel strength increased, reaching the stable pressure for each injection rate required more time.

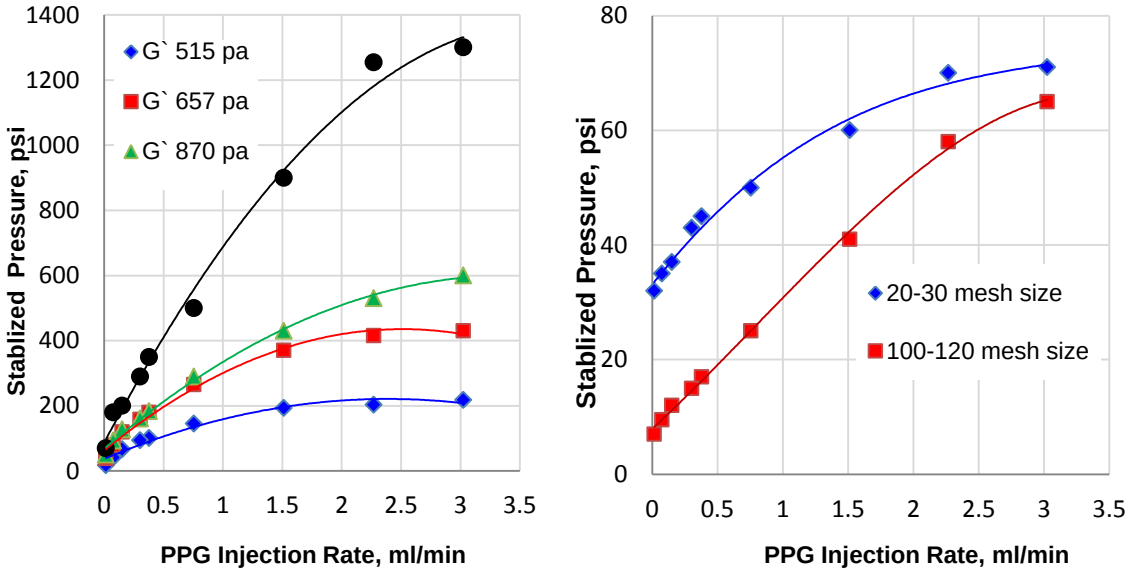

(a) 20-30 mesh size PPG *(b)* PPG swollen in 1% NaCl

Figure 7-2—Stable pressures versus injection rate for gel strengths and particle sizes.

7.6.1.2 **Resistance factor calculation.**

PPG is a shear thinning or pseudo plastic material. The resistance factor (Fr) is used to measure PPG resistance to flow when it extrudes through fractures. Similar to the porous media experiment, Fr was estimated from the injectivity index and geometry of the fracture. It can be defined as the ratio of the particle gel injection pressure drop to the brine injection pressure drop at the same flow rate.

The resistance factor was calculated during the gel extrusion process against the velocity for each different gel strength and particle size. **Figures 7-3*a*** and **7-3*b*** illustrate the resistance factor results obtained for different gel strengths and gel particle sizes, respectively. The PPG resistance factor increased as the gel strength and gel particle size increased. For example, at a velocity of 29 ft/day, the Fr of gel strengths 515, 657, 870, and 1300 pa were 74981, 158294, 208282, and 291595, respectively. The Fr determined for each PPG strength decreased sharply as the superficial velocity increased. For

instance, the resistance factor for 100-120 mesh size was 8750 at a velocity of 10 ft/day. When the velocity was doubled, the resistance factor decreased substantially to 1683.

The data in **Figure 7-3** were fitted according to the power law equations. **Table 7-2** lists the fitting equations for the resistance factors obtained for both effects. The elasticity index (*n*) measured for the effects of gel strength were plotted against the storage moduli, as presented in **Figure 7-4**. As the gel strength increased, the gel elastic value decreased.

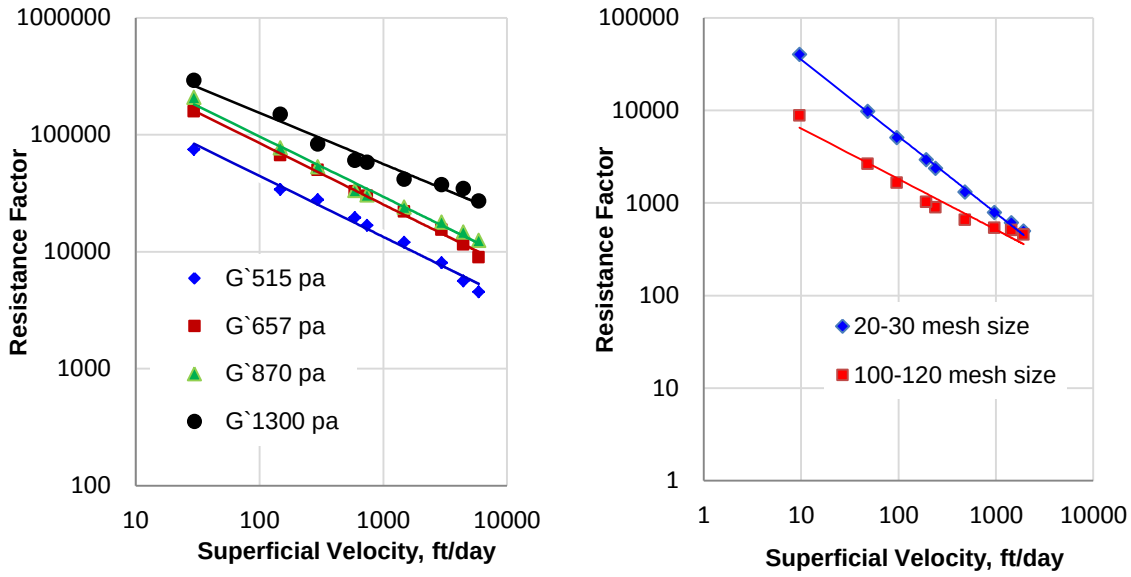

(a) 20-30 mesh size PPG *(b)* PPG swollen in 1 % NaCl

Figure 7-3—Resistance factor calculated for both gel strength and gel particle size.

Table 7-2—Summary of fitting equations for resistance factor measurements.

Storage Moduli G´(Pa)	Particle Size(mesh)	Fitting Equations	Elasticity Index (*n*)	R^2
515	20-30	FR = 490150 u $^{-0.530}$	0.530	0.986
657		FR = 955622 u $^{-0.525}$	0.525	0.996
870		FR = 1E+06 u $^{-0.50}$	0.50	0.988
1300		FR = 1E+06 u $^{-0.437}$	0.437	0.981
870	20-30	FR = 238927 u $^{-0.829}$	0.829	0.997
	100-120	FR = 22514 u $^{-0.547}$	0.547	0.957

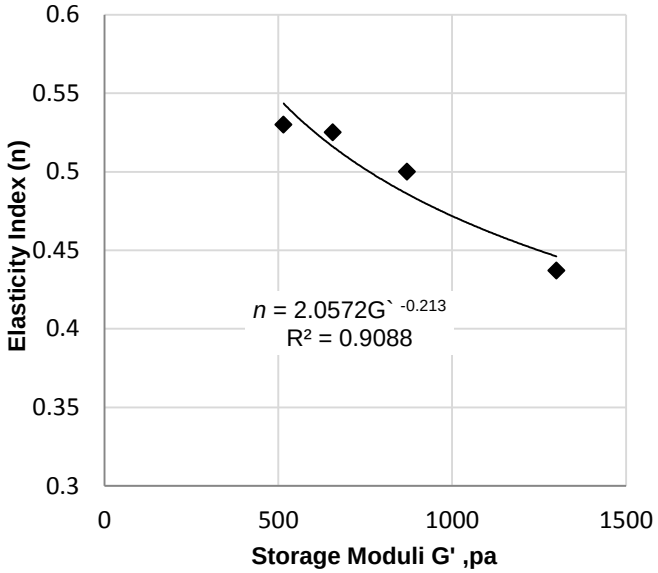

Figure 7-4—Elasticity index as a function of gel strengths.

7.6.1.4 **Residual resistance factor to brine and oil**

Residual resistance factors were determined by dividing the pressure drop of the injection of either brine or oil into the fracture after gel placement by the pressure drop of the injection of either brine or oil into the fracture before gel placement.

7.6.1.5.1 Effect of gel strength on DPR

Figure 7-5*a* illustrates the F_{rrw} determined for brine injected through different strength PPGs. The results indicate that the gel strength does affect the F_{rrw}; the F_{rrw} increased as the gel strength increased. As the gel strength increased from 515 pa to 1300 pa, the increase in the F_{rrw} became significant. After determining the F_{rrw}, oil was

injected through the same internal diameter with the same velocity to obtain the F_{rro}. **Figure 7-5 *b*** depicts the measurements of oil with a viscosity of 37 cp injected through swollen PPGs. The results indicate that the gel strength also affects the F_{rro}; the F_{rro} increased as the gel strength increased. For all of the gel strengths, the F_{rro} was less than the F_{rrw}.

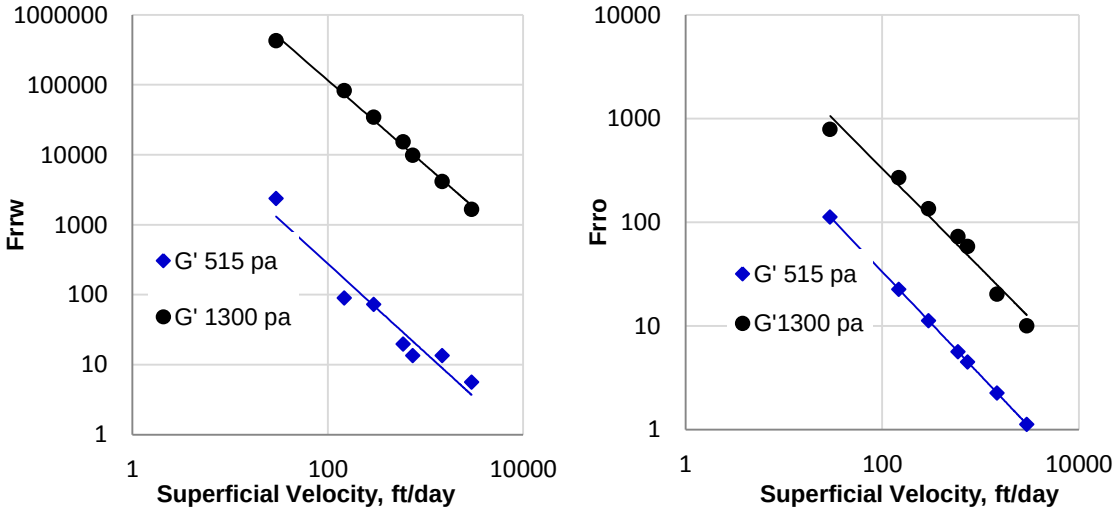

Figure 7-5—Residual resistance factor for brine and oil.

7.6.1.5.5 Effect of opening size on DPR

PPGs with a mesh size of 20-30 swollen in a 1% NaCl solution were used to observe the effect of the fracture width on the residual resistance factors. **Figure 7-6 *a*** and ***b*** presents the results obtained from injecting a 1% NaCl solution and 37 cp oil through gel placed in fractures 0.069 and 0.12 inches wide. These data suggest that F_{rrw} and F_{rro} increased as the fracture widened. F_{rro} was less than F_{rrw} regardless of the fracture width.

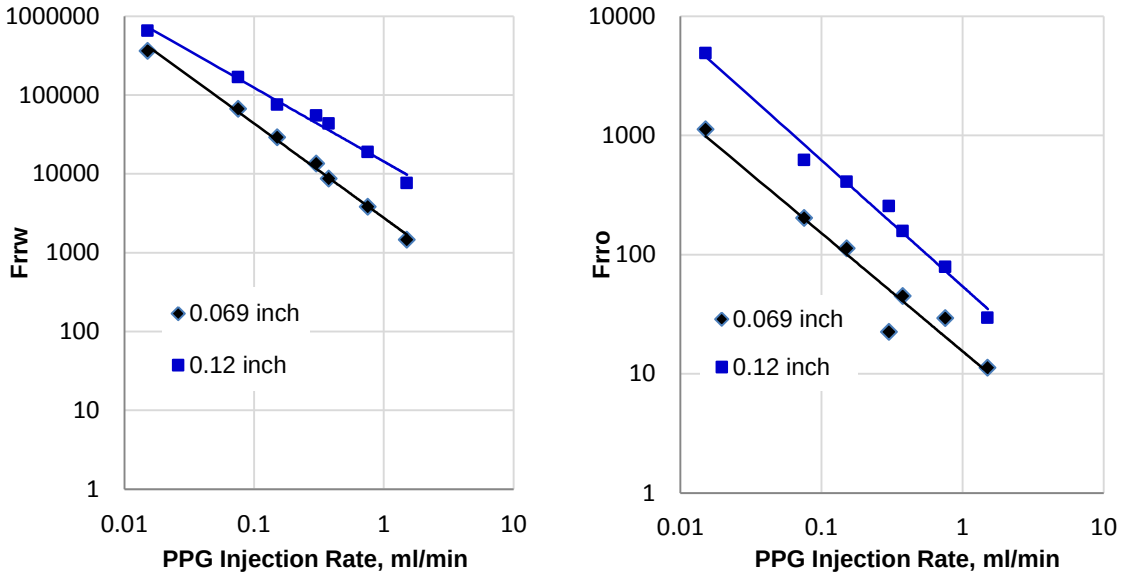

(a) Inject 1% brine *(b)* inject 37 cp oil

Figure 7-6—Residual resistance factor for brine and oil as a function of both flow rate and fracture width.

7.6.2 Brine and Oil Cycles Measurements

This section discusses the results obtained from injecting different cycles of brine and oils through gel-filled fractures. During these several cycles, the residual resistance factors to brine and oil for each cycle were determined to evaluate PPG performance.

Seven velocities were used to inject brine, and the stable pressure was observed at each. **Figure 7-7*a*** illustrates the F_{rrw} determined for the two particle sizes as a function of superficial velocity. The F_{rrw} for both particle sizes decreased as the velocity increased. This decrease was significant at a low velocity. For example, the F_{rrw} value at 100-120 mesh size decreased from almost 200,000 to 50,000 as the velocity increased from 10 to 50 ft/day. The results also suggest that the F_{rrw} was greater for larger than for smaller particle sizes.

After the F_{rrw} values were determined, oils with different viscosities (37 cp and 195 cp) were injected consecutively to determine the F_{rro}. **Figures 7-7*b*** and ***c*** illustrate the F_{rro} measurements for both particle sizes at different oil viscosities. Both figures

indicate that the F_{rro} determined for the two PPG mesh sizes decreased as the superficial velocity increased. The change in particle size does not appear to have a significant effect on the F_{rro} when compared to the first cycle of brine. For the oil with a viscosity of 37cp injected with a velocity of 10 ft/day, the F_{rro} measurements for both 20-30 mesh and 100-120 mesh particle sizes was 4900 and 3400, respectively. The results also indicate that the F_{rro} decreased as the oil viscosity (at the same given particle size) increased.

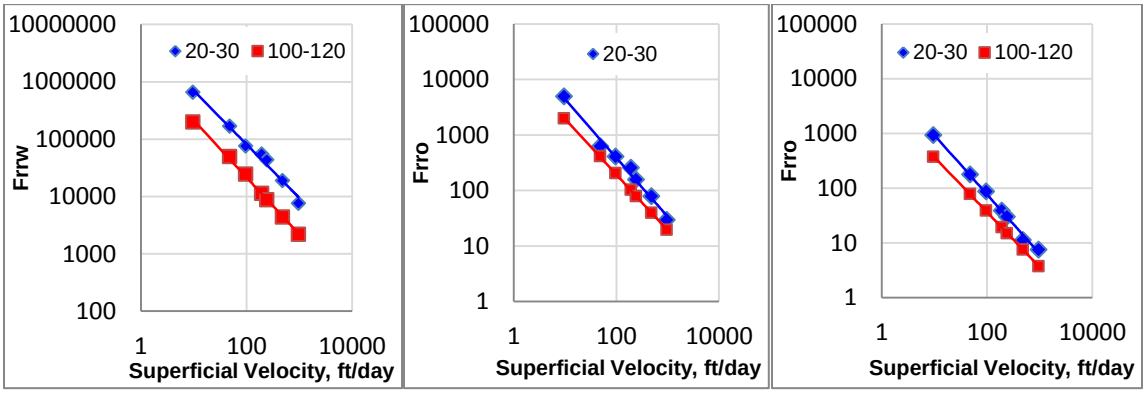

a). First 1% brine cycle *b).* First 37cp oil cycle *c).* First 195 cp oil cycle

Figure 7-7—*Frrw* and *Frro* determined for the first cycles.

The water loss (dehydration) from PPG and the injection pressure were both obtained during the process of injecting 37 cp oil through 20-30 mesh. **Figure 7-8** illustrates that a significant gel breakdown occurred during the oil injection process. Oil was injected at a constant flow rate of 0.3025 ml/min. The differential pressures (stable pressure) across the gel and the water loss from the gel were measured. The pressure began to build during the early stages of oil injection, eventually reaching 53 psi before falling and finally fluctuating between 3 and 7 psi. When compared to the first water cycle injection process, the differential pressure at the same flow rate (0.3025ml/min) was 29 psi. This significant drop in pressure suggests that gel could fail during the oil injection process.

Cumulative water loss data from the gel during the oil injection process were collected. **Figure 7-8** shows that the cumulative water loss from the gel began to build rapidly until the cumulative oil injected reached approximately 150 ml. The cumulative water loss then began to level off at 14 ml. We continued to inject oil until observing a stable pressure across the gel to ensure that no more water loss would occur.

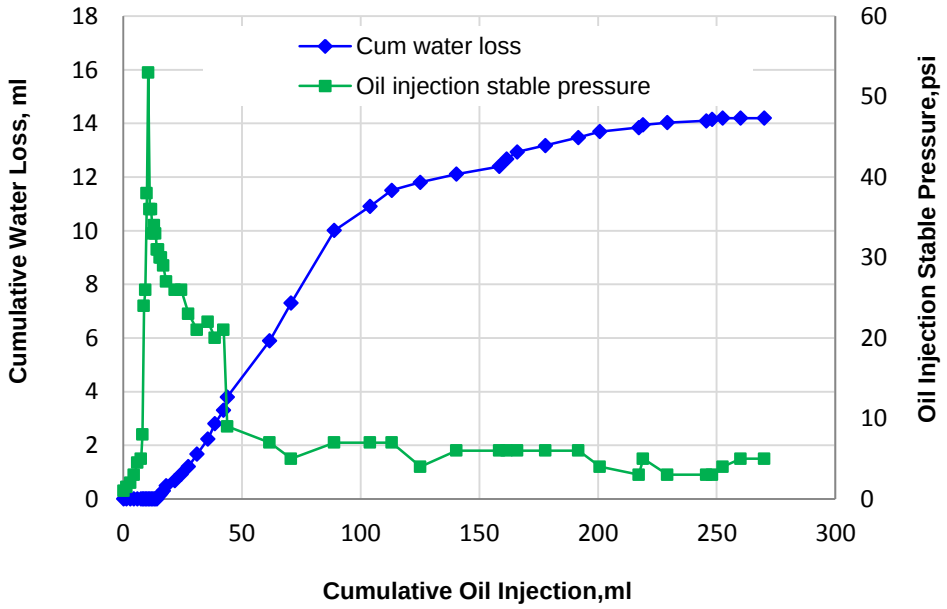

Figure 7-8—PPG breakdown during two-phase flow.

7.6.2.1 Frro and Frrw obtained from first cycle

Figure 7-9 depicts the comparison of the first cycle of 1% brine with the first cycle of two oil viscosities to identify the extent to which gel can reduce permeability to water more than to oil.

The results show that the residual resistance factor was much lower during oil injection than during water injection. At a velocity of 10 ft/day, the *Frrw* to water was 653414, and the *Frro* for oil with a viscosity of 195cp was 930, which means that the *Frro* decreased by around 700 times. A number of reasons may exist for this phenomenon; some of the reasons observed in our experiments will be explained in the Discussion section.

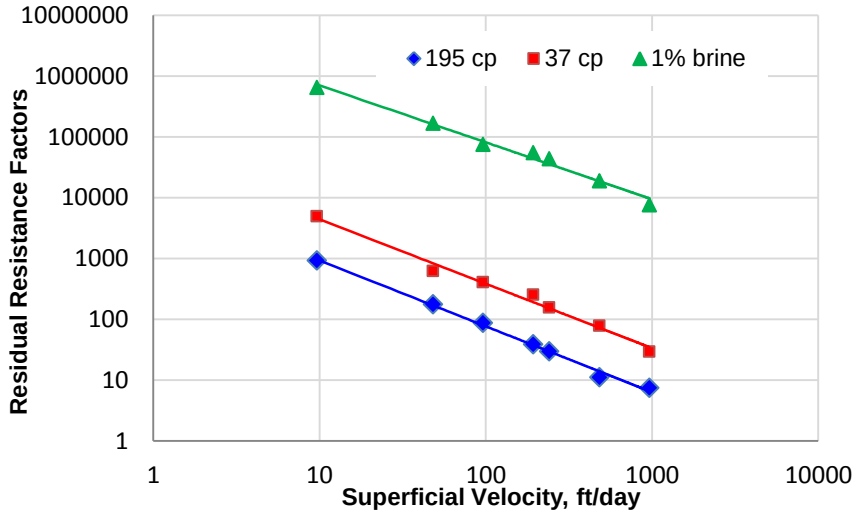

Figure 7-9—Comparisons between *Frrw* and *Frro* during the first cycle of flooding.

7.6.2.3 Brine and oil reinjection measurements.

After the first cycles of brine and oil injections were completed, we continued to inject multiple cycles of brine and oil through the same gel sizes. **Figure 7-10*a*** shows the results obtained for the second brine cycles. The *Frrw* measurements observed during the second water injection cycle were almost the same for both particle sizes. For instance, the *Frrw* measurements for particle sizes 20-30 and 100-120 were 544.5 and 726, respectively, at the same velocity (964 ft/day). In this example, the oil may have dehydrated both particle sizes to the same extent. The effect of different particle sizes on the *Frrw* was not significant after oil was injected through the gel.

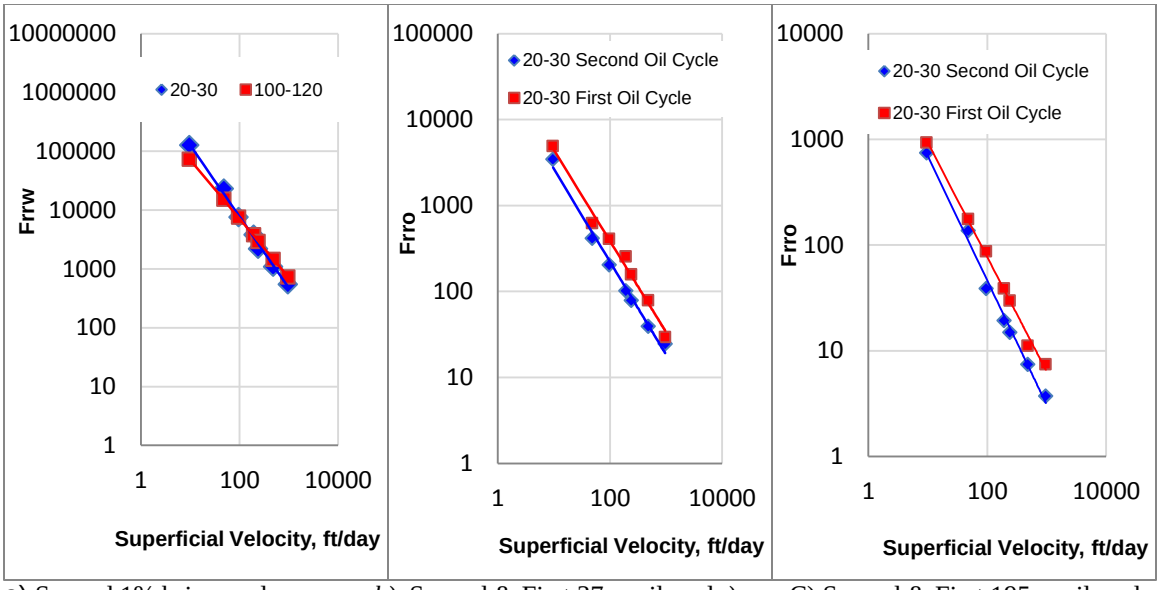

a) Second 1% brine cycle *b).* Second & First 37cp oil cycle*).* C) Second & First 195cp oil cycle

Figure 7-10—*Frrw* and *Frro* determined for the second cycles.

Figures 7-10 *b* and ***c*** provides a comparison of the *Frro* determined during the first and second oil injection cycles, respectively. The results obtained during the second oil injection cycle for both oil viscosities suggest a decrease in the *Frro*, even when compared to the first cycle. This decrease indicates further gel breakdown, thus continuously increasing the gel's permeability during oil injection. For example, the *Frro* determined for oil with a viscosity of 37 cp at the same velocity (100 ft/day) decreased almost two times less than the *Frro* measured during the first oil injection cycle. The *Frro* was 407 for the first oil injection cycle and 203 for the second.

Figure 7-11 compares the results from the first, second, and third water cycles for the same particle size. A third water cycle was injected after the second oil cycles. The *Frrw* measurements taken during the third brine cycle indicate a slight decrease when compared to the *Frrw* measured during the second brine cycle. For instance, at a velocity of 10 ft/day, the *Frrw* for the second cycle was 127052; it decreased slightly to 108902 during the third cycle. A comparison of all three water cycles indicates that *Frrw*

decreased substantially after the first oil injection. The *Frrw* for both the second and third cycles were very similar. These measurements indicate further particle gel breakdown but to a lesser extent than during the second cycle.

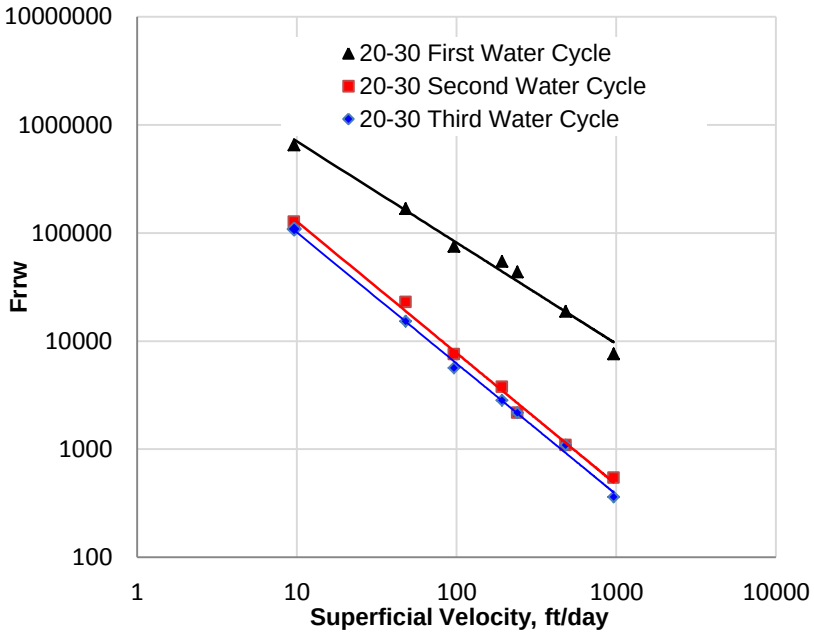

Figure 7-11—*Frrw* determined for the different 1% brine cycles.

7.7 Summary and Conclusions

This work investigated the characterization of disproportionate permeability reduction for PPG placed in closed fractures. The following conclusions were drawn from this investigation:

- The particle gel injection pressure increased as the particle size, gel strength, and flow rate increased but decreased as the fracture width increased.
- Elasticity indices (*n*) were successfully obtained and fitted as a function with gel strength. The results indicated that as the gel strength increased, the gel elastic value decreased.
- The results also indicated that the greater the gel strength, the more time is needed to achieve a stable pressure for each injection rate. Additionally, wider fractures require less time to reach a stable pressure than do narrower fractures for each injection flow rate.

- The *Frro* was always much less than the *Frrw* during all alternating water and oil floods. The DPR also increased with increases in the oil viscosity, particle size, gel strength, and fracture width.
- The first oil injection (first cycle of oil) can significantly degrade the gel properties. This finding explains why the residual resistance factor *Frrw* obtained from the second brine cycle decreased significantly compared with the *Frrw* obtained from the third brine cycle.
- The injection pressure for different water cycles increased as more water cycles were performed. However, these injection pressure increases were not significant at different oil cycles.
- A different disproportionate permeability reduction mechanism of the particle gel was investigated. The gel strength greatly affected the DPR and is an important parameter that should be considered.

Section 8: Use Consolidated Sandstone Rock to Evaluate Nanoparticle Gel Transport and Blocking Behavior

8.1 Summary

The application of nanoparticles in enhanced oil recovery (EOR) continues to gain attention in the oil industry due to its apparent potential. However, previous studies have focused on the evaluation of stiff particles, such as silica and aluminum oxide. Nanogel preformed particles with sizes ranging from 100-285 nm were used to represent deformable nanoparticles. Core flooding tests were run using sandstone cores with water permeabilities ranging from 42 to 1,038 mD.

8.2 Objectives

Study the behavior of injecting deformable nanoparticle preformed gel through low permeability sandstone cores.

8.3 Experimental Description

8.3.1 Nanogel.

The nanogel used in this study was an acrylamide-based crosslinked polymer from Poweltec in France. A 1.0 wt.% potassium chloride (KCL) aqueous solution was used to prepare the nanoparticle solutions. A Sysmex FPIA-3000 (Malvern) particle size analyzer was used to determine the particle size distribution of elastic nanogels. **Figure 8-1** shows the result of the 1% nanoparticle prepared by 1% KCl brine. The average particle size was 158 nm.

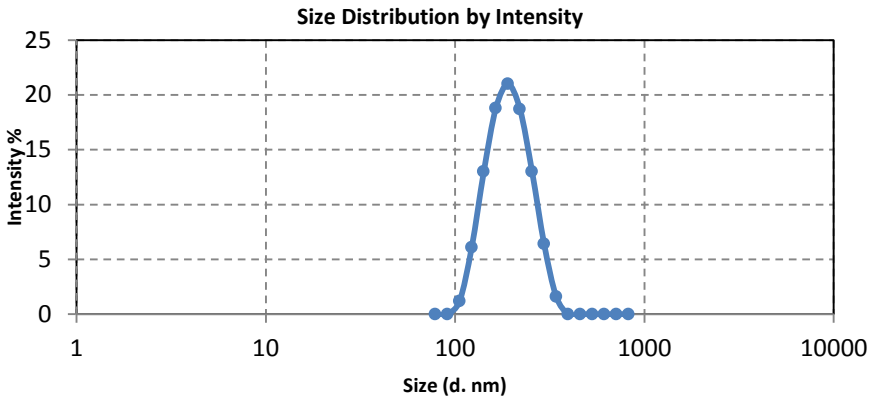

Figure 8-1. Nanoparticle characterization using the Sysmex FPIA-3000 (Malvern) nanoparticle distribution analyzer

8.3.2 Sandstone Cores.

Several low-medium permeability (water-wet) Berea sandstone core plugs ranging from 41.2 to 555.4 mD were used in this study. In addition, a higher permeability (1038 mD) core plug from Missouri sandstone also was employed. The length of the cores ranged from 6.95 to 7.1 cm, and the diameters ranged from 2.5 to 2.53 cm. The liquid permeability, pore volume, and porosity of the cores were determined by routine core analysis. **Table 8-1** summarizes the measured dimensions and average petrophysical properties.

Table 8-1. Dimensions and Petrophysical Properties at Initial Condition

Core ID	Length (cm)	Diameter (cm)	Porosity (%)	Pore Volume (cc)	Avg. Liq. Permeability (mD)
A1	7.00	2.52	18.98	6.43	41.20
A2	7.00	2.51	20.90	7.36	143.4
A3	7.00	2.52	20.49	7.14	143.2
A4	7.00	2.52	20.36	7.10	143.0
B1	7.00	2.53	23.79	8.30	311.5
C1	7.00	2.53	22.00	7.45	555.4
C2	7.00	2.50	22.00	7.45	556.2
C3	7.00	2.53	21.25	7.45	555.6
D1	6.99	2.53	18.93	6.73	1038.1

8.4 Experimental Setup

The core was mounted in a Hassler type core holder designed for cores 2.6 cm in diameter and up to 8 cm in length. The core flooding apparatus appears in **Figures 8-2**. All data, such as the injection pressure and flow rate, were recorded automatically.

8.5 Experimental Procedure

1) Vacuum and saturate the core, and then measure the porosity and pore volume
2) Core placement: load the core into the Hassler type core holder
3) Fill the core holder with confining fluid (water)
4) Inject brine at different flow rates, and determine the absolute permeability
5) Inject the nanogel at a rate of 0.25-5.0 cc/min starting from 0.25 cc/min (lowest to highest) until the pressure is stable at each flow rate and the mobility reduction can be calculated.
6) Inject brine at different flow rates (from 0.25-5.00 cc/min) to determine the permeability reduction.

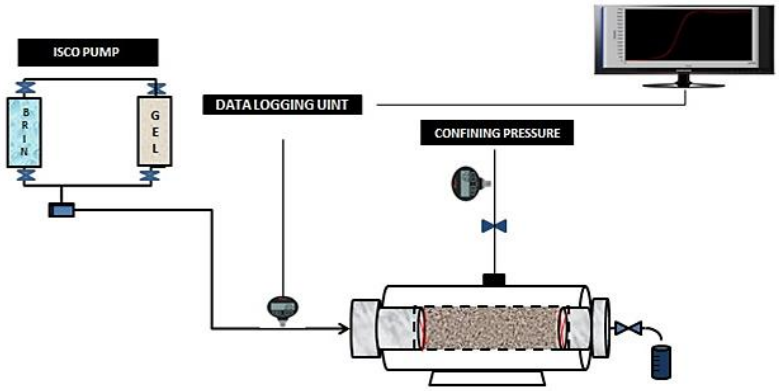

Figure 8-2. Schematic of experimental setup

8.6 Results and Analysis

The experimental setup allowed us to measure the pressure drop throughout each sandstone core. We injected nanogel solution into a core initially at the lowest velocity until the injection pressure became stable, and then we increased the injection rate and continued the injection until the pressure stabilized again. The process continued for several velocities. The stabilized pressures at the different velocities were used to calculate the resistance factor. In this work, different core plugs with a variety of liquid

permeabilities in the range of 41 -1038 mD were used to evaluate the nanogel performance at different injection rates (0.25-5.0 ml/min), at ambient conditions. We studied the effect of the rock permeability, nanogel concentration, and swelling degree of the nanoparticle on the resistance factor and residual resistant factor to water.

8.6.1 Gel Injection Behavior

8.6.1.1 Effect of Permeability on Injection Pressure and Resistance Factor (Fr)

0.1 wt% nanoparticle solution was injected into five rocks with permeabilities of 41.2, 143.2, 311, 555.4, and 1038 mD, respectively, at different injection rates. Stabilized pressures were recorded at different injection rates. **Figure 8-3** shows the relationship between the injection pressure and the superficial velocity, indicating that the injection pressure increased as the permeability decreased, as expected. The core with a permeability of 41.2 mD had a much higher injection pressure than the other four cores. As shown in Figure 3, when the injection rate reached 1.75 mL/min, the injection pressure increased to 2379.21 psi. To determine whether the nanogel transported through the low-permeability rock, we made a few 1-cm cuts for the low-permeability rock from the inlet and then measured the pressure drop across the remaining core. **Table 8-2** provides the results. The expected pressure was calculated based on the assumption that the core was very homogenous and that the nanogel plugged uniformly throughout the core. The expected pressure was much higher than the measured pressure after the first cutting, indicating that the nanogel sufficiently plugged the inlet. However, the measured pressure was almost the same as the expected pressure for the second and third cutting, indicating that the nanogel had already transported through the rock and had been well distributed across its length, except for at the inlet.

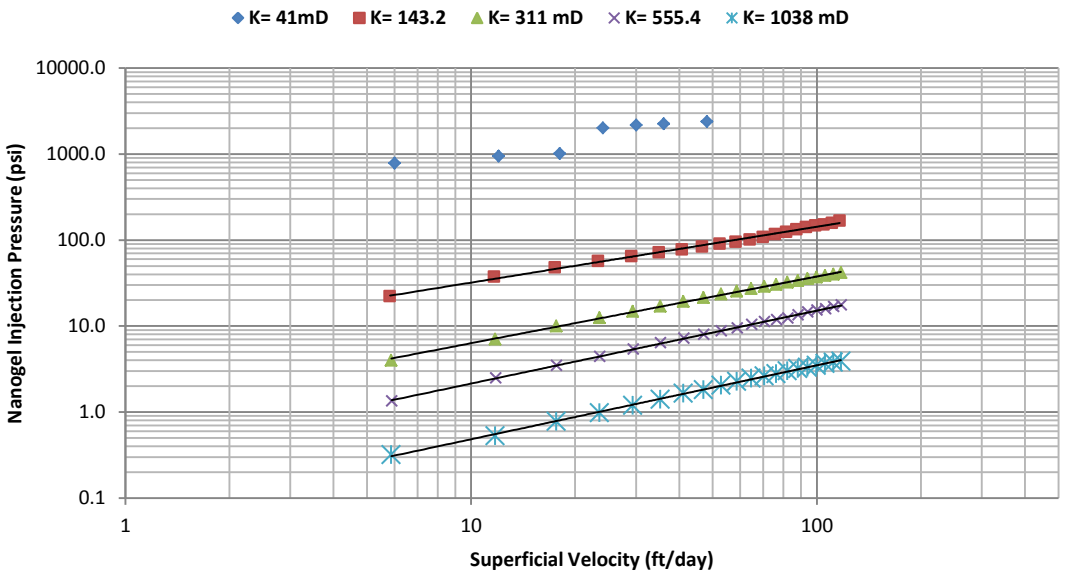

Figure 8-3. Injection pressure as a function of permeability and superficial velocity.

Table 8-2. Gel Propagation inside Low-Permeability Core

Flow Rates	Brine injection before cleaning the surface	Brine injection after cleaning the surface	Cut 1 Brine injection after cutting		Cut 2 Brine injection after cutting		Cut 3 Brine injection after cutting	
	(6.9 cm)	(6.9 cm)	(5.87 cm)		(4.9 cm)		(4.0 cm)	
Q(mL/min)	ΔP(psi)	ΔP(psi)	Expected ΔP(psi)	Measured ΔP(psi)	Expected ΔP(psi)	Measured ΔP(psi)	Expected ΔP(psi)	Measured ΔP(psi)
0.25	1412.4	1010	872	201	164	150	122.4	117
0.5	1826.8	1585	1368	327	267	240	195.9	183
0.75	2072.3	1861	1606	442	361	320	261.2	241
1	2268.4	2241	1935	565	461	396	323.3	300

Figure 8-4 depicts the resistance factor as a function of the superfical velcocity for the five coreflooding results. The resistance factor of the four high-permeability cores (143.4, 311.2, 555.4, and 1038 mD) decreased as the velocity increased and decreased as the permeability increased. This permeability effect directly corresponds to the standard expectation that the narrower the pore size, the more resistance forces exist for the

particle solution to pass through. On the other hand, with the lowest rock permeability (**Figure 8-4**, k = 41.2 mD), we observed a different trend as the injection rate increased. For the first three injection rates, the trend indicated shear thinning behavior. However, as the injection rate increased to 24 ft/day (corresponding to 103.7 s^{-1}), the resistance factor increased, indicating shear-thickening behavior. This could be attributed to the change in microstructure of a colloidal dispersion [Wagner, 2009]. In equilibrium, random collisions among particles make them naturally resistant to flow. As the shear rate increases, however, particles become organized in the flow, which lowers their viscosity. At even higher shear rates, hydrodynamic interactions between particles dominate over stochastic interactions, causing transient fluctuations in the particle concentration. The difficulty with which particles flow around each other in a strong flow leads to a higher rate of energy dissipation and an immediate increase in viscosity. In addition, further increases in the flow rate (as more shear rate was applied) in the same core (41.2 mD) decreased the resistance factor, which can be attributed to mechanical degradation [Seright et. al., 2011].

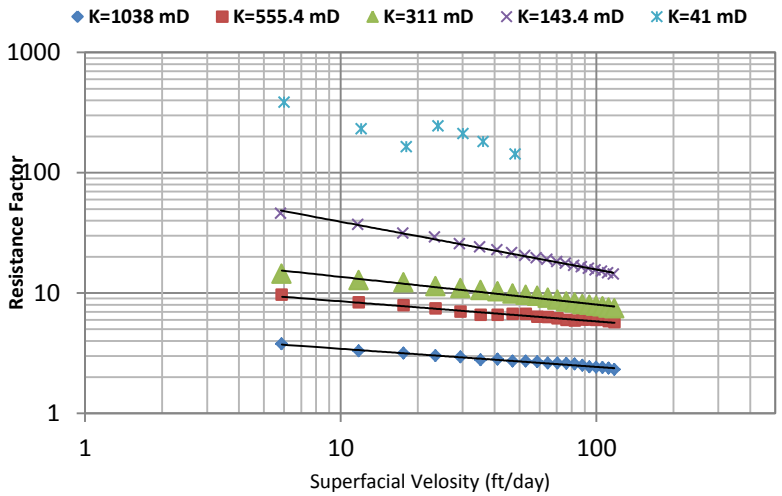

Figure 8-4. Resistance factor as a function of permeability and superficial velocity

8.6.1.2 Effect of Nanogel Concentration on Injection Pressure and Resistance Factor (Fr)

Berea sandstone cores with the same permeability of ~555.4 mD were selected to investigate the effect of nanogel concentrations on the injection pressure. Three concentrations of nanogel solutions (0.1, 0.25, and 0.5 wt.%) were used. **Figure 8-5** shows the effect of the nanogel concentration on the injection pressure at different superficial velocities. The injection pressure increased significantly as the concentration increased.

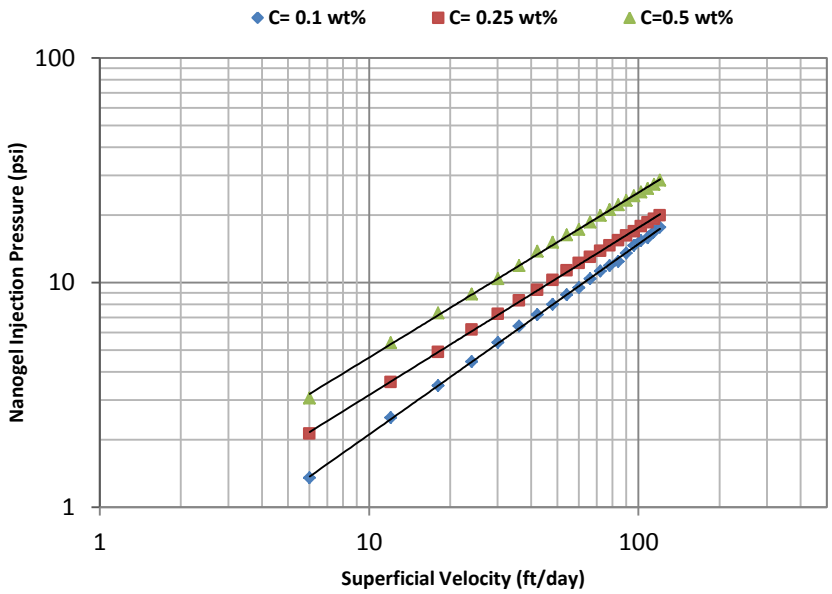

Figure 8-5. Injection pressure as a function of concentration and superficial velocity

Figure 8-6 shows that the the resistance factor (RF) increased as the particle concentration increased. Additionally, the resistance factor decreased with an increase in the injection rate for all nanogel concentrations ranging from 0.1 to 0.5 wt%. This indicates that the nanoparticle solutions exhibited shear thinning or pseudoplastic behavior in the tested porous media.

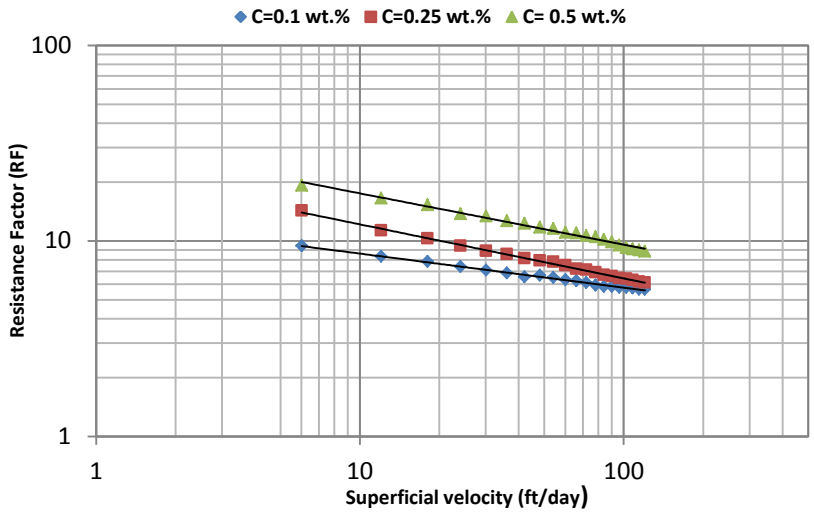

Figure 8-6. Resistance factor as a function of concentration and superficial velocity

8.6.1.3 Effect of Swollen Degree of Nanogels on Injection Pressure and Resistance Factor (Fr)

Like other particle gels, nanogels can swell when certain environmental parameters change, such as the temperature, brine salinity, and pH [Bai et al., 2013]. The particles will become much weaker the more they swell, which makes them more deformable. This raises the question as to which type of particle can flow mostly easily through porous media: small, strong particles or large, weak particles. Zhang's experimental results confirmed that large, fully swollen particles transport much more easily through open fractures than small, partially swollen particles [Zhang and Bai, 2011]. However, no research has been conducted to determine whether particle gel behaves the same in porous media. We used three cores with similar water permeabilities of approximately 143 mD to study the effect of the size of the deformable particles on the injection pressure and resistance factor. Three samples with an average size of 158, 265, and 285 nm, respectively, were used for the comparison. Note that the different sample sizes were

prepared from the same size particles. In another word, the particle size was increased by additional swelling rather than using different particle samples.

Figure 8-7 shows the stable pressure measurement results at different superficial velocities. The results showed that the sample with the smaller particle size had a higher injection pressure than the sample with the larger particle size, indicating that the elasticity or deformability of the swollen nanogels has a more pronounced effect on the injection pressure than does the size of the swollen nanogel**. Figure 8-8** shows that the resistance factor decreased with an increase in the swollen particles, which indicates that the smaller swollen nanogel had a higher apparent viscosity than the two samples with larger volumes, even though the former was larger than the latter. Overall, the results suggested that particles with a more controlled swelling rate are not better than particles that swell quickly in terms of particle transportation and injectivity, which is very consistent with our experimental results in fractures, openings, and screens (Zhang and Bai, 2011; Imqam et al., 2014; Muhammed et al., 2014).

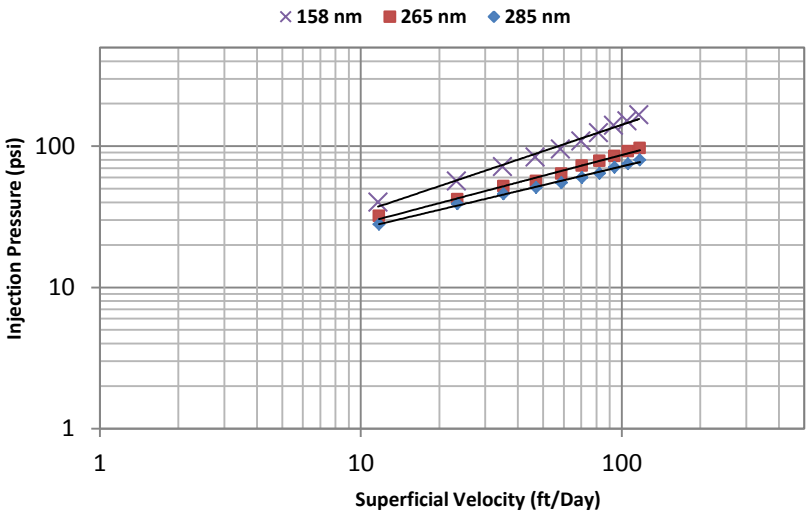

Figure 8-7. Injection pressure as a function of swollen particles

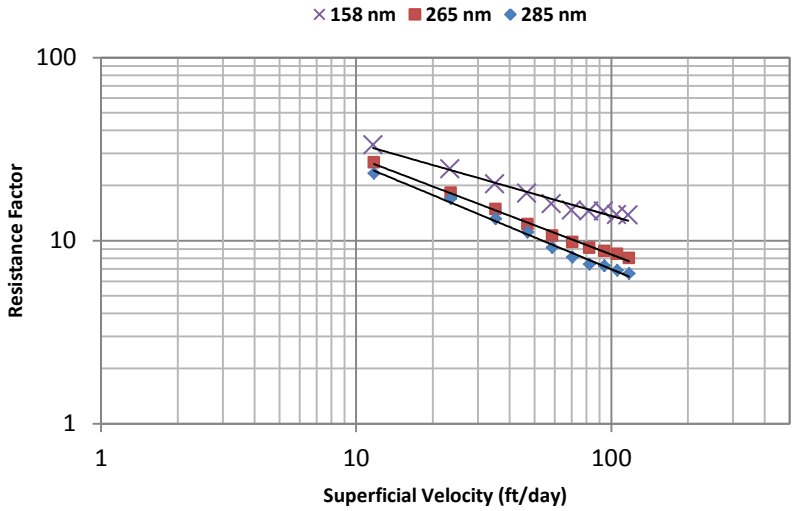

Figure 8-8. Resistance factor as a function of superficial velocity and swollen particles

8.6.2 Nanogel Resistance to Water Flow

8.6.2.1 Residual Resistance Factor (Frr)

After gel placement, the brine was injected at different flow rates from high to low. The stabilized pressure was recorded at different flow rates to calculate the Frr. The

results **(Figure 8-9)** show that the nanogel effectively reduced the permeability of the rocks with initial permeabilities of 143.4, 311, and 555.4 mD. However, the Frr of the high-permeability rock (1038 mD) was relatively small, ranging from 2.67 to 4.39, indicating that the particle is not very efficient for use in a reservoir with high-permeability streaks. Also, it appears that the Frr increased with a higher solution concentration and decreased as the superficial velocity increased, as shown in **Figure 8-10**. Furthermore, **Figure 8-11** shows that the Frr decreased with an increase in the size of the nanogel particles, indicating that more swollen nanogels have less resistance to water flow than less swollen nanogels, even though the former are larger than the latter. This finding is consistent with our other observations for millimeter-sized particle blocking in open fractures (Zhang and Bai, 2011).

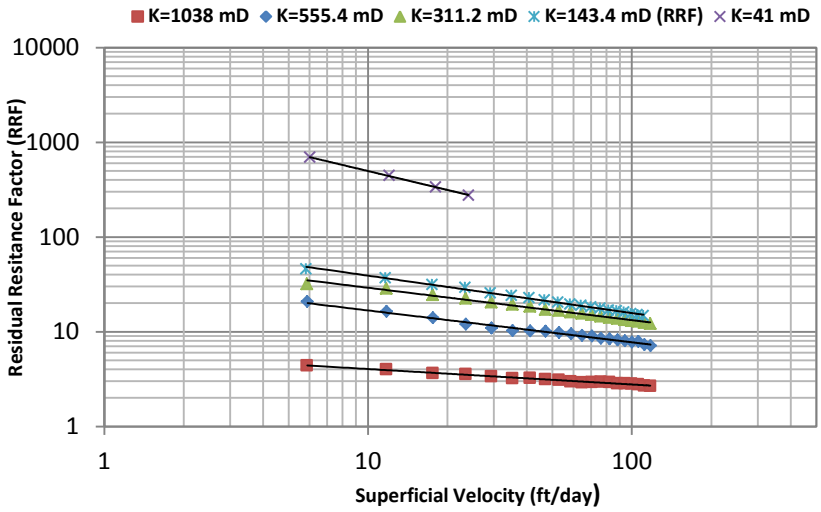

Figure 8-9. Residual resistance factor as a function of permeability and superficial velocity

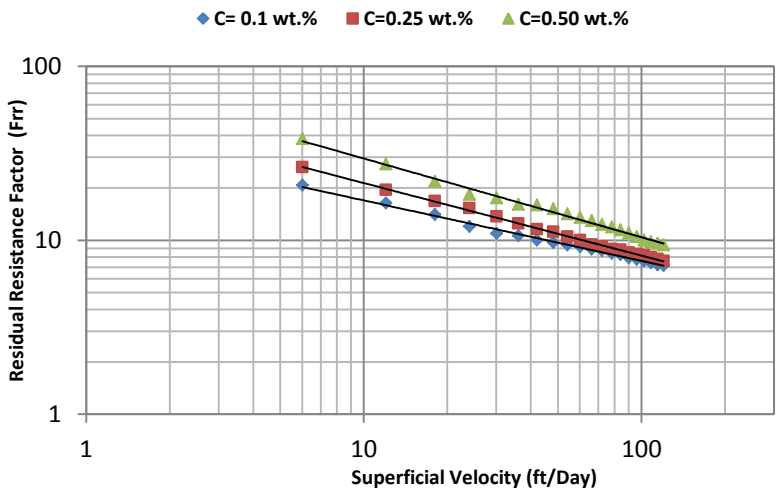

Figure 8-10. Residual resistance factor as a function of concentration and superficial velocity

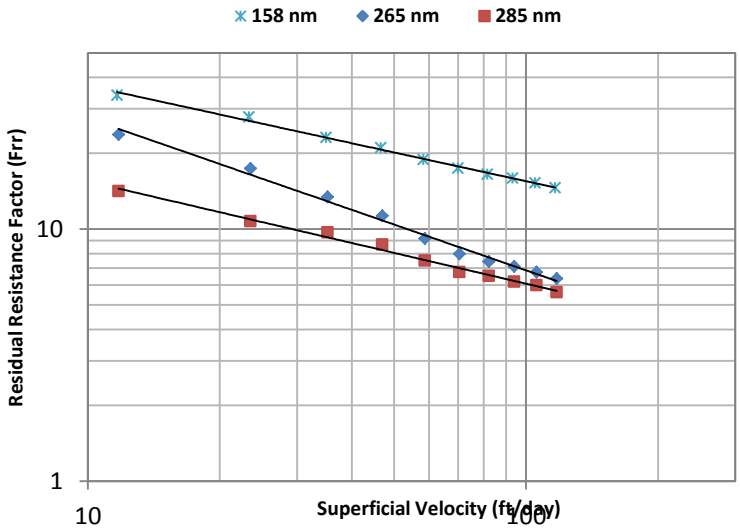

Figure 8-11. Residual resistance factor as a function of superficial velocity and swollen nanogel particles

8.6.2.2 Dynamic Jamming Ratio (JR) and Particle Pore Throat Ratio

The adsorption thickness and dynamic JR for each core flooding result were calculated using as shown in **Table 8-3**. The adsorption thickness was much higher than the particle size (158 um=0.158 µm) for all cases, indicating that the particles adsorbed

on the rock surface on multiple layers. Comparing the dynamic JR with the residual resistance factor data showing in **Figure 8-9**, we found that the permeability reduction decreased with the increase JR, which has a good agreement with the statement of Shi et al. (2011). In addition, the particle adsorption layer is elastic and deformable, which can explain why the dynamic JR increased with the shear rate, as shown in **Tables 8-3** and **8-4**. **Table 8-4** summarizes the values of the JR with different nanogel concentrations. The adsorption layer thickness increased as the concentration increased, yet, the dynamic JR values decreased as the nanogel concentration increased.

Table 8-3. Summary of JR with Different Permeabilites and Shear Rates

K=1038 mD			K=555.4 mD			K=311 mD			K=143.4 mD			K=41.2 mD		
r_p= 6.56 µm			r_p= 4.75 µm			r_p= 3.20 µm			r_p= 2.35 µm			r_p= 1.31 µm		
γ (s^{-1})	ε_H	JR	γ (s^{-1})	ε_H	JR	γ (s^{-1})	ε_H	JR	γ (s^{-1})	ε_H	JR	γ (s^{-1})	ε_H	JR
5.04	2.03	6.48	7.55	2.43	3.91	10.31	1.85	3.46	14.02	1.45	3.24	25.93	1.05	2.50
10.08	1.92	6.85	15.10	2.30	4.13	20.63	1.81	3.54	28.04	1.40	3.36	51.86	1.02	2.57
15.12	1.81	7.27	22.65	2.21	4.30	30.94	1.76	3.64	42.06	1.35	3.48	77.78	1.00	2.62
20.16	1.78	7.39	30.20	2.11	4.50	41.25	1.73	3.70	56.08	1.34	3.51	103.71	0.99	2.65
25.20	1.72	7.65	37.76	2.06	4.61	51.57	1.69	3.79	70.10	1.30	3.62	-	-	
30.24	1.66	7.93	45.31	2.01	4.73	61.88	1.67	3.83	84.12	1.29	3.64	-	-	
35.27	1.67	7.88	52.86	2.01	4.73	72.19	1.66	3.86	98.14	1.27	3.70	-	-	
40.31	1.63	8.07	60.41	2.01	4.73	82.51	1.63	3.93	112.16	1.26	3.73	-	-	
45.35	1.62	8.12	67.96	1.99	4.77	92.82	1.62	3.95	126.18	1.24	3.79	-	-	
50.39	1.57	8.38	75.51	1.96	4.85	103.13	1.60	4.00	140.20	1.23	3.82	-	-	
55.43	1.53	8.60	83.06	1.94	4.90	113.45	1.59	4.03	154.22	1.22	3.85	-	-	
60.47	1.55	8.49	90.61	1.93	4.92	123.76	1.57	4.08	168.25	1.21	3.88	-	-	
65.51	1.55	8.49	98.16	1.89	5.03	134.07	1.56	4.10	182.27	1.20	3.92	-	-	
70.55	1.54	8.54	105.72	1.88	5.05	144.39	1.55	4.13	196.29	1.19	3.95	-	-	
75.59	1.51	8.71	113.27	1.87	5.08	154.70	1.54	4.16	210.31	1.18	3.98	-	-	
80.63	1.50	8.77	120.82	1.85	5.14	165.02	1.53	4.18	224.33	1.17	4.02	-	-	
85.67	1.49	8.83	128.37	1.83	5.19	175.33	1.52	4.21	238.35	1.16	4.05	-	-	
90.71	1.47	8.95	135.92	1.84	5.16	185.64	1.51	4.24	252.37	1.16	4.05	-	-	
95.75	1.44	9.14	143.47	1.78	5.34	195.96	1.49	4.30	266.39	1.15	4.09	-	-	
100.78	1.43	9.20	151.02	1.77	5.37	206.27	1.48	4.32	280.41	1.14	4.12	-	-	

Table 8-4. Summary of the JR with Different Nanogel Concentrations and Shear Rates

K=555.4 mD; C=0.1 wt.%			K=555.2 mD; C=0.25 wt.%			K=555.6 mD C=0.5 wt.%		
rp= 4.496 µm			rp= 4.496 µm			rp= 4.498µm		
γ (s^{-1})	ε_H µm	JR	γ (s^{-1})	ε_H µm	JR	γ (s^{-1})	ε_H µm	JR
7.55	2.39	3.76	7.56	2.50	3.60	7.55	2.67	3.37
15.10	2.26	3.98	15.12	2.34	3.84	15.10	2.51	3.58
22.65	2.17	4.14	22.68	2.26	3.98	22.65	2.40	3.75
30.20	2.08	4.32	30.25	2.21	4.07	30.20	2.31	3.90
37.76	2.02	4.44	37.81	2.15	4.19	37.75	2.28	3.94
45.31	2.00	4.49	45.37	2.09	4.30	45.29	2.24	4.02
52.86	1.97	4.57	52.93	2.04	4.40	52.84	2.23	4.03
60.41	1.95	4.61	60.49	2.03	4.44	60.39	2.20	4.08
67.96	1.93	4.66	68.05	1.99	4.53	67.94	2.16	4.16

75.51	1.91	4.70	75.62	1.96	4.60	75.49	2.14	4.21
83.06	1.89	4.75	83.18	1.92	4.69	83.04	2.11	4.26
90.61	1.88	4.78	90.74	1.90	4.72	90.59	2.08	4.32
98.16	1.86	4.85	98.30	1.88	4.78	98.14	2.06	4.36
105.71	1.84	4.88	105.86	1.87	4.80	105.69	2.04	4.41
113.27	1.82	4.95	113.42	1.85	4.86	113.24	2.01	4.47
120.82	1.80	4.99	120.99	1.84	4.90	120.79	1.99	4.53
128.37	1.79	5.03	128.55	1.83	4.92	128.33	1.96	4.60
135.92	1.77	5.08	136.11	1.81	4.96	135.88	1.94	4.63
143.47	1.75	5.13	143.67	1.80	5.01	143.43	1.93	4.66
151.02	1.75	5.15	151.23	1.78	5.06	150.98	1.92	4.70

8.6.3 Empirical Correlation Model for FR and FRRW

Resistance factor. The resistance factors shown in Figures **8-4**, **8-6**, and **8-8** have a linear relationship with the superficial velocity in the log-log plot, except for the 41.2 mD rock. A general power law equation can be used to express the relationship:

$$F_r = K \cdot v^{-n} \qquad (8\text{-}1)$$

where *K* and *n* are the flow consistency constant and flow behavior index, respectively. **Table 8-5** summarizes the K and n values for each straight line in the three figures and their corresponding correlation factors.

Table 8-5. Fitting Equations for Resistance Factor as a Function of Velocity

Effect	Value	Fitting Equation	R^2
Permeability	K = 40 mD	-	-
	K = 143.4 mD	$F_r = 97.749 \cdot v^{-0.397}$	0.996
	K = 311 mD	$F_r = 23.145 \cdot v^{-0.230}$	0.971
	K = 555.4 mD	$F_r = 12.543 \cdot v^{-0.167}$	0.970
	K = 1038 mD	$F_r = 4.8608 \cdot v^{-0.150}$	0.984
Concentration	C = 0.1%	$F_r = 37.704 \cdot v^{-0.347}$	0.994
	C = 0.25%	$F_r = 55.683 \cdot v^{-0.417}$	0.998
	C = 0.5%	$F_r = 83.566 \cdot v^{-0.452}$	0.993
Swelling	Particle Size = 158 nm	$F_r = 84.904 \cdot v^{-0.397}$	0.975
	Particle Size = 265 nm	$F_r = 88.384 \cdot v^{-0.511}$	0.991
	Particle Size = 285 nm	$F_r = 86.209 \cdot v^{-0.545}$	0.992

Residual resistance factor. The residual resistance factor shown in **Figures 8-9**, **8-10**, and **8-11** also has a good linear relationship with the superficial velocity in the log-log plot. This relationship can be expressed using the following general power law equation:

$$F_{rr} = a \times v^{b} \qquad (8\text{-}2)$$

where a and b are constants related to the deformability of the adsorption layers. **Table 8-6** provides a, b and the correlation factor R^2 for each line.

Table 8-6. Fitting Equations for Residual Resistance Factor as a Function of Velocity

Effect	Value	Fitting Equation	R^2
Permeability	K = 41.2 mD	$F_{rr} = 2296 \cdot v^{-0.664}$	0.999
	K = 143.4 mD	$F_{rr} = 97.083 \cdot v^{-0.395}$	0.996
	K = 311 mD	$F_{rr} = 23.145 \cdot v^{-0.932}$	0.989
	K = 555.4 mD	$F_{rr} = 36.376 \cdot v^{-0.336}$	0.986
	K = 1038 mD	$F_{rr} = 5.88 \cdot v^{-0.163}$	0.989
Concentration	C = 0.1 wt.%	$F_{rr} = 32.051 \cdot v^{-0.262}$	0.988
	C = 0.25 wt.%	$F_{rr} = 22.959 \cdot v^{-0.2.70}$	0.998
	C = 0.5 wt.%	$F_{rr} = 12.871 \cdot v^{-0.174}$	0.997
Swelling	Particle Size = 158 nm	$F_{rr} = 84.904 \cdot v^{-0.397}$	0.996
	Particle Size = 265 nm	$F_{rr} = 96.264 \cdot v^{-0.53.2}$	0.992
	Particle Size = 285 nm	$F_{rr} = 100.13 \cdot v^{-0.578}$	0.991

8.7 Summary and Conclusions

Core flooding tests were run to study the transport behavior of nanogel through sandstone and the effect of the nanogel on water flow was investigated. The following conclusions can be drawn from the work:

- The tested nanogel had good injectivity for the cores with permeabilities above 143.4 mD, but the injectivity was fairly low for the rock with a permeability of 41.2 mD.
- The resistance factor decreased as the flow velocity increased for all rocks except the one with the lowest permeability of 41.2 md; this relationship can be expressed well by exponential equations.
- The residual resistance factor decreased as the flow velocity increased for all rocks; this relationship can be expressed well by exponential equations.
- Both the resistance factor and the residual resistance factor decreased with an increase in the size of the swollen particles, which were prepared from the same nanoparticle sample, because the larger particles were weaker than the small

particles, indicating that the gel strength is more important than the particle size for nanogel particle injectivity and permeability reduction.

- Both the resistance factor and the residual resistance factor increased with reduced rock permeability and increased nanogel concentration.
- The nanogel particle adsorption layer thickness decreased with the shear rate from water flow.

Section 9: Use Sand Pack Model to Evaluate Gel Transport through High Permeability Streaks

9.1 Summary

High-permeability streaks can expedite an undesirable water channeling and early water breakthrough during water flooding. PPGs was injected and placed through Super-K permeability cores to reduce unwanted water production and increase oil recovery. Extensive experiments were conducted to examine the effect of the sand permeability, PPG size, concentration, and water salinity on the PPG injection process, passing criteria, and plugging efficiency to water flow.

9.2 Objectives

PPGs swollen in different brine concentrations were injected into two ranges of sand permeability to determine the following:

- Examine the effect of unconsolidated sand pack permeability, gel strength, gel size, and gel concentrations on the gel injection pressure.
- Study the effect of injection flow rate on the PPG injection pressure.
- Determine the gel threshold pressure (defined as the minimum pressure required to enable gel to propagate through high permeability streaks).
- Study associated mechanisms with PPG injections (e.g., retention and adsorption).

9.3 Description of Experiments

The following are descriptions of the materials and equipment used to investigate the mechanisms of PPG propagation through Super- K permeability streaks.

9.3.1 Preformed Particle Gel (PPG).

A superabsorbent polymer was used as a PPG to conduct the experiments. Dry particles with mesh sizes of 170-200 and 80-100 were swollen in a 1% sodium chloride (NaCl) brine concentration. Gel concentrations of 800 and 2000 ppm were used. **Table 9-**

1 lists the PPG swelling ratios and PPG strength measurements for PPGs swollen in 0.05% NaCl and 1% NaCl. PPGs swollen in the low brine concentration (0.05% NaCl) were more swellable and weaker than PPGs swollen in the high brine concentration (1% NaCl).

Table 9-1—PPG swelling ratio and strength in 0.05% and 1% NaCl.

No	Brine Concentration: C ,NaCl %	Swelling Ratio	Gel Strength: G` ,pa
1	0.05	165	515
2	1	50	870

9.3.2 Brine Concentration and Oil Viscosity.

Both 0.05% and 1 wt% NaCl were used for brine injection and to prepare the swollen PPGs. Oil with a viscosity of 37 cp at 70 °F was used to saturate the sand pack model.

9.3.3 Magnetic Stirring Vessel.

An accumulator with a 1200 ml capacity and a maximum adjusted impeller speed of 1800 r/min was used to inject PPGs into a high permeability sand pack model. The impeller was placed at the bottom of the accumulator so that the PPGs remained dispersed in brine before they were injected into the model.

9.3.4 Sand Packs. Silica sand was used to obtain different permeability sand packs. A vibrator machine was used to pack the sand carefully to obtain the desired permeability. A range of mesh sizes was used to obtain an approximate sand permeability of 65.4 and 26.5 Darcy. **Table 9-2** illustrates the sand pack permeability and PPG properties used for each experiment.

Table 9-2—Sand pack permeability and PPG properties used in each experiment.

Experiment	Sand Pack Permeability, Darcy	PPG Concentration, ppm	NaCl Concentration, %	PPG Size, micron
1st Experiment	26.5	2000	1	75
2nd Experiment	65.4	2000	1	75
3rd Experiment	26.5	800	1	75
4th Experiment	26.5	2000	0.05	75
5th Experiment	26.5	2000	1	150

9.4 Experimental Setup

The experimental setup used in this study (see **Figure 9-1**) was constructed from a stainless steel tube 91.4 cm in length and 2.5 cm in diameter. It was packed with different sand grains to test the effect of various Super-K permeabilities on the PPG injection process. A syringe pump was used to inject suspensions of PPG, brine, and oil from accumulators to the sand pack model. Four pressure transducers were mounted on both the inlet and along the sand pack to monitor the pressure during the gel treatment injection and brine injection processes. Test tubes mounted at the model outlet were used to record the PPG and brine production volumes in the effluent.

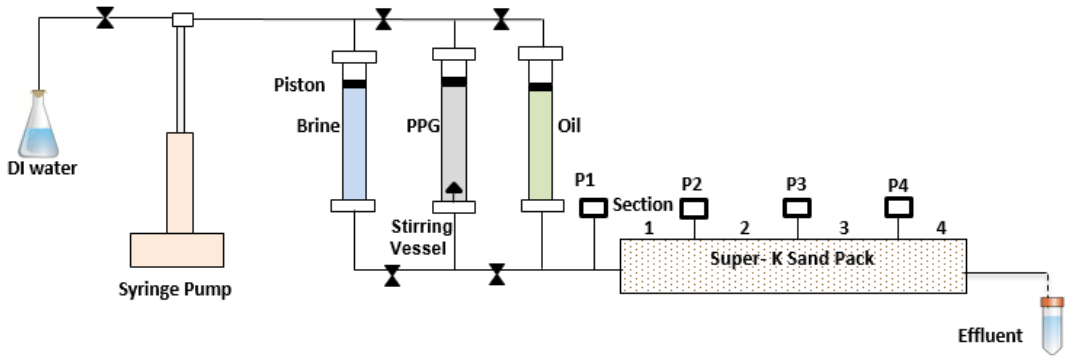

Figure 9-1—A micron-size PPG injection apparatus.

9.5 Experimental Procedures

Several procedures were followed when conducting the PPG treatment injection processes and water injection processes. These procedures are described as follows:

9.5.1 Preparing and Saturating Sand Pack Models

A vibrator machine was used to prepare different sizes of silica sand so that the desired sand pack permeability could be obtained. Sand was poured at a regular rate; then vibration was kept constant until the entire tube was filled with sand. The sand pack models were then vacuumed for at least 1 hr before being fully saturated with 1% NaCl to determine the pore volume, porosity, and permeability. The sand pack model was next flushed with brine at different injection flow rates (1, 2, 3, 4, 5, 6, and 7 ml/min) to ensure that the model was 100% saturated with brine. Oil viscosity with a 37 cp was injected from the accumulator into the sand pack at 2 ml/min to determine the connate water saturation.

Oil was injected until no water was produced and the injection pressure became stable. A variety of oil injection flow rates (1, 3, 4, 5, 6, and 7 ml/min) was then used to determine the effective oil permeability at connate water saturation.

9.5.2 Preflush

Brine was injected into the Super-K permeability sand at a rate of 2 ml/min to simulate secondary oil recovery conditions. The brine was injected into the sand packs until no oil was produced and the brine injection pressure became stable. The Super-K permeability sand was flushed again with brine at flow rates of 1, 3, 4, 5, 6, and 7 ml/min to determine the effective water permeability at residual oil saturation

9.5.3 PPG Treatment

Swollen suspended PPGs were injected into sand packs at a rate of 2 ml/min after the first water flooding processes were completed. The PPG was injected until began to produce

at effluent and the PPG injection pressure became stable in all four pressure sensors. The gel threshold pressure, gel breakthrough pressure, and gel injection stable pressure were each recorded so that the gel propagation mechanisms through the Super-K permeability sand at different injection conditions could be diagnosed. The PPG injection was then resumed at different flow rates (1, 3, 4, 5, 6, and 7 ml/min) to study the effect of injection flow rates and to calculate the gel resistance factor.

9.5.4 Post-flush Water Injection

Brine was injected at 2 ml/min after the PPG treatment was complete to test the gel's resistance to water flow. The injection started with low flow rates moving to high flow rates; this was repeated in reverse order, from high to low flow rates. The rationale for using these brine cycles was to determine the gel stability during water flow at different water injection flow rates. A series of brine cycles was run until no discrepancies occurred between the repeated cycles.

9.6 Results and Analysis

This section discusses the PPG injection mechanisms, resistance factor calculations, and PPG resistance to water flow.

9.6.1 PPG Injection Mechanisms

Preformed particle gels were injected through the sand pack until they produced at effluent and the injection pressure became stable. **Figures 9-2** and **9-3** show the injection pressure recorded at the different pressure points across the sand pack for both PPG swollen in 1% and 0.05% NaCl solutions, respectively. For both experiments, the PPG was injected through nearly the same permeability of approximately 26.5 Darcy. The PPG was injected at rate of 2 ml/min. PPG injection continued until it produced at effluent and the pressure became stable in each pressure point across the sand pack. The PPG swollen in 0.05% NaCl was larger than the PPG swollen in 1% NaCl. Yet, the PPG

injection pressure recorded at pressure point P1 for PPG swollen in 1% NaCl was twice as great as the injection pressure recorded for the PPG swollen in 0.05% NaCl. The gel injection pressure for the PPG swollen in 1% NaCl was approximately 1600 psi, while the injection pressure recorded for the PPG swollen in 0.05% NaCl was approximately 800 psi. The results also indicated that the pressure changes took place at all the points, which shows that the PPG propagated deeply across the core. Also, it was observed that the PPG injection pressure increment at point 1 was much higher than at other points, which implies that most of the gel particles had been caught in the front part of the core by retention or a trap mechanism. For the PPG swollen in 1% NaCl, the injection pressure recorded at P1 became stable at approximately 1600 psi, while at P2, P3, and P4, the pressure was 600 psi, 450 psi, and 30 psi, respectively.

The injection pressure change at all points for the PPG swollen in a 1% NaCl solution was higher and more visible than the pressure change recorded for the PPG swollen in a 0.05% solution. Very small changes in injection pressure were recorded across the sand core at the last points of the PPG swollen in the 0.05% solution. The gel injection pressure was approximately 5.37 psi, 2.58 psi, and 1.39 psi at points P2, P3, and P4, respectively. This small change in pressure was caused by the gel rheology of the gels swollen in different NaCl concentrations. Table 1 indicates that the PPG swollen in the 1% brine solution was stronger than the gel swollen in the 0.05% brine solution. The monitored gel production in the effluent showed that the gel swollen in the 0.05% solution had broken into very tiny particles to propagate. As a result, a small change in the injection pressure across the sand pack occurred during the PPG propagation for the gel swollen in the lower brine concentration. This result was also observed by Imqam *et al.* (2014) where they indicated that gel particles swollen in 0.05% brine broke into very small sizes to pass, while gel particles swollen in 1% brine experience a slight change in sizes but required higher injection pressure to transport.

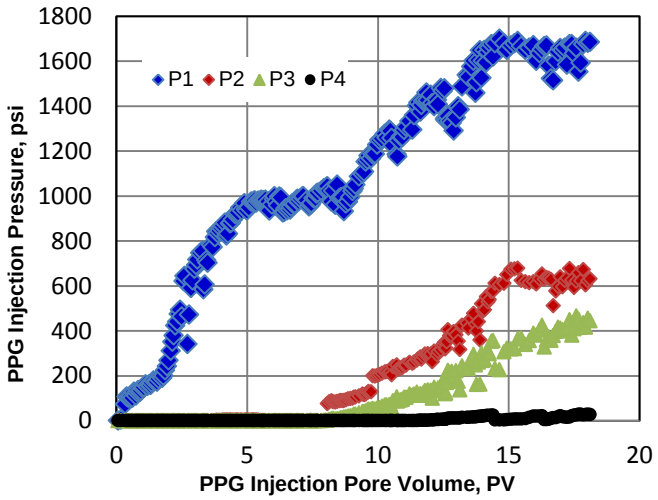

Figure 9-2—PPG injection pressure across the sand pack of the gel particles swollen in 1% NaCl.

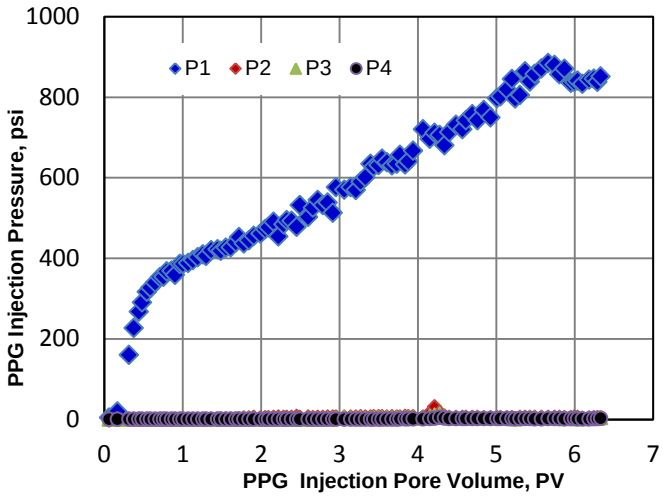

Figure 9-3—PPG injection pressure across sandpack of the gel particles swollen in 0.05% NaCl.

9.6.2 Gel particle retention in sand pack cores

PPG was propagated deeply into sand pack and gel particles were produced in the effluent. However, the PPG injection pressure distribution across the sand pack was varied and based on the PPG properties and pore throat geometry. The results indicated that some gel particles remained in some pore throats and blocked them. The injection pressure recorded at the inlet section of sand was greater than any injection pressure

measured in the remaining sections. The trapped or retained particles reduced the void space volume available for flow in the inlet section more than in the other sand sections. **Table 9-3** summarizes the injection stable pressure measured across the sand pack for the effects of sand permeability, PPG concentration, brine concentration (PPG strength), and PPG size. The results show that the effect of retention was varied and caused by the pressure gradient, pore throat geometry, PPG size, and strength.

Table 9-3—PPG injection pressure at injection rate of 2 ml/min across sandpack.

Effects		PPG Injection Stable Pressure, psi			
		P1	P2	P3	P4
Permeability (Darcy)	26.5	1680	593	320	28
	65.4	27.5	10.3	7.3	3
PPG Concentration (ppm)	800	183.5	84.8	47.7	13.21
	2000	1680	593	320	28
NaCl Concentration (%)	0.05	835	5.37	2.58	1.39
	1	1680	593	320	28
PPG Size (micron)	75	1680	593	320	28
	150	2589.5	4.39	3.49	0.7

Injection pressure was increased through the entire sand core when a gel was swollen in 1% and when used PPG size of 75 microns. A slight change in injection pressure was observed when the PPG was swollen in 0.05% brine and when using PPG size of 150 microns. Our previous work; (Imqam *et al*. 2014) indicated that PPG swollen in 0.05% brine broke down into very small pieces when it was injected through a pore throat size larger than 6. Imqam *et al*. (2014) also indicated that PPG swollen in 0.25, 1, and 10% brine did not break down significantly into small pieces like the PPG swollen in 0.05% brine, but the PPG needed a larger injection pressure gradient to transport than PPG swollen in 0.05% brine. Therefore, some of the gel particles broke and were entrapped in the inlet section, which caused the injection pressure to increase accordingly. The other gel particles continued to propagate deeply and produced at effluent; therefore, the injection pressure increase was based on the PPG size change across the sandpacks.

9.6.3 PPG passing criteria

A threshold pressure, breakthrough pressure, and injection stable pressures were determined for each experiment during the PPG injection process. The threshold pressure is the minimum pressure required to initiate PPG propagation through sand. The breakthrough pressure is the pressure at which PPGs begin to produce at the outlet. The evaluation of these pressures is crucial to understanding PPG propagation mechanisms and injection performance through Super-K sand formations. PPG is not like other solid materials, due to its elasticity and deformability. The injection pressure measurements and the pore volume associated with these pressures are listed in **Table 9-4**.

The threshold pressure was significantly affected by the pore throat size, PPG concentration, brine concentration, and PPG size. The threshold pressure rose significantly as the PPG concentration, brine concentration, and PPG size increased. Three PPG injection patterns were observed during the PPG propagation. These patterns were determined according to the threshold pressure measurement and the pressure difference between the sand face injection pressure and the other pressure points across the sand pack. The first pattern was the low gel particle retention and pass pattern, which was deduced by the low threshold pressure and low pressure change distribution measured for the permeability of 65.4 Darcy and gel concentration of 800 ppm. The second pattern was the high gel particle retention and pass pattern, where a high threshold pressure was required and a large pressure change was noticed across the sand pack for the PPG swollen in 1% NaCl. The third pattern was the high gel particle retention, breaking, and pass pattern shown for the PPG swollen in 0.05% NaCl and the PPG size of 150 micron.

Table 9- 4—Passing criteria for the PPG injection processes.

Effects		Threshold Pressure, psi	Volume at Threshold, PV	Breakthrough Pressure, psi	Volume at Breakthrough, PV	Stable Pressure, psi	Volume at Stable Pressure, PV
Permeability (Darcy)	26.5	817	3.68	983	7.34	1680	14.07
	65.4	6.7	1.83	26.6	15.17	27.18	17.9
PPG Concentration (ppm)	800	88.6	9.91	184.2	38.02	183.5	40.3
	2000	817	3.68	953	7.34	1680	14.07
NaCl Concentration (%)	0.05	421.7	1.47	666.8	3.94	856	5.01
	1	817	3.68	953	7.34	1680	14.07
PPG Size (micron)	75	817	3.68	953	7.34	1680	14.07
	150	2646	10.8	2670.9	32.9	2545.4	34.3

The PPG injection pressure at the inlet of sand pack increased as the PPG propagated deeply through the sand cores, as indicated by the breakthrough pressure measurements. The breakthrough pressure was greater than the threshold pressure. With permeability of 26.5 Darcy, the threshold pressure was 817 psi, and the injection pressure continued to increase until PPG was produced in the effluent and reached 983 psi. Most of the results also indicated that the PPG injection pressure continued to increase and became stable at values larger than the breakthrough pressures.

The calculated pore volume indicated that a smaller PPG volume was required for the PPG to reach the effluent when using a low brine concentration, small PPG size, and large PPG concentration. Injecting 800 ppm of PPG, approximately two times the injection pore volume of PPG was used than injecting 2000 ppm of PPG. A 40.3 PV of 800 ppm of PPG was required to reach the effluent compared to a 14.07 PV of 2000 ppm of PPG. The variation in PPG injection pore volume was created by both the PPG retention and the PPG strength factors.

9.6.4 Effect of injection flow rate

When the PPG was visibly produced in the effluent and the pressure became stable at all the different sections, the PPG continued to be injected through the sand pack but at different injection rates. The PPG was injected initially at a low flow rate, with the rate increased gradually. A stable pressure occurred at each injection rate. Seven flow rates were used to inject the PPG through the sand pack. A sharp increase in the PPG injection pressure was noticed during the early injection flow rates.

Figure 9-4 illustrates the injection pressure measurements at different injection flow rates for the two PPGs concentrations. The gel injection pressure for all of the injection flow rates was higher in the high PPG concentrations than it was in the low gel concentrations; the low PPG concentrations were more injectable than the high PPG concentrations. At an injection flow rate of 4 ml/min, the injection pressure for 2000 ppm was 2524 psi while the injection pressure for 800 ppm was 261.6 psi.

The gel injection pressure increased a great deal during the early flow rates. A smaller increase in range occurred at higher flow rates. The gel injection pressure with a gel concentration of 800 ppm, increased approximately1.5 folds (from 180 psi to 250 psi) when the injection rate increased from 1 to 3 ml/min. However, when the injection rate was increased from 5 to 7 ml/min, the injection pressure rose by only 1.1 fold. This result was consistent with Imqam *et al*. (2014), where the PPG injection pressure did not increase linearly through all of the gel injection velocities but rather tended to reach a plateau after a certain injection velocity.

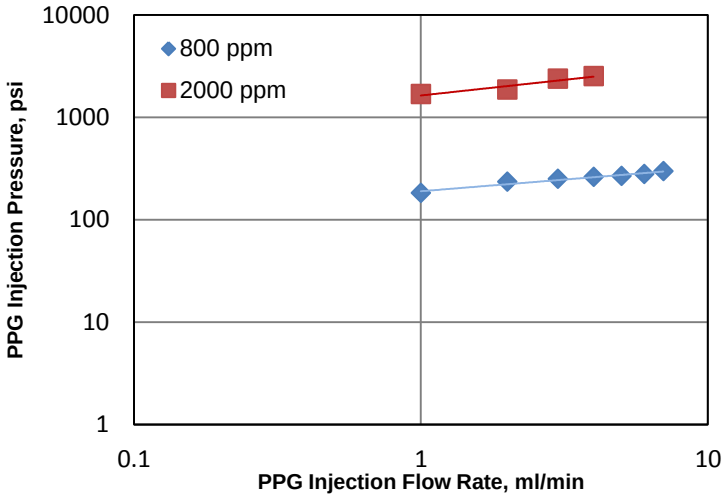

Figure 9-4—Effect of the injection flow rate on the PPG injection pressure.

The power law equation was successfully used to fit the injection pressure data as a function of the injection flow rates. The fitting equations for the pressure injection measurements obtained from the power law equation are summarized in **Table 9-5**.

Table 9- 5—Fitting equations for injection pressure as a function of the injection flow rate.

Effects		Fitting Equation	R^2
Permeability (Darcy)	26.5	$P= 1634.3\ q^{0.3056}$	0.91
	65.4	$P=30.018\ q^{0.2379}$	0.91
PPG Concentration (ppm)	800	$P= 189.85\ q^{0.2278}$	0.95
	2000	$P= 1634.3\ q^{0.3056}$	0.91
NaCl Concentration (%)	0.05	$P= 497.2\ q^{0.8302}$	0.96
	1	$P= 1634.3\ q^{0.3056}$	0.91
PPG Size (micron)	75	$P= 1634.3\ q^{0.3056}$	0.91
	150	$P= 2157.5\ q^{0.2433}$	0.99

9.6.5 Resistance Factor Calculation

The resistance factor (Fr) is defined as the effective viscosity of a gel in porous media relative to that in water. It can be calculated from this equation:

$$\mathrm{Fr} = \frac{(\Delta p)_{\mathrm{ppg}}}{(\Delta p)_{\mathrm{brine}}}$$

where $(\Delta p)_{ppg}$ is the injection pressure measured during the gel injection and $(\Delta p)_{brine}$ is the injection pressure before PPG placement.

The resistance factor was calculated at each sand pack section and plotted as a function of the injection pore volume. **Figure 9-5** illustrates the resistance factor calculated for a PPG concentration of 800 ppm. The PPG was injected at a flow rate of 2 ml/min; injection continued until gel was produced in the effluent. The resistance factor determined at the inlet sand pack section (section 1) was greater than in any other sections. The resistance factor calculated at sections 1, 2, 3, and 4 was approximately 2474, 1005, 807, and 69, respectively. This result indicated that the PPGs propagated deeply through the Super-K sand, but their movement was not like a piston. Large quantities of gel particles were entrapped in section 1, and their volume decreased as they approached the effluent section.

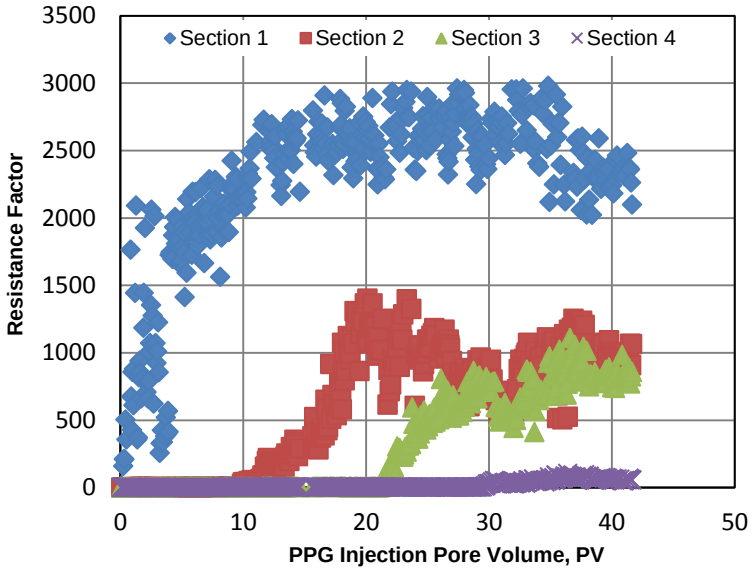

Figure 9-5—Resistance factor calculated for the four sections, with a PPG concentration of 800 ppm.

Table 9-6 provides a summary of the resistance factor (Fr) calculated across the sand pack. The results indicate that the Fr for the first section was higher than for any other sand pack sections. A much larger retention occurred in section 1 compared to the other sections.

The resistance factor determined at the inlet section increased as the sand pack permeability, PPG concentration, and PPG size decreased. However, Fr increased as the brine concentration increased. The PPG swollen in 0.05% NaCl was larger than the PPG swollen in 1% NaCl, but the Fr calculated (in section 1) for the 0.05% brine was much less than the Fr calculated for 1% brine. Similarly, 150 micron PPG had a smaller Fr than 75 micron PPG. This occurred because the PPG was broken into small pieces to pass through the core, which created a lower resistance factor than if their size had not been reduced. Results also indicated that the resistance factor was affected more significantly by the brine concentration and pore throat size than by the PPG size and concentration.

Table 9-6—Resistance factor across the sand pack.

Effects		Resistance Factor Values			
		Section 1	Section 2	Section 3	Section 4
Permeability (Darcy)	26.5	2090.3	1046.4	1813.3	560
	65.4	22.63	16.67	61.4	33.3
PPG Concentration (ppm)	800	2474	1005	807	69
	2000	2090.3	1046.4	1813.3	560
NaCl Concentration (%)	0.05	151.1	139.5	14.87	13.9
	1	2090.3	1046.4	1813.3	560
PPG Size (micron)	75	2090.3	1046.4	1813.3	560
	150	1233.5	30	279	7

9.6.6 Effect of injection flow rate

The resistance factor determined for gel concentrations of 800 and 2000 ppm were plotted against the injection flow rate as illustrated in **Figure 9-6**. The resistance factor was calculated for the entire sand pack section. The resistance decreased significantly during the early injection flow rates. It became less dependent on the injection flow rates

when the injection rates rose above 4 ml/min. The resistance factor increased as the PPG concentration increased. The Fr determined for 2000 ppm was 3380 at the injection rate of 1 ml/min; it was 1215 for 800 ppm. Results also imply that particle gels exhibit a shear thinning behavior during propagation through Super-K permeability streak cores.

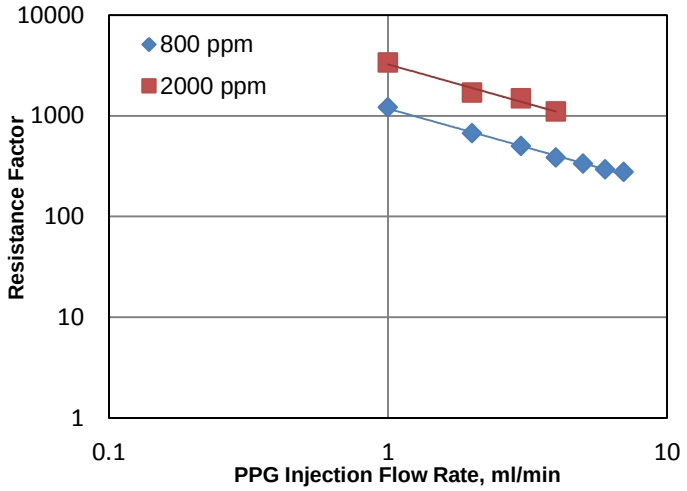

Figure 9-6—Resistance factor determined for the PPG concentration effect.

The power law equation was used to fit the resistance factors determined for the effect of sand pack permeability, PPG concentration, brine concentration, and PPG size. The equations were fairly fitted as functions of flow rates with a high accuracy (R^2) as listed in **Table 9-7**.

Table 9-7—Empirical correlation for the resistance factor.

Effects		Fitting Equations	R^2
Permeability (Darcy)	26.5	$Fr= 3245.8\ q^{-0.78}$	0.97
	65.4	$Fr= 372.95\ q^{-0.628}$	0.99
Gel Concentration (ppm)	800	$Fr= 1175.4\ q^{-0.774}$	0.99
	2000	$Fr= 3245.8\ q^{-0.78}$	0.97
Brine Concentrations (%)	0.05	$Fr= 932.45\ q^{-0.466}$	0.98
	1	$Fr= 3245.8\ q^{-0.78}$	0.97
Particle Size(micron)	75	$Fr= 3245.8\ q^{-0.78}$	0.97
	150	$Fr= 4258.6\ q^{-0.824}$	0.99

9.6.7 PPG Resistance to Water Flow

Initially brine was injected at a flow rate of 2 ml/min to maintain consistency when comparing its injection pressure with the PPG injection pressure. Brine continued to be injected until the pressure became stable at all the pressure measurement points. **Figure 9-7** depicts the brine injection pressure as a function of the brine injection pore volume for a PPG concentration of 800 ppm. The injection pressure at point 1 was higher than at any other pressure points; the injection pressure decreased as the water injection was transported deeply into the sand pack. The PPG resistance to water flow was significant at the sand pack inlet but not in other sections.

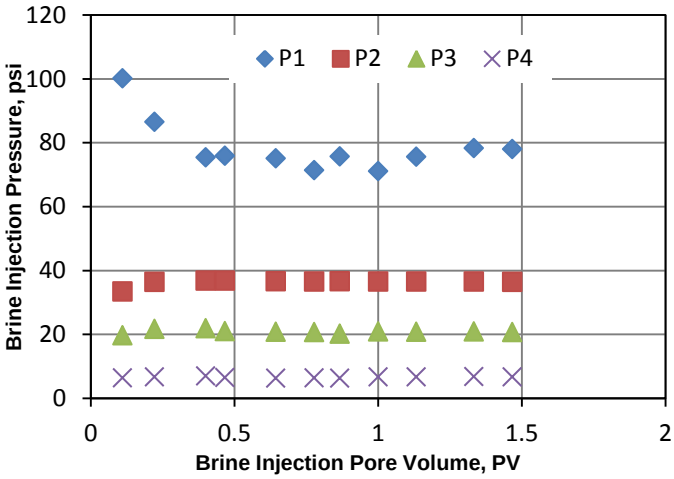

Figure 9-7—Brine injection pressure across the sand pack for a PPG concentration of 800 ppm.

Table 9-8 lists the brine injection pressures across the sand pack related to the effect of sand permeability, PPG concentration, NaCl concentration, and PPG size. The brine injection pressure distribution was varied and it decreased as the brine was injected deeply through the sand pack. The water injection pressure measured at each point was high when using a high PPG concentration, high NaCl concentration, and small PPG size. Referring to **Table 9-3**, the brine injection pressure was smaller than the PPG injection pressure. This reduction might have occurred because of PPG washout or brine injection

change path mechanisms. However, the brine injection pressure after the PPG injection was still larger than the brine injection pressure before the PPG treatment.

Table 9-8—brine injection pressure at an injection flow rate of 2 ml/min across sand pack **cores.**

Effects		Brine Injection Stable Pressure, psi			
		P1	P2	P3	P4
Permeability (Darcy)	26.5	1592	1316	1334	39
	65.4	15.9	12.6	8.93	1.51
PPG Concentration (ppm)	800	78	36.4	20.7	6.62
	2000	1592	1316	1334	39
NaCl Concentration (%)	0.05	168.8	1.28	0.74	0.3
	1	1592	1316	1334	39
PPG Size (micron)	75	1592	1316	1334	39
	150	1216	0.88	1.54	0.44

9.6.7.1 **PPG washout and water change path mechanisms**

Cycles of brine were injected into the sand packs not only to test the PPG's resistance to water flow but also to evaluate the pore throats blocking efficiency. A low-to-high injection rate procedure was used to inject the water through the sand pack. A stable pressure was required for each flow rate. Water was next injected into the sand packs using a high-to-low injection rate procedure to determine whether or not the gel was washed out of the pore throat as a result of the increased injection rate. If the injection pressure measured from the repeated injection rate procedure overlapped the previous injection pressure results, it implies that the gel did not move from the pore throat. The brine injection cycles stopped when the injection pressure did not change with repeated injections cycles. The final residual resistance factor (Frrw) to water was calculated for the final injection cycle and the blocking degree of PPG to water was then determined.

Figures 9-8 and **9-9** illustrate the water injection stable pressures at the seven injection flow rates determined for PPG concentrations of 800 and 2000 ppm, respectively. Seven cycles of 1% NaCl were injected into a sand pack filled with a PPG concentration of 800 ppm. The injection pressure rose with increased injection flow rates during the first brine cycle. The injection pressure continued to rise until it reached an injection flow rate of 5 ml/min, after which it declined and then increased slightly. PPG

failure started to occur at a rupture pressure of 118 psi. The second water cycle was performed and the injection rate decreased gradually until it reached 1 ml/min. The injection pressure measured from a second water injection showed considerable discrepancies with previously measured pressure. These discrepancies continued to occur during the water cycles. They decreased and became negligible as additional water injection cycles were run. A similar trend was observed for the PPG concentration of 2000 ppm, but with a higher PPG rupture pressure of 1643 psi and smaller water injection cycles. The injection pressure measured for PPGs of 2000 ppm was maintained at a higher level than the injection pressure measured for PPGs of 800 ppm after the water injection cycles ended. The injection pressure for PPGs of 2000 ppm was 314 psi at the same injection rate (7 ml/min); the injection pressure for PPGs of 800 ppm was 44 psi. Four water injection cycles were performed to reach the final pressures for PPGs of 2000 ppm, while seven water injection cycles were performed for PPGs of 800 ppm.

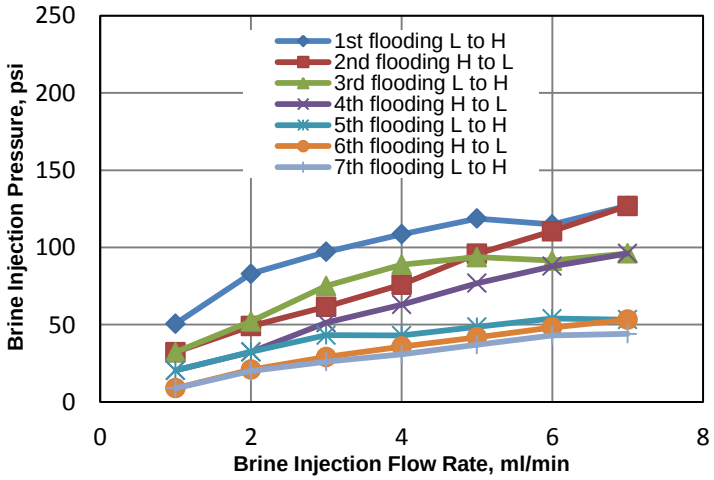

Figure 9-8—Water injection pressure for a PPG concentration of 800 ppm.

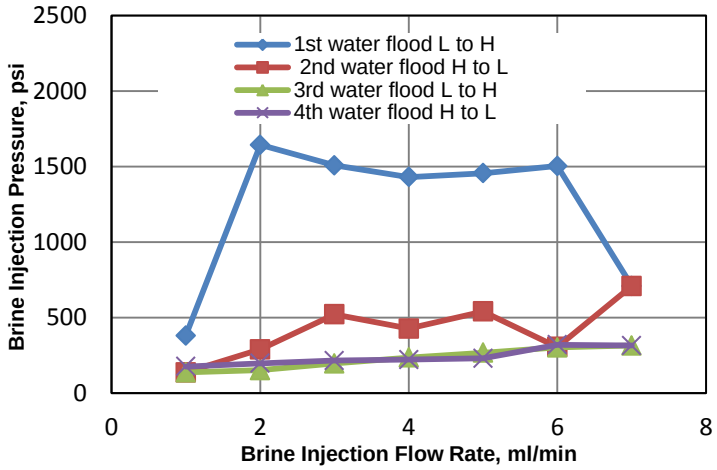

Figure 9-9—Water injection pressure for a PPG concentration of 2000 ppm.

Table 9-9 summarizes the water injection cycles and the ruptured PPG injection pressure results. Large number of brine cycles was performed, when both a smaller PPG concentration and a smaller brine concentration were used. The PPG's resistance to water flow increased as the brine concentration and the PPG concentration increased, as was indicated by the rupture pressure measurements.

Table 9-9—brine injection cycles performed and ppg failure pressures.

Effects		Number of Brine Injection Cycles	Rupture Pressure, psi
Permeability (Darcy)	26.5	4	1643
	65.4	4	28.7
PPG Concentration (ppm)	800	7	118
	2000	4	1643
NaCl Concentration (%)	0.05	6	160
	1	4	1643
PPG Size (micron)	75	4	1643
	150	4	2010

9.6.7.2 PPG blocking to water flow Results The residual resistance factor to water (Frrw) is defined as the ratio of the water phase permeability before and after particle gel treatment. The Frrw was determined for the different water injection cycles as a function of the injection flow rates. **Figure 9-10** illustrates the F_{rrw} calculated for the PPG concentration of 2000 ppm. The F_{rrw} results did not decrease systematically with the injection flow rates as a result of the gel washout effects. The F_{rrw} determined at the four cycles decreased linearly with increasing injection flow rates. The Frrw decreased significantly at the early injection rate, but when the injection flow rate exceeded 4 mm/min, the F_{rrw} tended to be independent of the increased injection flow rates. The F_{rrw} decreased from 351 to 179 when the injection rate increased from 1 to 2 ml/min. The F_{rrw} only decreased from 89 to 75 when the injection rate increased from 6 to 7 ml/min. The power law equation is used to fit the F_{rrw} as a function of the injection flow rates with a fair fit.

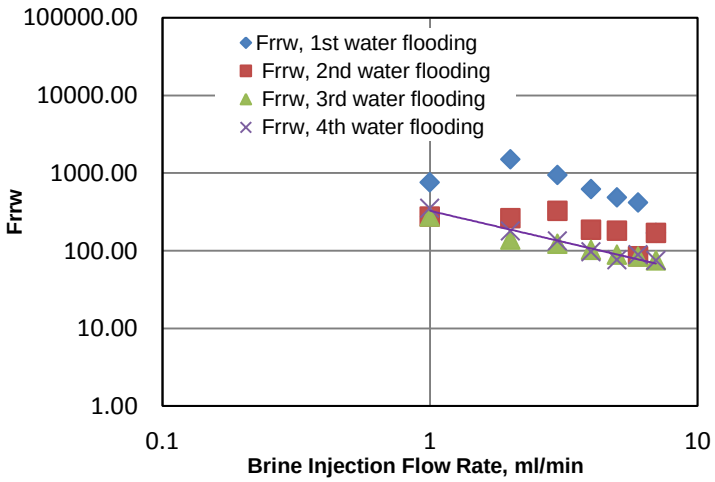

Figure 9-10—The residual resistance factor for a PPG concentration of 2000 ppm.

Blocking efficiency (*E*) to water flow refers to the percentage of permeability reduction that can be calculated from E= [1-(1/Frrw)]*100. The stabilized water injection pressures measured at the final water injection cycle at an injection flow rate of 2 ml/min were used to calculate the Frrw and the blocking efficiency. **Table 9-10** shows the

blocking efficiency to water flow determined relation to the sand permeability, gel concentration, brine concentration, and particle size. PPG blocking efficiency to water flow was too high during all experiments. It reached 90% and above, which indicates that the PPG can be used efficiently to plug the large pore throat sizes or channels that exist within the Super-K permeability features. This unvaried high percentage of blocking was reached because a sufficient PPG volume was injected into the sand pack model.

Table 9-10—blocking efficiency to water flow determined at 2 ml/min.

Effect		Water Injection Pressure Before PPG, psi	PPG Injection Pressure, psi	Water Injection Pressure after PPG, psi	F_{RRW}	PPG Blocking, %
SandPack Permeability	26.5 Darcy	1.1	1680	197.5	179.5455	99.44304
	65.4 Darcy	0.15	27.1	1.6	10.66667	90.625
Gel Conc.	800 ppm	0.4	183.5	21	52.5	98.09524
	2000 ppm	1.1	1680	197.5	179.5455	99.44304
Brine Conc.	0.05% NaCl	1.9	856	52.2	27.47368	96.36015
	1%NaCl	1.1	1680	197.5	179.5455	99.44304
Effect of Particle Size	75 micron	1.1	1680	197.5	179.5455	99.44304
	150 micron	1.8	2545.4	1272.1	706.7222	99.8585

9.7 Summary and Conclusions

A number of factors that affect preformed particle gel transport and the PPG's resistance to water flow through Super-K sand permeability were examined in this study. The effect of sand permeability, PPG concentration, brine concentration, and PPG size on PPG injection and placement were each investigated. The following conclusions can be drawn from the study:

- PPG was propagated deeply into the sand pack and gel particles were produced in the effluent. However, the PPG injection pressure distribution across the sand pack varied and based on the PPG's properties and the pore throat geometry.
- High PPG injection pressure was measured in the front part of the sand pack as a result of gel particle retention. The retention was controllable by selecting proper PPG strength, concentration, and size.

- The PPGs transport through Super-K permeability sand exhibited three patterns: low gel particle retention and pass; high gel particle retention and pass; and high gel particle retention, breaking, and pass.
- The PPG injection pressure at the inlet section increased as the PPG propagated deeply through the sand cores, as indicated by the breakthrough pressure measurements. A small PPG injection pore volume was required to reach the effluent when using a low brine concentration, small PPG size, and high PPG concentration.
- In field applications, it is very common that operators often are concerned about particle size for better injection performance. Contrary to the conventional concepts in PPG treatment practices, PPG injection was more sensitive to the PPG's strength than the PPG's size.
- The results show that fully swollen gel particles have a better injectivity than partially swollen particles with a larger diameter. The injection pressure rose as the PPG's concentration, water salinity, and gel particle size increased.
- The PPG injection pressure did not increase linearly through all of the gel injection flow rates but rather tended to reach a plateau after a certain injection flow rate.
- A high resistance factor was developed across the sand pack, but it was greater at the inlet section, demonstrating that PPGs did not propagate like a piston through the Super-K sand pack. This occurred because gel particles were retained in the sand pack.
- After the PPG injection process were completed, cycles of saline water were injected into the sand pack to test the PPG's resistance to water flow. The PPG's blocking efficiency to water flow increased as the PPG's strength, size, and concentration increased.
- Brine injection pressure measurements after the PPG treatment showed that permeability reduction developed across the sand pack cores. However, the in-depth permeability reduction varied according to the PPG's strength, size, and concentration.
- The PPG stability within the pore throat size was significantly affected by the brine concentration (gel strength) and the PPG concentration. The PPG significantly resisted brine flow, but this resistance decreased with a continuous increase in brine injection flow rates.

Section 10: Use Heterogeneous Model to Evaluate Gel Sweep Efficiency

10.1 Summary

Preformed particle gels were used as a diversion agent to correct permeability heterogeneity present in mature oil fields. The factors affecting the PPG's ability to increase oil recovery and decrease water production in non-cross flow heterogeneity reservoirs are discussed in this section.

10.2 Objectives

This work was conducted in an attempt to study the behavior of the micron-size PPGs propagation through both high and low permeabilities by evaluating the following:

- Study the effect of permeability contrast ratio on the oil recovery factor before, during, and after PPG treatment.
- Determine the injection profile change after the gel treatment for both low and high permeabilities.
- Compare the oil recovery and water cut results obtained during the initial water flooding with results obtained after PPG treatment.
- Determine the oil produced from low permeability/un-swept zones after PPG treatments are introduce.

10.3 Experimental Description

The following are descriptions of the materials and equipment which used to conduct the non-cross flow heterogeneity experiment.

10.3.2 Preformed Particle Gel (PPG)

A superabsorbent polymer was used as a PPG to conduct these experiments. Dry particles with a mesh size of 170-200 (90-75 microns) were swollen in a 1% Sodium Chloride (NaCl) brine concentration.

10.3.3 Brine Concentration and Oil Viscosity

1 wt% NaCl solution was used for brine flooding and to prepare the swollen PPGs. Oil with a viscosity 195 cp at 70 °F was used to saturate the sand pack model.

10.3.4 Magnetic Stirring Vessel

An accumulator with a1200 ml capacity and a maximum adjusted impeller speed of 1800 r/min was used to inject PPGs into a heterogeneity sand pack model. The impeller was placed at the bottom of the accumulator to keep PPG dispersed in brine before it was injected into the model.

10.3.5 SandPacks

Three sizes of silica sand were used to obtain different permeability contrasts between the models. Mesh sizes of 18-20, 50-60, and 100-120 were used to obtain low and high permeability sandpacks. Silica sand was packed into two separate tubes that had the same length and area.

10.4 Experimental Setup

The experimental setup used in this experiment is depicted in **Figure 10-1**. Two same dimensions tubes (with 20 cm in length and 2.7 cm in diameter) were used to contain the silica sand pack. A syringe pump was used to inject brine, oil and PPG from accumulators into the sand pack models. Two pressure transducers were mounted in front of each sand pack model to acquire the injection pressure change during the brine flooding and gel treatment. The test tubes were kept at the outlets of each sand pack to collect the volume of the effluents. The collected volume was used to determine gel penetration into each sandpack permeability.

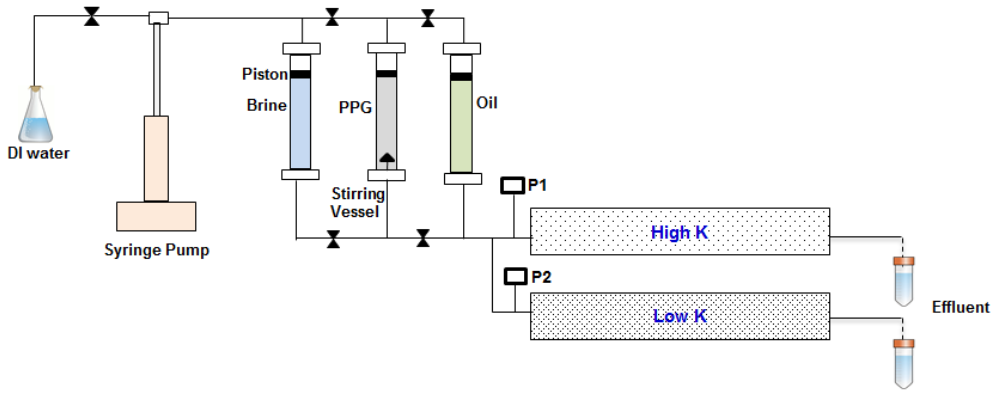

Figure 10-1—A schematic diagram of the non-cross flow experiment apparatus.

10.5 Experimental Procedures

Parallel sand packs were used to emulate the non-cross flow heterogeneities present in oil reservoirs. The ratio between the high permeability and low permeability layers is an important factor to be considered during PPG treatment. Three experiments were conducted with varying layer permeability contrast ratio. The permeability contrast ratio was as follows: 4, 20, and 44.The high permeability sand pack was kept nearly constant for all the three experiments. The low permeability sand pack, however, was varied.

The following subsections are the procedures used to carry out the experiments. They are briefly explained as follow:

10.5.1 Preparing and Saturating Sand Pack Models

A vibrator machine was used to prepare the different sizes of silica sand so that the desire sand pack permeability could be obtained. Sand pack models were vacuumed for at least 6 hr. It then fully saturated with 1% NaCl to determine pore volume, porosity, and permeability.

Heavy oil viscosity was injected from the accumulator into each sand pack at a rate of 1 ml/min. Oil was injected until no water was produced and the injection pressure became stable. **Table 10-1** summaries results obtained for the permeability, pore volume, porosity, irreducible water saturation, and original initial oil in place.

Table 10-1—Sand core heterogeneity properties for different permeability contrast ratio.

Case #	Permeability Contrast Ratio	Permeability, Darcy	Pore volume, gm	Porosity, %	Swi, %	OIIP, cc
1	4	High 21.7	35.7	33.64	25	26.70
		Low 6.2	39.60	37.31	8	36.60
2	20	High 22.4	32.60	30.72	27	21.93
		Low 1.1	35.40	33.35	18	32.60
3	44	High 22.1	41.87	34.84	26	30.8
		Low 0.5	24.9	20.72	12	21.8

Both sandpacks with low and high permeability were connected to each other as shown in **Figure 10-1** and then water flooding cycles began.

10.5.2 First Water Flooding

1% NaCl was injected into both low and high permeabilities at a rate of 1 ml/min to simulate secondary oil recovery conditions. During the first water flooding, both oil recovery and water cut were determined for low and high sand pack permeability layers.

10.5.3 PPG Treatment

Swollen PPGs in 1% NaCl with a concentration of 2000 ppm were injected into the sand packs at a rate of 1 ml/min after the first water flooding processes were complete. During the 0.5 PV of PPG injection treatments, volumes of oil and water production were collected. The gel injection pressure was also recorded to determine the gel propagation response into low and high permeability layers.

10.5.4 Second Water Flooding

A 1% NaCl was injected again at the same injection rate after PPG treatment to test the gel blocking efficiency for high permeability. Oil recovery measurements from low and high permeability cores were also determined.

The above procedures were all repeated for each experiment. The oil recovery factor, the water cut, and the injection pressure were each determined for the low and the high permeability sand pack models.

10.6 Results and Analysis

10.6.1 Oil Recovery Results

The oil recovery results of the water flooding cycles, the PPG injection, and the polymer flooding of the layer permeability contrast ratio of 4 are plotted in **Figure 10-2**. The oil recovery was determined for low and high permeability layers as a function of the water pore volume production of each layer. In the initial water flooding stage, a large volume of oil was recovered from high permeability layer compared to a very small volume of oil was recovered from low permeability layer. The oil recovered from high permeability layer was 80%. In contrast, oil recovered from low permeability was only 20%. Production pore volume results indicated a larger amount of water was flew through the high permeability layer than it was through the low permeability layer. Therefore, low oil recovery was obtained from the low permeability layer. Nearly all of the injected water during this stage was diverted into the high permeability layer. More than 4 PV of water was injected through high permeability layers. In contrast, less than 0.2 PV of water was injected through low permeability layer.

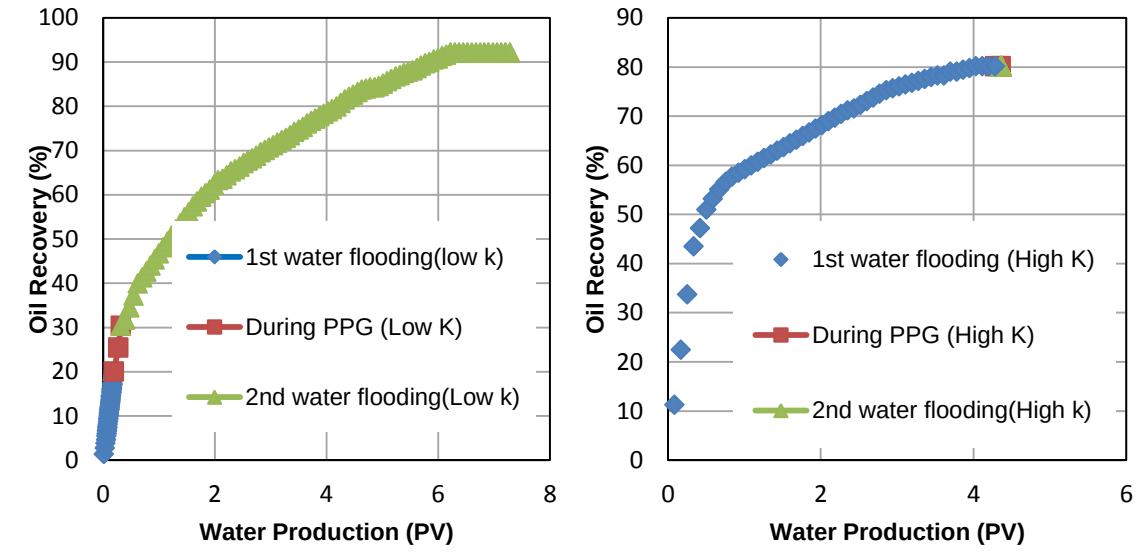

a) Oil recovery for a low permeability of 6.1 Darcy **b) Oil recovery for a high permeability of 21 Darcy**

Figure 10-2—The oil recovery for permeability: a) 6.1 Darcy and b) 21 Darcy.

During PPG injection, the sweep efficiency of the heterogeneity cores improved and oil recovered from low permeability began to rise. The oil recovered from low permeability increased substantially more than that recovered from high permeability layers. The recovery factor obtained from the low permeability layer was increased by 11.7%. While, oil recovery factor obtained from the high permeability layer increased by only 0.2%.

A large amount of PPG remained in the high permeability layers helping reduce the permeability contrast between layers. These PPGs also helped to improve sweep efficiency of the heterogeneity layers and increase the amount of oil recovered from the low permeability during the second water flooding. The oil recovered from low permeability rose substantially more than it did in the high permeability layers. The recovery factor obtained from the low permeability was increased by approximately 60%. In contrast, oil recovery from high permeability remained unchanged. Production pore

volume results indicated a significant improve in water injection through the low permeability layer. As result, significant amount of oil was produced from the low permeability layer. Nearly all of the injected water during the second water flooding was diverted into the low permeability layer.

Figure 10-3 illustrates the total oil recovery as a function of total injection pore volume. The oil recovery was calculated for both low and high permeability cores. The oil recovery from both cores before PPG injection reached approximately 45%. It increased substantially to approximately 85% after PPG injection.

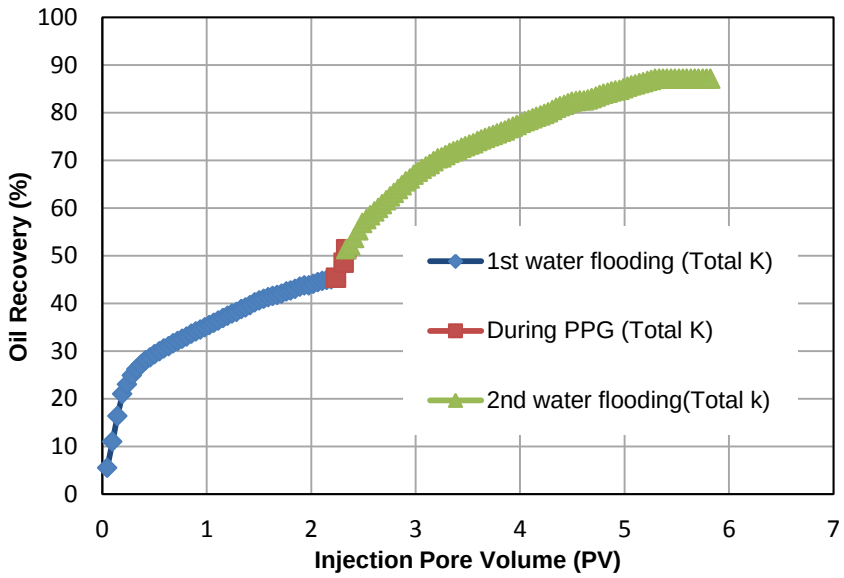

Figure 10-3—The oil recovery obtained from the total permeability cores.

10.6.2 Water Cut Results

The water cut results obtained during the water flooding cycles and PPG injection of the layer permeability contrasts ratio of 4 are plotted in **Figure 10-4**. During the first water flooding, water cut increased substantially during the first 1 PV brine injection. It

began to stable when 2PV of brine was injected. The water cut was higher than 90% at the end of the first water flooding.

When PPG was injected, the water cut dropped sharply into less than 60%. When the water flooding was resumed, the water cut slightly increased to approximately 80%. Water cut fluctuated during the second water flooding between approximately 80 and 90%. The water cut during this stage was much less than it was in the first water flooding, before PPG injection. This declined in water cut indicates that PPG effectively blocking the water channels and divert the water floods to displace more oil from the low permeability layer.

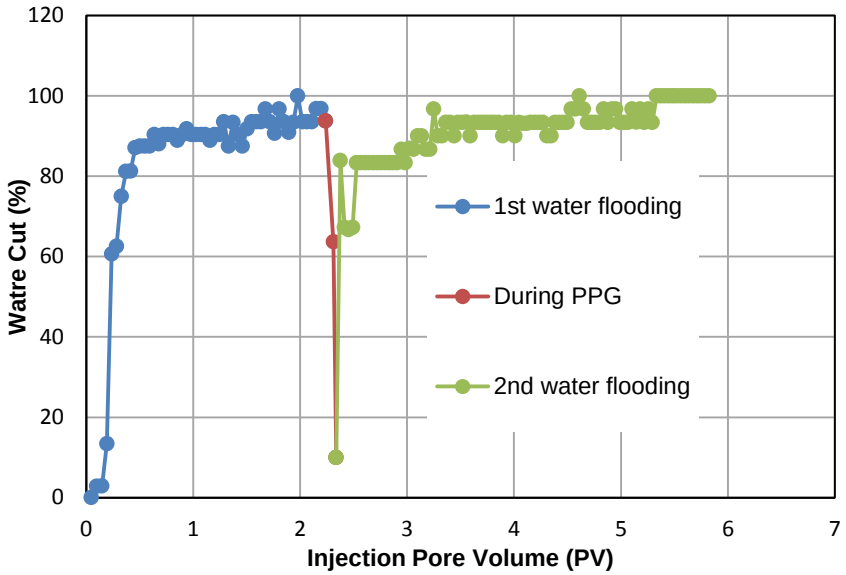

Figure 10-4—Water cut for permeability contrast ratio of 4.

10.6.3 Effect of permeability contrast ratio

Different ranges of permeability contrast ratio were performed to study their effect on oil recovery change. The oil recovery result of the permeability contrast ratio of 4 was compared to the oil recovery results obtained from permeability contrast ratio of 20 and

44. The oil recovery results obtained for each permeability contrast ratio during the water flooding cycles and during the PPG injection are listed in **Table 10-2**.

The incremental recovery ratio and the final total oil recovery are listed also in this table. The incremental oil recovery ratio was calculated based on ratio of the oil recovery increase from low and high permeabilities.

$$\text{Incremental Oil Recovery Ratio} = \frac{\text{Oil recovery incremental from low Permeability core}}{\text{Oil recovery incremental from high permeability core}}$$

The incremental ratio results were used to determine at which permeability ratio PPGs could be more efficient to increase oil recovery from the low permeability, un-swept layer.

The incremental oil recovery ratio results indicate that high permeability contrast ratio produced a larger oil recovery more than did the low permeability contrast ratio. The PPGs ability to increase the amount of oil recovered from a low permeability layers increased as the permeability contrast ratio increased. In permeability contrast ratio of 4, the oil recovery incremental after PPG injection from low permeability was 4.6 (92.1/20) while it was 1 (80.2/80) from high permeability. Therefore, the incremental oil recovery ratio equal 4.6 (4.6/1). The incremental oil recovery ratio increased to 31.5 and 40 as the permeability ratio increased to 20 and 44, respectively. These lab results are consistent with previous simulation results conducted by Imqam *et al.* (2015). The lab and simulation results indicated that PPG increased the oil recovered from the un-swept low permeability layers when the permeability layers became more heterogeneous.

Table 10-2—A summary of permeability contrast ratio results.

Permeability Contrast Ratio	Permeability, Darcy	Oil Recovery, %			Incremental Oil Recovery Ratio
		Before PPG	During PPG	After PPG	
4	High 21.7	80	80.1	80.2	4.6
	Low 6.2	20	31.7	92.1	
20	High 22.4	74	74	74	31.5
	Low 1.1	1.9	1.9	60	
44	High 22.1	52.2	52.2	53	40
	Low 0.5	0.9	0.9	36	

Evaluate the Injection Profile Improvement after PPG Injection.

Water injection is one of the most common reservoir problems created by reservoir heterogeneity. The injection profile was determined to evaluate water injection volume change through high and low permeability cores after PPG treatments. It is defined as the ratio of the total production volume of oil and water obtained from each permeability layer to the total brine injection volume. It can be calculated as:

$$\text{Injection profile} = (\frac{\text{Vp}}{\text{Vi}}) \times 100$$

where V_p is the cumulative volume of total fluid produced at each permeability and *Vi* is the cumulative volume of water injected.

Injection profile results examine the water injection changes as a result of PPG treatments. It provides a quantitative value of how much fluid is produced during the first water flooding, during the PPG, and after the second water flooding.

If injection profile increased gradually to 100% means water injection through that certain layer began to increase. If it is decreased gradually to less than 100% means water injection through that certain layer began to decrease. When it equals 100%, means the entire amount of water injection was flew through that layer.

The injection profile of the first water flooding, the PPG injection, and the second water flooding of the layer permeability contrast ratio of 4 is plotted in **Figure 10-5**. A poor injection profile was identified during the first water flooding. A low injection profile trend was identified for the low permeability layer. The injection profile was less than 5% in the low permeability, means less than 5% of total water injection that was used in the first water flooding was flew into low permeability layer. The injection profile, however, was above 90% in the high permeability layers. Thus, more than 90% of the total water injection was transported into the high permeability layers. This large water injection transport through the high permeability layer produced large amount of oil as illustrated in **Figure 10-2**.

The injection profile began to improve in the low permeability layers once the PPGs were injected into the heterogeneous permeability. The injection profile in the high permeability declined by approximately 10% while it increased in the low permeability by approximately 3%. The profile change indicates that the PPG plugged the high permeability layer and diverted the water injection to the low permeability layer.

The injection profile was significantly improved after the PPG treatment was complete. It began to increase in the low permeability layer during the second water flooding; it began to decrease in the high permeability layers. Thus, the PPG effectively diverted most of the injection water to sweep the large remained oil in the low permeability layers. The injection in the low permeability layer was improved significantly more than in the high permeability layers. It improved approximately to 60% in the low permeability layers and decreased approximately to 30% in the high permeability layer. Therefore, PPG can effectively divert more than 60% of the water injection into the low permeability layers and sweep more oil from the un-swept layer.

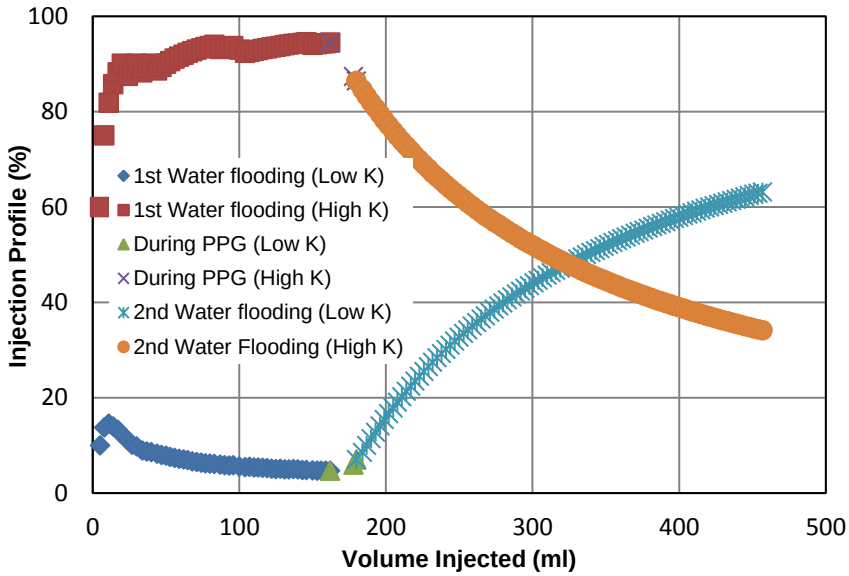

Figure 10-5—The injection profile for permeability contrast ratio of 4.

10.7 Summary and Conclusions

This section was focusing on evaluate the use of PPG to improve the conformance control in non-heterogeneity formations. Three different ranges of permeability contrast were tested. Water cut, oil recovery, and injection profile were determined. The following are the main conclusions drawn from this section:

- The effect of PPG on improving sweep efficiency and recovering more oil from low permeability became more obvious and effective as the sand pack model became more heterogeneous.
- Oil recovery from the low permeability sand packs improved significantly after the PPG injection was complete. The oil recovery incremental was strongly dependent on the permeability contrast ratio.
- The oil recovery incremental from that was obtained from the low permeability was larger than that obtained from the high permeability. The oil recovery incremental ratio revealed better oil improvement at a large permeability contrast ratio.
- Injection profile improved significantly after the PPG treatment. In some cases (e.g., permeability contrast of 4) the injection profile in low permeability was improved much larger than in high permeability layers. It reached approximately 63% in the low permeability and approximately 34 % in the high permeability.

Section 11: Simulation Study of Preformed Particle Gels (PPG) for Conformance Control

11.1 Introduction

Preformed particle gel (PPG) is an improved super absorbent polymer (SAP) for conformance control. Traditional SAPs cannot be used for conformance control due to their low strength, instability at high temperatures, and fast swelling time (Bai *et al.*, 2008). However, new series of SAPs, known as preformed particle gel (PPG), were developed for conformance control (Bai *et al.*, 2004a, 2007a). There are different types of PPGs, such as preformed bulk gels (Seright, 2004), partially preformed gels (Sydansk *et al.*, 2004), millimeter-sized preformed particle gels (Bai *at al.*, 2004a), and pH sensitive crosslinked polymers (Huh *et al.*, 2005). The main differences are in their swelling times and particle sizes. There have been several well tests using a temperature sensitive microgel system, called BrightWater® from TIORCO (Cheung *et al.*, 2007). Swelling gels were also successfully employed to control CO_2 breakthrough in CO_2 enhanced oil recovery projects (Wu and Bai, 2008).

Bai *et al.* (2007b, 2010) performed extensive experimental research to investigate the propagation of PPG through porous media and the influencing parameters, such as particle size, swelling capacity, injectivity, etc. However, no mathematical model has been proposed for propagation of gel and very few simulation studies have been done to model laboratory results.

Transport ability of PPG through pores depends on several parameters, such as pore diameter, structure of particles, particle size, and salinity. In fact, particle size is not

the diameter of each particle, but it is the average size of randomly selected number of particles through a sample. Particles can swell considerably; swelling ratio is a function of salinity. The particles, depending on the salinity, are defined as weak or strong.

Based on the study by Li and Bai (2001), parameters for evaluating gel performance were swelling capacity, elastic modulus, swelling rate, and fracture stress. The swelling capacity, A, can be defined as

$$A = \frac{M_l - M_s}{M_s}, \tag{11.1}$$

where M_l is the volume after swelling, and M_s is the dried gel volume. The change in elastic modulus versus time can be used as an indication of thermal stability and strength. It should be noted that gel strength is a function of both monomer and crosslinker concentrations and by increasing the crosslinker concentration, the strength will increase due to the rapid increase in network density. However, swelling capacity will be lost if the crosslinker concentration is too high and this is an important consideration for designing gel treatments. Thermal stability can be enhanced from 90 ^{0}C to 120 ^{0}C when only 0.2 wt% thermal stabilizing agent is added. Higher temperatures are favorable, as the swelling capacity of gels increases considerably at higher temperatures.

In this chapter, PPG experiments are presented first. Experiments discussed in this chapter are all conducted by Dr. Bai and his research staff at Missouri University of Science and Technology, Rolla. Next, we describe the mechanistic model developed and implemented in an in-house reservoir simulator, UTGEL. The simulation results are validated with different experimental and field data.

11.2 Experimental Procedure

11.2.1 Gels and Materials

A superabsorbent polymer comprised mainly of a potassium salt of cross-linked polyacrylamide copolymer was used as the PPGs in all experiments. When dry, these PPGs are white, sugar-like, granular powder. Table 11-1 lists the typical characteristics of the PPGs used in this study. In aqueous solution, PPGs can absorb a large amount of water because of their hydrophilicity which allows hydrogen bonding with water molecules, although the swelling solution salinity affects ability to adsorb water.

Table 11-2 shows that PPG swelling ratio is greatly affected by brine salinity. Figure 11-1 shows a comparison of dry gel particles and fully swollen particles in 1.0 wt. % sodium chloride (NaCl) solution. The laboratory data shows that swelling ratio decrease as brine concentration increases as shown in Figure 11-2.

Table 11-1: Characteristics of PPG used in the experiments.

Properties	Value
Absorption Deionized Water (g/g)	>200
Apparent Bulk Density (g/l)	540
Moisture Content (%)	5
pH Value	5.5-6.0 (+/- 0.5; 1% gel in 0.9% NaCl)

Table 11-2: Effect of brine salinity on swelling ratio.

Brine Salinity, wt. % NaCl	Swelling Ratio, g/g
0.05	194
0.25	98
1	52
10	32

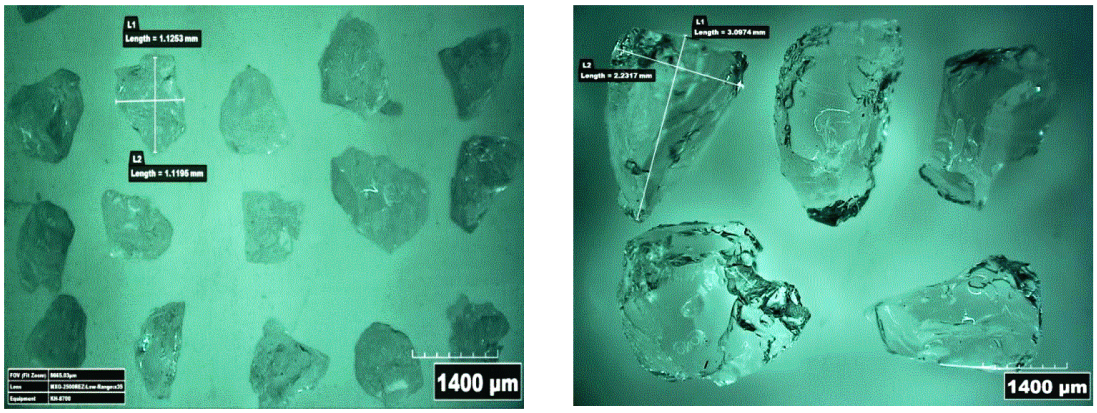

(a) (b)

Figure 11-1: Comparison of dry and swollen PPG particles: (a) Dry PPGs with 18/20 mesh size, (b) Fully swollen PPGs in 1.0 wt. % NaCl (Bai, 2013).

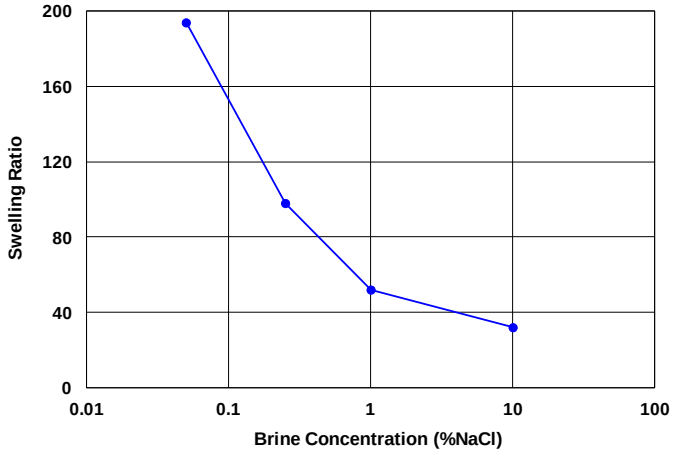

Figure 11-2: The swelling ratio as a function of brine concentration.

The following section represents different experiments designed and conducted for evaluating PPG performance. Experimental data is used to model the flow and transport of PPG in porous media.

11.2.2 Transparent Open Fracture Experiment

A 1-D transparent model constitutes two parallel acrylic plates between which

there is a rubber O-ring. Bolts, nuts, and shims are used to fix the two parallel acrylic plates and control the fracture width. On one side of the plate, there is a hole as inlet for the injection of fluids and PPG; on the other side, there is another hole as the outlet to discharge fluids and PPG. In addition, there are three extra holes on a plate as pressure taps, connecting to the pressure transducers. The schematic diagram of the experimental setup is shown in Figure 11-3. The model was used to study the particle strength and size effect on the injectivity and to visually observe particle movement in a single fracture. Brine was injected at different flow rates and then PPG was extruded into the fracture to evaluate the injection pressure. Before PPG injection, the fracture system is saturated with brine to characterize using flow measurements. Completely swollen PPG sample with 40-mesh size was prepared with four different brine salinities (0.05, 0.25, 1, and 10 wt% NaCl) for the experiment.

The test was conducted in three fracture widths (0.5, 1, and 1.5 mm) and at different salinities. After gel placement, water was injected to evaluate plugging efficiency of the gel. The gel moves along the fracture like a piston and gravity effects on PPG shape and movement are neglected. Injection pressure measurements were recorded at different injection flow rates and used for comparison with simulation results. The measured PPG injection pressures for different fracture widths (0.5, 1, 1.5 mm) are shown in Figure 11-4 through Figure 11-6. The pressure gradient remained stable during the experiment and there was no considerable plugging (continuous pressure gradient increase) at the end of gel injection. Also, resistance factor and residual resistance factor data were measured at different salinities and different fracture widths which helped us to develop a model for resistance factor and residual resistance factor as a function of

salinity and injection rate.

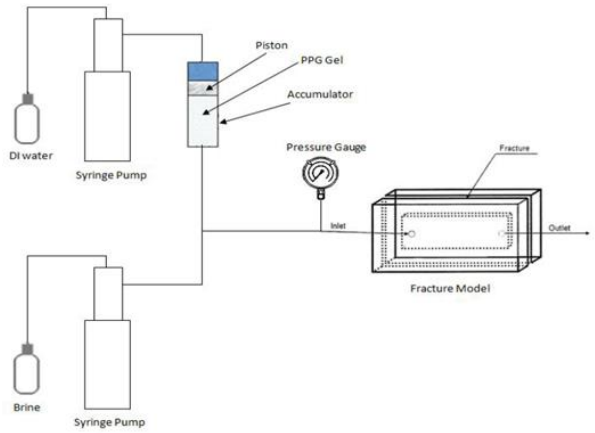

Figure 11-3: Experimental setup for PPG injection into an open fracture (Bai, 2013).

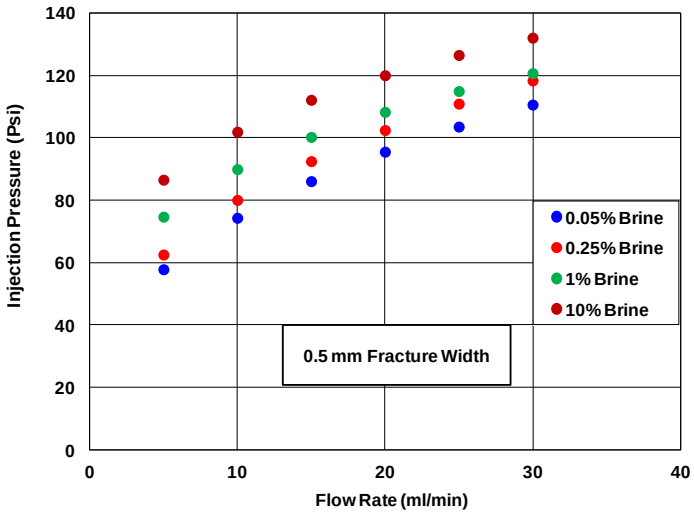

Figure 11-4: PPG injection pressure vs. flow rate for 0.5 mm fracture width: 0.05 wt.% NaCl, (b) 0.25 wt.% NaCl, (c) 1 wt.% NaCl, (d) 10 wt.% NaCl.

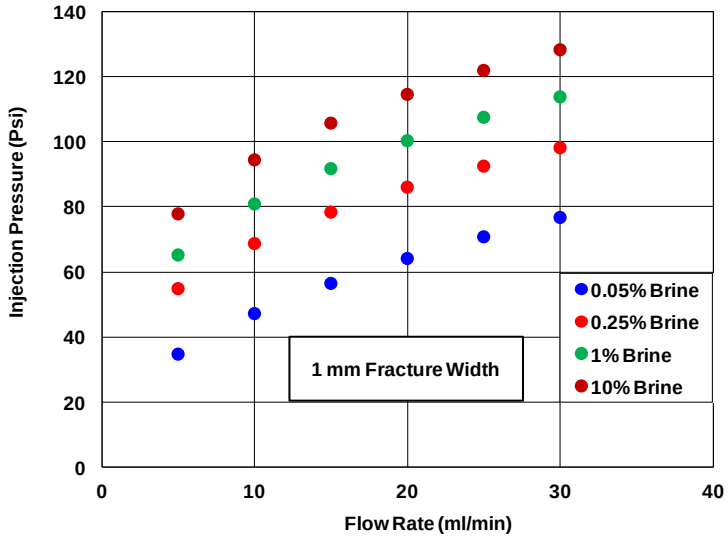

Figure 11-5: PPG injection pressure vs. flow rate for 1 mm fracture width: 0.05 wt.% NaCl, (b) 0.25 wt.% NaCl, (c) 1 wt.% NaCl, (d) 10 wt.% NaCl.

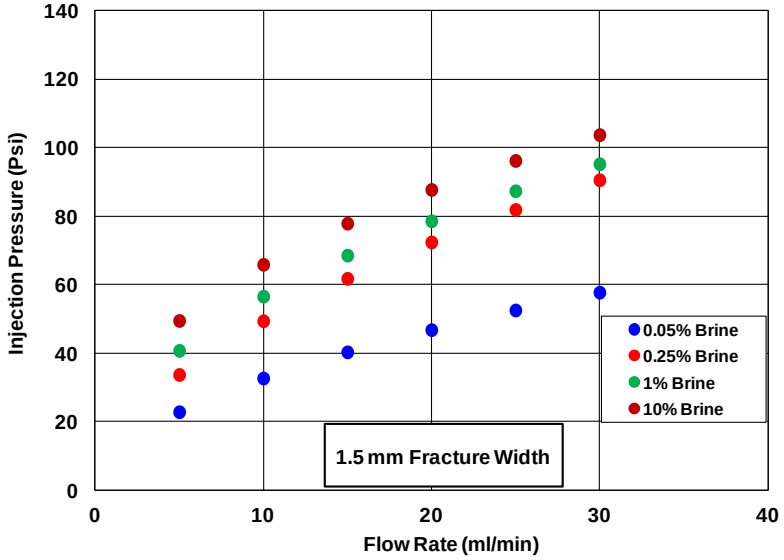

Figure 11-6: PPG injection pressure vs. flow rate for 1.5 mm fracture width: 0.05 wt.% NaCl, (b) 0.25 wt.% NaCl, (c) 1 wt.% NaCl, (d) 10 wt.% NaCl.

11.2.3 Homogeneous Sandpack Experiment

Sandpack with 1 inch diameter and 20 inches length (Figure 11-7) was divided into four sections with equal lengths by three pressure taps. Four pressure transducers

were mounted on the inlet and on the pressure taps along the sand pack for monitoring the pressure behavior of the injection process. Stainless steel screens were used on each end of the sand pack and all pressure taps to prevent sand migration. Dry Ottawa sands with particle size of 354 - 420 micron (40/45 mesh) were used with a measured water permeability of 27.29 Darcy. Figure 11-8 shows sand particles and homogeneous sandpack porous media. Sands were gradually packed into the model with a constant packing pressure (200 psi) to ensure all sections of the sandpack having the same porosity. Consistent permeability value was measured for each section of the sandpack as shown in Figure 11-9 and homogenous porous media model was assumed in the following experimental discussion and simulation work. The pore volume of the sand pack was 49.7 ml with the porosity of the sandpack measured as 0.193. The brine used in the experiment was 1 wt.% KCl and 2000 ppm preformed particle gel was used for the gel injection. The experimental procedure is presented below:

- Sandpack was initially saturated with 1 wt% KCl brine and the pore volume was calculated.
- Brine was injected at different flow rates and the absolute permeability was calculated.
- Oil was injected to displace water until no water came out and the oil in place was calculated based on the volume of water displaced.
- Brine was injected at 2 ml/min rate and the differential pressure with time was recorded in each section of the sandpack to obtain the injectivity curve. The volume of oil produced was also recorded every 2.5 minutes to obtain the oil recovery curve for the water flooding process.
- PPG was injected at 2 ml/min. The injection pressure was monitored in each section and the oil production was recorded.
- Brine was injected again at 2 ml/min rate and the pressure behavior, oil recovery, and water cut were observed.

The sandpack results of oil recovery and water cut are given in Figure 11-10 and Figure 11-11. Waterflood oil recovery was 62% OOIP and PPG and subsequent

waterflood increased the recovery by additional 20%. The water cut was reduced from 99% to almost 79% during microgel injection which is a good indication for effectiveness of this microgel in reducing water cut.

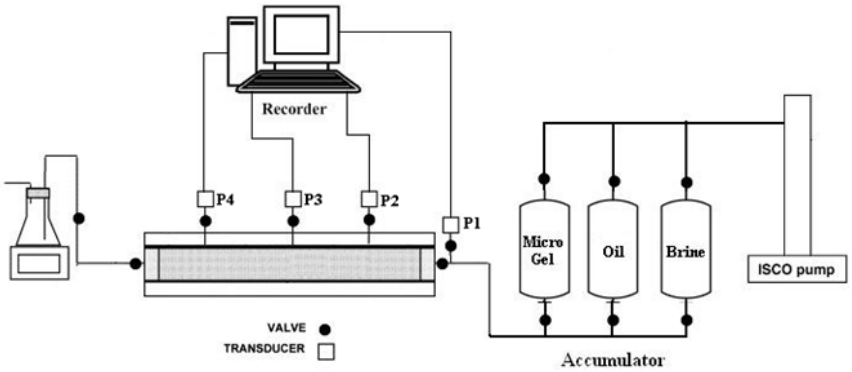

Figure 11-7: Schematic representation of homogeneous sandpack model for PPG injection (Bai, 2013).

Figure 11-8: Dry Ottawa sands used in the sandpack model (homogeneous porous media is achieved for sandpack experiment).

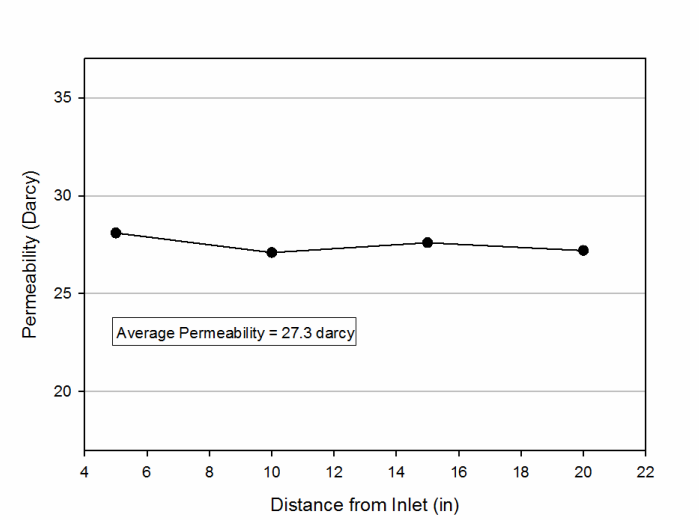

Figure 11-9: Permeability profile along the sandpack model (Bai, 2013).

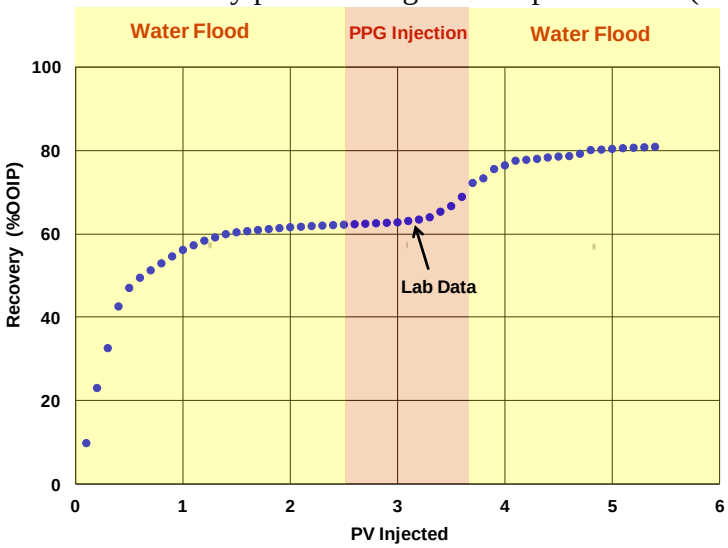

Figure 11-10: Measured oil recovery for homogeneous sandpack experiment (Bai, 2013).

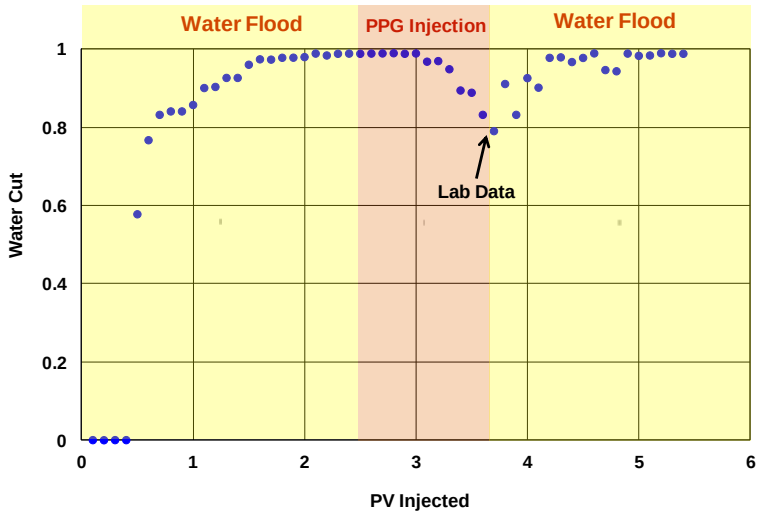

Figure 11-11: Measured water cut for homogeneous sandpack experiment (Bai, 2013).

11.2.4 Heterogeneous Sandpack Experiment (No Crosslow)

The main objective of these experiments is to evaluate PPG performance in heterogeneous porous media and to achieve this two different heterogeneous systems are designed. The first is two parallel sandpacks with different permeabilities and without any crossflow between two packs as shown in Figure 11-12. The flow rates are the same for both sandpacks and the PPG performance in each pack will be evaluated based on the measured oil recovery and water cut.

The experimental procedure is presented below:

- Both Sandpacks were initially saturated with 1 wt% KCl brine and the pore volumes were calculated.
- Brine was injected at different flow rates and the absolute permeability of each sanpack was calculated.
- Oil was injected to displace water until no water was produced and the oil saturation is calculated based on the volume of water displaced.
- Brine was injected at 1 ml/min and the differential pressure with time was recorded to obtain the injectivity curve. The volume of oil produced from each sandpack was also recorded every 2.5 minutes to obtain the oil recovery curve for the water flooding process in both sandpacks.

- PPG (2000 ppm concentration) was injected at 1 ml/min for 0.2 PVs. The injection pressure was monitored in each section and the oil production was recorded.
- Brine was injected again at 1 ml/min and the pressure behavior, the oil recovered, and the water cut were observed.

The sandpack results of oil recovery and water cut are given in Figure 11-13 and Figure 11-14. Waterflood oil recovery was 39% OOIP and PPG and subsequent waterflood increased the recovery by about 17%. The water cut was reduced from 99% to almost 79% during microgel injection which is a good indication for effectiveness of this microgel in reducing water cut.

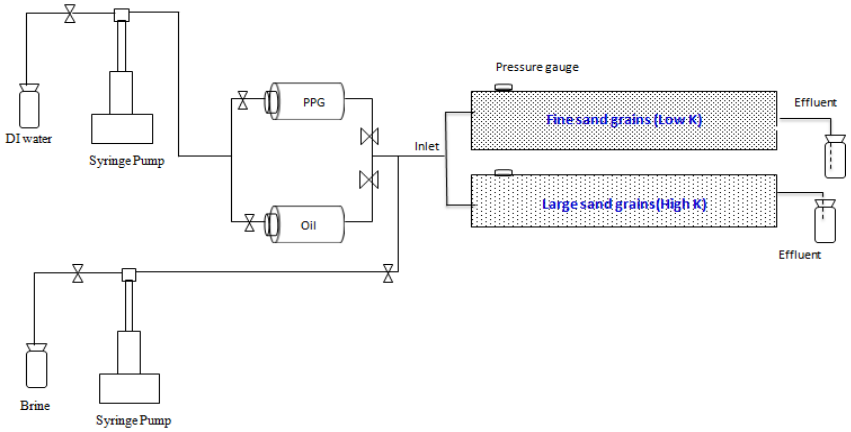

Figure 11-12: Schematic representation of heterogeneous sandpack model with different permeabilities (no crossflow) for PPG injection (Bai, 2014).

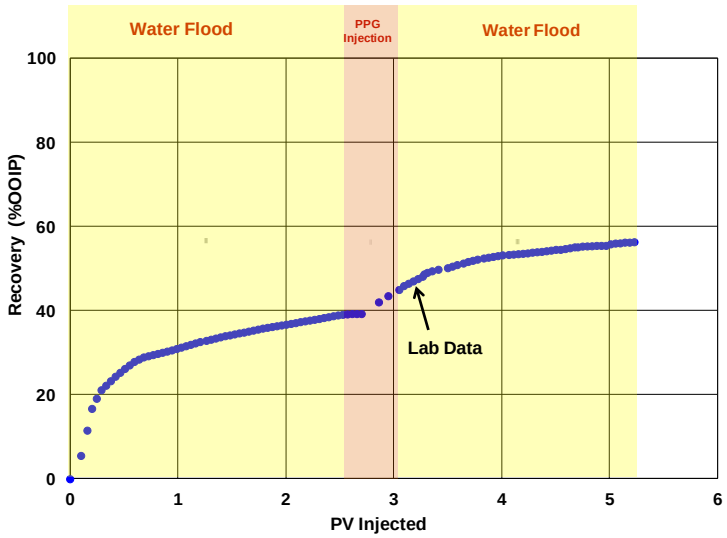

Figure 11-13: Measured oil recovery for heterogeneous sandpack experiment without crossflow (Bai, 2014).

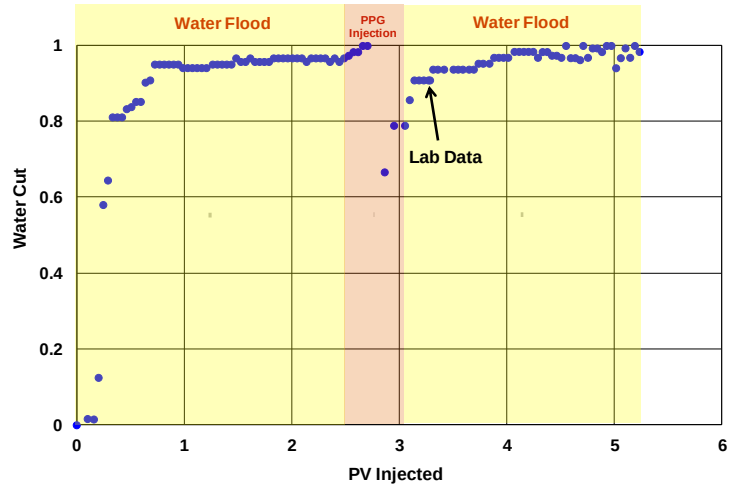

Figure 11-14: Measured water cut for heterogeneous sandpack experiment without crossflow (Bai, 2014).

11.2.5 Heterogeneous Sandpack Experiment (With Crosslow)

The second heterogeneous system is two parallel sandpack with different permeabilities (inner low permeability zone and outer high permeability zone) and with

crossflow between two porous media as shown in Figure 11-15. A perforated screen tube with diameter less than 1 inch was placed inside the stainless steel round tube to design high and low permeability zones in contact with each other. Large sand grain was poured first inside the stainless steel around perforated screen tube to create high permeability media. Fine sand grain was then poured inside perforated screen to obtain low permeability zone. The outer high permeability zone was filled with sand of 20-30 mesh size and the inner low permeability zone was filled with sand of 80-100 mesh size. The oil recovery and water cut from the combined sandpack system were measured at the effluent. The size of the sandpacks was 5.08 cm in diameter and 30.48 cm in length.

The coreflood results of oil recovery and water cut for heterogeneous case with no crossflow are given in Figure 11-16 and Figure 11-17. Waterflood oil recovery was 65% OOIP and PPG and subsequent waterflood increased the recovery by about 6%.

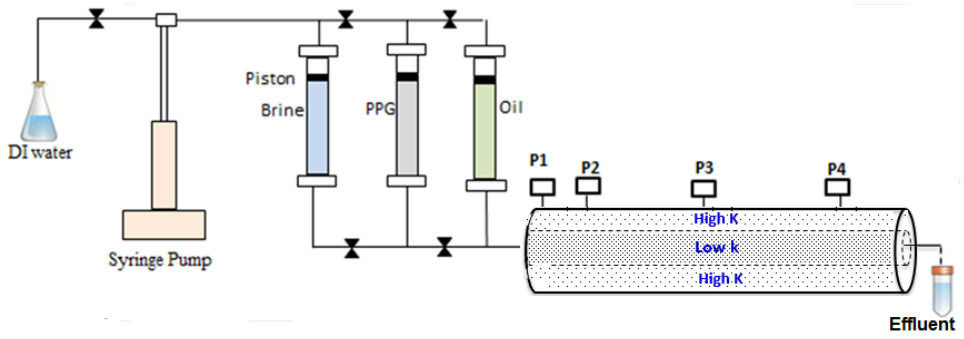

Figure 11-15: Schematic representation of heterogeneous sandpack model with different permeabilities (with crossflow) for PPG injection (Bai, 2014).

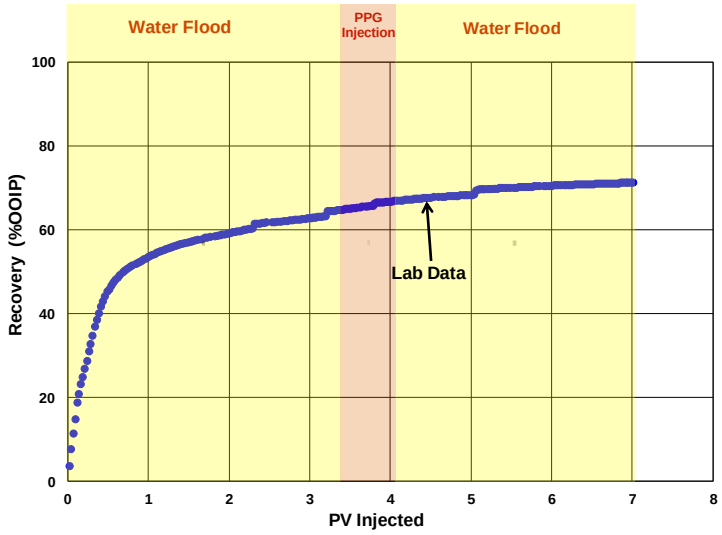

Figure 11-16: Measured oil recovery for heterogeneous sandpack experiment with crossflow (Bai, 2014).

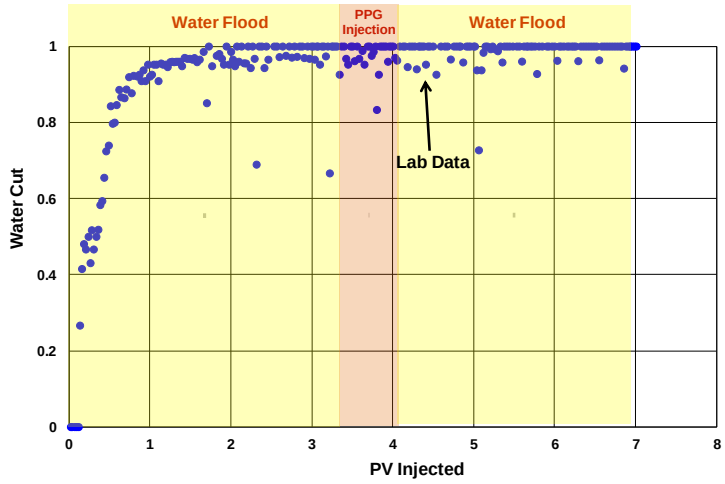

Figure 11-17: Measured water cut for heterogeneous sandpack experiment with crossflow (Bai, 2014).

11.2.6 Nanogel Berea Sandstone Coreflood Experiment

A high permeability Berea sandstone core was used in this study (Figure 11-18).

Liquid permeability, pore volume, and porosity of the core were determined by routine core analysis. The core is homogeneous with dimensions of 3.9×3.9×53.1 cm, porosity of 0.23, permeability of 550 mD, and pore volume of 185.1 cm^3.

The microgel used in the work was provided by Poweltec in France. It is crosslinked hydrophilic gel with the particle size of 100-200 nanometers. It was in liquid form with 30 wt% of solid. 1000 ppm microgel composed of 1 wt% KCl brine was prepared using energic stirring (warring blender 11000 rpm for 10 minutes) for coreflooding tests. Figure 11-19 shows the image of particles from ESM (Environmental Scanning Electron Microscope). Figure 11-20 shows the particle size distribution of the microgel prepared by 1 wt% KCl brine at 25 ^{0}C measured by a sysmex FPIA3000 (Malvern) particle size analyzer.

Figure 11-21 shows the experimental set up which consists of one ISCO pump to inject brine, oil, and microgel. A hassler type core holder is designed for the core with the dimension of 3.85×3.85×60 cm. The coreholder has five pressure taps enabling pressure drop measurements at different sections: 12-24 cm, 24-32 cm, 32-36 cm, 36-48 cm, and total length 0-60 cm. The core holder contains rubber sleeve that provides a seal around the core in order to prevent any leakage. The seal is achieved by hydraulic pumping water into the annular space between the rubber sleeve and the core holder outer wall.

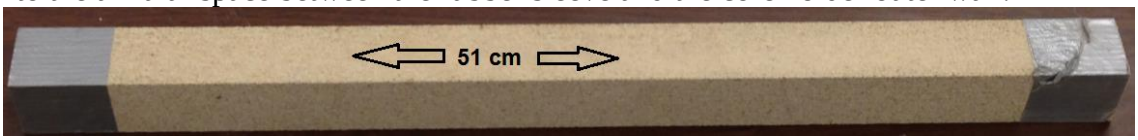

Figure 11-18: The image of the long Berea sandstone core used for gel conformance control study.

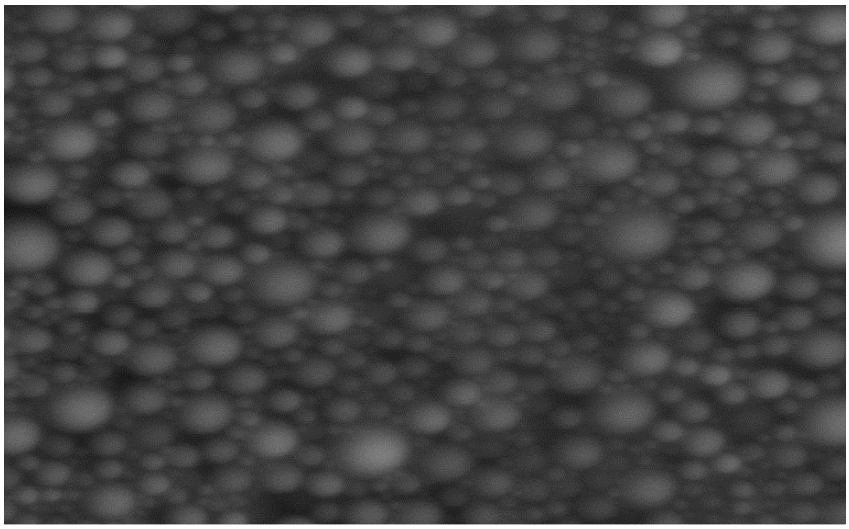

Figure 11-19: The image of the swollen microgel before injection (Bai, 2013).

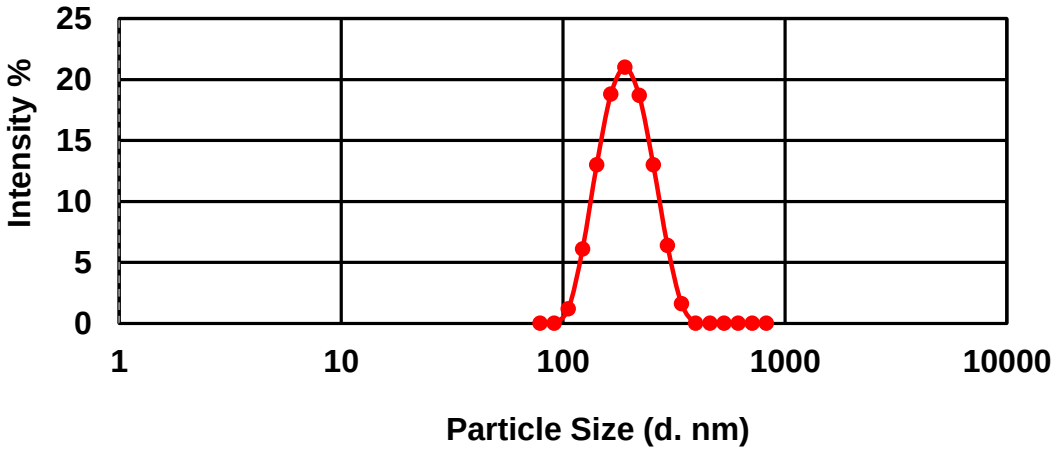

Figure 11-20: Microgel characterization with microparticle distribution analyzer using Sysmex FPIA3000 (Malvern) with a salinity of 10,000 mg/L (Bai, 2013).

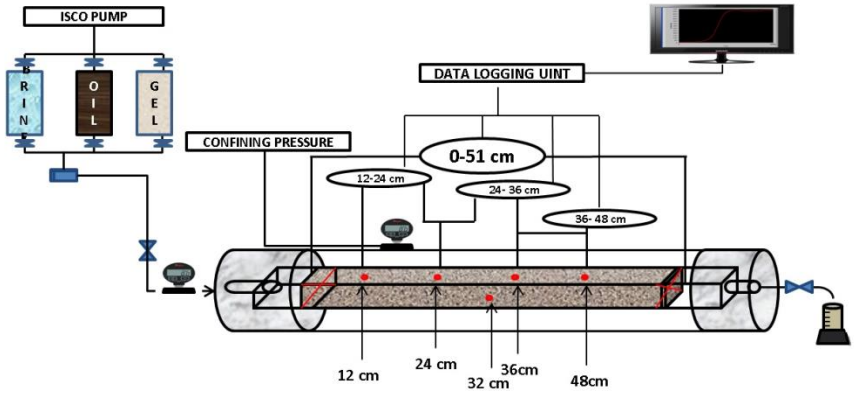

Figure 11-21: Experimental set up used for Berea sandstone coreflood experiment (Bai, 2013).

The experiment is designed to determine microgel propagation, permeability reduction, oil recovery, and water cut. The Berea sandstone core with water permeability of 558.62 mD was used for this experiment at room temperature of 25 ^{0}C. After saturating and preparing the core, it was flooded with 0.97 PV of brine at the flow rate of 1.5 cm^3/min and then flooded with 0.9 PVs of microgel at the rate of 1.5 cm^3/min. Finally, 1.16 PVs of post water was injected again at the same rate of 1.5 cm^3/min. The mineral oil from Fisher Scientific was used for the oil recovery experiment. A brief summary of the experimental procedure is outlined as

- The core was prepared, dry weight was measured and then it was under vacuum for one day.
- The core was saturated with 1 wt% KCl brine and the pore volume was calculated.
- Brine was injected at different flow rates and the absolute permeability was calculated using measured pressure drop.
- Mineral oil was injected at 1.5 cm^3/min to displace water until no water comes out and the oil in place was calculated based on the volume of water displaced.
- Brine was injected at 1.5 cm^3/min rate and the differential pressure with time was recorded. The volume of produced oil was also recorded every few minutes to obtain waterflood oil recovery curve.
- One PV of microgel was injected at the same injection rate of 1.5 cm^3/min. The

injection pressure was monitored in each section and the oil production was recorded every few minutes.

- Brine was injected again at 1.5 cm^3/min rate and the pressure behavior, the oil recovered, and water cut were monitored.

The coreflood results of oil recovery and water cut are given in Figure 11-22 and Figure 11-23. Waterflood oil recovery was 40% OOIP and PPG and subsequent waterflood increased the recovery by about 20%. The water cut was reduced from 99% to almost 90% during microgel injection which is a good indication for effectiveness of this microgel in reducing water cut. The experimental results indicated that residual oil saturation was reduced from 0.374 during primary waterflood to 0.289 during microgel injection and finally to 0.223 during post water injection.

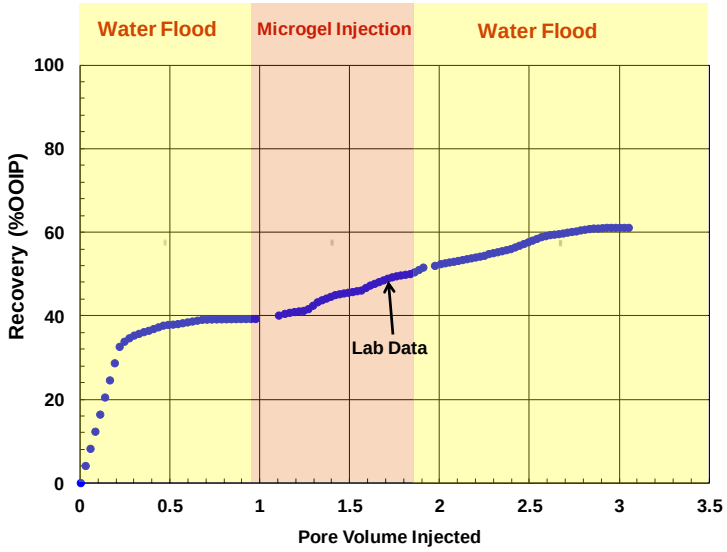

Figure 11-22: Measured oil recovery for Berea sandstone coreflood (Bai, 2013).

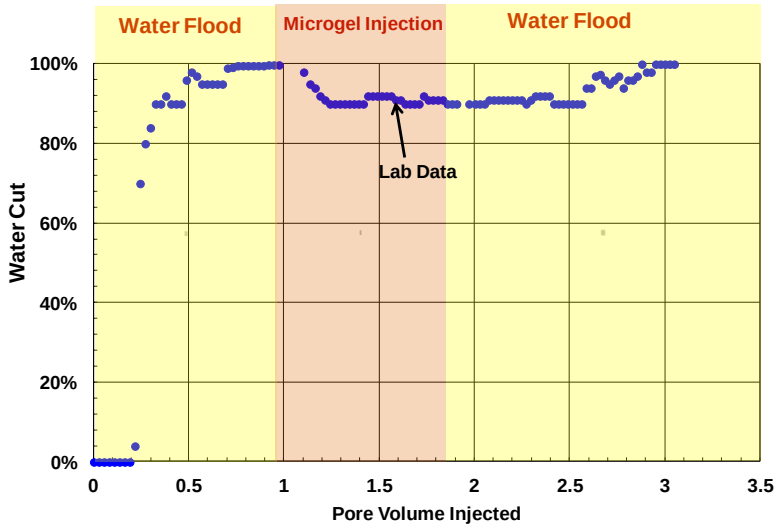

Figure 11-23: Measured water cut for Berea sandstone coreflood (Bai, 2013).

11.3 PPG Model Description

11.3.1 PPG Transport Model

There are different conditions for particles to flow and transport through porous media. Viscosity and resistance factor are two important properties for modeling PPG flow in porous media. The resistance factor is a function of salinity and flow rate based on the laboratory results. The swelling ratio and subsequent size of swelled particles are calculated.

The average pore throat radius is calculated using porosity and permeability.

$$r_h = 1.15\sqrt{\frac{8\bar{k}}{\phi}}, \tag{11.2}$$

where the average permeability, $\bar{k}$, is approximated from

$$\bar{k} = \left[\frac{1}{k_x}\left(\frac{u_{x\ell}}{u_\ell}\right)^2 + \frac{1}{k_y}\left(\frac{u_{y\ell}}{u_\ell}\right)^2 + \frac{1}{k_z}\left(\frac{u_{z\ell}}{u_\ell}\right)^2\right]^{-1}, \tag{11.3}$$

where k_x, k_y, k_z are directional permeabilities, $u_{x\ell}, u_{y\ell}, u_{z\ell}$ are components of fluxes in each direction for the aqueous phase and u_ℓ is aqueous phase flux.

In each grid cell, we calculate the pore throat size using Eq. (11.2) and permeability and porosity assigned to that grid cell. PPG will move out of a gridblock depending on the size of particles in comparison to the pore throat diameter assigned to the gridblock. If PPG cannot pass through the gridblock, the resistance factor is calculated and the aqueous viscosity is increased accordingly. The conditions for passing PPG particle through the pore throat for weak and strong PPG particles (Bai *et al.*, 2004b) are as follows:

- For weak PPG particles: If PPG particle diameter is less than $5.7 \times d_p$.
- For strong PPG particles: If PPG particle diameter is less than $1.3 \times d_p$.

Under the above criteria for weak and strong gels, the PPG particles will pass through the pore throat. If above conditions for a specific gridlock hold and PPG can pass through pore throat, gel particles will enter that specific gridblock and resistance to water flow by PPG will happen (Goudarzi *et al.*, 2013, 2014). The PPG will increase the viscosity of aqueous phase and new effective viscosity for water will be calculated as defined below:

$$\mu_{effective} = RF \times \mu_{aqueous\ phase}, \qquad During\ \ PPG\ Injection \tag{11.4}$$

$$\mu_{effective} = RRF \times \mu_{aqueous\ phase}. \qquad During\ \ Post Water\ Injection \tag{11.5}$$

The resistance factor (RF) is used during PPG injection and residual resistance factor (RRF) is for post water injection and will be explained in more detail later. This increase in water viscosity will lead to reduction of water phase mobility, improvement in

mobility ratio, and subsequently delay water production.

11.3.2 Swelling Ratio

Swelling ratio is defined as the ratio of PPG particle volume after and before swelling. Bai (2010) and Imqam *et al.* (2014) reported a relationship for swelling ratio as a function of salinity based on laboratory measurements. They showed that the particles can swell very fast within 60 minutes and the final swelling ratio depends on salt concentration, with higher salt concentration leading to the smaller swelling ratio. It is presumably due to the static electric repulsive force and charge balance. At low salt concentrations, the electric repulsive force will separate the gel molecules and create more space for water to enter (Bai *et al.*, 2004b).

We developed an empirical correlation for swelling ratio vs. effective salinity to fit their laboratory data.

$$SF = a_p (C_{SEP})^{n_p}, \tag{11.6}$$

where a_p and n_p are model parameters, *SF* is the swelling ratio, and C_{SEP} is the effective salinity $\left(C_{SEP} = C_5 + \beta_p C_6\right)$ in meq/ml which takes into account the combined effect of anions (C_5) and divalent cations (C_6) on swelling ratio. The effect of pH is not considered in this model.

11.3.3 PPG Viscosity

UTGEL models viscosity of aqueous solution containing gel as a function of gel concentration and water viscosity as shown below (Thurston *et al.*, 1987):

$$\mu_1 = \mu_w \left[1 + A_{ppg,1} C_{ppg,1} + A_{ppg,2} C_{ppg,1}^2\right], \tag{11.7}$$

where $C_{ppg,1}$ is the PPG concentration in aqueous phase, μ_w is the water viscosity, and $A_{ppg,1}$ and $A_{ppg,2}$ are model parameters.

11.3.4 PPG In-situ Rheology

The viscosity of gel decreases by increasing shear rate. The relationship between gel viscosity and shear rate is modeled using Meter's equation (Meter and Bird, 1964) as follows:

$$\mu_1 = \mu_w + \frac{\mu_1^0 - \mu_w}{1+\left(\frac{\dot{\gamma}_{eq}}{\dot{\gamma}_{1/2}}\right)^{P_\alpha - 1}}, \tag{11.8}$$

$$\dot{\gamma}_{eq} = \frac{\dot{\gamma}_c |u_\ell|}{\sqrt{k k_{r\ell} \phi S_\ell}}, \tag{11.9}$$

where μ_1^0 is the gel solution viscosity at low shear rate, $\dot{\gamma}_{1/2}$ and P_α are model parameters, $\dot{\gamma}_c$ is the shear rate correction, $|u_\ell|$ is magnitude of flux, and $k_{r\ell}$ is relative permeability of phase ℓ.

The empirical correlations for resistance factor/apparent viscosity are developed based on the measured resistance factor at different salinities, injection rates, and fracture widths. The proposed models use resistance factor as major input parameters with consideration of flow rate and salinity on resistance factor.

11.3.5 PPG Resistance Factor with Salinity Effect

Gel can reduce the water effective permeability where the degree of permeability reduction depends on gel type, salinity, hardness, shear effects, and rock properties. Resistance factor (RF) is determined by the ratio of the differential pressure for

microgel injection to that of initial water injection as

$$RF = \frac{(k_w/\mu_w)_{BaseWater}}{k_{microgel}/\mu_{microgel}} = \frac{\Delta P_{microgel}}{\Delta P_{BaseWater}}, \quad (11.10)$$

where k_w, $k_{microgel}$ are effective permeabilities during waterflood and microgel injection, and μ_w, $\mu_{microgel}$ are water and microgel viscosities, and ΔP_w, $\Delta P_{microgel}$ are the pressure drop during waterflood and microgel injection.

Measured data for resistance factor as a function of flow rate and salinity for different fracture widths are reported. Table 11-3 gives the empirical correlations developed based on measured resistance factor at different salinities and fracture widths. It is clear that resistance factor decreases as flow rate increases indicating the shear thinning behavior of microgels (Zhang et al., 2010). The viscoelastic behavior of PPG is related to coil structure of polyacrylamide molecules with a flexible nature (Green and Willhite, 1998).

For each fracture width, the coefficient "a_1" varies significantly with salinity but relatively a minor variation in the exponents "b_1". Therefore, an exponential function was used to fit the data as shown in Figure 11-24. We believe that resistance factor is sensitive to the water hardness (i.e. calcium and magnesium concentrations). We have proposed the following correlation but additional laboratory data are required to validate it (Goudarzi *et al.*, 2015).

$$a_1 = a_{11}(C_{SEP})^{a_{12}}. \quad (11.11)$$

The resistance factor is expressed as

$$RF = a_{11}(C_{SEP})^{a_{12}}(\dot{\gamma}_{eq})^{b_1}, \quad (11.12)$$

where a_{11}, a_{12}, and b_1 are model parameters, $\dot{\gamma}_{eq}$ is shear rate, and C_{SEP} is the effective salinity $\left(C_{SEP} = C_5 + \beta_p C_6\right)$ in meq/ml which takes into account the combined effect of anions (C_5) and divalent cations (C_6) on resistance factor. The proposed model considers the effect of shear rate and salinity on resistance factor.

Table 11-3: Resistance factor correlations based on fracture experiments (Zhang and Bai, 2010).

Fracture Width (mm)	Salinity (wt%)	Resistance Factor
0.5	0.05	$RF = 24130\,q^{-0.616}$
	0.25	$RF = 27640\,q^{-0.643}$
	1	$RF = 37976\,q^{-0.731}$
	10	$RF = 46353\,q^{-0.764}$
1	0.05	$RF = 106646\,q^{-0.556}$
	0.25	$RF = 203784\,q^{-0.674}$
	1	$RF = 247784\,q^{-0.689}$
	10	$RF = 311457\,q^{-0.72}$
1.5	0.05	$RF = 207954\,q^{-0.48}$
	0.25	$RF = 291839\,q^{-0.446}$
	1	$RF = 400038\,q^{-0.525}$
	10	$RF = 536435\,q^{-0.585}$

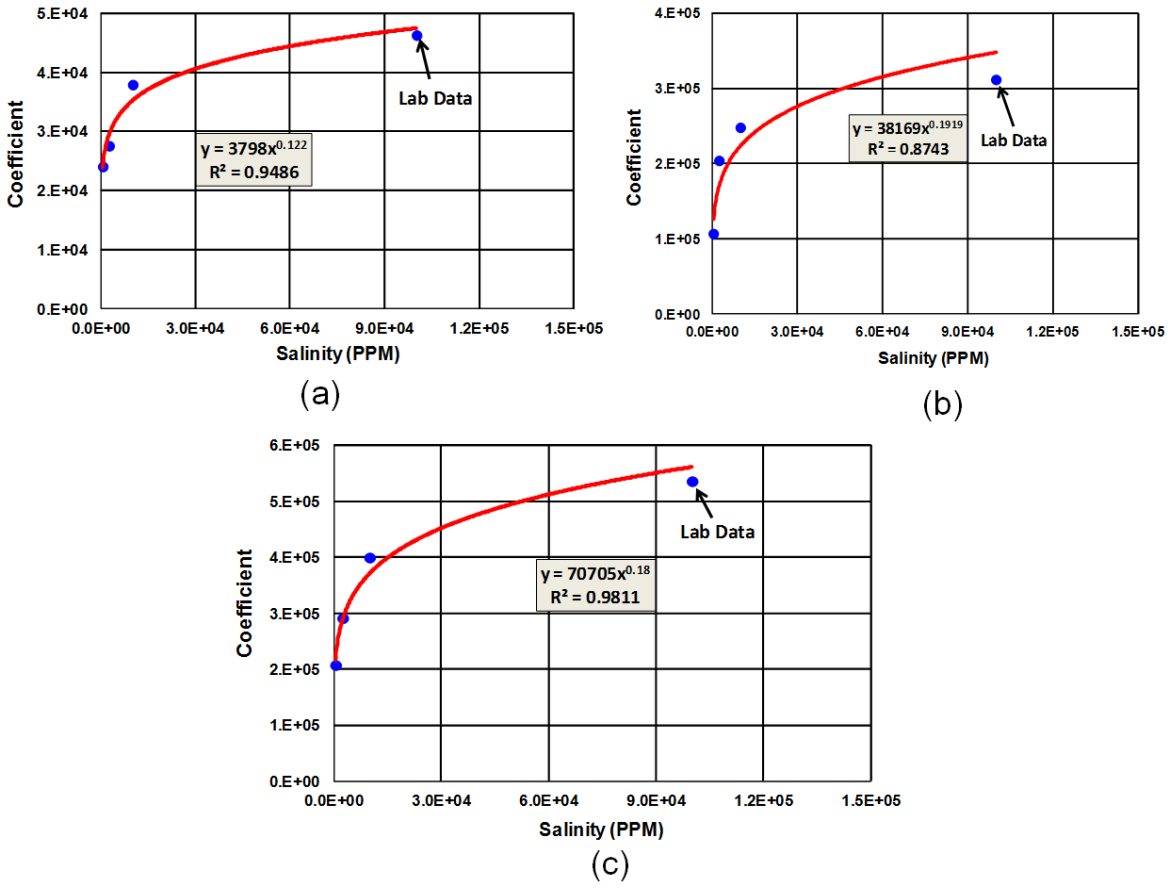

Figure 11-24: Calculated (curve) and measured (points) resistance factor coefficients (a_1) as a function of salinity for different fracture widths: (a) 0.5 mm, (b) 1 mm, (c) 1.5 mm.

11.3.6 Residual Resistance Factor with Salinity Effect

Residual resistance factor, RRF, is defined to ensure that permeability reduction will remain in post water injection. RRF is defined as the ratio of pressure drop during post water injection to the pressure drop during initial waterflood as follows:

$$RRF = \frac{(k_w/\mu_w)_{BaseWater}}{(k_w/\mu_w)_{PostWater}} = \frac{\Delta P_{PostWater}}{\Delta P_{BaseWater}}. \tag{11.13}$$

where $\Delta P_{BaseWater}$, $\Delta P_{PostWater}$ are the pressure drop during initial water and post water injection.

Measured data for residual resistance factor as a function of flow rate and salinity for different fracture widths are reported.

Table 11-4 gives the empirical correlations developed using measured residual resistance factor for different salinities and fracture widths. Similar to resistance factor, residual resistance factor decreases as flow rate increases.

The coefficient "a_2" is changing with salinity considerably for each fracture width with minor change in the exponents "b_2". Therefore, an exponential function can be used to fit the data as shown in Figure 11-25. We believe that residual resistance factor is sensitive to the brine hardness (i.e. calcium and magnesium concentrations). We have used the following correlation but need additional laboratory data for validation.

$$a_2 = a_{21}(C_{SEP})^{a_{22}}. \tag{11.14}$$

Accordingly final developed model for resistance factor will be expressed as following:

$$RRF = a_{21}(C_{SEP})^{a_{22}}(\dot{\gamma}_{eq})^{b_2}, \tag{11.15}$$

where a_{21}, a_{22}, and b_2 are model parameters. The proposed model considers combined effects of shear rate and salinity on residual resistance factor.

Table 11-4: Residual resistance factor correlations based on fracture experiments (Zhang and Bai, 2010).

Fracture Width (mm)	Salinity (wt%)	Residual Resistance Factor
0.5	0.05	$RRF = 4439.3q^{-1.057}$
	0.25	$RRF = 5490.4q^{-1.062}$
	1	$RRF = 21766q^{-1.482}$
	10	$RRF = 30776q^{-1.503}$
1	0.05	$RRF = 26980q^{-0.975}$
	0.25	$RRF = 48265q^{-1.155}$
	1	$RRF = 59764q^{-1.199}$
	10	$RRF = 136059q^{-1.418}$
1.5	0.05	$RRF = 76385q^{-1.012}$

11.3.7 PPG Retention Model

A new retention model was developed and implemented into the simulator to consider the PPG retention. UTGEL uses Langmuir isotherm for PPG retention (adsorption) and includes PPG concentration and salinity as shown below:

$$\hat{C}_{PPG} = \frac{a_{14}\left(C_{PPG,1}\right)}{1 + b_{14}C_{PPG,1}}, \tag{11.16}$$

$$\mathrm{a}_{14} = \left(\mathrm{a}_{14,1} + \mathrm{a}_{14,2}\mathrm{C}_{\mathrm{SEP}}\right), \tag{11.17}$$

where $C_{PPG,1}$ is the PPG concentration in the aqueous phase 1 and the parameters $\mathrm{a}_{14,1}$, $\mathrm{a}_{14,2}$, and b_{14} are input parameters.

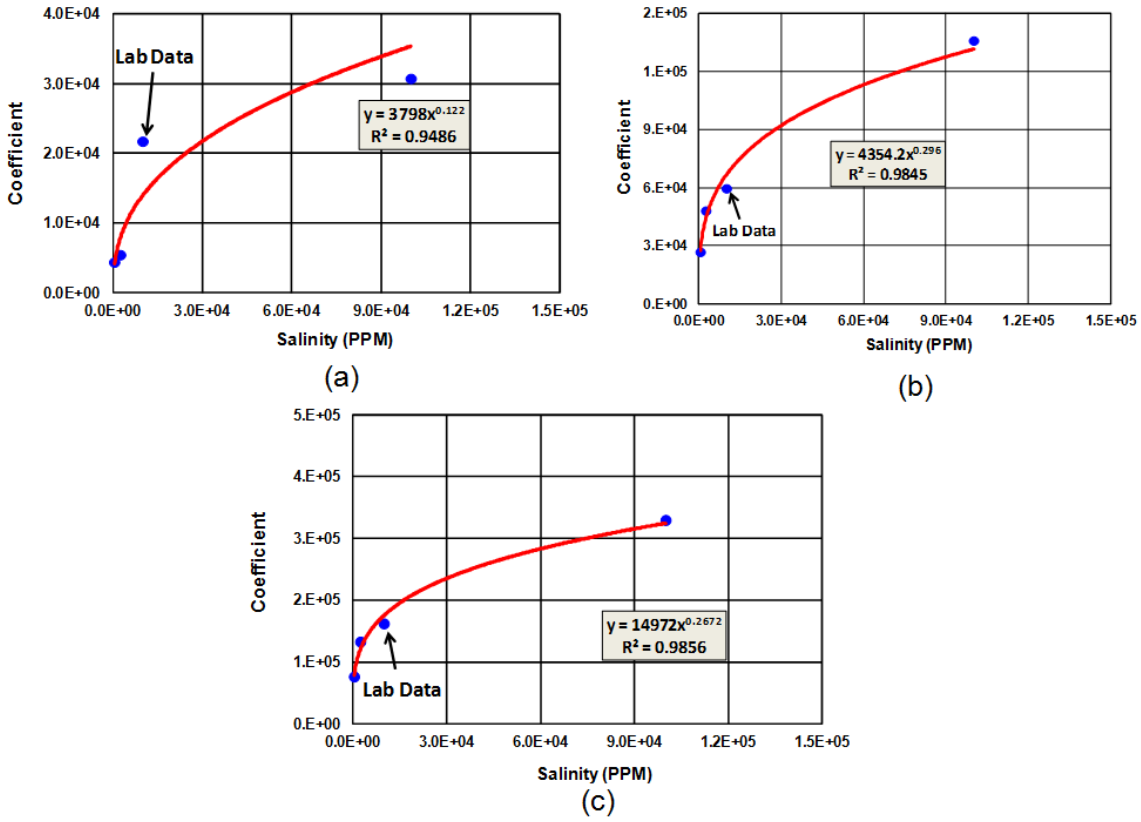

Figure 11-25: Calculated (curve) and measured (points) residual resistance factor coefficients (a_2) as a function of salinity for different fracture widths: (a) 0.5 mm, (b) 1 mm, (c) 1.5 mm.

11.3.8 PPG Transport Kinetics

Wang *et al.* (2012) proposed a novel mathematical model that reflects pore-throat plugging by PPG, particle plugging to reduce the permeability, pressure gradient, throat size, and plugged particle restarting to deform and flow through pore throats. The plugging will happen when PPG particle diameter is larger than the pore throat. However, under the effect of large pressure gradient, the PPG particle will deform and pass through the pore throat. Hence, the net rate of PPG plugging will be the difference between the

rate of plugging, r_p, and the rate of restarting of previously plugged particles, r_r (Wang *et al.*, 2013). Therefore the following equation represents a kinetic model for this statement:

$$\frac{\partial \sigma}{\partial t} = r_p - r_r. \tag{11.18}$$

The plugging probability of PPG particles through the pore throat is related to the diameter distribution of PPG and pore throats. The extensive laboratory research showed that PPG diameter has normal distribution after drying, crushing and swelling. The experimental results by Wang (2013) showed that the critical restarting pressure gradient of PPG has exponential relationship with the ratio of particle diameter to pore throat diameter.

$$\nabla p_G = K_A * \exp(K_B * D_{PPG} / 2r_h), \tag{11.19}$$

where K_A, and K_B are model parameters. According to Eq. (11.19), it can be seen that under a pressure gradient less than critical pressure gradient, the plugging will happen and under higher gradient than critical pressure gradient, the particles will pass though the pore throat. Generally, larger particles are trapped first when passing through the pore throat and the concentration of PPG suspension decreases. As PPG particles transport in the reservoir, the plugging particles will deform and restart if the pressure gradient is higher than critical restarting pressure gradient. The restarting rate is proportional to particle concentration, pressure gradient, and flow rate and the following function can be used to describe the rate of particle restarting r_r of previously plugged particle:

$$r_r = \chi\sigma v_{\mathrm{p}} \frac{\nabla p - \nabla p_{\mathrm{G}}}{\nabla p} \cdot \Theta\left(\nabla p - \nabla p_{\mathrm{G}}\right), \tag{11.20}$$

$$\Theta\left(\nabla p - \nabla p_{\mathrm{G}}\right) = \begin{cases} 0 & \nabla p < \nabla p_{\mathrm{G}} \\ 1 & \nabla p \geq \nabla p_{\mathrm{G}} \end{cases}, \tag{11.21}$$

Where χ is the removal coefficient of plugging particles which is used for characterizing the probability of particles restarting, $\Theta(x)$ is the Heaviside function, v_{p} is the flow velocity, and ∇p is the instantaneous pressure gradient.

The PPG is approximately regarded as a sphere and the expansion is a 3D volume expansion. The swelling of three kinds of PPG is shown in Figure 11-26. It can be seen from the figure that the initial swelling ratio of PPG with water increases drastically with time and tends to reach stable plateau after almost 120 mins. In fact, swelling of PPG and suspension property of particles in solution determines whether the PPG can reach deep into the reservoir to change the flow direction. The experimental results show that PPG swelling can increase to some extent at temperatures above 80 ^{0}C as shown in Figure 11-27.

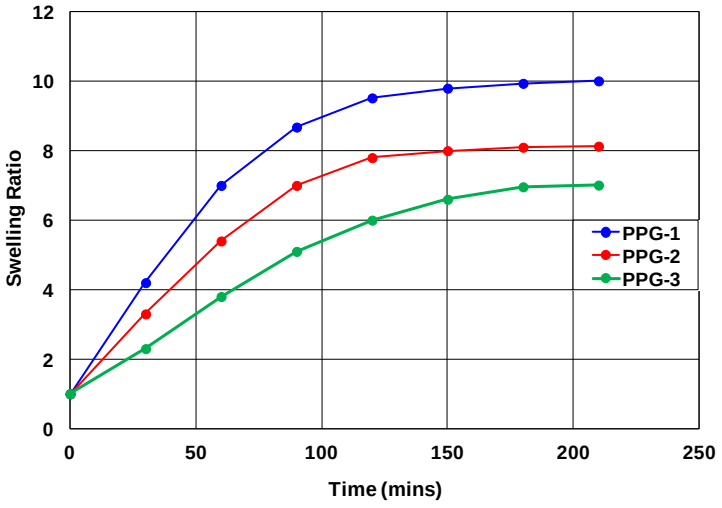

Figure 11-26: PPG swelling as a function of time (Wang *et al.*, 2013).

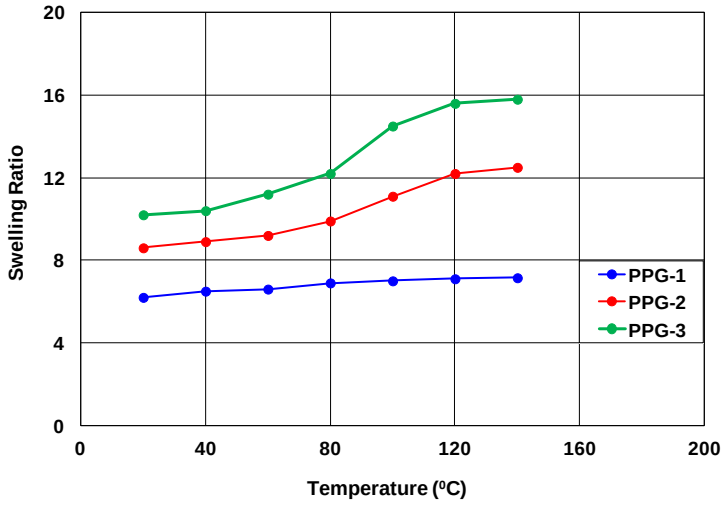

Figure 11-27: PPG swelling dependence on temperature (Wang *et al.*, 2012).

11.3.9 Embedded Discrete Fracture Model (EDFM)

The conformance control processes including PPG treatment are usually performed in mature waterflooded reservoirs which typically contain fractures or very high permeability streaks. Modeling the propagation of PPG through these fractures and conduits was considered as new challenges for this research study. Numerical simulation of fluid-flow in fractured reservoirs is complex due to the large contrast between matrix and fracture permeabilities, the extremely small size of fracture apertures, and the unstructured grid.

Several approaches have been proposed to model fracture networks that can be classified into two major classes of models: Dual continuum (Dual Porosity/Dual Permeability, DPDP) and Discrete Fracture Models (DFM). The Dual continuum models provide an efficient approach to describe highly heterogeneous fractured formations

using two domains, one for fracture system and other one for rock matrix. However, they suffer from high degree of simplification in a way that they cannot consider the effect of each fracture explicitly. On the other side, discrete fracture models are limited by unstructured gridding algorithms and simulation times even though they are more accurate. Unstructured gridding imposes more complexity for field-scale simulations (Figure 11-28).

To overcome problems associated with unstructured gridding, a new model has been developed called Embedded Discrete Fracture Model (EDFM). First, Li and Lee (2008) adopted a hierarchical modeling approach to represent fractures with different length scales. Later, Moinfar *et al.* (2013) employed this model to represent fractures with different dip and orientations in GPAS (in-house fully implicit parallel compositional reservoir simulator). A 3D synthetic illustration of fracture inclination which comprises eight fractures is shown in Figure 11-29.

In this model, fracture planes are discretized by cell boundaries. In fact, for flow in rock matrix, the structured grid is used and unstructured grid is used to model flow in fracture network. The fracture control volumes are considered as non-neighboring connections (NNC). A preprocessing step is developed to locate the fractures and to calculate the transmissibility factors among non-neighboring connections (Cavalcante Filho *et al.*, 2015). Since the fracture control volumes are introduced inside the matrix grid domain, three new connections are defined based on non-neighboring connections. For each of these new connections, a transmissibility factor is calculated as a preprocessing step explained briefly in the following:

a) For matrix-fracture connection (Connection type I)

$$T = \frac{kA}{d}, \tag{11.22}$$

where A is the area of fracture cell inside the grid block, k is the harmonic average of permeability, and d is the normal distance between center of matrix gridblock and fracture cell.

b) For fracture-fracture intersection (Connection type II)

$$\frac{kA}{d} = \frac{T_1 T_2}{T_1 + T_2}, \tag{11.23}$$

$$T_1 = \frac{k_{f_1} \omega_{f_1} L}{d_{f_1}}, \tag{11.24}$$

$$T_2 = \frac{k_{f_2} \omega_{f_2} L}{d_{f_2}}, \tag{11.25}$$

where k is the fracture permeability, ω is the fracture aperture, L is the length of intersection line between two fractures bounded in a gridblock, and the subscripts f_1 and f_2 represent the intersected fracture number 1 and number 2.

c) For fracture-fracture connection of the same fracture plane (Connection type III)

$$T = \frac{kA}{d}, \tag{11.26}$$

where k is the fracture permeability, A is the length of intersection times the aperture, and d is the distance between center of two segments.

The EDFM approach was implemented into UTGEL to provide efficient and robust tool to study the flow of gels in complex fracture system (Shakiba, 2014). The EDFM implementations created a more realistic environment to study the behavior of fractured reservoirs and aid in designing gel injection through fractures and conduits.

Taksaudom (2014) investigated the effect of PPG for a complex fracture conduit model which contains many fracture streaks with different dip angles and the results showed that there was approximately 7% improvement in oil recovery with PPG treatment compared to waterflood.

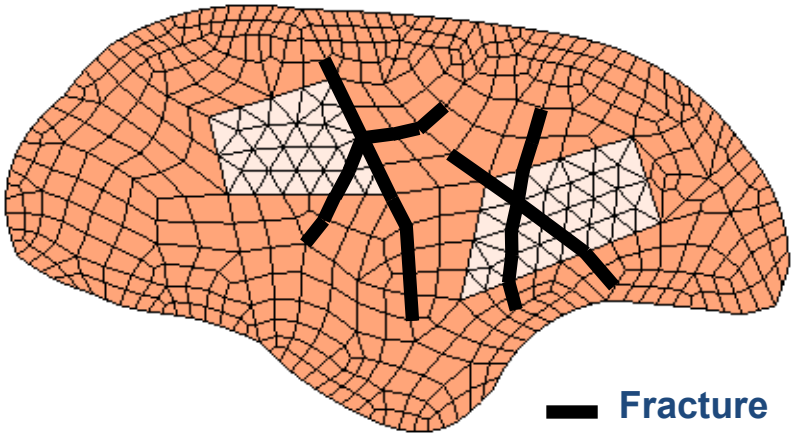

Figure 11-28: Discrete fracture model using unstructured grid.

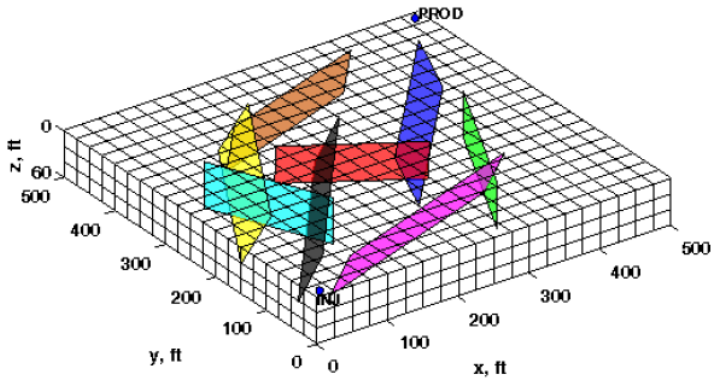

Figure 11-29: A synthetic 3D fractured reservoir with eight inclined macro-fractures (Moinfar *et al.*, 2012).

11.4 Results and Discussion

11.4.1 Simulation of Open Fracture Experiment

A Cartesian 1-D model was set up to simulate the fracture with single phase gel injection (Figure 11-30). Similar to the fracture experiment, six injection rates of 5, 10, 15, 20, 25, and 30 ml/min were selected and the simulation continued until the point where injection pressure became stable at steady state conditions. The PPG injection concentration, swelling ratio, and resistance factor information were selected based on the measured data from the lab. The open fracture media has porosity of one and the permeability was calculated for each fracture width using the equation for laminar flow between two parallel plates. The simulations are done at room temperature with twelve hours simulation time. The injection was at constant rate and production was at constant pressure. Totally, twelve simulations were performed to model the effect of salinity, flow rate, and fracture widths on PPG injection pressure and injectivity.

The injection pressure depends on flow rate, salinity, fracture width, and gel properties. Different simulations were performed to investigate the effect of these properties on injection pressure. Table 11-5 gives the summary of data used for different fracture width simulations. Comparisons of lab data and simulations are shown in Figure 11-31 through Figure 11-33. The comparison of injection pressure shows that there is good agreement between lab data and simulation results. The results demonstrate that PPG injection pressure increases with flow rate and salinity. The injection pressure depends on softness and deformability of swollen PPG particles rather than the particle size and PPG particles are softer and deformable at lower salinity brine which justifies the reason for high PPG injection pressure at higher salinity. The comparison shows that

PPG injection pressure decreases and the fracture width increases. This can be due to more conductivity of fracture at higher widths which lowers the injection pressure.

Table 11-5: Model parameters for the open fracture experiment.

Model	1-Dimensional Cartesian
No. of grids	20×1×1
$\Delta x, \Delta z$	55, 10 cm
Porosity	100 %
Δy (fracture width)	0.5, 1, 1.5 mm
Fracture Permeability	20833, 83333, 187500 Darcy
Water Saturation	100 %
Temperature	25 ^{0}C
Injection Rate (constant rate)	5, 10, 15, 20, 25, 30 ml/min
Outlet Pressure	14.7 psi
Simulation Time	12 hour

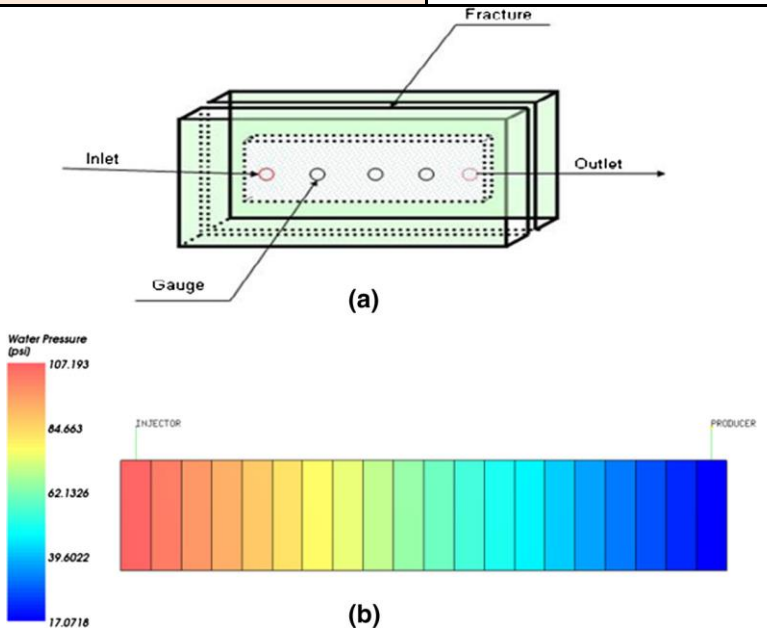

Figure 11-30: Open fracture experiment: (a) experimental setup, (b) simulation model.

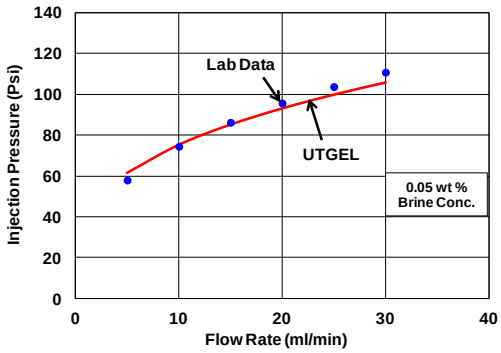

(a)

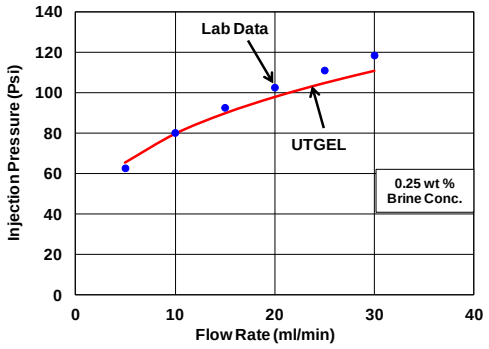

(b)

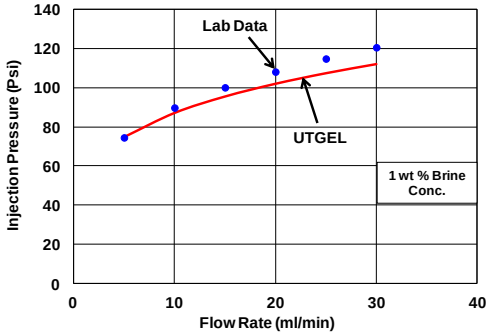

(c)

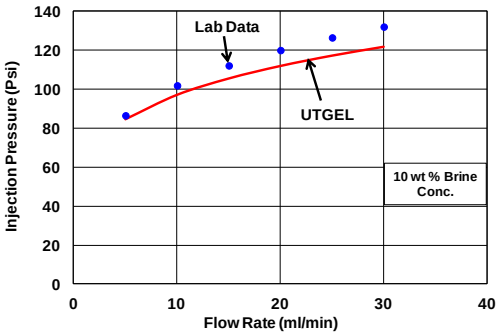

(d)

Figure 11-31: Comparison of measured and simulated PPG injection pressures as a function of flow rate for 0.5 mm fracture width:
(a) 0.05 wt.% NaCl, (b) 0.25 wt.% NaCl, (c) 1 wt.% NaCl, (d) 10 wt.% NaCl.

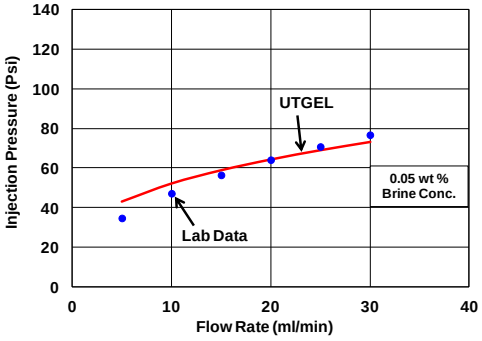

(a)

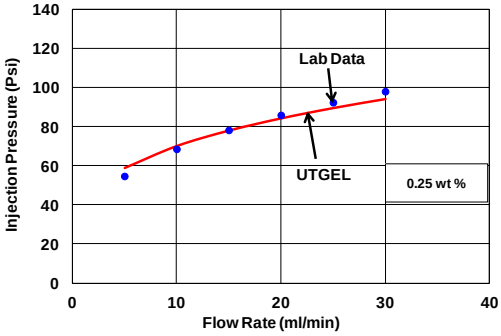

(b)

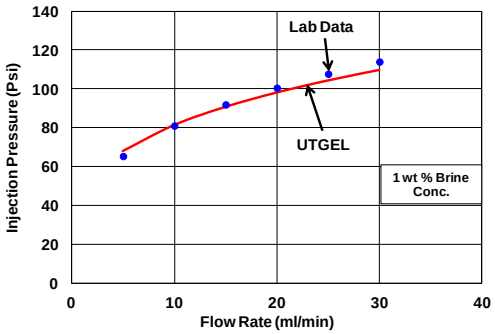

(c)

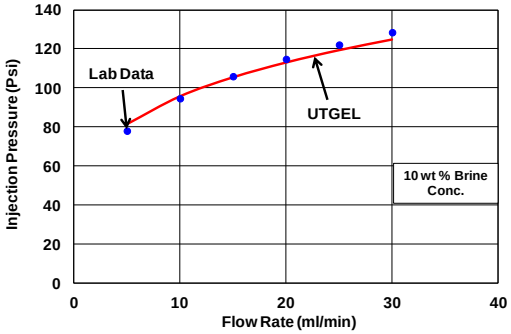

(d)

Figure 11-32: Comparison of measured and simulated PPG injection pressures as a function of flow rate for 1 mm fracture width:
(a) 0.05 wt.% NaCl, (b) 0.25 wt.% NaCl, (c) 1 wt.% NaCl, (d) 10 wt.% NaCl.

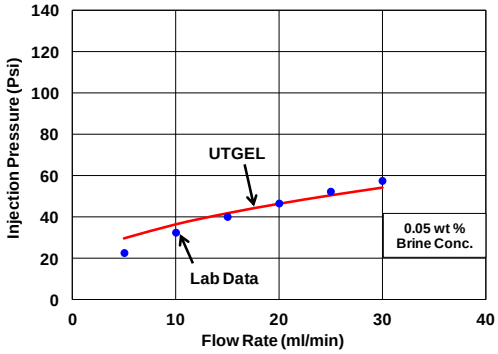

(a)

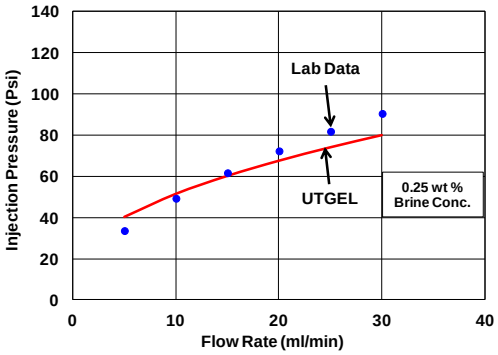

(b)

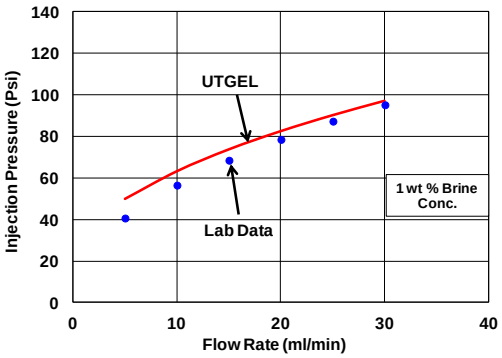

(c)

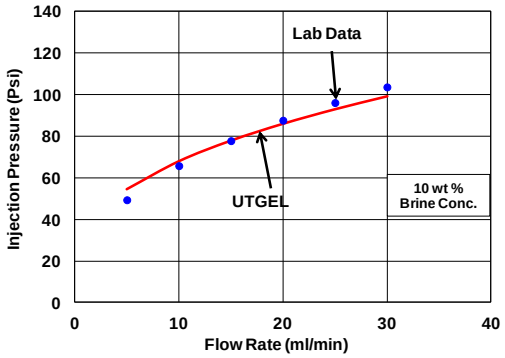

(d)

Figure 11-33: Comparison of measured and simulated PPG injection pressures as a function of flow rate for 1.5 mm fracture width:
(a) 0.05 wt.% NaCl, (b) 0.25 wt.% NaCl, (c) 1 wt.% NaCl, (d) 10 wt.% NaCl.

11.4.2 Simulation of Homogeneous Sandpack Experiment

A Cartesian 1-D model was used to simulate the water and PPG injection into the sandpack to history match the measured oil recovery and water cut (Figure 11-34). After packing and saturating the sandpack, it was flooded with 2.5 PVs of brine at a flow rate of 2 ml/min and then flooded with 1.2 PVs of PPG at the rate of 2 ml/min. Finally, 1.7 PVs of post-water was injected at the same rate of 2 ml/min. The mineral oil from Fisher Scientific was used for this experiment. Oil recovery was nearly 81% OOIP. A summary of rock and fluid properties is shown in Table 11-6.

In order to history match the oil recovery and water cut results, parameters were assigned for swelling ratio, resistance factor, and residual resistance factor. The coefficient and exponent parameters for swelling ratio were used based on the lab data to calculate swelling ratio as a function of salinity shown below:

$$SF = 34.26(C_{SEP})^{-0.343}. \tag{11.27}$$

In addition, resistance factor and residual resistance factor parameters were assigned in the INPUT file based on measured data. The following equations for resistance factor (RF) and residual resistance factor (RRF) are used.

$$RF = 203503(C_{SEP})^{-0.52}(\dot{\gamma}_{eq})^{-0.619}, \tag{11.28}$$

$$RRF = 86220(C_{SEP})^{-0.54}(\dot{\gamma}_{eq})^{-1.21}. \tag{11.29}$$

A comparison of measured and simulated oil recovery is shown in Figure 11-35. Water cut is compared in Figure 11-36. The favorable comparison of the simulated and the experimental results indicate that the gel transport model implemented in the simulator can accurately model gel injection behavior.

Table 11-6: Fluid and petrophysical properties for homogeneous sandpack experiment.

Diameter and Length	2.54 cm, 50.8 cm
Porosity, Permeability	0.386, 27290 md
Initial oil Saturation	0.88
Irreducible Water Saturation	0.12
Pore Volume	99.4 cm^3
Temperature	22.5 ^0C
Salinity	1 wt% KCl (0.134 meq/ml)
Mineral Oil Viscosity	37 cp
Residual Oil Saturation	0.265
Duration of Experiment	268 min
Gel flood:	Pore volumes injected:
1 wt% KCl flood	2.5 PV
2000 ppm PPG in 1 wt% KCl	1.2 PV
1 wt % KCl post flush	1.7 PV

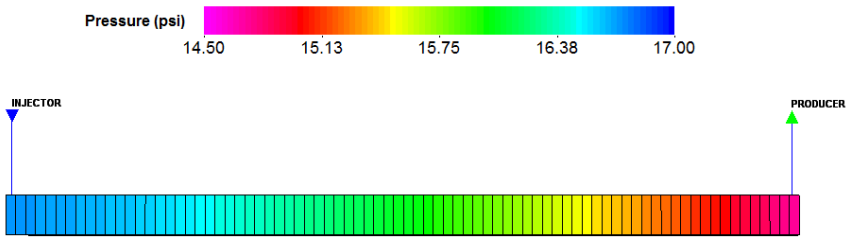

Figure 11-34: The simulation model for homogeneous sandpack experiment.

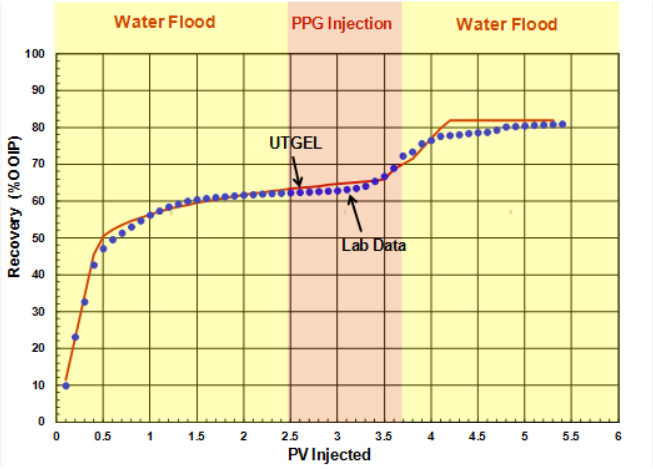

Figure 11-35: Comparison of measured (blue circles) and simulated (red curve) oil recoveries.

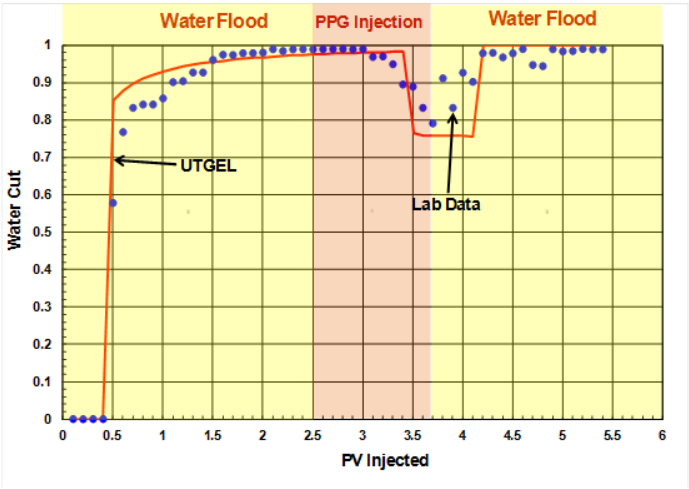

Figure 11-36: Comparison of measured (blue circles) and simulated (red curve) water cuts.

11.4.3 Simulation of Heterogeneous Sandpack Experiment (Without Crossflow)

A Cartesian 2-D model (two layers) was used to simulate the water and PPG injection into the heterogeneous sandpack experiment without crossflow to model and history match the oil recovery and water cut measurements (Figure 11-37). The mineral oil from Fisher Scientific was used. After saturating and preparing both sandpacks, it was flooded with 2.86 PVs of brine at the flow rate of 1 ml/min and then flooded with 0.2 PVs of PPG at the rate of 1 ml/min. Finally, 2.18 PVs of post-water was injected again at the same rate of 1 ml/min. A summary of rock and fluid properties with is given in Table 11-7. Oil recovery was nearly 56% OOIP.

Resistance factor and residual resistance factor parameters were assigned in the input file based on measured data. To model heterogeneous sandpack experiment, the following equations as a function of salinity and flow rate for resistance factor (RF) and

residual resistance factor (RRF) are used.

$$RF = 60(C_{SEP})^{-0.52}(\dot{\gamma}_{eq})^{-0.30}, \tag{11.30}$$

$$RRF = 83(C_{SEP})^{-0.54}(\dot{\gamma}_{eq})^{-1.21}. \tag{11.31}$$

Different values of residual oil saturation and relative permeability parameters are used for high and low permeability sandpacks. A comparison of measured and simulated oil recovery is shown in Figure 11-38. Water cut is compared in Figure 11-39. The favorable comparison of the simulated and the experimental results indicates that the gel transport model implemented in the simulator can accurately model gel injection behavior.

Table 11-7: Fluid and petrophysical properties for heterogeneous sandpack experiment without crossflow.

Diameter and Length	2.6 cm, 20 cm
Porosity for each region	0.272 (High perm), 0.375 (Low perm)
Permeability for each region	6778 md (High perm), 1005 md (Low perm)
Initial oil Saturation	0.74 (High perm), 0.82 (Low perm)
Irreducible Water Saturation	0.26 (High perm), 0.18 (Low perm)
Residual Oil Saturation for each region	0.09 md (High perm), 0.32 md (Low perm)
Oil Relative Permeability Endpoint for each region	0.85 md (High perm), 0.68 md (Low perm)
Oil Relative Permeability Exponent for each region	1.6 md (High perm), 2.4 md (Low perm)
Ratio of k_v/k_h	0
Temperature	22.5 ^{0}C
Salinity	1 wt% KCl (0.134 meq/ml)
Mineral Oil Viscosity	195 cp
Duration of Experiment	360 min
Microgel flood:	Pore volumes injected:

1 wt% KCl flood	2.86 PV
2000 ppm PPG in 1 wt% KCl	0.2 PV
1 wt % KCl post flush	2.18 PV

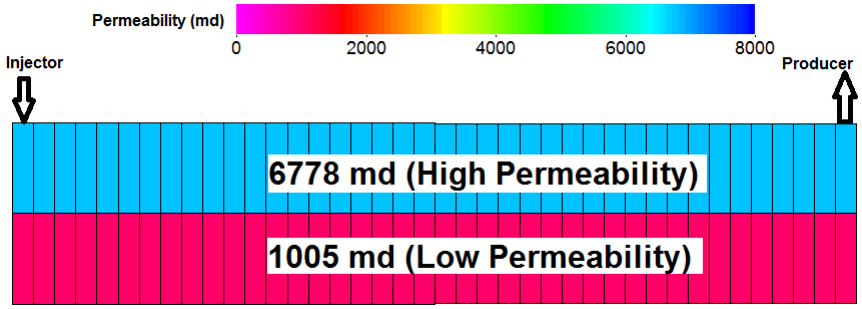

Figure 11-37: The simulation model for heterogeneous sandpack experiment (without crossflow).

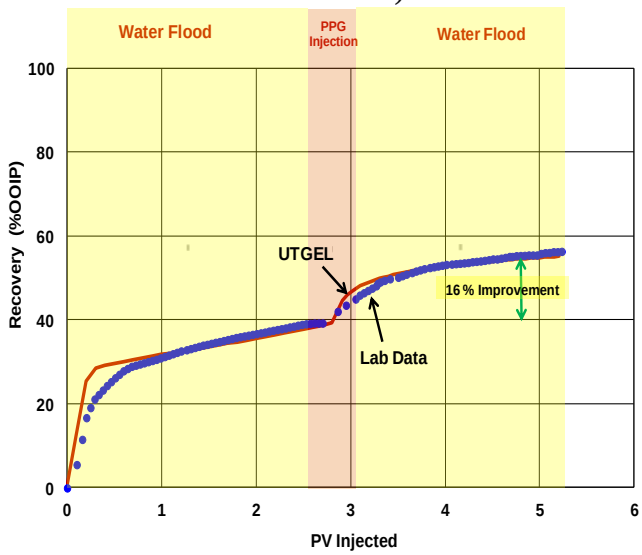

Figure 11-38: Comparison of measured (blue circles) and simulated (red curve) oil recoveries.

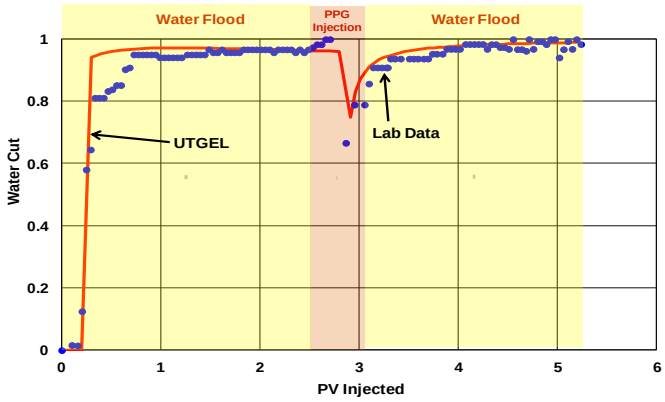

Figure 11-39: Comparison of measured (blue circles) and simulated (red curve) water cuts.

11.4.4 Simulation of Heterogeneous Sandpack Experiment (With Crossflow)

A Cartesian 2-D model (three layers) was used to history match the water and PPG injection into the heterogeneous sandpack experiment with crossflow (Figure 11-40). After preparing and saturating the sandpack with oil to reach irreducible water saturation, it was flooded with 3.19 PVs of brine at the flow rate of 2 ml/min and then flooded with 0.59 PVs of PPG at the rate of 2 ml/min. Finally, 3.23 PVs of post-water was injected again at the same rate of 2 ml/min. The mineral oil from Fisher Scientific was used for this experiment. A summary of rock and fluid properties is shown in Table 11-8. Oil recovery was nearly 71% OOIP.

Different values of residual oil saturation and relative permeability parameters are used for both high and low permeability sandpacks. A comparison of measured and simulated oil recovery is shown in Figure 11-41. Water cut is compared in Figure 11-42. PPG can selectively penetrate into the higher permeability sand while minimizes its penetration into the lower permeability sand or unswept zone. To model heterogeneous sandpack experiment, the following equations as a function of salinity and flow rate for

resistance factor (RF) and residual resistance factor (RRF) are used.

$$RF = 47(C_{SEP})^{-0.52}(\dot{\gamma}_{eq})^{-0.32}, \tag{11.32}$$

$$RRF = 73(C_{SEP})^{-0.51}(\dot{\gamma}_{eq})^{-1.27}. \tag{11.33}$$

Table 11-8: Fluid and petrophysical properties for heterogeneous sandpack experiment with crossflow.

Outside Diameter, Inside Diameter and Length	5.08 cm, 2.54 cm, 30 cm
Porosity for each region	0.272 (High perm), 0.375 (Low perm)
Permeability for each region	6778 md (High perm), 1005 md (Low perm)
Initial oil Saturation	0.72
Irreducible Water Saturation	0.28
Residual Oil Saturation for each region	0.09 md (High perm), 0.32 md (Low perm)
Oil Relative Permeability Endpoint for each region	0.85 md (High perm), 0.68 md (Low perm)
Oil Relative Permeability Exponent for each region	1.6 md (High perm), 2.4 md (Low perm)
Ratio of k_v/k_h	0.1
Temperature	22.5 ^{0}C
Salinity	1 wt% KCl (0.134 meq/ml)
Mineral Oil Viscosity	37 cp
Duration of Experiment	867 min
Microgel flood:	Pore volumes injected:
1 wt% KCl flood	3.19 PV
2000 ppm PPG in 1 wt% KCl	0.59 PV
1 wt % KCl post flush	3.23 PV

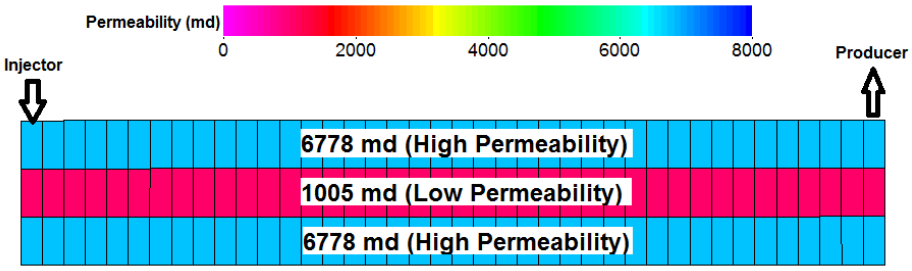

Figure 11-40: The simulation model for heterogeneous sandpack experiment (with crossflow).

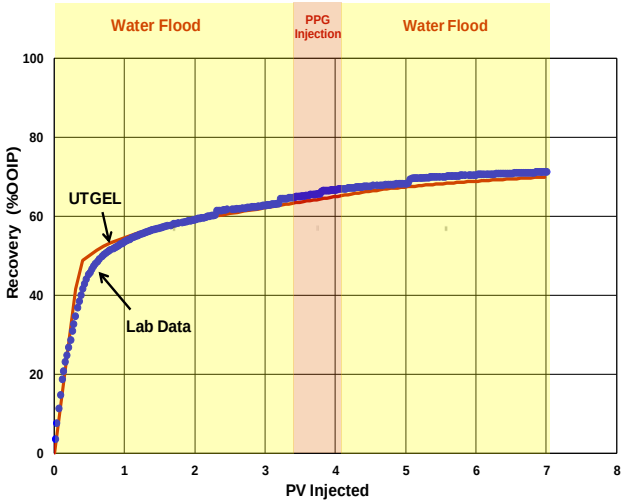

Figure 11-41: Comparison of measured (blue circles) and simulated (red curve) oil recoveries.

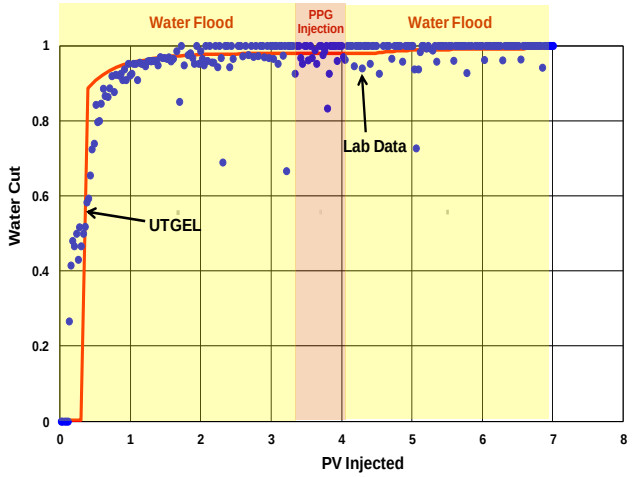

Figure 11-42: Comparison of measured (blue circles) and simulated (red curve) water cuts.

11.4.5 Simulation of Berea Sandstone Coreflood Experiment

1-D numerical model was set up (Figure 11-43) to simulate the water and microgel injection into the Berea sandstone core to history match the measured oil recovery and water cut measurements during both waterflood and microgel injection. A comparison of measured and simulated oil recovery is shown in Figure 11-44 and water cut is compared in Figure 11-45. The comparison shows that simulated oil recovery and water cut were in good agreement with the lab data. The residual oil saturation was reduced by increasing PPG concentration in gridblocks during microgel injection. However, based on experimental results, oil relative permeability endpoint remained constant at 0.654 during whole experiment which shows the minimum effect of microgel on oil relative permeability; the main goal is to reduce water relative permeability. A summary of rock and fluid properties is shown in Table 11-9.

Residual oil saturation measured during gel injection was reduced below that of waterflood. The phenomena have been reported for viscoelastic polymer solutions injected into consolidated cores (Huh and Pope, 2008; Delshad et al., 2008; Li et al., 2014). Many researchers have attributed the effect to increased pressure gradient, pulling effect of elastic polymers, among others. More experimental and theoretical research is required to understand the mechanism causing the reduction in residual oil saturation observed in our PPG experiment. However, in order to history match the oil recovery behavior, we propose a preliminary linear correlation to describe residual oil saturation reduction by increasing gel concentration as

$$w(i) = \frac{C_{PPG,i} - C_{PPG,0}}{C_{PPG,inj} - C_{PPG,0}}, \tag{11.34}$$

$$S_{res,i} = w(i)(S^0_{res,PPG} - S^0_{res,primary}) + S^0_{res,primary}, \tag{11.35}$$

where $C_{PPG,i}$, $S_{res,i}$ are the gel concentration and residual oil saturation in each gridblock, $C_{PPG,0}$, $C_{PPG,inj}$ are the initial and injected gel concentrations, $S^0_{res,primary}$, $S^0_{res,PPG}$ are the residual oil saturation during initial waterflood and end of gel injection. For this experiment, the initial gel concentration in the core, $C_{PPG,0}$, was zero and the injected gel concentration, $C_{PPG,inj}$ was 1000 ppm.

Table 11-9: Fluid and core properties used in microgel experiment.

Width, Height, and Length	2.54 cm, 2.54 cm, 50.8 cm
Porosity, Permeability	0.23, 558.34 md
Initial oil Saturation	0.66
Irreducible Water Saturation	0.34
Pore Volume	185.1 cm^3
Temperature	22.5 ^{0}C
Salinity	1 wt% KCl (0.134 meq/ml)
Mineral Oil Viscosity	37 cp
Residual Oil Saturation	0.374 (Water Inj.), 0.289 (Gel Inj.), 0.223 (Post flush)
Duration of Experiment	376 min
Gel flood:	Pore volumes injected:
1 wt% KCl flood	0.97 PVs
1000 ppm Microgel	0.91 PVs
1 wt % KCl post flush	1.17 PVs

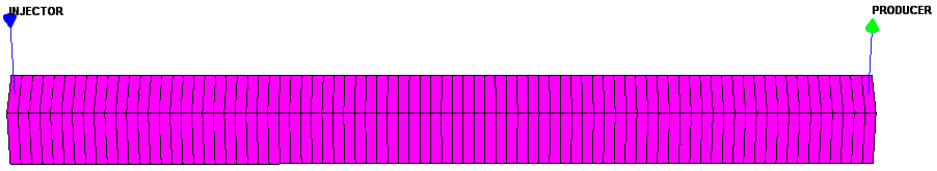

Figure 11-43: The simulation model used for history matching Berea sandstone microgel experiment.

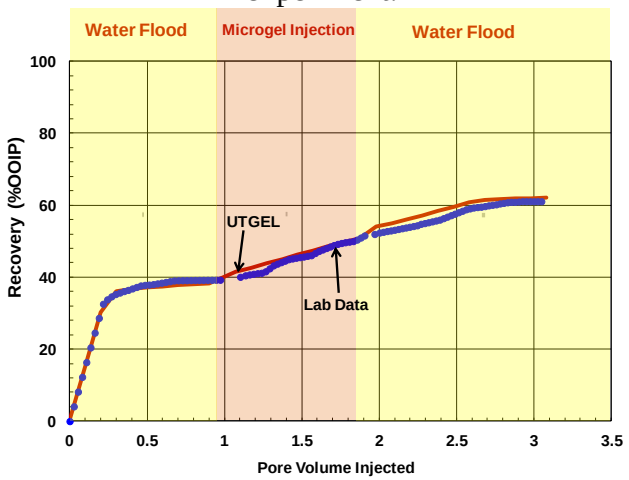

Figure 11-44: Comparison of measured (blue circles) and simulated (red curve) oil recoveries for Berea coreflood.

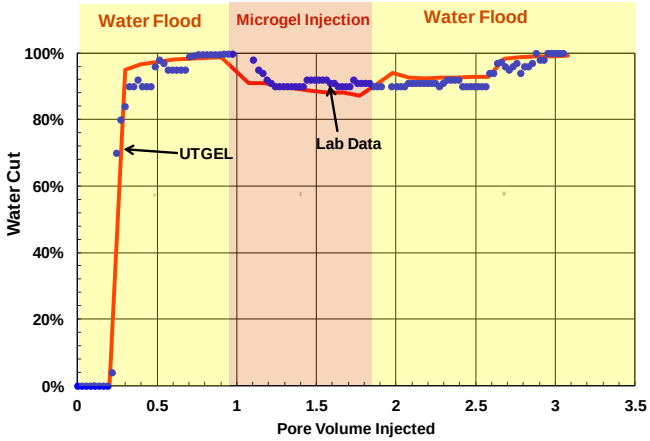

Figure 11-45: Comparison of measured (blue circles) and simulated (red curve) water cuts for Berea coreflood.

11.5 Synthetic Simulations

11.5.1 Base Case

A Cartesian model was set up to simulate the PPG injection with constant rate injection and production at constant pressure. The base case has a high permeability layer of 1500 md located in the middle and upper and lower layers have a permeability of 50

md (Figure 11-46). Table 11-10 gives the input data including model properties and PPG injection design. Waterflood was compared with PPG flood and the results indicated considerable improvement in oil recovery (around 7% OOIP incremental) and reduction in water cut as shown in Figure 11-47 and Figure 11-48. Oil saturation maps at the end of simulation (2.5 PVs) are shown in Figure 11-49 and Figure 11-50. It is clear from the figures that the layer with higher permeability is more favorable for injected PPG and injected water will divert into upper and lower layers. Several simulations were performed to study the impact of injection design and reservoir properties.

11.5.2 PPG Treatment Size

The typical treatment size is around 5% of the channel volume (CV). However, this can vary from 5% to 15% depending on PPG dilution, vertical to horizontal permeability ratio, and dispersion, among other factors. Figure 11-51 and Figure 11-52 show the incremental oil recovery and water cut sensitivity to gel treatment size. The results demonstrate that higher treatment size is favorable. However, it should be noted that increasing PPG slug above 15% will not have considerable improvement in oil recovery and it will increase cost.

11.5.3 PPG Concentration

The PPG treatment concentration for base case was chosen to be 1000 ppm. However, concentrations of 10,000 and 15,000 ppm were used to investigate the PPG concentration effect on oil recovery. Figure 11-53 and Figure 11-54 show the incremental oil recovery and water cut sensitivity to gel concentration. The results demonstrate that higher PPG concentration is favorable. However, it should be noted that increasing PPG

concentration above 15000 ppm will not improve oil recovery.

11.5.4 Permeability Contrast

Permeability contrast between high permeability zone and the rest of the reservoir is one of the key factors affecting the success of conformance treatment. As shown in Figure 11-55, higher contrast in permeability is desirable for better efficiency because thief zone takes more of the injected PPG to divert the flow to the lower permeability zones.

11.5.5 Crossflow

The vertical to horizontal permeability ratio (k_v/k_h) is another factor that can impact the performance of PPG treatment. The lower the k_v/k_h ratio, more PPG will be placed in high permeability with more effective permeability reduction. However, for the large k_v/k_h ratio, PPG can cross flow into low permeability zones, which is undesirable. Figure 11-56 shows the impact of k_v/k_h ratio on incremental oil recovery.

Table 11-10: Base case data used for PPG study and sensitivity simulations.

Model	3-Dimensional Cartesian
No. of Grids	15×15×3
Δx , Δy , Δz	1.5, 1.5, 1.5 m
Porosity and permeability	0.449, (50, 1500, 50) md
Initial Water saturation	30 %
K_v/K_h	0.1
Injection Rate (constant rate)	2.8 m^3/day
Production Pressure (constant pressure)	101.35 Kpa
PPG Concentration	1000 ppm
Waterflood:	**PVs injected:**
1 wt% KCl flood	2.5 PVs
PPG flood:	**PVs injected:**
1 wt% KCl flood	1 PV

1000 ppm PPG in 1 wt% KCl	0.5 PV
1 wt % KCl post flush	1 PV

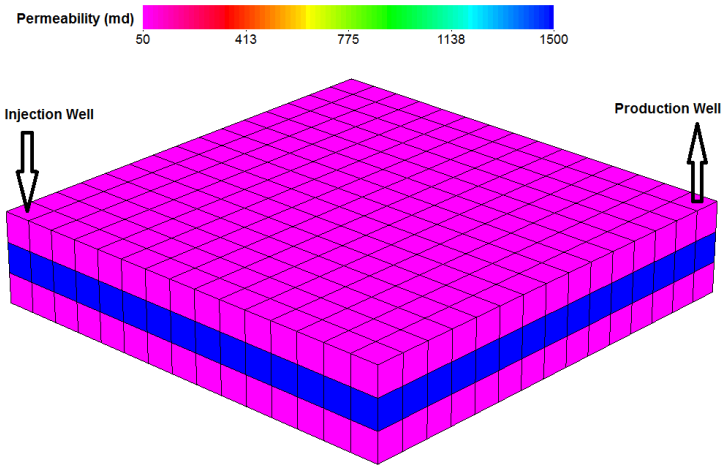

Figure 11-46: Simulation model and permeability representation.

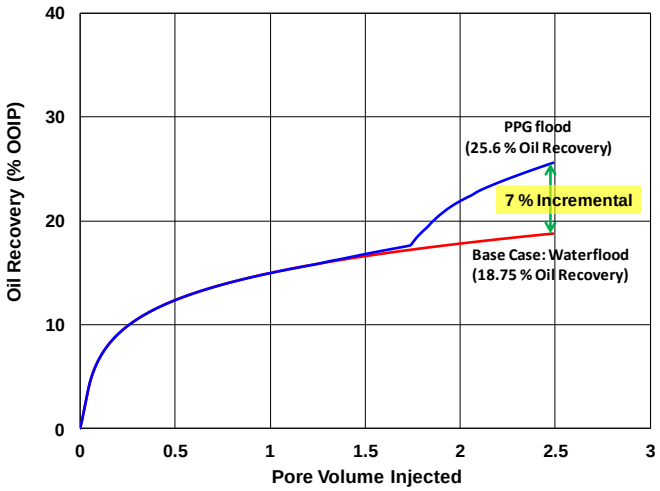

Figure 11-47: Comparison of oil recovery between waterflood and PPG flood for the base case.

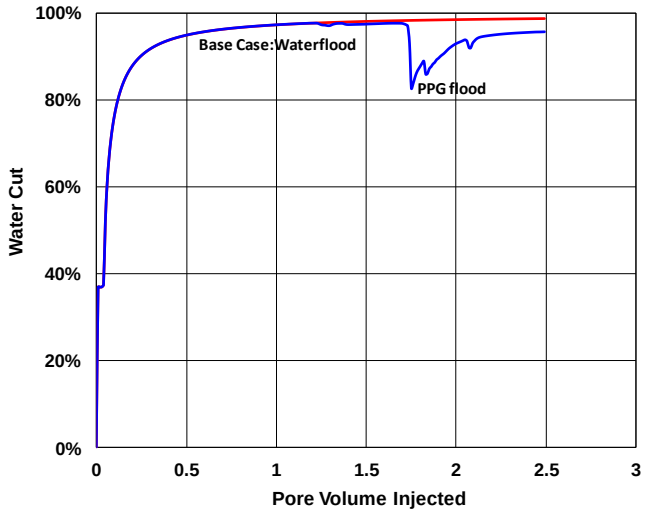

Figure 11-48: Comparison of water cut between waterflood and PPG flood for the base case.

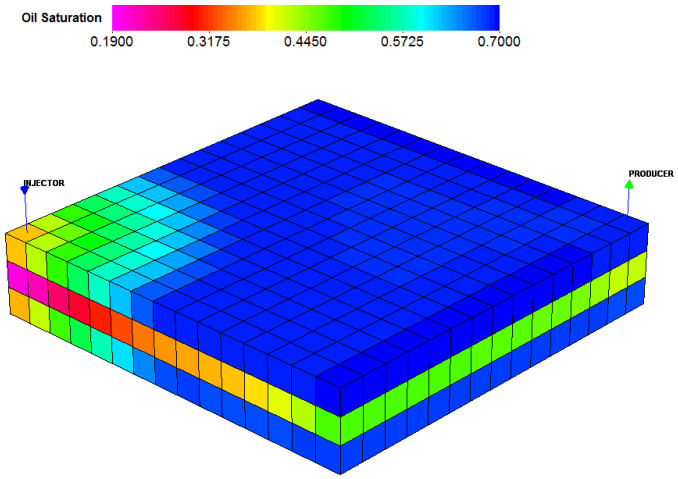

Figure 11-49: Oil saturation after 2.5 PVs for waterflood in the base case simulation.

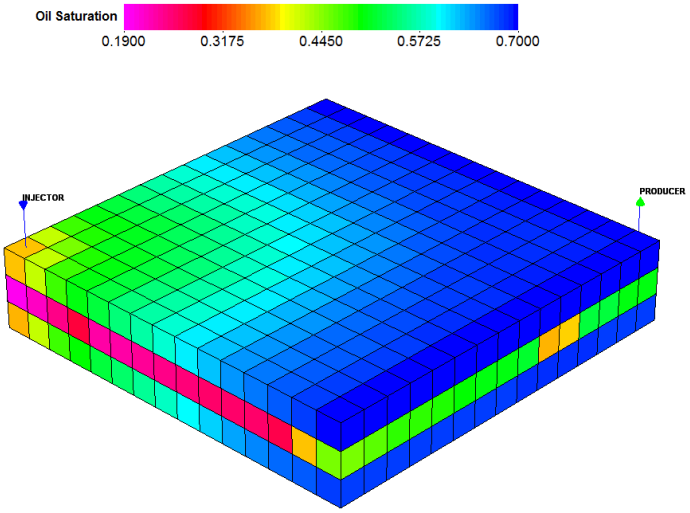

Figure 11-50: Oil saturation after 2.5 PVs for PPG flood in the base case simulation.

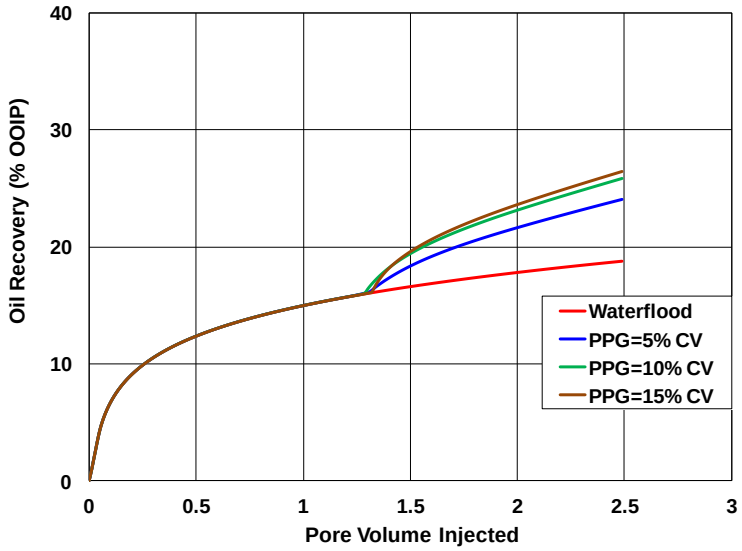

Figure 11-51: Comparison of oil recovery for different treatment sizes.

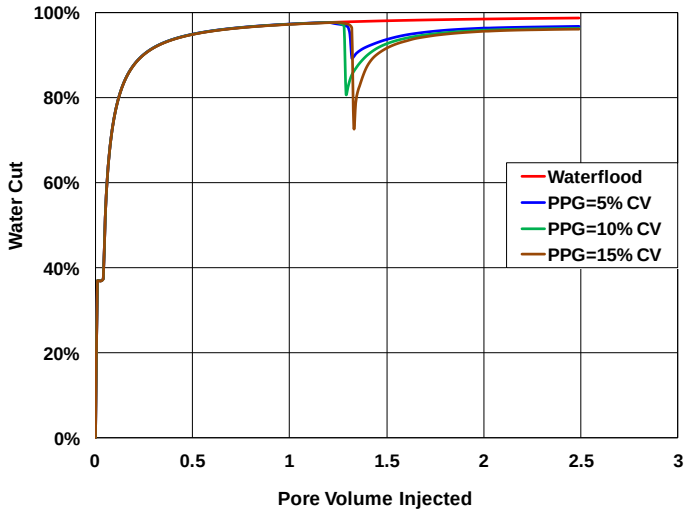

Figure 11-52: Comparison of water cut for different treatment sizes.

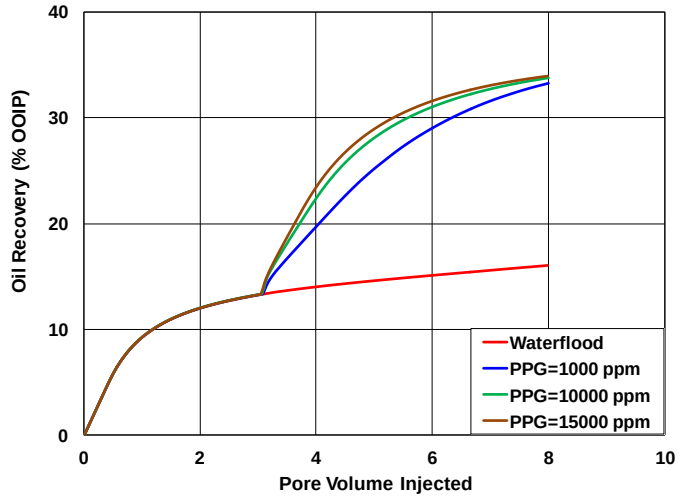

Figure 11-53: Comparison of oil recovery for different PPG concentrations.

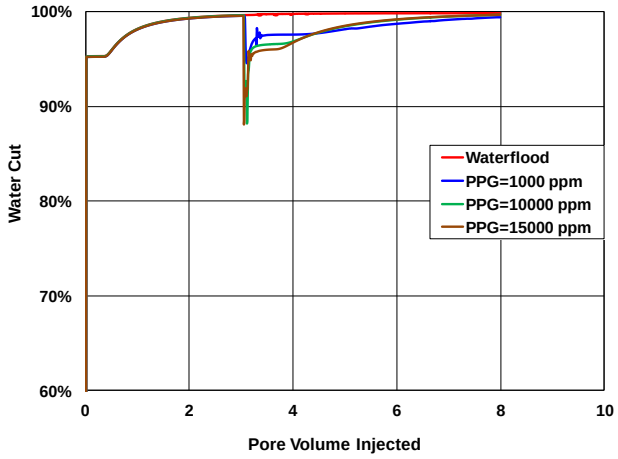

Figure 11-54: Comparison of water cut for different PPG concentrations.

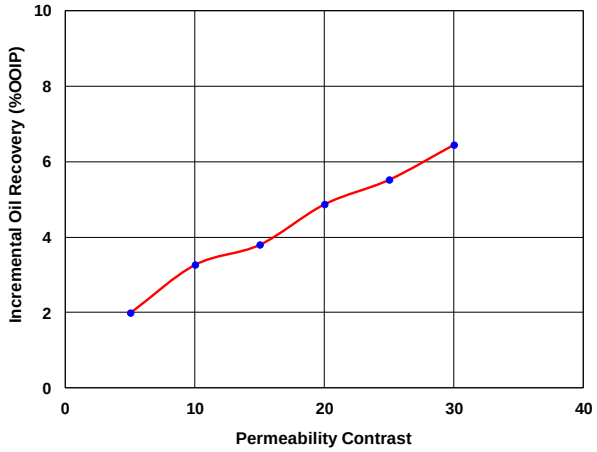

Figure 11-55: Impact of permeability contrast (thief zone and the rest of the reservoir) on incremental oil recovery.

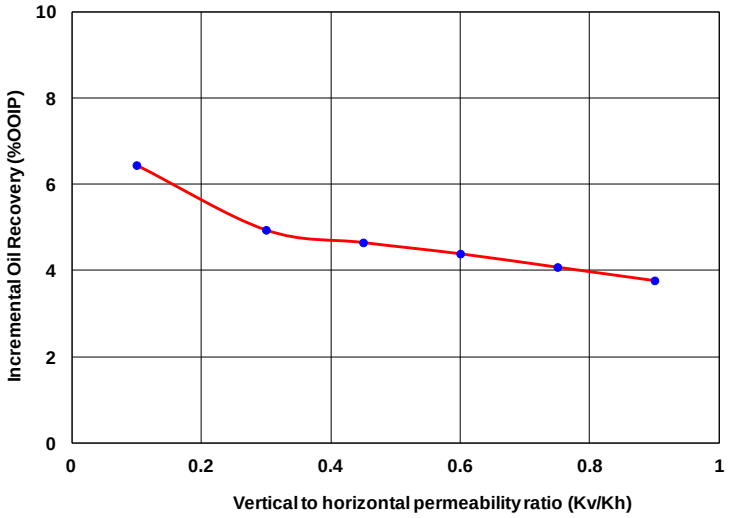

Figure 11-56: Impact of k_v/k_h ratio on incremental oil recovery.

11.6 Field-scale simulations

11.6.1 Karamay Field PPG Conformance Control

The Karamay oil field is an onshore sandstone reservoir in northern China (Delshad et al., 1998). We used the geomodel and well conditions of Karamay as a candidate reservoir for PPG treatment. A pilot area of 42.67×42.67 m2 containing 13 wells was used. The top of the pay zone is at the depth of 289.56 m with a thickness of 10 m. Crude oil and water viscosities at the reservoir temperature of 60 °C are 17.2 and 0.9 cp, respectively. The pay zone has three geological layers and stochastic permeability maps were generated for each layer by use of the matrix-decomposition method and conditioned to the well data (Figure 11-57). The pay zones are isolated from each other by non-communicating shale layers. A Cartesian model with 19×19×3 gridblocks in X, Y, and Z directions is used for this field study.

Table 11-11 gives the reservoir and fluid properties. Figure 11-58 shows initial oil

saturation distribution. The PPG input parameters were chosen based on measured experimental data. The simulation includes 100 days of waterflood followed by PPG flood for 300 days and followed by post water injection for 600 days.

The comparison of oil recovery and water cut with and without PPG treatment are shown in Figure 11-59 and Figure 11-60. Oil recovery increases by about 14% with significant reduction in water cut using PPG. The success of PPG can be related to heterogeneity of reservoir in which the middle layer has the highest permeability compared to the other two and this made it possible for PPG to block the high permeability gridblocks and water diverts into low permeability zones. The oil saturation distribution after 400 days of waterflood and PPG flood in Figure 11-61 and Figure 11-62 clearly shows that PPG improved sweep efficiency considerably and most of the reservoir oil was produced. However, salinity, temperature, particle sizes, and reservoir heterogeneity control how far PPG propagates into the formation from the injection well. The PPG concentration and also resistance factor at the end of PPG flood (400 days) are shown in Figure 11-63 and Figure 11-64.

Table 11-11: Karamay field and fluid properties for PPG field scale conformance control study.

Model	3-Dimensional Cartesian
No. of grids	19×19×3
Δx, Δy, Δz	10, 10, (3-6-3) m
Reservoir Porosity	0.3
Initial Reservoir Pressure	12238 Kpa
Oil and Water Relative Permeability Endpoint	0.95, 0.20
Temperature	60 ^{0}C
Crude Oil Viscosity	40 cp
Simulation Time	1000 days
PPG Design:	**Time injected:**

Waterflood	100 Days
PPG flood with Concentration of 1000 ppm	300 Days
Post Water Injection	600 Days

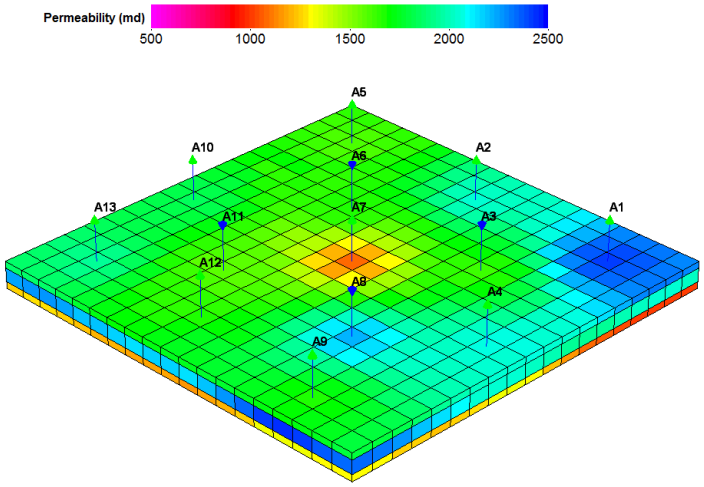

Figure 11-57: Permeability distribution in Karamay field.

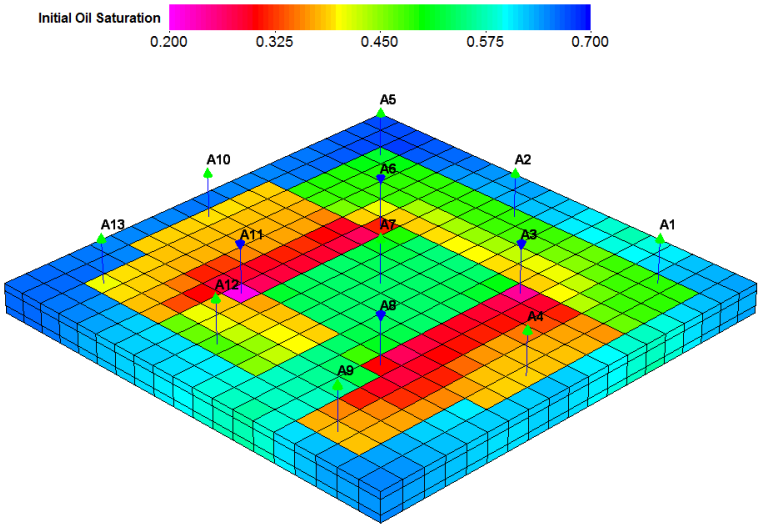

Figure 11-58: Initial oil saturation distribution in Karamay field.

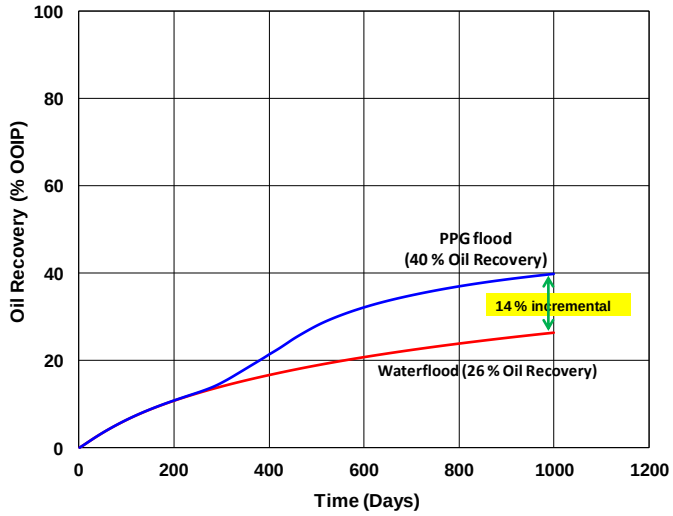

Figure 11-59: Comparison of waterflood and PPG flood oil recoveries in Karamay oil field.

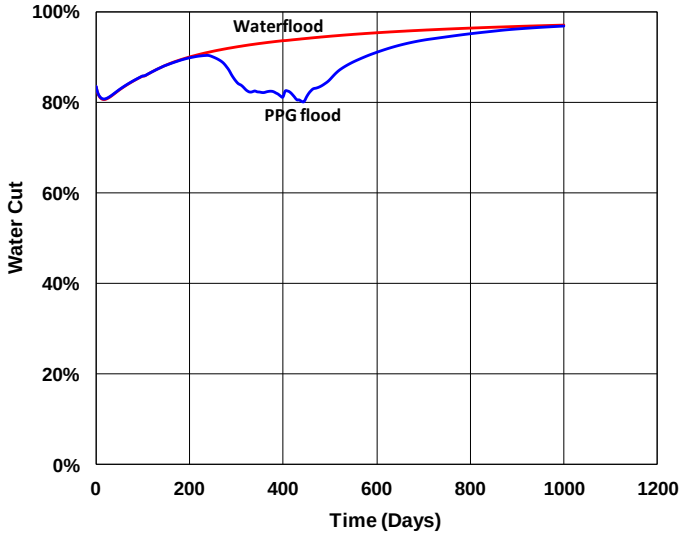

Figure 11-60: Comparison of waterflood and PPG flood water cuts in Karamay oil field.

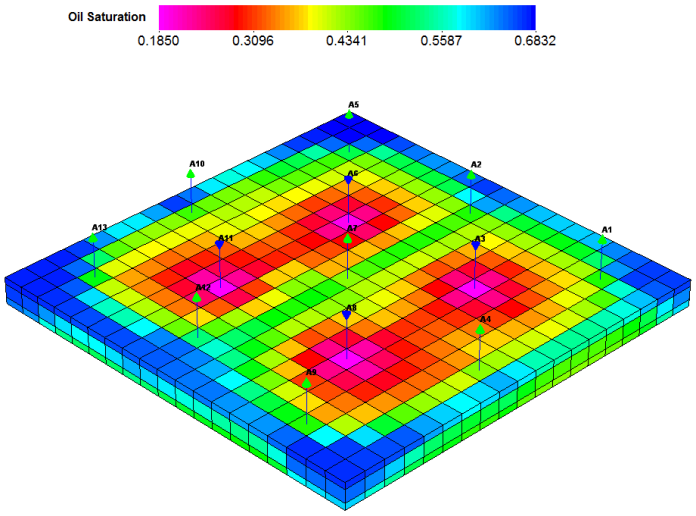

Figure 11-61: Oil saturation after 400 days for waterflood.

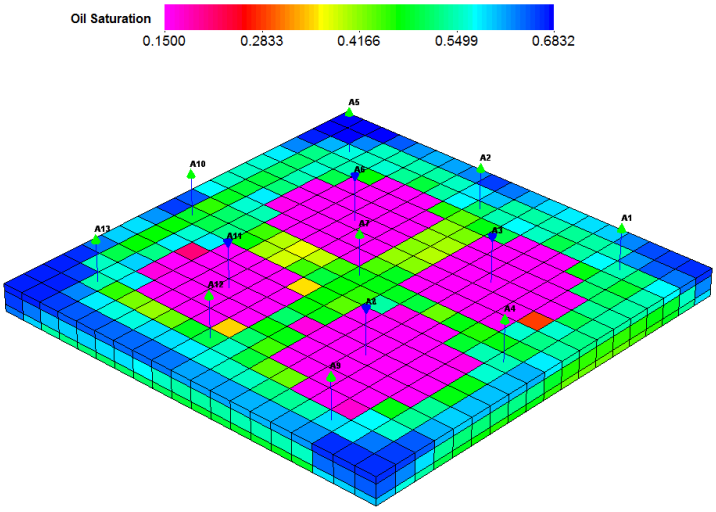

Figure 11-62: Oil saturation after 400 days for PPG flood.

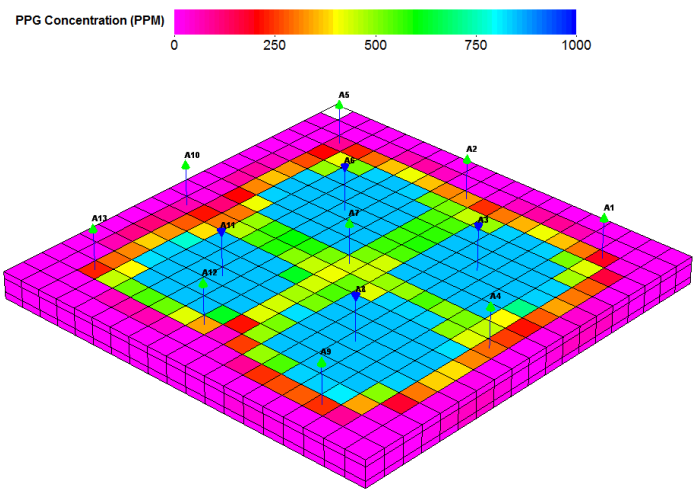

Figure 11-63: PPG concentration after 400 days for PPG flood.

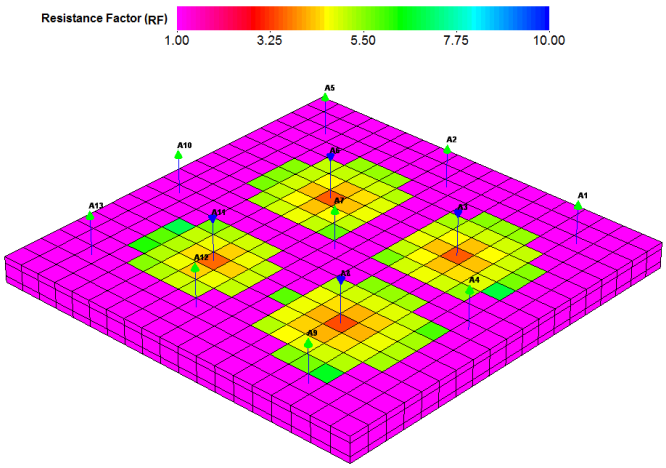

Figure 11-64: Resistance factor after 400 days for PPG flood.

11.6.2 Heterogeneous Permeability Large Scale Model

A Cartesian model was set up where PPG injection is simulated. The injection was at constant rate and production was at constant pressure. Table 11-12 gives the data used. The base case has a high average permeability of 3000 md with Dykstra-Parsons coefficient of 0.88, correlation length of 0.1 in x-axis, correlation length ratio Lx/Ly of 1, and correlation length ratio Lx/Lz of 1000. The generated heterogeneous permeability distribution is shown in Figure 11-65. The model consists of one inverted 5-spot pattern (4 produces, 1 injector) and PPG concentration for injection was 2000 ppm. The base case model (PPG flood) was compared with waterflood and the results indicated that PPG injection has considerable improvement compared to waterflood.

A comparison of simulated oil recovery for PPG flood vs. waterflood is shown in Figure 11-66. Oil recovery increases by about 15% with significant decrease in water cut using PPG. The oil saturation at the end of waterflood and PPG flood in areal direction are shown in Figure 11-67 and Figure 11-68. Also, the oil saturation at the end of waterflood and PPG flood in vertical direction are shown in Figure 11-69 and Figure 11-70. It is clear from the figures that the areas with higher permeability is more favorable for PPG injection and gives better sweep efficiency. Therefore it can be concluded that both areal and vertical sweep efficiency are improved using PPG compared to waterflood.

Figure 11-71 and Figure 11-72 show the incremental oil recovery and oil production rate sensitivity to gel concentration. This sensitivity analysis was performed to optimize the incremental oil recovery from PPG treatment by increasing PPG concentration. Three PPG concentrations of 500, 2000, and 15000 ppm were chosen for

sensitivity simulations and the duration of PPG injection was 200 days. The results demonstrate that higher PPG concentration is favorable. However, it should be noted that increasing PPG concentration above 2000 ppm will not have any impact in oil recovery.

Table 11-12: Simulation input parameters for large scale heterogeneous case.

Model	3-Dimensional Cartesian
No. of grids	40×40×3
Δx, Δy, Δz	10, 10, 10 ft
Reservoir Porosity	0.35
Initial Water Saturation	0.15
K_v/K_h	0.1
Crude Oil Viscosity	25 cp
Injection Rate	2500 ft^3/day
Production Bottomhole Pressure	500 psi
Simulation Time	800 days
Waterflood:	**Time injected:**
1 wt% KCl Flood	800 Days
PPG Design:	**Time injected:**
Waterflood	300 Days
PPG flood with Concentration of 2000 ppm	200 Days
Post Water Injection	300 Days

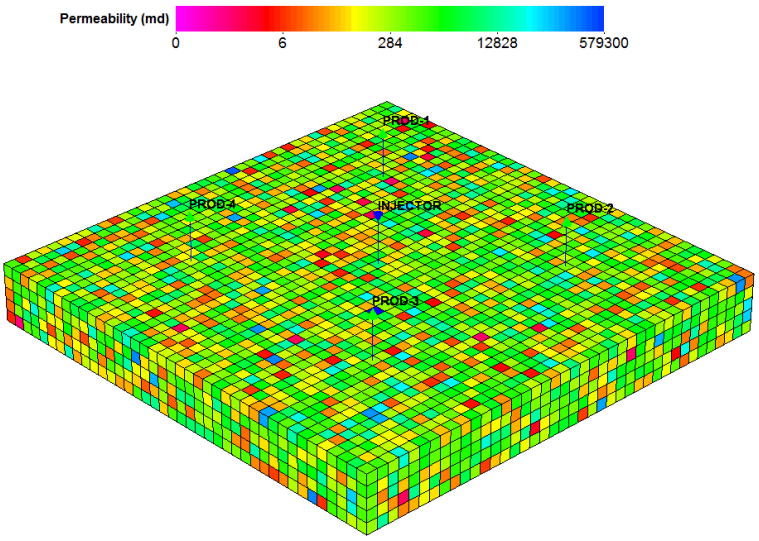

Figure 11-65: The base case heterogeneous permeability distribution representation.

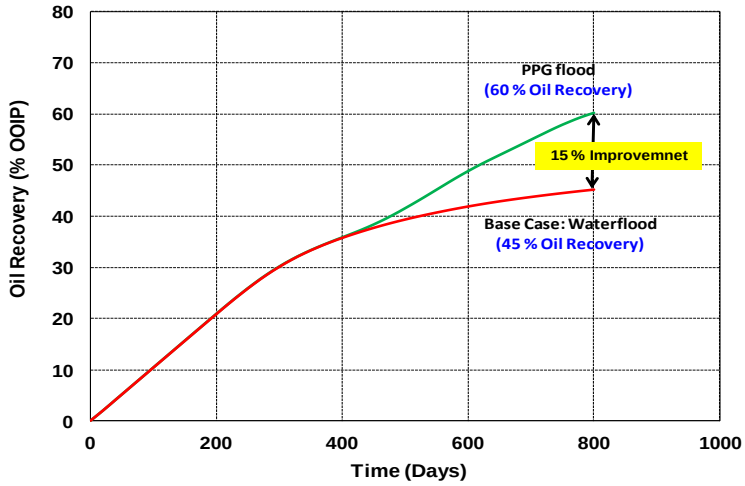

Figure 11-66: Comparison of simulated oil recovery for PPG vs. waterflood.

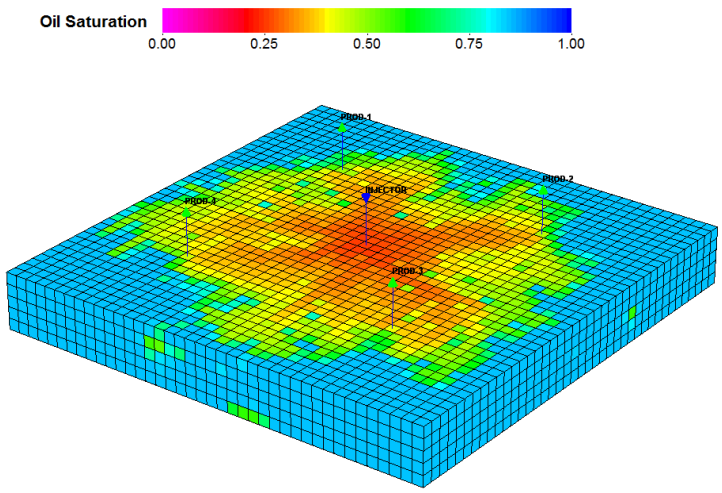

Figure 11-67: Oil saturation distribution at the end of waterflood scenario in areal direction.

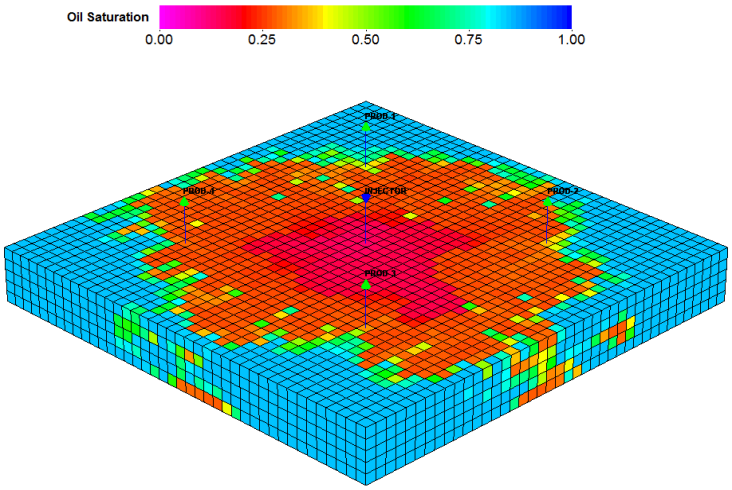

Figure 11-68: Oil saturation distribution at the end of PPG flood scenario in areal direction.

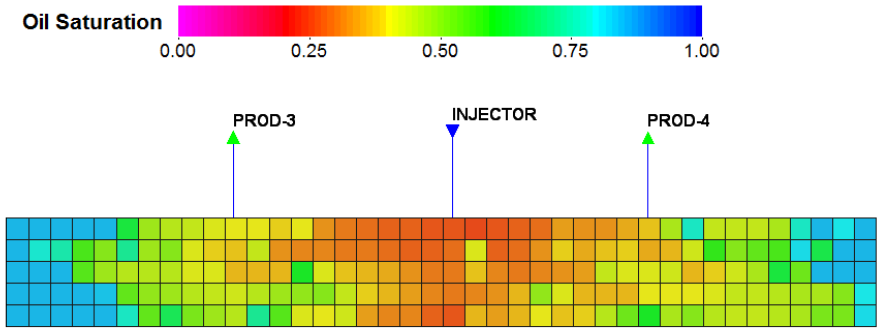

Figure 11-69: Oil saturation distribution at the end of waterflood scenario in vertical direction.

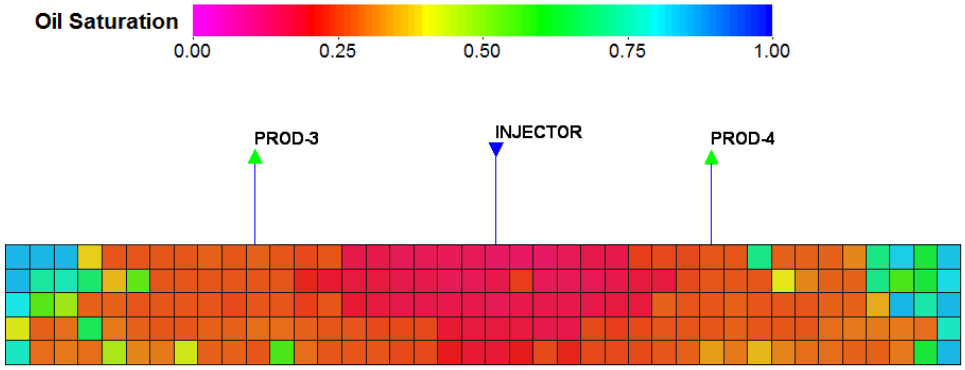

Figure 11-70: Oil saturation distribution at the end of PPG flood scenario in vertical direction.

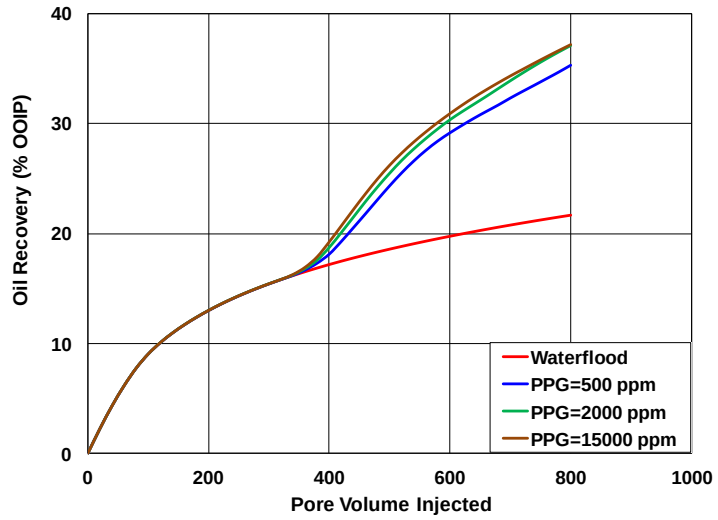

Figure 11-71: Comparison of oil recovery for different PPG concentrations.

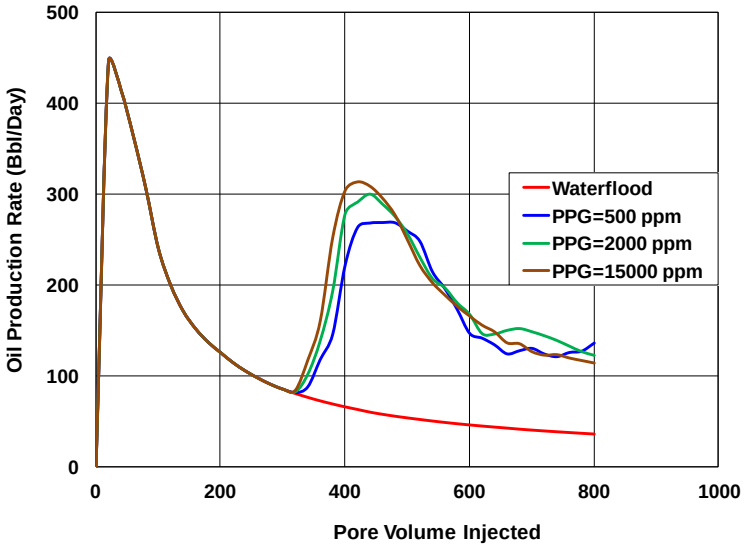

Figure 11-72: Comparison of oil production rate for different PPG concentrations.

11.6.3 PPG vs. Bulk Gel Conformance Control for a Heterogeneous Onshore Field

We used the geomodel and well conditions of a candidate onshore field to

compare PPG versus Bulk Gel treatments. A pilot area of 983×1075 m^2 containing 10 injection wells and 7 production wells, all of which are vertical wells with perforation over the entire pay zone, was selected for this study. The average reservoir porosity is around 0.25 but it varies between 0.1 and 0.3, as shown in Figure 11-73. The reservoir permeability is very heterogeneous and varies from 0.1 to 17,000 md (in both vertical and areal direction) as shown in Figure 11-74. The top of the pay zone is at the depth of 1916 ft with a thickness of 37 ft. Crude oil and water viscosities at the reservoir temperature of 72.5 °F are 3.4 and 0.37 cp, respectively. A Cartesian model with 43×47×19 gridblocks in X, Y, and Z directions is used for this field study. Table 11-13 gives the reservoir and fluid properties. The PPG and Bulk Gel input parameters for comparison were chosen based on measured experimental data. Different simulations were performed to investigate the performance of two types of gels, namely; Bulk Gel, and PPG. The production scenarios are summarized as following:

- Base case waterflood: comprised of 7.3 PV of water injection.
- Bulk in-situ gel treatment: comprised of 5.0 PV of pre-treatment water injection, followed by 0.3 PV of bulk gel treatment, and 2.0 PV of post water injection.
- PPG treatment: comprised of 5.0 PV of pre-treatment water injection, followed by 0.3 PV of PPG injection, and 2.0 PV of post water injection.

The comparison of oil recovery and water cut for different production scenarios are shown in Figure 11-75 and Figure 11-76. The oil recovery increases by about 9% for Bulk Gel Flood compared to waterflood. However, PPG flood shows around 21% improvement in oil recovery compared to waterflood. This illustrates that injection of PPG as microgel can be more efficient than generation of in-situ bulk gel in the reservoir

by injecting polymer and crosslinker since polymerflood has some disadvantages, such as shear degradation, higher adsorption, and high pressure drop requirement for injection.

Table 11-13: UTGEL simulation input parameters.

Model	3-Dimensional Cartesian
No. of grids	43×47×19
Δx, Δy, Δz	75, 75, 2 ft
Initial Water Saturation	0.2
Crude Oil Viscosity	3.4 cp
Injection Rate	Variable for each well
Production Bottomhole Pressure	300 psi
Total Pore Volume Injected	7.3 PV
Waterflood:	**Pore Volume Injected:**
1 wt% KCl Flood	7.3 PV
PPG Design:	**Pore Volume Injected:**
Waterflood	5 PV
PPG flood with Concentration of 2500 ppm	0.3 PV
Post Water Injection	2 PV
Bulk Gel Design:	**Pore Volume Injected:**
Waterflood	5 PV
0.5 %wt Polymer and Crosslinker	0.3 PV
Post Water Injection	2 PV

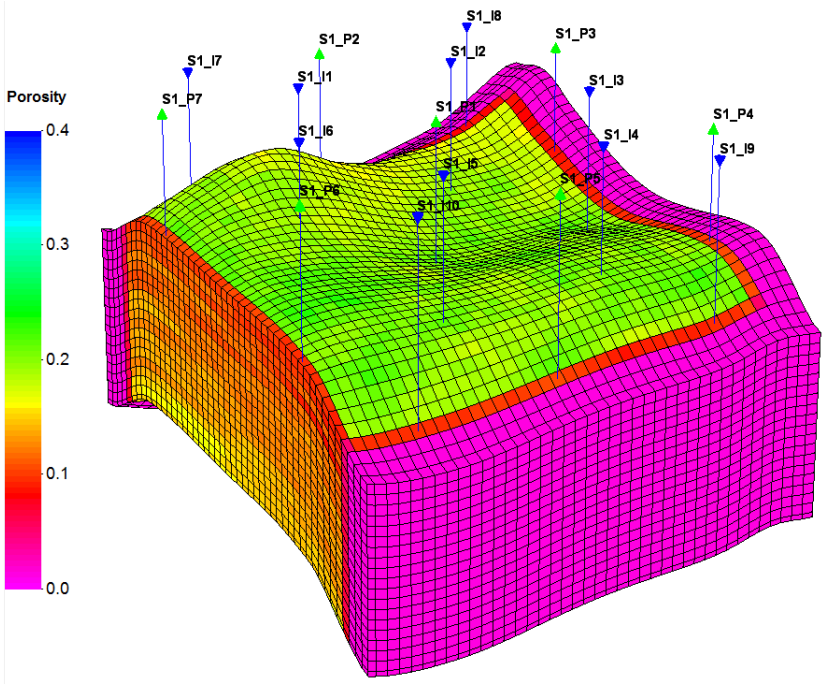

Figure 11-73: Porosity distribution of the heterogeneous onshore field.

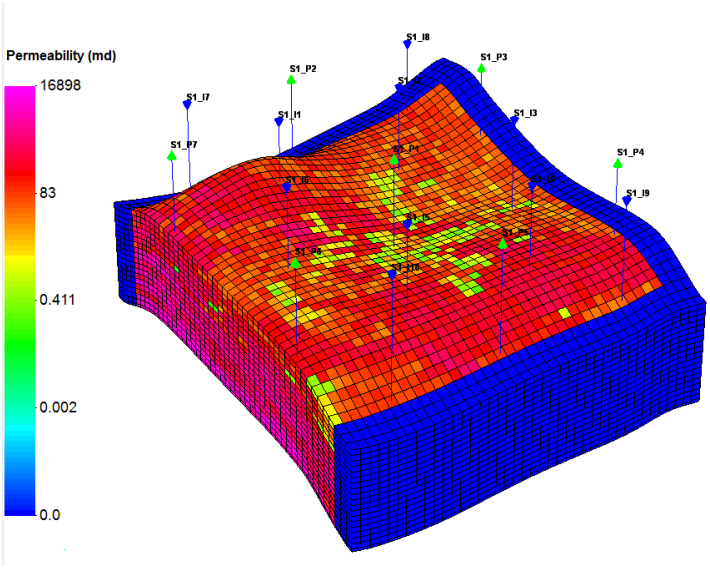

Figure 11-74: Permeability distribution of the heterogeneous onshore field.

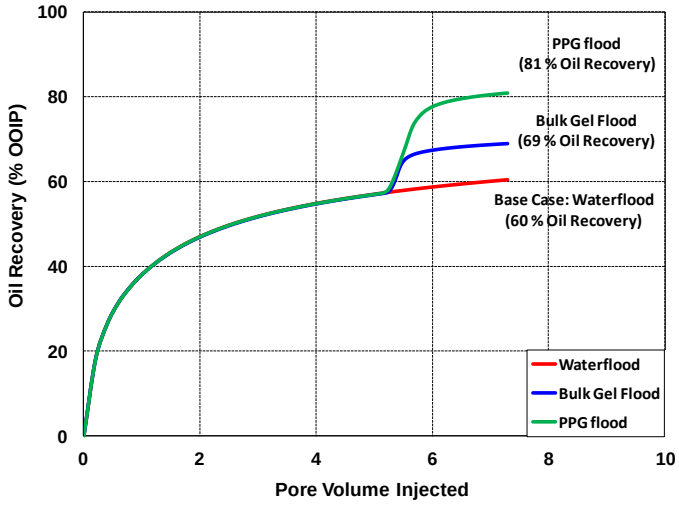

Figure 11-75: Comparison of waterflood, Bulk Gel flood, and PPG flood oil recoveries.

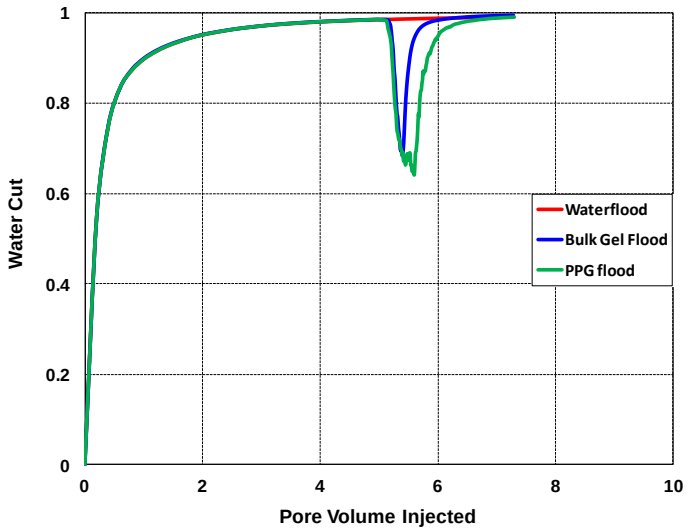

Figure 11-76: Comparison of waterflood, Bulk Gel flood, and PPG flood water cuts.

11.7 Summary and Conclusions

- PPG experiments in both fracture and sandpack models were performed successfully to investigate the effect of PPG on improving conformance and reducing water cut.

- PPG injection pressure increased with the increase in flow rate and salinity but decreased with the increase of fracture width.
- Berea coreflood experiment was conducted to understand the transport of PPG microgels and their impact on flow conformance and reducing water production.
- Coreflood results indicated that residual oil saturation after PPG flood is lower than the waterflood residual oil saturation. A simple model is proposed but more mechanistic understanding is underway supported by additional laboratory and theoretical studies.
- Empirical correlations are developed for resistance factor (RF) and residual resistance factor (RRF) using different size conduits and for a wide range of flow rate and brine salinity and hardness.
- We have developed models for gel rheology, adsorption, swelling ratio, resistance factor, and residual resistance factor.
- The gel transport models were implemented in a reservoir simulator and validated against laboratory experiments.
- The numerical studies indicated that main PPG design variables are treatment size, PPG concentration, permeability contrast, and the ratio of vertical to horizontal permeability.
- The normal and rule-of-thumb estimate for slug size is between 5-15% of the Channel Volume (CV). However, the sensitivity simulations showed that increasing slug volume above 10 % CV will not have considerable impact on final oil recovery. The sensitivity simulations also illustrated that higher concentration is favorable for PPG treatment. However, 10,000 ppm can be considered as the criteria where increasing concentration above that will not increase the final oil recovery. For reservoir properties, higher permeability contrast between layers and lower vertical to horizontal permeability ratio (k_v/k_h) are favorable design parameters for PPG treatment. Higher k_v/k_h will cause the crossflow of PPG from high permeability layer into low permeability layer which brings adverse effect on blocking high permeability channels.
- UTGEL can model the performance of PPG in improving oil recovery in the parallel sandpack systems (with crossflow and without crossflow) which represented a degree of heterogeneity in the experiment design. Resistance factor and gel retention model parameters were used as history matching parameters.
- To history match heterogeneous parallel sandpack experiments (with crossflow and without crossflow), different relative permeability, capillary pressure, and residual saturations are used for high and low permeability zones.
- PPG can preferentially penetrate into the higher permeable layer while minimizing its penetration into the lower permeable layer.

- Pilot scale simulations of Karamay oil field showed that PPG is capable of generating high resistance factor in the high permeability thief zone and increased the incremental recovery by 14% over waterflood.

12. PUBLICATIONS

1. **A. Almohsin** et al.," Transport of Nanogel through Porous Media and Its Resistance to Water Flow," SPE paper 169078, SPE Improved Oil Recovery Symposium, Tulsa, OK, April 2014.
2. **F. Muhammed** et al., "A Simple Technique to Determine Gel Strength of Millimeter-sized Particle Gel," SPE paper 169106, SPE Improved Oil Recovery Symposium, Tulsa, OK, April 2014.
3. **Goudarzi**, A. et al "Water Management in Mature Oil Fields using Preformed Particle Gels," SPE paper 165356, SPE Western Regional & AAPG Pacific Section Meeting, 2013 Joint Technical Conference, Apr 19 - 25, 2013, Monterey, CA, USA.
4. **Goudarzi**, A. et al., "Novel Experiments and Mechanistic Models for Conformance Control Microgels," SPE paper 169159, SPE Improved Oil Recovery Symposium, Tulsa, OK, April 2014.
5. **Goudarzi**, A., Zhang, H., Varavei, A., Taksausdom, P., Hu, Y., Delshad, M., Bai, B., and Sepehmoori, K. 2015. A laboratory and simulation study of preformed particle gels for water Conformance Control. Fuel Journal*;* 140**:** 502-513.
6. **Imqam**, A. et al., "Preformed Particle Gel Extrusion through Open Conduits during Conformance Control Treatments," SPE paper 169107, SPE Improved Oil Recovery Symposium, Tulsa, OK, April 2014.
7. **Imqam** A. et al "Characterizing the Disproportionate Permeability Reduction of Preformed Particle Gels during Extrusion through Fractures" SPE-171531-MS**,** Asia Pacific Oil & Gas Conference and Exhibition, October 2014, Adelaide, Australia.
8. **Imqam**, A., Bai, B., Al-Ramadan, M., Delshad, M., Sepehmoori, K. 2014. Preformed Particle Gel Extrusion through Open Conduits during Conformance Control Treatments. SPE Journal. SPE-169107-PA.
9. **Imqam**, A., Bai, B., Delshad, M. 2015. Preformed Particle Gel Propagation through Super-K Permeability and its Resistance to Water Flow during Conformance Control. Paper SPE 176429 accepted to present at the SPE Asia Pacific Oil & Gas Conference and Exhibition held in Bali, Indonesia, 20–22 October.
10. **Imqam**, A., Goudarzi, A., Delshad, M., Bai, B. 2015. Development a Mechanistic Numerical Simulator for Preformed Particle Gel Applications in Non-Cross Flow Heterogeneous Reservoirs. Paper SPE **175058** accepted to present to the SPE Annual Technical Conference and Exhibition held in Houston, Texas, USA, 28-30 September.

Additional publications

1. Ayman Almohsin (PhD student at MS&T)

   Dissertation title: " An Investigation of Deformable Nanogel-Particles through Sandstone Porous Media"

1. Ali Abdulmohsen Al Brahim (Ms student at MS&T)

   Thesis title: "Evaluation of Millimeter-Sized Preformed Particle Gel for Conformance Control Treatments Using Simple Models"

4. Ze Wang (Ms student at MS&T))

   Thesis title: "Preformed Particle Gel propagation and recovery improvement in heterogeneous fractured reservoir"

4- Ali Goudarzi (PhD Student at UT-Austin)

   Dissertation title: "Modeling Chemical EOR and Conformance Control Processes Using Different Reservoir Simulators, Aug. 2015."